Searching for more π-acceptor phosphines:

From α-pyridiniophosphines to α-cationic phospholes

Dissertation

zur Erlangung des mathematisch-naturwissenschaftlichen Doktorgrades

„Doctor rerum naturalium"

der Georg-August Universität Göttingen

im Promotionsprogramm Chemie

der Georg-August University School of Science (GAUSS)

vorgelegt von

Tim Johannsen

aus Heide

Göttingen, 2022

Betreuungsausschuss

Prof. Dr. Manuel Alcarazo (Institut für Organische und Biomolekulare Chemie, Tammannstr. 2, 37077 Göttingen)

Prof. Dr. Dietmar Stalke (Institut für Anorganische Chemie, Tammannstr. 4, 37077 Göttingen)

Mitglieder der Prüfungskommission

Referent: Prof. Dr. Manuel Alcarazo (Institut für Organische und Biomolekulare Chemie, Tammannstr. 2, 37077 Göttingen)

Korreferent: Prof. Dr. Dietmar Stalke (Institut für Anorganische Chemie, Tammannstr. 4, 37077 Göttingen)

Weitere Mitglieder der Prüfungskommission:

Jun.-Prof. Dr. Johannes Walker (Institut für Organische und Biomolekulare Chemie, Tammannstr. 2, 37077 Göttingen)

Dr. Lisa Vondung (Institut für Anorganische Chemie, Tammannstr. 4, 37077 Göttingen)

Dr. Alessandro Bismuto (Institut für Organische und Biomolekulare Chemie, Tammannstr. 2, 37077 Göttingen)

Dr. Daniel Janßen-Müller (Institut für Organische und Biomolekulare Chemie, Tammannstr. 2, 37077 Göttingen)

Tag der mündlichen Prüfung: 17.03.2022

Declaration

Hiermit versichere ich, dass ich die eingereichte Dissertation selbständig verfasst und keine anderen als die angegebenen Quellen und Hilfsmittel benutzt, sowie Zitate kenntlich gemacht habe.

Göttingen,

Tim Johannsen

The presented thesis was prepared in the group of Prof. Dr. Manuel Alcarazo at the Institute of Organic and Biomolecular Chemistry of the Georg-August University Göttingen between June 2017 and December 2020.

Parts of this thesis were published in the following publications:

H. Tinnermann, L.D.M. Nicholls, T. Johannsen, C. Wille, C. Golz, R. Goddard, M. Alcarazo, *ACS Catal.* **2018**, *8*, 10457-10463.

T. Johannsen, C. Golz, M. Alcarazo, *Angew. Chem. Int. Ed.* **2020**, *59*, 22779-22784.

Acknowledgements

Abbreviations

Å	ångström/angstrom (10^{-10} m)
Ad	adamantyl
Alk	alkyl
aq.	aqueous
Ar	aryl
ATR	attenuated total reflection
bdmim	1-butyl-2,3-dimethylimidazolium
Bn	benzyl
Bp.	boiling point
c	concentration
CAAC	cyclic(alkyl)(amino)carbene
cat.	catalytic
Cbz	benzyloxycarbonyl
conc.	concentrated
conv.	conversion
Cy	cyclohexyl
Cp	cyclopentadienyl anion
CV	cyclic voltammetry/voltammogram
δ	chemical shift (NMR)
d	days
d	doublet (NMR)
dba	dibenzylideneacetone
DCE	1,2-dichloroethane
DCM	dichloromethane
DFT	density functional theory
dipp	di*iso*propylphenyl
ee	enantiomeric excess
EE	ethyl acetate
e.g.	*exempli gratia* / for example
EDG	electron donating group
EI	electron impact ionization
eq.	equivalents
equiv.	equivalents
ESI	electrospray ionization
et al.	*et alii* / and the others
etc	*et cetera* / and more
EtOAc	ethyl acetate
EWG	electron withdrawing group
h	hours
HOMO	highest occupied molecular orbital
HR	high resolution

HSAB	hard and soft acids and bases
*i*Pr	*iso*-propyl
IR	infrared
J	coupling constant
L	ligand
LUMO	lowest unoccupied molecular orbital
M	generic metal
m	meta
m	multiplet (NMR)
ᴍ	molar (mol · L^{-1})
m/z	mass to charge ratio
Me	Methyl
MeCN	acetonitrile
Mes	Mesityl
MHz	megahertz
min	minutes
MS	mass spectrometry
$\tilde{v}$	wavenumber
n.d.	not determined
n-Bu	*n*-Butyl
NHC	N-heterocyclic carbene
NMR	nuclear magnetic resonance
Nu	nucleophile
ovn.	overnight
OAc	acetate
p	pentet
p	*para*
PE	petrol ether
Ph	phenyl
PMA	phosphomolybdic acid
ppm	parts per million
q	quartet (NMR)
quant.	quantitative
R	residue
rac	racemic
R$_f$	retention factor
rt / r.t.	room temperature
s	singlet (NMR)
sat.	saturated
SPhos	2-dicyclohexylphosphino-2',6'-dimethoxybiphenyl
SPS	solvent purification system
SWV	squared-wave voltammetry/voltammogram

|	
T	temperature
t	triplet (NMR)
t	time
t-Bu	*tert*-butyl
TEP	Tolman electronic parameter
THF	tetrahydrofuran
Tf	triflyl (F_3CSO_2)
TLC	thin layer chromatography
TMS	trimethylsilyl
Tol	tolyl
TPPTS	triphenylphosphine trisulfonate
Ts	tosyl
UV	ultraviolet light
X^-	generic anionic ligand
XPhos	2-dicyclohexylphosphino-2',4',6'-tris(propan-2-yl)biphenyl

Table of contents

1. Introduction

1.1 Phosphine ligands

To obtain the desired reactivity, it is often needed to alter the original catalyst. For this purpose, specific ligands are designed to modify the electronic and steric properties of the catalytic active center. In transition-metal catalysis, phosphine ligands are the most used and widespread ligands. This is due to their versatility and relative strong bonding to the metal center. Also, the phosphorus itself has a rich chemistry allowing for great varieties in structures and properties.[1,2]
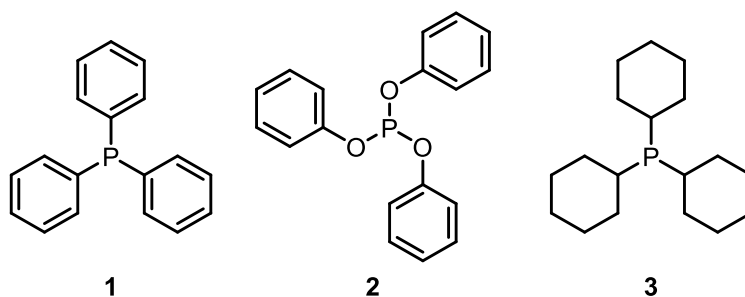
Scheme 1: structures of commonly used phosphines and phosphites.

The prime example of a phosphine ligand is triphenylphosphine **1** (PPh$_3$). Depending on the metal it coordinates to, it serves as a ligand in many different reactions. With gold as the metal, it catalyzes reactions where gold acts as a π-acid; however its probably most famous applications are as ligand with rhodium in the Wilkinson-catalyst[2,3] (**4**) and with palladium in Pd-catalyzed cross-couplings. In tetrakis-triphenylphosphine-palladium(0) (Pd(PPh$_3$)$_4$) (**5**) PPh$_3$ is only type of ligand present and the resulting complex is quite active in Suzuki-cross-coupling reactions.[4]
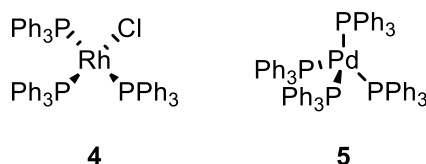
Scheme 2: structures of catalysts with phosphine as ligand.

The phenyl as a substituent for the phosphorus is an example of a mildly electron-donating substituent. If a more electron rich phosphine is needed, alkyl substituents are used, like *t*Bu or cyclohexyl (**3**). For electron poorer phosphine, fluorinated phenyls or phosphites (**2**) are normally used. To obtain even further electron deficient phosphines, the phosphorus can be directly decorated with halogens. PCl$_3$ and PF$_3$ have been used for this purpose. These molecules are however toxic and quite sensitive, so it may be advocated to look for more stable phosphines with similar reactivity.[5]

Besides the ubiquitous applications in scientific research, phosphines as ligands are also present in several industrial processes, like the Shell higher olefin process (SHOP) [6] (**6**) or the Ruhrchemie/Rhône-Poulenc oxo process (**7**).[7]
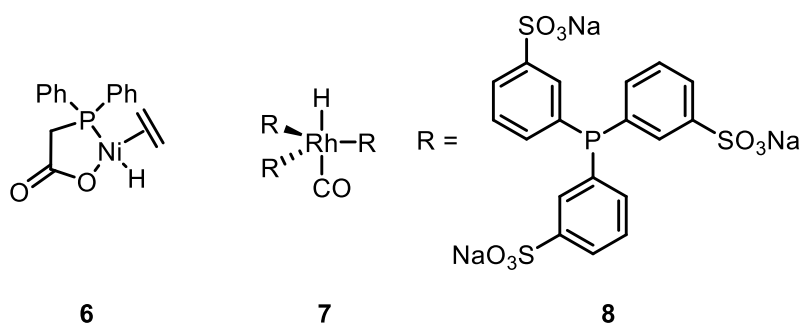
Scheme 3: Phosphine catalysts in industrial use.

The ligand of the latter one (**8**) allows for a rather decent solubility in water, again showcasing the great variety of possible phosphines.

1.2 Phospholes

Phospholes (**9**) are one of the many derivatives of phosphines. They consist of a five-membered unsaturated ring with a single phosphorus as heteroatom, so they are also a derivative of cyclopentadiene (**10**). Compared to their lighter homologue pyrrole (**11**), they show a stronger pyramidalization at the phosphorus. This indicates a greatly diminished degree of aromaticity, especially in comparison to the highly aromatic heterocycles like pyrrole and thiophene (**12**) and even the relatively weakly aromatic furane (**13**).[8]
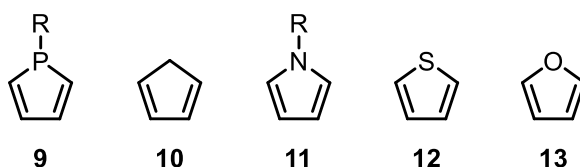
Scheme 4: Phosphole and its homologues.

Besides the aromaticity, the phosphole contains other interesting electronic properties. As the phosphorus atom refuses to hybridize and form sp-hybrid orbitals, mainly p-electrons are used to establish C-P bonds. While this is also responsible for the strong pyramidalization, it leads as well to a strong s-character of the lone pair. Since the s-like free electron-pair is unsuitable for delocalization into the π-system, phospholes as a whole exhibit only a weak aromatic character, as only the hyperconjugation between the exocyclic P-R σ-bond and the π-system contributes to the aromaticity.[8,9]

Another interesting property of phospholes is the quite low inversion barrier of the pyramidal phosphorus center.[10] The value ranges for simple phospholes, depending on the substituents, between 15 and 16.1 kcal/mol.[11] This is far lower than their saturated homologues with values around 36.5 kcal/mol and energies between 23.7 and 26.2 kcal/mol needed to invert benzene-fused phospholes, namely phosphindoles (**14**) and

dibenzophopholes (**15**). These experimental values, published in 1971 by the Mislow-group[11], are in the same range as modern theoretical calculations.[12–14] The inversion barrier can also be lowered by either introducing electro-positive substituents on the phosphorus or π-accepting substituents at the ring.[12,14] It also has been calculated that the planar transition state of the inversion is very aromatic, depicting similar values on different criteria of aromaticity as benzene or pyrrole, thus compensating the phosphorus´ instability at sp^2-like configurations.[13]
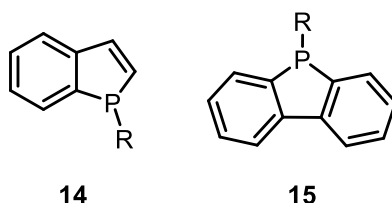
Scheme 5: Phoshindole and dibenzophosphole.

In recent years phospholes have gained much attention as ligands in catalysis, but also in material science for their unique electronic properties.[8] The first synthesis of a non-fused phosphole was described in 1959 independently by both the Hübel[15] and the Johnson groups[16] by condensation of a dichlorophosphine with an 1,4-dilithio-1,2,3,4-tetraphenylbutadiene. The first phosphole without any carbon substituents on the diene was synthesized 8 years later by Quin and Bryson. They started from an oxidized and partly saturated ring synthesized by the McCormack-reaction[17] and generated the phosphole by reduction and elimination.[18]
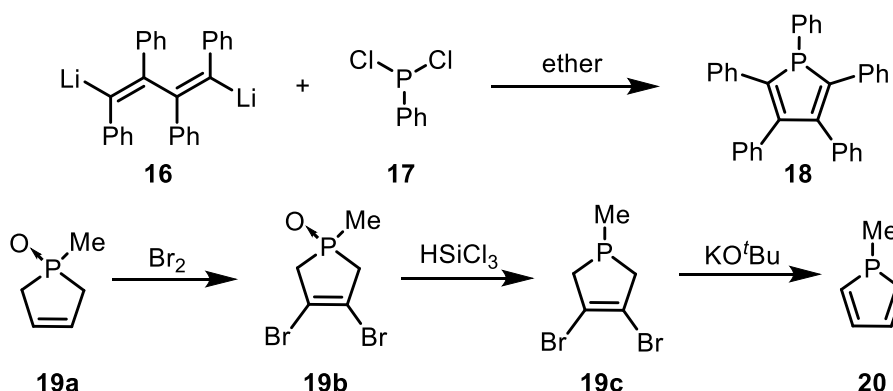
Scheme 6: Early syntheses of phospholes by Johnson (top) and Quin.

The simplest phosphole without any substituents except the hydrogen on the phosphorus was elusive until 1983, when it was first identified by the Mathey group. The phosphole **22** is very reactive, and readily undergoes hydrogen shifts (usually [1,2]) and subsequent Diels-Alder reactions when kept above -70 °C. It was synthesized by protonation of the phospholyl anion and identified by ^{31}P-NMR.[19] It was later fully characterized by NMR.[20]
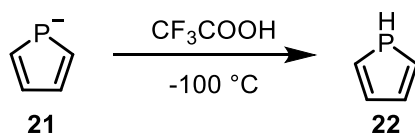
Scheme 7: Synthesis of the parent phosphole.

The phospholyl anion **21** can be prepared by synthesizing the corresponding 1-phenyl phosphole and subsequent cleavage of the P-substituent by addition of an alkali metal.[21]

Today there are several syntheses available to prepare phospholes in reasonable quantities. The two routes shown in Scheme 6 are still in use. Besides these, one can use the cycloaddition of 1,3-diynes with primary phosphines.[22] This reaction, which could also produce pyrrols if primary amines are used, is only applicable for the synthesis of 1,2,5-trisubstituted phospholes. As an advantage however, the substituents in 2- and 5-position can be quite large. This allows for example the relatively easy synthesis of chiral phosphole catalysts like **25**.[23]
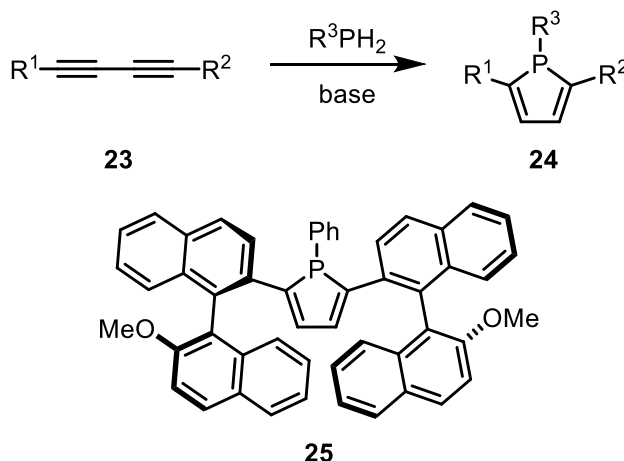
Scheme 8: Synthesis of the phospholes from diynes and an example for a chiral phosphole ligand.

An extremely versatile and efficient route towards phospholes is the one developed by Fagan and Nugent in 1988, as it can be done as a one-pot reaction.[24] In this synthesis, zirconocene dichloride **26** is reduced by *n*-BuLi in the presence of alkynes, leading to the formation of five-membered zirconium metallacycles **28**. The zirconium can then be transmetallated by addition of a dichlorophosphine yielding the corresponding phosphorus-containing ring **29**.[25] This reaction not only produces phospholes and their homologues, but also a variety of metallacycles.[24] One drawback is however the generation of stoichiometric amounts of zirconium-waste and with zirconocene dichloride the use of a relatively elaborate starting material.
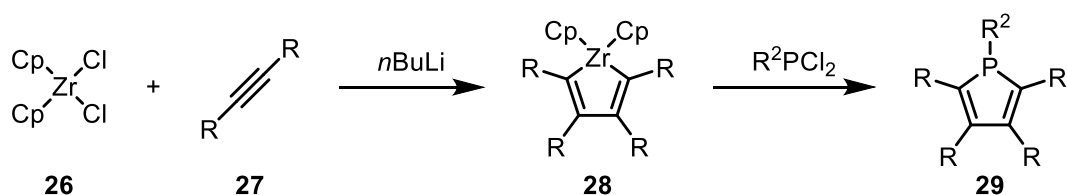
Scheme 9: Synthesis of phospholes as described by Fagan and Nugent.

Chiral phosphole-catalysts cannot only be prepared directly in the synthesis of the phospholes themselves, but also by introduction or modification of substituents, usually at the phosphorus unit. One such example is given by Hydrio *et al.* They replaced a phenyl group of the phosphole with the chiral pyrrolidine **32**, yielding the chiral phosphole **33** which could be coordinated to palladium and used chiral allylic substitutions.[26]
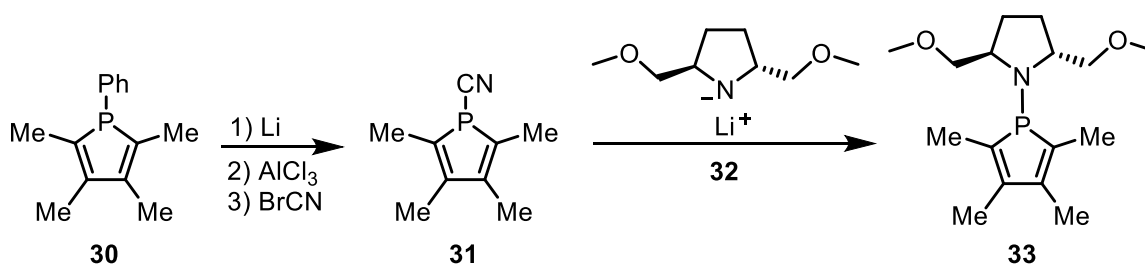
Scheme 10: Synthesis of a chiral phosphole by modification.

1.2.1 Applications of phospholes in catalysis

Though not as frequently used as their non-cyclic counterparts, phospholes have found several uses in catalysis. Due to their highly modular synthesis, it is relatively easy to prepare differently substituted phospholes. Judging by the number of total publications, the simple monophospholes are the most used among the phosphole-based ligands.[27] The electronic values are dependent on the substitution pattern. Monophospholes bearing a phenyl group on the phosphorus with alkyl-substituents on the carbon atoms (Scheme 11, **30** and **34**) are usually less π-accepting than PPh$_3$, while phospholes with aryls in these positions (**18** and **35**) are more π-accepting. The differences however are small. A stronger effect can be seen for the σ-donor properties. Phospholes with methyl groups as substituents on the carbon atoms are better σ-donors, being better than PPh$_3$ in this regard, while the phenyl-substituted phospholes are significantly weaker σ-donors.
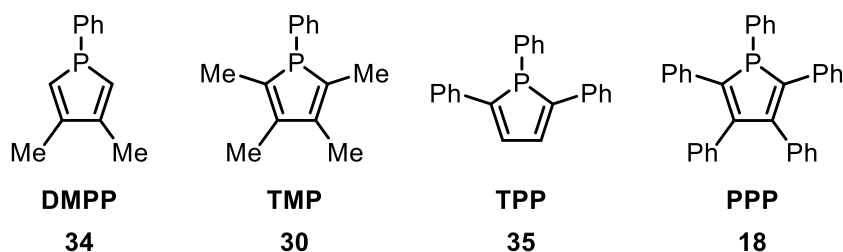
Scheme 11: Selection of standard phospholes used in catalysis and their commonly used abbreviations. DMPP: 3,4-dimethyl-1-phenylphosphole; TMP: 2,3,4,5-tetramethyl-1-phenylphosphole; TPP: 1,2,5-triphenylphosphole; PPP: pentaphenylphosphole.

As the catalytic hydrogenation with the Wilkinson-catalyst[3] is one of the prime examples for catalysis with phosphine ligands, it was one of the first examples tried using phospholes as ancillary ligands instead of the normal PPh$_3$ (Scheme 12). Attempts to use that new catalyst indicated that although reactivity could be achieved, the hydrogenation rates of the standard Wilkinson-catalyst could not be reached.[28]
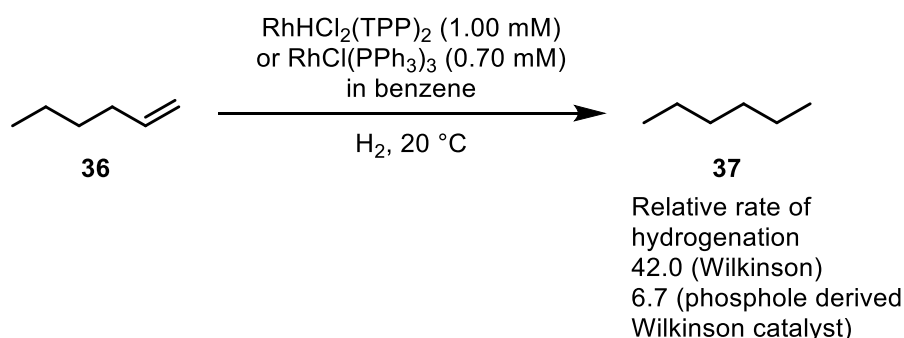
Scheme 12: Comparison of hydrogenation rates with different rhodium catalyst. The hydrogenation rate of the catalyst RhH(CO)(PPh$_3$)$_3$ (1.00 mM) was set as standard with a rate of 10.0.[28]

In the case of hydroformylations, Neibecker and Réau could show that the use of certain phospholes improves the yield and selectivity in comparison to triphenylphosphine (Scheme 13). The system they chose was the hydroformylation of 1-hexene with [Rh(CO)$_2$Cl]$_2$ as precatalyst, 20 bar of syngas (CO/H$_2$, 1:1) and triethylamine as additive at 80 °C. The ligand **35** showed 95% yield after 30 min with 80% selectivity for the linear product. With PPh$_3$ the results after the same time were 91% yield and 71% selectivity. The other tested phospholes (**34** and **18**) showed similar selectivities but considerably worse yields, 13% and 50%, respectively.[29]

6
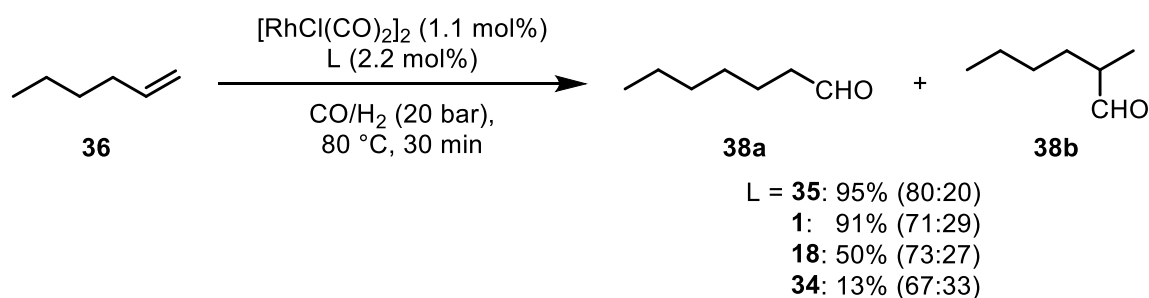
Scheme 13: Hydroformylation of 1-hexene using phospholes as ligands.

Good activity and selectivity could also be achieved with other substrates, for example styrene. Neibecker *et al.* showed that using the same condition as with hexene, but with a temperature of only 25 °C, the use of the TPP (**35**) showed a great improvement of the yield over the use of PPh3, but at a slightly worse selectivity (Scheme 14). However in contrast to the reaction with 1-hexene (**36**), the branched product is now the major one, regardless of the ligands used.[30]
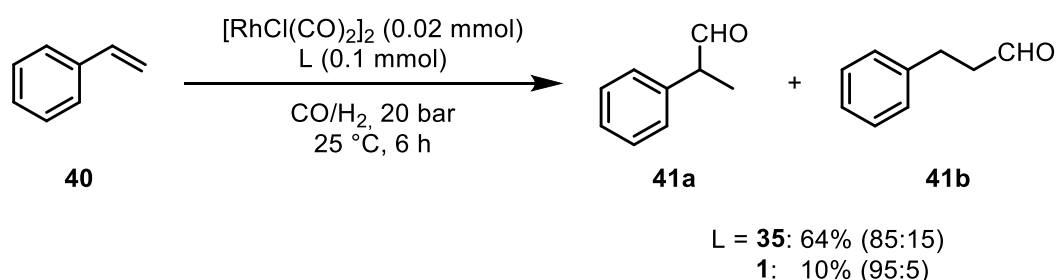
Scheme 14: Hydroformylations of styrene; comparison of phosphole and phosphine.

Phospholes also proved to be suitable ligands for Palladium-catalyzed CN-couplings. Thoumazet *et al.* tested different phosphine-ligands as well as different phospholes and benzophospholes (Scheme 15). TPP (**35**) proved to be the best ligand, outcompeting all the other in the allylation of aniline with allylic alcohol at room temperature, achieving 100% conversion in one hour.[31]
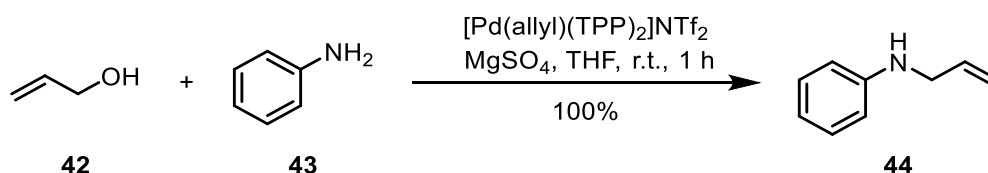
Scheme 15: Phospholes as ligands in the palladium-catalyzed allylation of aniline.

For a chiral application of phosphole ligands in catalysis, Hydrio *et al.* used **33** in the palladium catalyzed asymmetric allylic substitution (Scheme 16). At 25 °C in DCM for 1 h, the product was obtained with an *ee* of 58%. In THF the reaction was completed after 30 min, but with a slightly diminished *ee* of 55%. The authors gave no yield for specific ligands, only reporting a general yield of 93% for this reaction.[26]
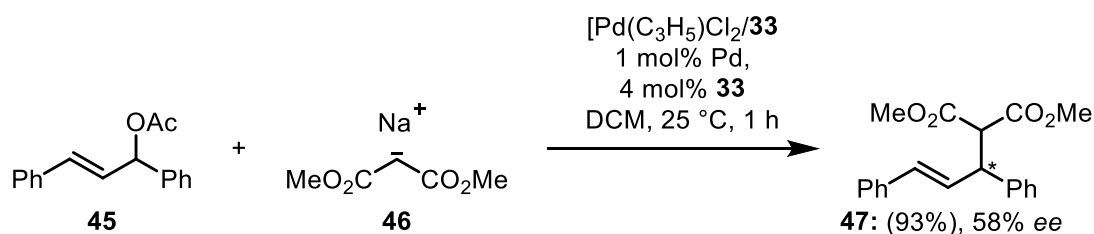
Scheme 16: Asymmetric allylic substitution with a Pd-phosphole complex.

Another reaction where phospholes proved to be good ligands is the Au- or Pt-catalyzed activation of multiple bonds. As these reactions will be a central point of the experimental part of this thesis, they will be explained in more detail below.

1.3 π-acid catalysis

Gilbert N. Lewis proposed the concept that molecules having a reactive vacant atomic orbital or an unoccupied molecular orbital of low energy, should be considered "Lewis acids".[32] Cationic metals or metal complexes have these characteristics, as they are able to accept electron density because of their LUMOs (lowest unoccupied molecular orbital) lying at relative low energies. To clarify the reactivity of these acids, the HSAB (hard and soft acids and bases) concept developed by Ralph G. Pearson can be used.[33] The concept suggests that hard Lewis acids favor the reaction with hard Lewis bases and soft acids with soft bases. Although many exceptions to this concept are known and no quantification of reactivity is provided, its usefulness comes from its ability to predict the inherent reactivity in many cases.[34]

In contrast to many other transition metals, the bond strengths between Au or Pt and C are in a favorable range for catalysis. Mercury for example would activate the multiple bond stronger than Pt or Au could, the Hg-C bond however is kinetically stable and much harder to break than the Au-C oder Pt-C bond. Therefore the proto-demetallation cannot happen easily and a catalytic cycle is not achieved but a stoichiometric reaction generating mercury waste.[35] The LPt or LAu-complex also manages to activate the olefin or alkyne towards nucleophilic additions, but as the Au-C and Pt-C- bonds are kinetically labile the bond can often be cleaved in rather mild reaction conditions ensuring catalytic activity.[35] As in this thesis only Au^I-catalysis will be performed, the focus will lie on explaining the special example of Au-π-acid catalysis and the platinum variant will be neglected.

The gold complexes activate multiple bonds by a variety of orbital interactions. Figure 1 shows the most possible interaction between an alkyne and gold, according to quantitative analyses by means of high-level computational methods. From the four main orbital interactions, the σ-donation from alkyne ligand to the metal contributes 65% of the total orbital term, followed by the in-plane π-back-donation with 27%. The other two interactions, the orthogonal π-donation (7%) and the δ-symmetric back-donation (1%) contribute only a small part to the total orbital term. [35]
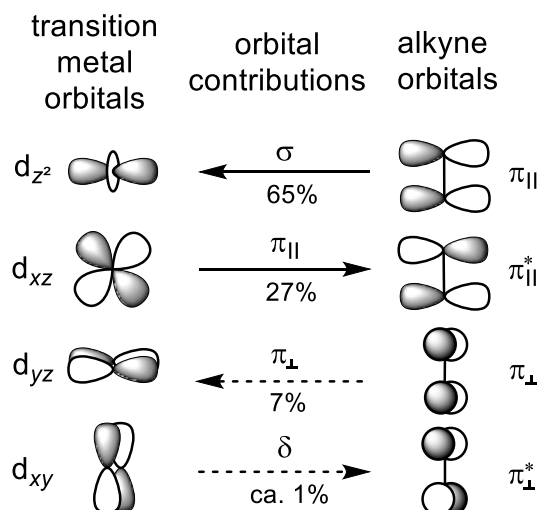
Figure 1: Interaction between transition metals and alkynes and their respective orbital contributions. Adapted from A. Fürstner, P. W. Davies, *Angew. Chem. Int. Ed.* **2007**, *46*, 3410.[35]

In the transition-metal (mainly Au and Pt) catalyzed activation of multiple bonds, the first step is usually the activation of the metal by abstraction of a ligand, mostly as a halide (Scheme 17, **I**). The now cationic metal complex coordinates the multiple bond side-on (**II**) which then turn into a proper π–complex (**III**). The metal can slip on one of the carbons, opening up the other to a nucleophilic attack (**IV**-**V**). The selectivity of this step can be influenced by tuning the substituents on the alkene or alkyne as well as the ligands of the metal center. After this reaction, the metal is now σ-bonded with the carbon (**VI**) and can proto-demetalate to release the desired product and reform the active catalyst.[36]

As already stated, the two most active metals in the catalyzed activation of multiple bonds are Au and Pt. Au hereby has a tendency for a coordination number of two, particular in complexes with phosphanes. Higher coordination numbers are also known, especially for gold in higher oxidation states, but not as frequently encountered. Platinum is more versatile, sporting frequently the coordination numbers two and four.[36]
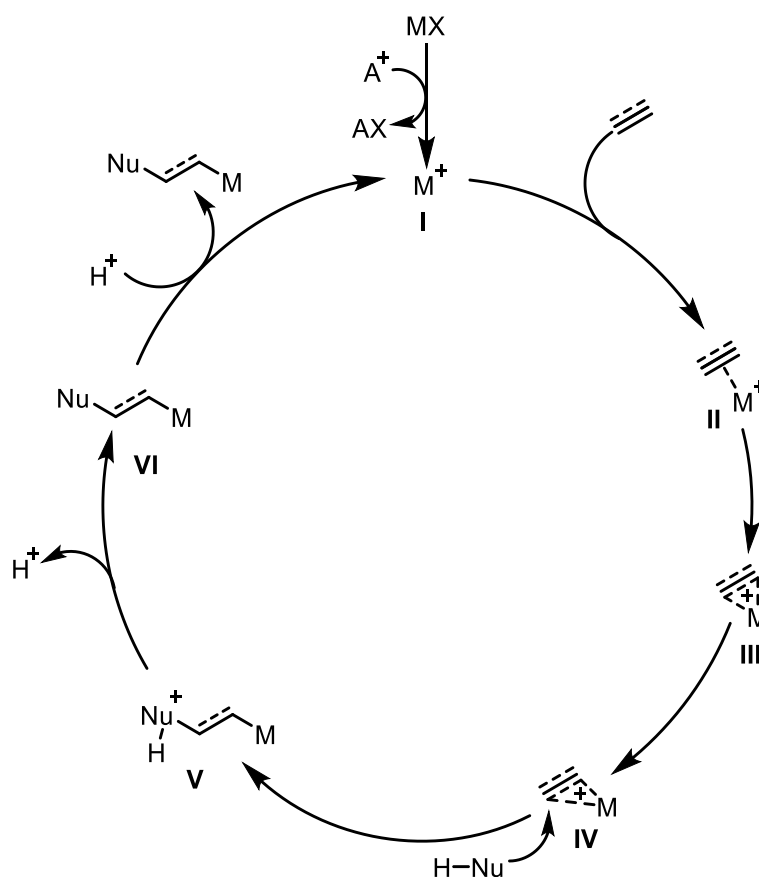
Scheme 17: General catalytic cycle for the activation of multiple bonds by transition metals as proposed by Fürstner.[36]

The Fürstner group was also able to support parts of the proposed catalytic cycle with some experiments. They could crystallize and analyze by X-ray crystallography an alkyne, in this case cyclododecyne and its respective gold complex (Scheme 18). The molecular structure shows the gold coordinating carbons C1 and C2 almost equally and being at a shorter distance to the center of the C1/C2-bond than any individual carbon atom, thus strongly supporting the existence of the intermediate **III** in scheme 13.[37]
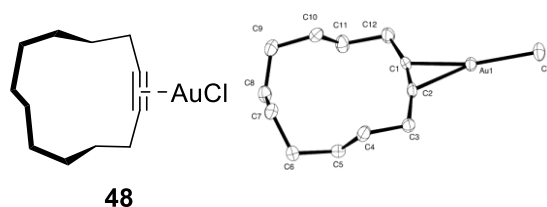
Scheme 18: Cyclododecyne gold chloride complex as formula and X-ray structure. Right figure taken out of: S. Flügge, A. Anoop, R. Goddard, W. Thiel, A. Fürstner, Chem. Eur. J. **2009**, *15*, 8558–8565.

Besides giving evidence for the catalytic cycle, the results of the experiment also shows nicely the bonding concepts shown in figure 1, as the π-back-donation from the gold to the alkyne weakens the alkyne bond and increases the C1-C2 distance from 1.196(4) Å (free cyclododecyne) to 1.224(5) Å in the metal complex. For the same reason, the C3-C2/C1-C12 angle get smaller from 175.9(9)° for the free alkyne to 165(1)° in the complex, straying away even further from the theoretical linear geometry.

1.3.1 Gold catalysis

Gold catalysis is a rather new field in chemistry as most catalytic cycles involve the change of redox-states, something that gold is reluctant to do. This was seen as a disadvantage at first, but later recognized as a possibility to open up new reaction pathways. The first examples involved the use of simple metal salts, like $AuCl_3$. The redox-inactivity made in some cases simple reaction setups possible, as inert conditions were not always needed, in contrast to many other transition metal catalyzed reactions.[34,38]

In gold catalysis the first step is the coordination of the substrate to the electron poor metal center. The active metal center is usually positively charged and bears at least one ligand. The positive charge is generated by abstracting a halide from the precursor and is usually done with a silver salt. In this step a counter ion is introduced to the complex. This counter ion should be weakly coordinating so the vacant coordination site on the metal is not blocked. Examples for these weakly coordinating anions are BF_4^-, SbF_6^- or NTf_2^-. The position of the attack on the gold can be influenced by electronic and steric factors. In accordance to the HSAB-concept gold in a higher oxidation state is considered harder and thus will likely activate harder donor sites. This makes them a valid option to activate hetero-elements.[35,36] As the metal complexes are quite polar, weakly donating polar solvents like dichloromethane are normally used as a reaction medium.

Besides the activation of hetero-elements, Au^I and Au^{III} differ in their ability to backdonate π-electron density to an alkyne, with Au^I being able to do this to a much larger extent. For this reason an alkyne activated by a Au^{III} will in most cases directly undergo an nucleophilic attack, while the Au^I may form a vinylidene intermediate (Scheme 19). As forming this intermediate involves a [1,2]-shift, usually of a hydride or halide, this may lead to a different regioisomeric outcome when compared to Au^{III}.
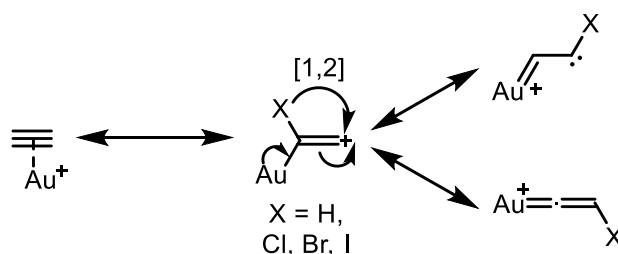
**Scheme 19:** Activation of alkyne by gold with possible vinylidene intermediates.

Gold catalysts are useful synthetic tools, as they show interesting new reactivities like strong activation of multiple bonds. They also tend to be more stable than other transition metals towards oxygen and moisture. They also show a strong affinity for π-systems, thus tolerating a variety of other functional groups in the reactants.[36,38]

1.3.2 Applications of gold catalysis

The role gold takes up often in a catalytic reaction is the activation of C-C multiple bonds or π-systems in general. The activated bonds then become a prime target for a nucleophilic attack, which usually leads to an 1,2-adduct. The first example in this regard was published by Fukuda *et al.* in 1987 (Scheme 20). While performing intramolecular hydroaminations with Pd[II] the authors were faced with unsatisfying yields and found Au[III] to be very effective in this reaction, producing high yields under mild conditions.[39]
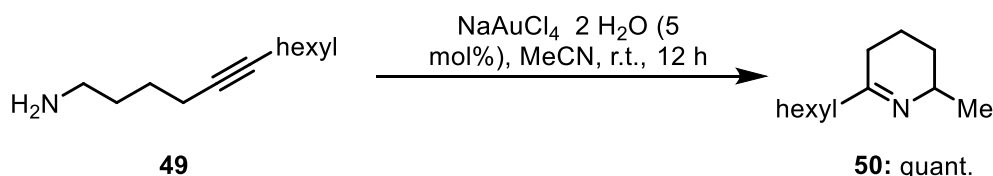
Scheme 20: First example of a gold-catalyzed hydroamination.

This founding sparked a new field of transition-metal chemistry which was heavily explored in the following years. Further examples for gold-catalyzed hydroaminations by Zhang *et al.* and Han *et al.* are shown in Scheme 21. In both the intra- and intermolecular reactions high yields and chemoselectivity could be achieved.[40]
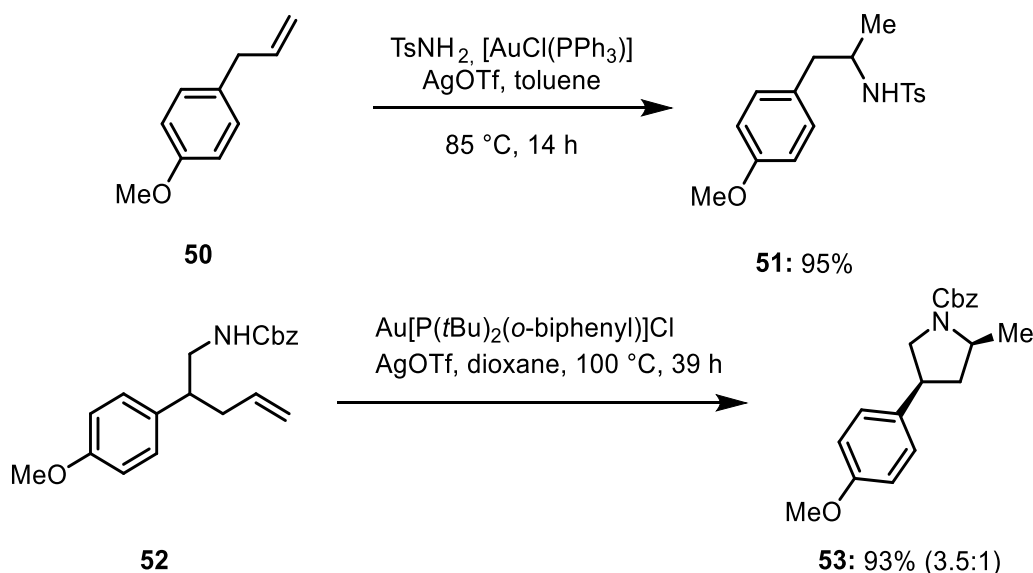
Scheme 21: Gold-catalyzed hydroaminations by Zhang *et al.* (top) and Han *et al.* (bottom).

Another interesting example was shown by the Gevorgyan group. Depending on the oxidation state of the gold catalyst chosen, different products can be obtained (Scheme 22).[41] The resulting regioselectivity can be explained with the HSAB-concept. The hard Au[III] activates the harder oxygen while the softer Au[I] activates the softer double bond. During the reaction with Au[III] a bromonium ion (Scheme 22, **I**) is formed, leading the different regioisomeric outcome.
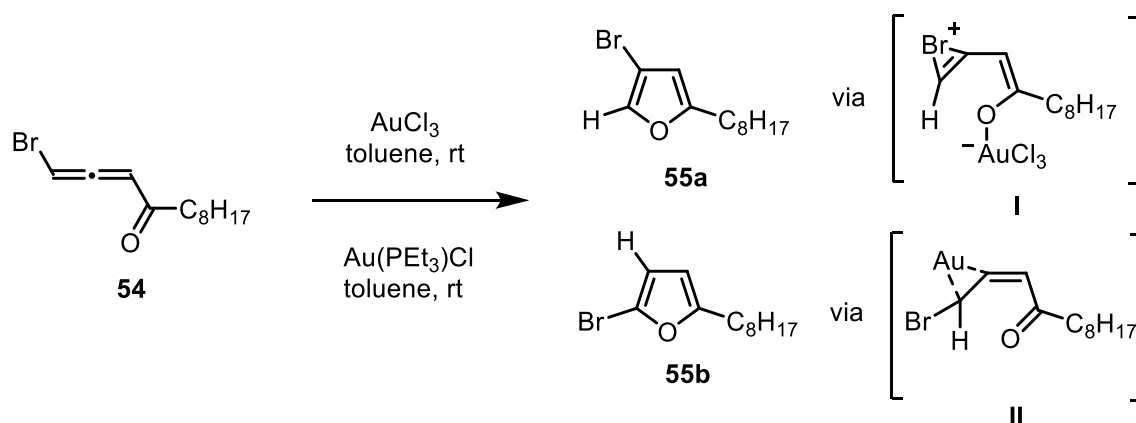
Scheme 22: Different selectivities of gold-catalyzed hydroaminations caused by different oxidation states of the metal.

A reaction which exemplifies the concept described in Scheme 19 was published by the Fürstner group (Scheme 23). During the hydroarylation of *ortho*-alkynylated biphenyls, the position of the substituent is different for Au[III] and Au[I]. When Au[III] is used, the direct hydroarylation happens, but with Au[I], the substituent undergoes a [1,2]-shift when the Au-vinylidene complex is formed, leading to different product.[42]
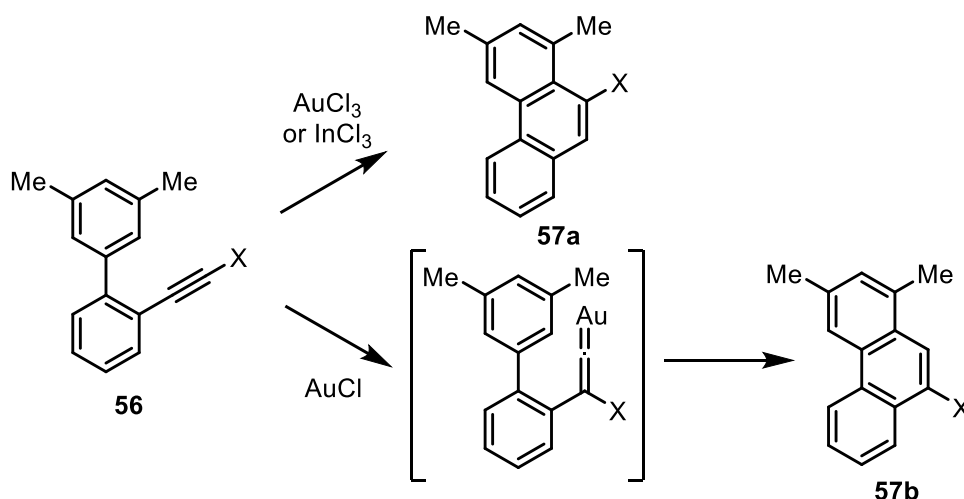
Scheme 23: Different regioisomers in the synthesis of phenantrenes, depending on the oxidation state of Au.

The relatively robust nature of gold catalysts also allows less inert reaction media resulting in additional reactivity. The Echavarren group performed a cyclization in methanol, resulting in a methoxycyclisation (Scheme 24).[43] Using the same starting material the Gagosz group showed that with a phosphole like **35** as a ligand the reaction proceeds satisfactorily as well. With an even lower loading of 1 mol% they were able to obtain the product with an even higher yield of 96%. It should be noted however that the reaction took with 75 minutes considerably longer. They also prepared the catalyst beforehand and not *in situ* like Echavarren, resulting in an additional step being needed.[44]

Scheme 24: Gold-catalyzed methoxycyclisation by the Echavarren group.

During recent years, much research has been conducted to try to overcome some of the shortcomings of Au catalysis. One of them being that usually an activating agent is needed to abstract the chloride from the gold, a role usually played by a silver salt added equimolarly to the gold catalyst. One of the possible solutions has recently been presented by the Gabbaï[45] and subsequently the Echavarren[46] groups. They introduced a functional group capable of being an H-bond donor (for example an amide) in close proximity to the chloride. They propose that during the catalytic cycle, the H-bond donor temporarily abstracts the chloride, allowing the resulting cationic gold center to catalyze the reaction.[46] The main difference between the two groups is the number of H-bond donors. While the Gabbaï group only employs one, the Echavarren group uses two, with the approach of Echavarren providing far superior results on the same substrate (Scheme 25).
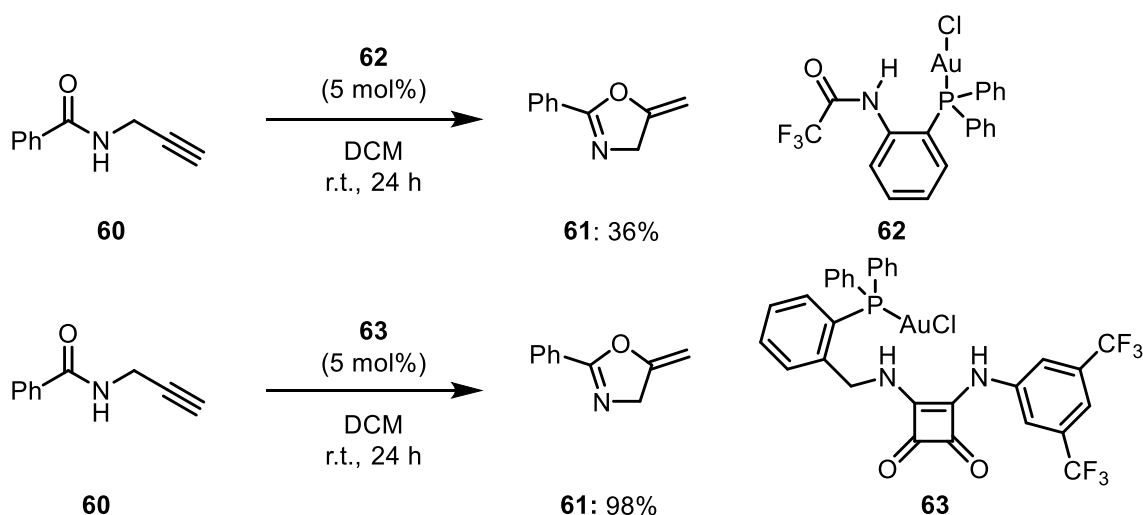
Scheme 25: Silver free gold catalyzed cycloisomerization of amindes into oxazolines by Gabbai (top) and Echavarren.

Differences in selectivity can not only be achieved by having catalysts in different oxidation states like Au[I] and Au[III], but also by modulating the electronic properties of a metal via its ligand without changing the oxidation state. An example of this can be in the [4+2] and [4+3] cycloadditions of allene-dienes performed by the Toste-group. When they used PPh$_3$ as a ligand, they were getting a 2:1 mixture between the [4+2] and [4+3] product. The use of di-*tert*-butybiphenylphosphine, a better σ-donor-ligand increased the proportion of the [4+3] product massively, leading to a 4:96 ratio. Going in the other direction, the use of

triphenylphosphite provided the same yield as the biphenylphosphine but was completely selective for the [4+2]-product (Scheme 26).[47]
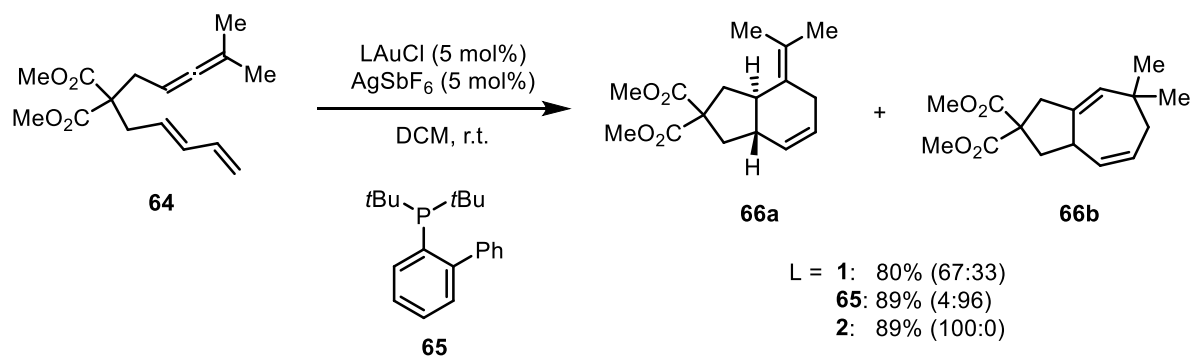
Scheme 26: Selectivity of [4+3] and [4+2] cycloadditions.

The Mascareñas group found the same connection between selectivity of the [4+3] and [4+2] cycloaddition and the electronic properties of the ligand for a similar substrate.[48] Interestingly, both groups could show with DFT calculations that the transition state for both final [4+2] and [4+3] products is identical. After the initial [4+3] cycloaddition, either a 1,2-hydrogen or 1,2-alky-shift lead to the final products (Scheme 27).[48,49]
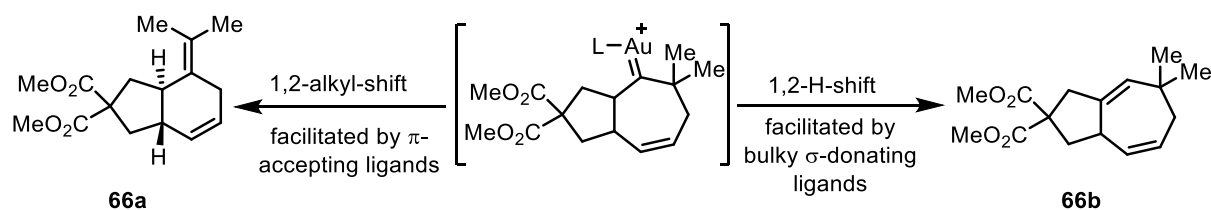
Scheme 27: Transition state and final products of [4+3] and [4+2] cycloadditions.

The effect of changing ligands for a specific reaction is in most cases not a change in selectivity, but just a change in the speed of the reaction. This can be caused by either steric or electronic factors, with the electronic factors often being easier to measure and predict. One way of showing the influence of the electronic factors is by making a Hammett plot.[50] To make a Hammett plot, a reaction is repeated multiple times under the exact same conditions, with the only variable changed being the ligand. The ligand should also have no structural differences besides the one substituent responsible for the change in the electronic properties. For this reason, the most common practice is to compare triaryl-phosphines, with the changing substituent being in the *para*-position, thus reducing the steric impact of the different substituents on the active center as much as possible. The different reaction rates are then plotted against σ, a constant roughly reflecting the electron-donating or withdrawing qualities of the substituent. Hydrogen is set as 0 on this scale, while usually electron withdrawing get positive and electron donation substituents negative values. The Toste group did a Hammett plot of a gold catalyzed hydroamination where they tested different arylphosphines (Scheme 28).[51]

$$y = 0.2236x - 0.0206$$
$$R^2 = 0.9572$$
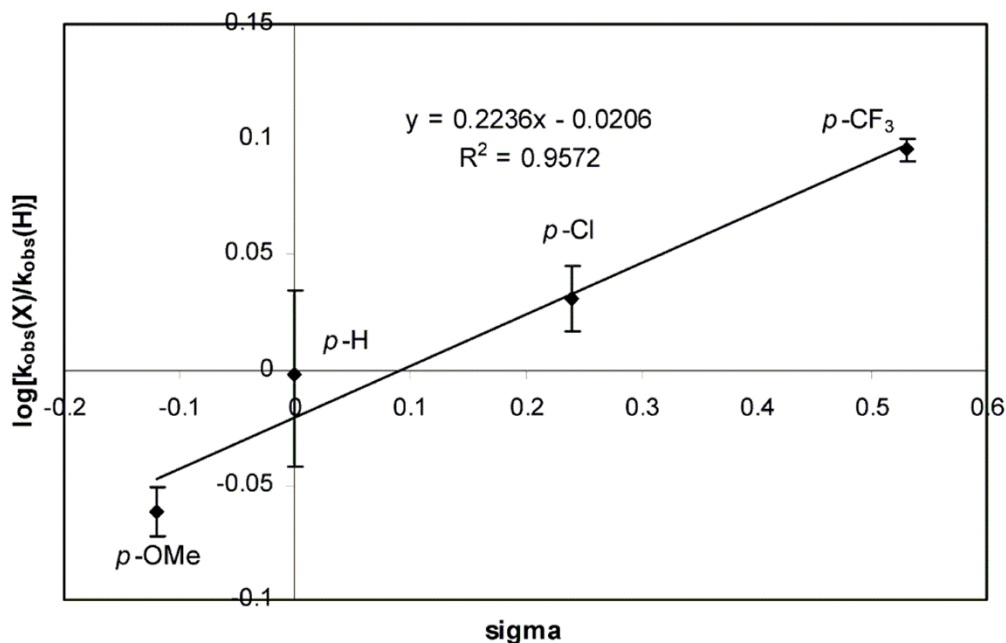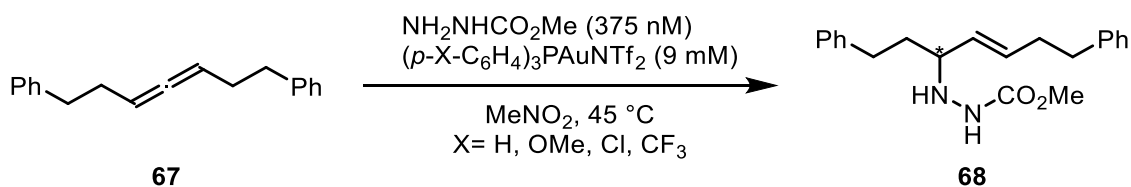
Scheme 28: Hammett-plot for gold-catalyzed hydroamination. Figure taken out of Wang *et al.*, *J. Am. Chem. Soc.* **2010**, *132*, 13064-13071.

The graph clearly shows an increase in the reaction rate for more electron withdrawing substituents. The reason lies in the rate determining step. For this reaction it was proposed to be the activation towards the nucleophilic attack, which is stronger if more electron withdrawing substituents are used. If the rate determining step would involve a transition state where an electron richer metal center would be preferable, the slope of the Hammett plot would be negative.

As the last two examples have shown, for reasons of selectivity and reactivity, electron poor phosphines are highly interesting. For this reason, our group has focused on the synthesis of extremely electron poor phosphines – by introduction of a positive charge in α-position to the phosphorus.

1.4 Cationic phosphines

In transition-metal catalysis, phosphines are among the most used ligands. Their properties can be easily altered and modulated by choosing the appropriate substituents. On their own, phosphines are weak σ-donors and good π-acceptors. The σ-donor qualities stem from the donation of electron density from the lone pair of the phosphorus (sp^3-hybridized but with very strong s-character) into an empty d-orbital of the metal. Responsible for the π-acceptor capabilities is the backdonation from filled d-orbitals of the metal into empty σ^*-orbitals of the phosphorus-substituent bond (Figure 2).
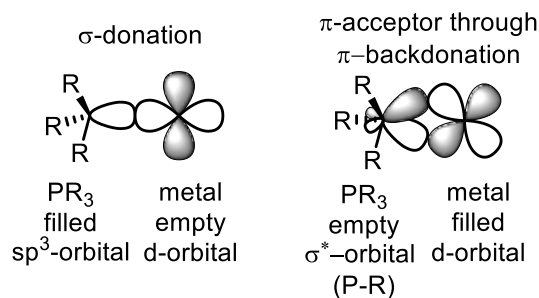
Figure 2: Orbital interactions between phosphines and metals, resulting in σ-donation and π-acceptance.

Most substituents on the phosphines are neutral because this allows easier coordination to lewis acidic metals. Phosphine ligands with cationic or anionic substituents are also known. However, often these charges are located at remote positions and not near the active center. Hence, the charged ligands are usually not used to directly influence the reactivity of the metal center, but to alter the physical properties of the whole complex. The desired effects could include higher solubility in polar solvents. For example the incorporation of sulfonates in compound **69** makes it more soluble in water,[52] while the ammonium rest in **70**[53] immobilizes the catalyst in the more polar aqueous phase (Figure 3). However, if the charge is introduced closer to the active center, for example in α-position, the electronic properties of the ligand are clearly influenced. This approach has opened up interesting new reactivities and lead to acceleration of already known reactions.[5,54]
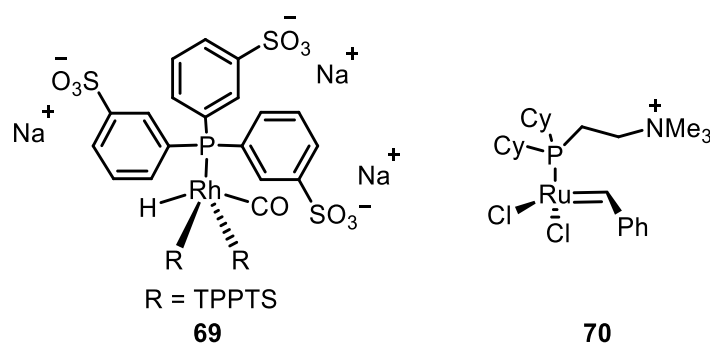
Figure 3: Ionic phosphines in metal complexes.

If the rate determining step of the catalytic reaction is the nucleophilic attack, then an electron poorer metal center is often beneficial. In phosphines this can be achieved by addition of electron-withdrawing groups to the phosphorus substituents. Examples from the literature are perfluorinated phenyl groups, in contrast to the normal carbohydrates like phenyl or cyclohexyl or by introducing heteroatoms, like in phosphites or phosphonites. It is also possible to use directly halogenated phosphines like PCl_3 or PF_3, but these compounds are hazardous gases which means higher security measures have to be established.

An alternative way of achieving the goal of electron-poor phosphines was accomplished by the Alcarazo group with the use of α-cationic phosphines.[54] The use of cationic or in general electron withdrawing substituents on the phosphorus enhances the inherent properties of phosphines: they become worse σ-donors and better π-acceptors as both the LUMO and the HOMO are lowered in energy (Figure 4). The lower energy makes it harder to transfer electron density out of the HOMO, lowering the σ-donor qualities, while lowering the LUMO makes it easier to accept electron density, resulting in a better π-acceptor. Responsible for the σ-donor properties is the non-shared electron pair of the phosphorus and the σ^*(P-C) orbital is the prime target for accepting π-electron density.[54]
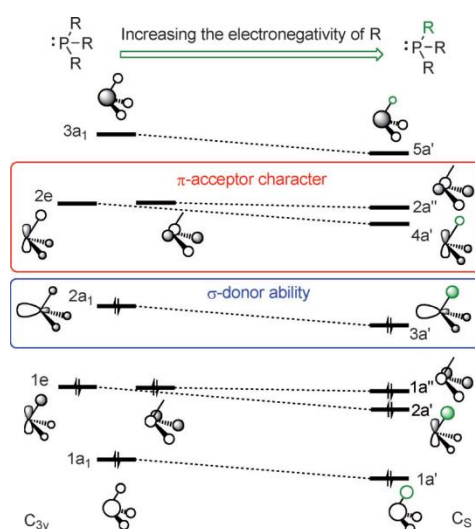
Figure 4: Effect of increasing electron-deficient substituent on the phosphorous. The y-axis shows qualitatively the energy. Figure taken out of *Chem. Eur. J.* **2014**, *20*, 7868-7877.

To measure how much the HOMO and LUMO are actually lowered by the introduction of a positive charge, the energies of theses orbitals can be determined by DFT-calculations (Figure 5). The calculations show indeed a strong decrease in both the HOMO and LUMO energy levels when a charge is introduced. When compared to the neutral phosphine PPh_3 (LUMO: -1.13 eV, HOMO: -5.28 eV) as a reference the LUMOs of the cationic phosphines are between 3 eV (cyclopropenium: -4.10 eV) and 5 eV (simple pyridinium: -6.07 eV) lower in energy. This rather large spread of the LUMO-energies of the different cationic phosphines shows also that the LUMO-energies are highly dependent on the respective nature of the cationic substituent and not only on the introduction of a positive charge. In contrast, the HOMO-energies are less susceptible to the exact structure of the substituent and are in a range between -9.05 eV (cyclopropenium) and -9.85 eV (CF_3-pyridinium). This is roughly 4 eV less than the HOMO of PPh_3. This also means that the HOMO- and LUMO-energies for cationic phosphines do only correspond to one another in their tendencies, but not in their exact values as the spread in the energy levels is much larger for the LUMO than the HOMO.[5]

Figure 5: Calculated HOMO and LUMO energies for several cationic phosphines and comparison with PPh₃. Figure taken out of: *Acc. Chem. Res.* **2016**, *49*, 1797-1805.

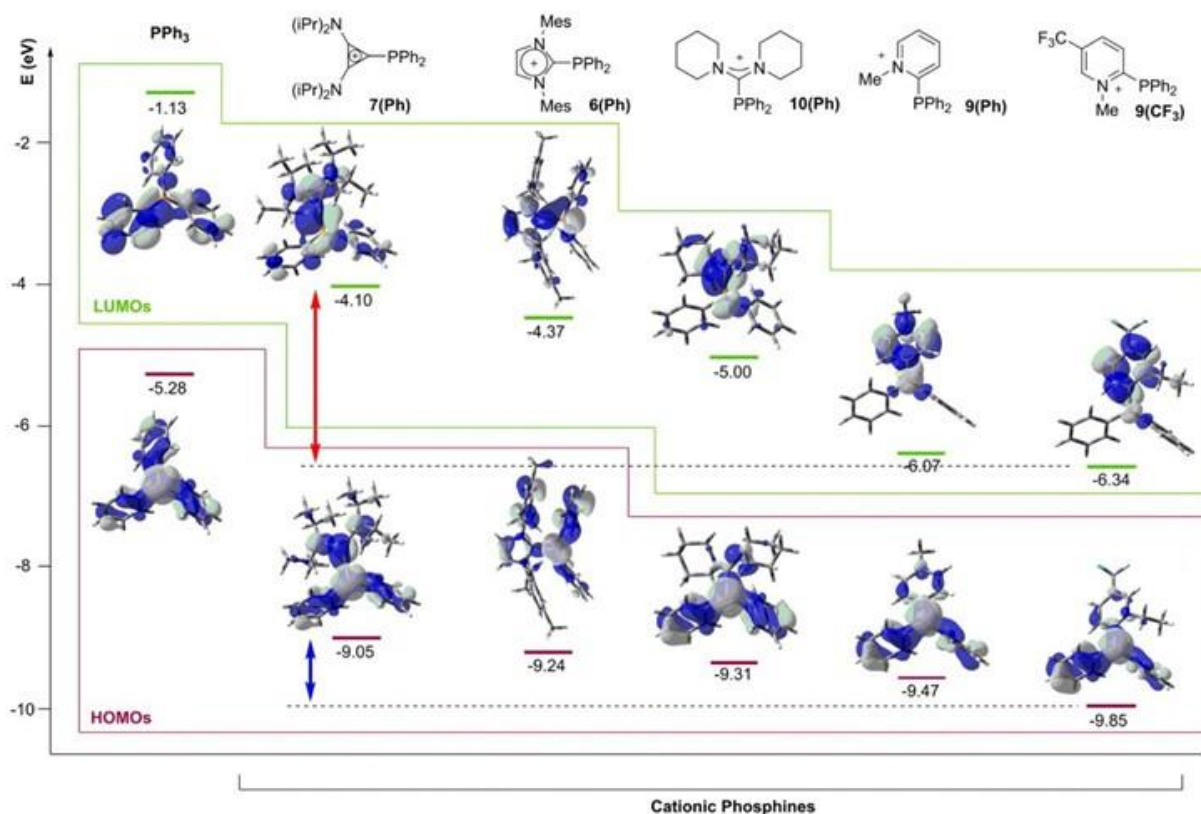With α-cationic phosphines, the electronic properties of halogenated phosphines like PCl_3 or $P(CF_3)_3$ can be mimicked, without working with highly toxic and sensitive gases.[55] The higher π-acidity of the metal has multiple effects on the catalysis: the coordination of electron rich substrates is easier and the speed of the nucleophilic attack is enhanced. Also, if redox-steps are involved in the catalytic cycle, the reductive elimination is faster. As a downside, the weaker σ-donation cannot be compensated by the better π-back donation from the metal, so the metal-ligand bond gets weaker. This makes the complexes more vulnerable towards decomposition by higher temperatures as well as moisture and air. Also, because of their positive charge, these complexes become extremely polar, which limits the scale of usable solvents. In most cases, halogenated solvents like DCM or fluorobenzene have to be used. When the phosphine has multiple cationic groups as substituents, this gets even worse and it may be necessary to work in high dilutions.[5]

To get a measure for the electronic properties of the phosphine ligands, Tolman introduced the measurement of stretching frequencies in metal-CO complexes.[56] He started by measuring complexes of the general formula [Ni(CO)₃L]. By comparison of the stretching frequencies with free CO (2143 cm⁻¹), the electronic properties of the ligand L can be estimated. The reason for this is the π-backbonding in the metal complex, where electron density is transferred to the ligand. In case of the carbonyl-ligands, this strengthens the metal-carbon bond, but also populates the anti-bonding π*-orbital in the CO, thereby lessening the strength of the carbon-oxygen bond in the CO (Figure 6). A weaker CO-bond

19

results in a lower CO-stretching frequency. The stretching frequency of the CO is now also indirectly affected by the other ligand introduced. If the ligand is π-donating, it increases the π-electron density on the metal, leading to even more π-backbonding to the CO-ligands, which lowers their stretching frequency even more. On the other hand, if the ligand is π-accepting, it competes with the CO-ligands for the π-electron density transferred by the metal via π-backbonding. This results in less electron density in the π^*-orbital of the CO, thereby the stretching frequency is lowered less and has a value closer to the one exhibited by the free CO.
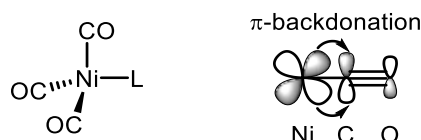

Figure 6: Nickel complex and π-backbonding to the CO-ligand.

The drawback of this scale to evaluate donor properties is the high toxicity of $Ni(CO)_4$, the starting material. Therefore it has been widely replaced by complexes like $[RhCl(CO)L_2]$ for monodentate or $[Mo(CO)_4L]$ for bidentate ligands. The use of the rhodium scale has a drawback as well: for ligands resulting in a square planar structure, it may deviate from a square planar coordination geometry if the ligands are too sterically demanding. If the geometry is disturbed the orbital overlap might be artificially reduced. This leads to changes in the strength of the π-backbonding to the CO caused by other factors than pure electronic properties and therefore to inaccuracies. If compared with the experimental values, calculated Tolman electronic parameters (TEPs) show similar results for the same compounds. So it may be a viable strategy to calculate the TEPs, if the experimental values cannot be obtained.[5]

Figure 7 shows an exemplary selection of phosphines in a Tolman map. This map plots the TEP in wavenumbers against the Tolman angle, an indicator for the steric bulk. On the scale of the TEP, the lowest values show the N-heterocyclic carbenes (NHC) with values around 2050 cm^{-1}. The phosphines (orange) occupy a wide range in the graph, ranging from 2070 cm^{-1} with alkyl-substituents to 2110 cm^{-1} with fluor as substituents. The phosphites lie between the alkyl- and halogen-substituted phosphines. The monocationic phosphines occupy an area between 2080 and 2100 cm^{-1}. The di- and tricationic phosphines have even higher TEP-values, reaching similar values as fluorinated phosphines and arsines.
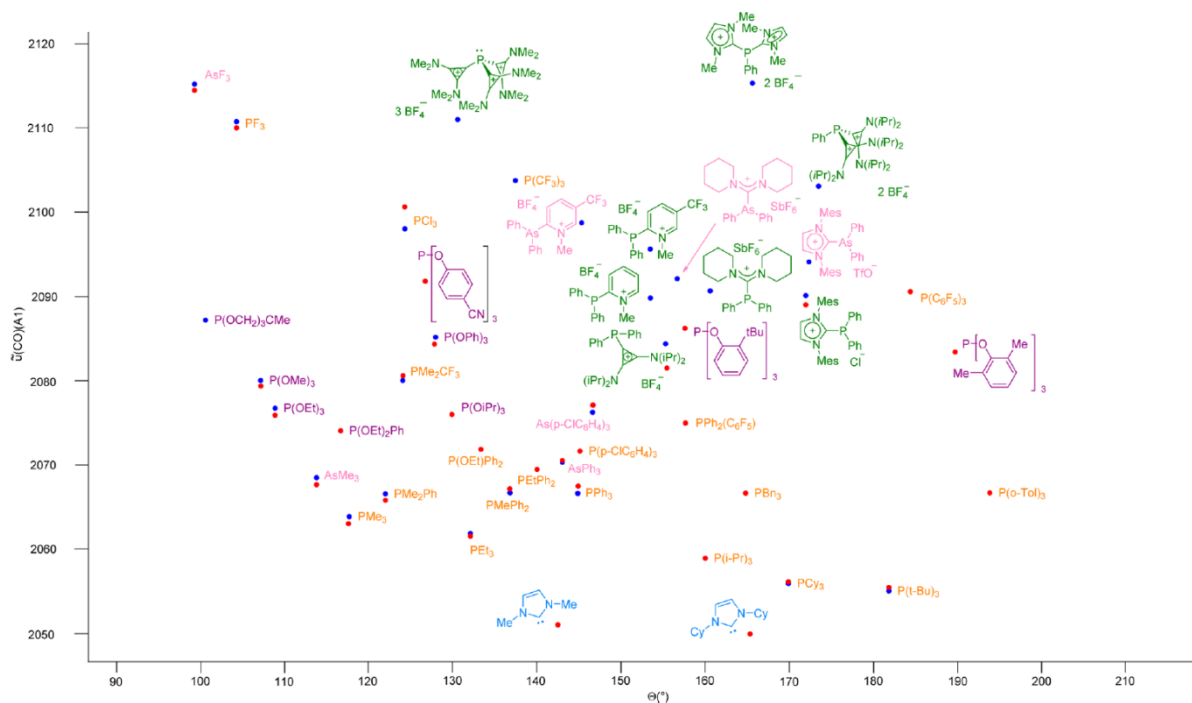
Figure 7: Tolman map including cationic phosphines and arsines. Taken out of *Acc. Chem. Res.* **2016**, *49*, 1797-1805. The phosphines are orange, phosphites violet, cationic phophines green, NHCs blue and arsines light pink. The red points show the experimental and the blue points the calculated values.

Besides the electronic value, Tolman also introduced a steric parameter in his map, the (Tolman) cone angle, the solid angle occupied by the respective ligand. The angle is determined by a point at 2.28 Å away from the phosphorus, mimicking the coordinating metal as the vertex and the van der Waals radii of the two outmost ligand atoms. This simple method is only applicable if the ligand follows the general formula PR_3. If the rests are not equivalent the half-angle of each substituent is measured independently. Then the three half-angles are averaged and the result doubled to estimate the cone angle (Figure 8).[56] The cone angle of the ligand has been shown to have a great effect on the stability of a metal complex and on the rate at which ligands are exchanged as well.[57]
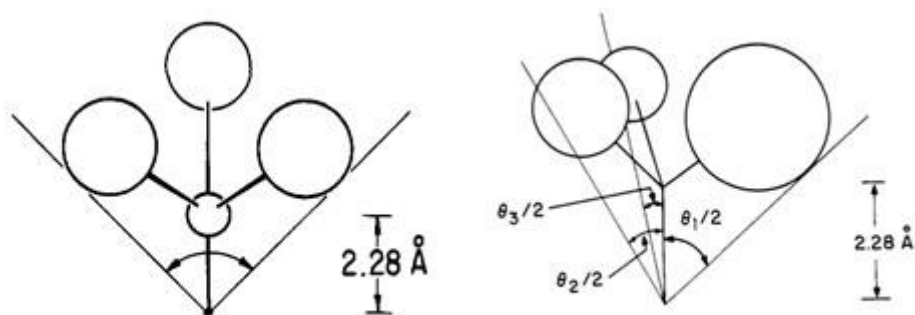

Figure 8: Determination of the Tolman cone angle for symmetrically (left) and unsymmetrically substituted phosphines. Figures taken out of: C.A. Tolman, *Chem. Rev.* **1977**, *77*, 313-348.

Another way to measure the electronic properties of cationic phosphines is to oxidize the phosphorus with selenium and measure the coupling constant between ^{31}P and ^{77}Se

(Scheme 29). The coupling constant of the resulting doublet is directly related to the charge distribution, as it becomes higher the more electronically depleted the phosphorus center is.[58] It has been shown however, that steric effects can also affect the coupling constants. Pinell *et. al.* measured the P-Se coupling constants of SeP(o-tolyl)$_3$, SeP(m-tolyl)$_3$ and SeP(p-tolyl)$_3$. In theory, all three selenophosphines should give similar coupling constants, as their electronic properties should be alike. The experiment showed indeed only a small deviation between SeP(m-tolyl)$_3$ with 726.3 Hz and SeP(p-tolyl)$_3$ with 723.5 Hz, but the sterically more demanding SeP(o-tolyl)$_3$ had a value of only 708.0 Hz. The difference caused by the steric effect between o and m/p (average at 724.9 Hz) is with roughly 17 Hz even higher than between SeP(p-tolyl)$_3$ and SePPh$_3$ (735.3 Hz, Δ = 11.8 Hz) or SeP(p-anisyl)$_3$ (719.3 Hz, Δ = 4.2 Hz) where the electronic effects should be dominant.
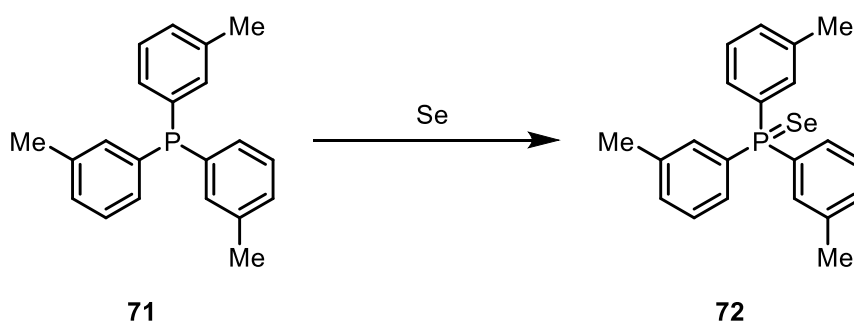
Scheme 29: Schematic oxidation of P(m-tolyl)$_3$ with selenium as oxidant.

From the experimental point of view, small obstacles could arise from the low abundance of the NMR-active isotope ^{77}Se with only 7.6%, which may lead to a poor signal-to-noise ratio. Also, selenium is not as good an oxidant as for example oxygen. The phosphorus in cationic phosphines is already quite electron poor and harsh reaction conditions may be needed to achieve the oxidation.

The last method often used to determine the electronical properties of phosphines is cyclic voltammetry (CV), where a changing potential is applied to the system and the corresponding current is measured. The strength of the potential is applied in a cyclic fashion, hence the name. If the potential reaches a point where either an oxidation or a reduction happens, the current changes which then can be clearly seen in the cyclic voltammogram (Figure 9). If the tested ligand has no easily to oxidize or reduce functional groups, the easiest oxidation or reduction should happen on the phosphorus, and therefore directly correspond to the electronic properties of the ligand. The first oxidation should remove an electron from the HOMO of the phosphorus, therefore correlate to the σ-donor-strength while the first reduction puts an electron in the LUMO, hinting to the strength of the π-acceptor qualities. A higher oxidation-potential means worse σ-donor-properties while a higher reduction-potential equals a better π-acceptor.
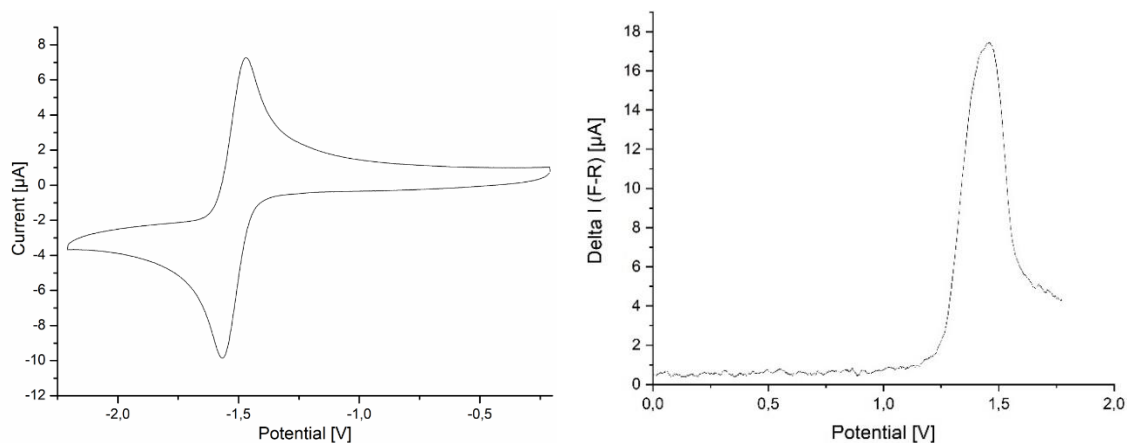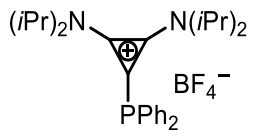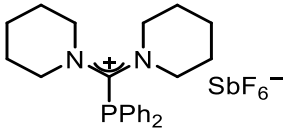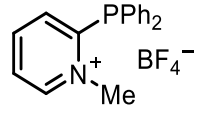
Figure 9: Cylic (left) and squarewave (right) voltammograms of **191c**.

It should be noted however, that the result is only comparable when the different compounds show reversible CVs and have similar structures. The ideal scenario would be completely reversible oxidations and especially reductions. Cationic phosphines often show different behaviors. The reduction is rarely reversible and often multiple reductions overlap, so it may be complicated to experimentally determine the π-acceptor properties. The situation with the oxidation is often more favorable. In the positive potential range the oxidation on the phosphorus is often the only oxidation to be observed. Because it is often not a reversible oxidation, the squarewave voltammetry experiment may be used instead of the classical CV-experiment to obtain more reliable results. From a not-reversible oxidation information of possible follow-up reactions cannot be obtained easily, thus the value of the oxidation potential can only be referenced to compounds of similar structure, in this case α-cationic phosphines. Direct quantitative comparisons to other phosphines may be inaccurate.

To check the capability of cyclic voltammetry in qualitative comparisons, the values have to be compared with other methods. Table 1 shows the oxidation potential of some of the phosphines where the HOMO/LUMO energy levels and the TEP have also been calculated.

Table 1: Ligands and their oxidation potential vs. Fc/Fc$^+$ in DCM with 0.1 M Bu$_4$NPF$_6$. Comparison with HOMO/LUMO-energies and TEP.

Ligand	E_{Ox} / V	HOMO / eV	LUMO /eV
PPh$_3$	0.536	-5.28	-1.13
(iPr)$_2$N, N(iPr)$_2$ ⊕ BF$_4^-$ PPh$_2$	1.207	-9.05	-4.10
N⁺N SbF$_6^-$ PPh$_2$	1.289	-9.31	-5.00
PPh$_2$ BF$_4^-$ N⁺ Me	1.480	-9.47	-6.07

As the trend in the oxidation potentials is the same as in the calculated energy levels (Figure 5) and TEPs (Figure 7), this shows that it is safe to assume that cyclic voltammetry delivers an accurate view of the electronic properties.

In the recent years a new technique saw increasing use for determining the steric properties of ligands, the buried-volume calculations. It functions similar to the method of Tolman, that the van-der-Walls radii are observed from a center, but instead of a cone angle, the complete occupied volume in a defined sphere is calculated. For this, the X-ray structure of a metal complex is needed. Then a sphere in a chosen distance around the metal is defined and divided into voxels. The size of these voxels can also be chosen. Then, each of these voxels is either defined as occupied or not, depending whether it is inside of the van-der-Waals radii of an atom in the molecule or not. In the calculation the radii of the metal is omitted, thus giving a reasonable value for the ligand alone. It should be noted however, that this approach slightly affects the calculated buried volume of the molecule, dependent on the size of the metal used to coordinate the ligand. As an advantage, not only an abstract angle is given but a complete picture, where the steric bulk can be exactly located (Figure 10).
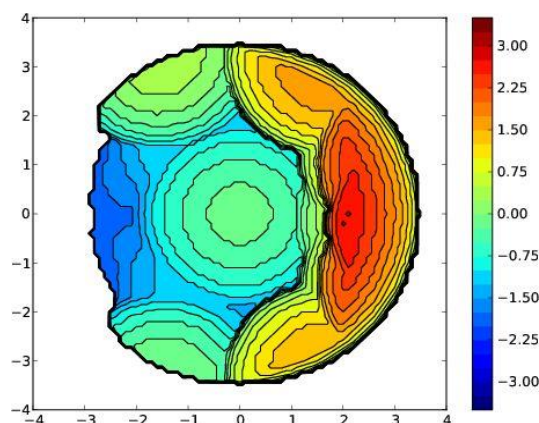
Figure 10: Buried volume plot of 191c. The colored scale indicates the position of the occupied volume.

1.4.1 Synthesis of α-cationic phosphines

In 1995, an early example for the synthesis of cationic phosphines is shown by Tolmachev *et al*. They prepared a phosphine with an imidazo[1,2a]pyridine backbone and turned the molecule cationic by addition of alkylation agents or Brønsted acids. While hydrochloric acid and the Meerwein-salt only reacted selectively via the N-position, the use of dimethylsulfate resulted in an product mixture, as both N- and P-alkylation took place.[59] While P-alkylation of a phosphine would in principle yield a cationic phosphonium salt (**75**), the lone pair of the phosphorus is used in the process. This drastically changes the properties of the phosphorus, making it impossible to coordinate it to a metal (Scheme 30).
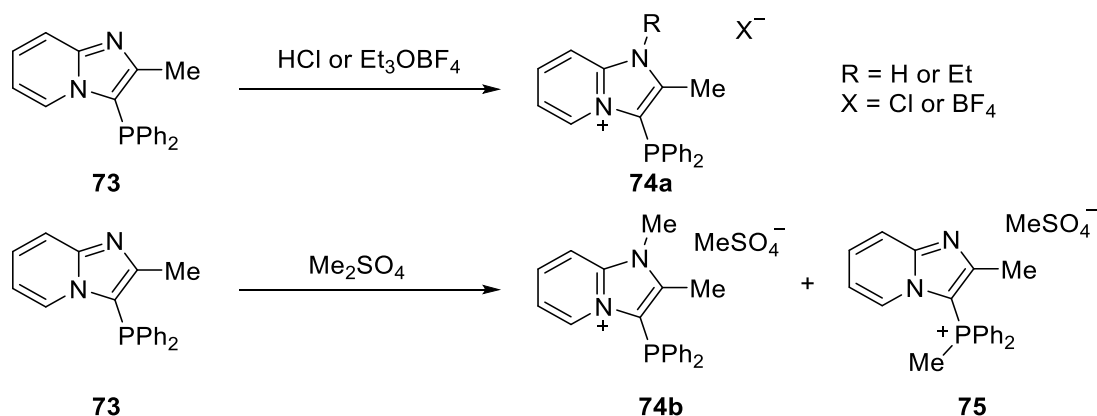
Scheme 30: Alkylation of imidazo-pyridine phosphines.

In the same year, Komarov and Kornilov published together with the Tolmachev-group a possible work-around to the P-alkylation problem. By coordinating the phosphine, this time with a simple imidazole-backbone (**76**), to tungsten they could selectively alkylate the nitrogen with dimethylsulfate, as the lone pair on the phosphorus was already blocked (Scheme 31).[60]
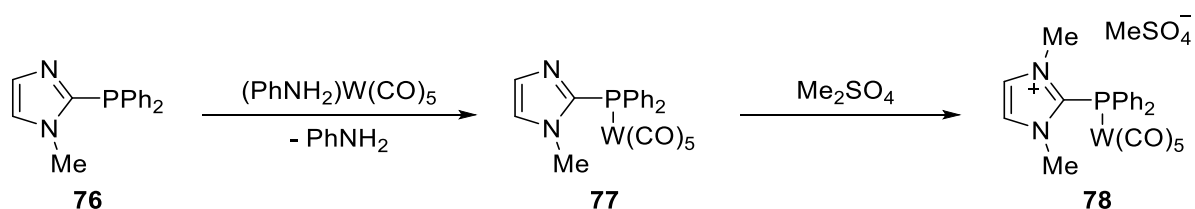
Scheme 31: Imidazolium-based cationic phosphine.

In 1999, Kuhn *et al.* were able to produce a cationic phosphine by reaction of an imidazolium carbene with Ph_2PCl. They were expecting a reductive coupling resulting in a diphosphine **81** and a chlorine-carbene adduct **82**, but the cationic phosphine **80** was the only product obtained in the reaction (Scheme 32).[61]
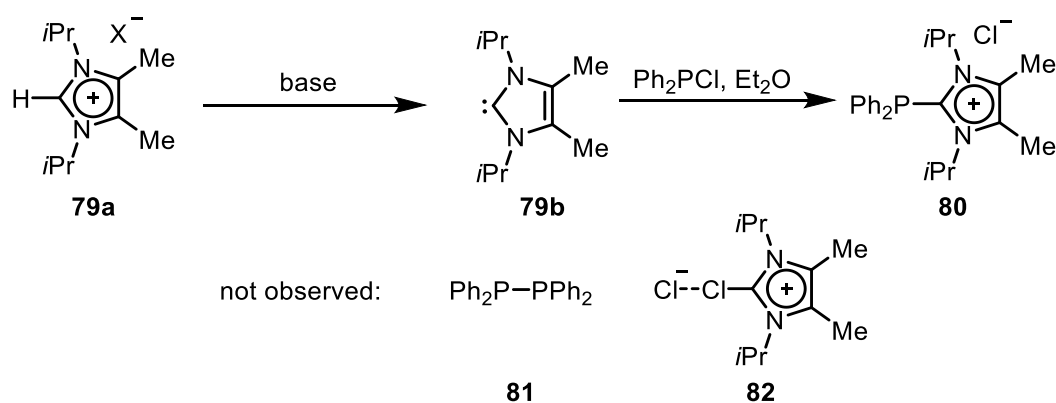

Scheme 32: Cationic phosphine synthesis via carbenes.

Testing the capabilities of their newfound cationic phosphine, Kuhn *et al.* were able to produce Pd and Pt complexes (**83**) with their ligand. When investigating the electronic properties of the ligand, it showed a behavior similar to neutral phosphines. The use of cationic phosphines and anionic metal fragments resulted in the synthesis of zwitterionic complexes (Scheme 33).[62]
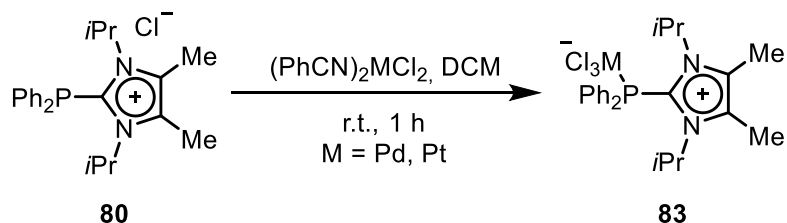
Scheme 33: Cationic phosphine metal complex.

In 2001 Brauer *et al.* published a complete synthesis of a cationic phosphine and showed a subsequent catalytic application of the ligand. They also used the imidazolium backbone, but with different substituents (Me and *n*Bu) on the two nitrogen atoms. Their metal of choice was rhodium and the metal complexes obtained were used in hydroformylation reactions.[63]

Another route to symmetrically substituted imidazolium-based cationic phosphines was published in 2007 by the Tkatchenko group. They were able to obtain the cationic phosphine

by reaction of the imidazolium-carboxylate **84** with a chlorophosphine. The advantage of this procedure is that it is an one-pot reaction, no strong bases have to be used and it does not involve isolated carbenes.[64] As a major drawback, the starting material imidazolium-carboxylate is synthesized under harsh conditions, requiring 120-130 °C for 24 h,[65] which significantly limits the modularity of the reaction in regards to more complex backbones than imidazolium (Scheme 34).
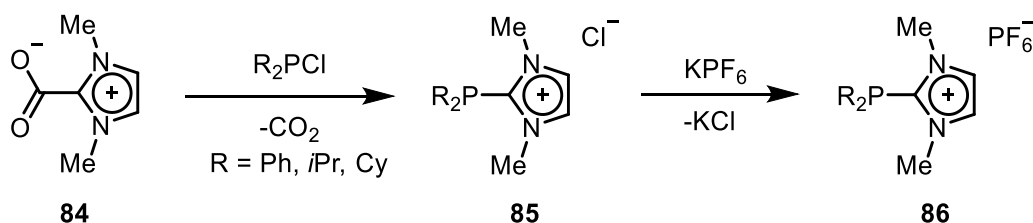
Scheme 34: Synthesis of cationic phosphines via imidazolium-carboxylates.

Because of these limitations, the Alcarazo group used for the synthesis of imidazolium-based cationic phosphines the approach by Kuhn *et al.* rather than the one published by Tkatchenko.

An overview for the syntheses of imidazolium-based cationic phosphines is shown in scheme 35. Three different approaches were followed. Either the cationic phosphine is synthesized by reaction of a chlorophosphine (general formula PR_2Cl, R = alkyl or aryl) with a Lewis basic deprotonated imidazole, thereby generating a free carbene (**87**), or the direct substitution of a silyl salt (**89**) could happen. As another possibility, an already synthesized phosphine can be made cationic, exemplified by the N-alkylation of the imidazoliophosphine **90**.[5,54] Depending on the starting materials used, the counterion can be either a chloride or a triflate.
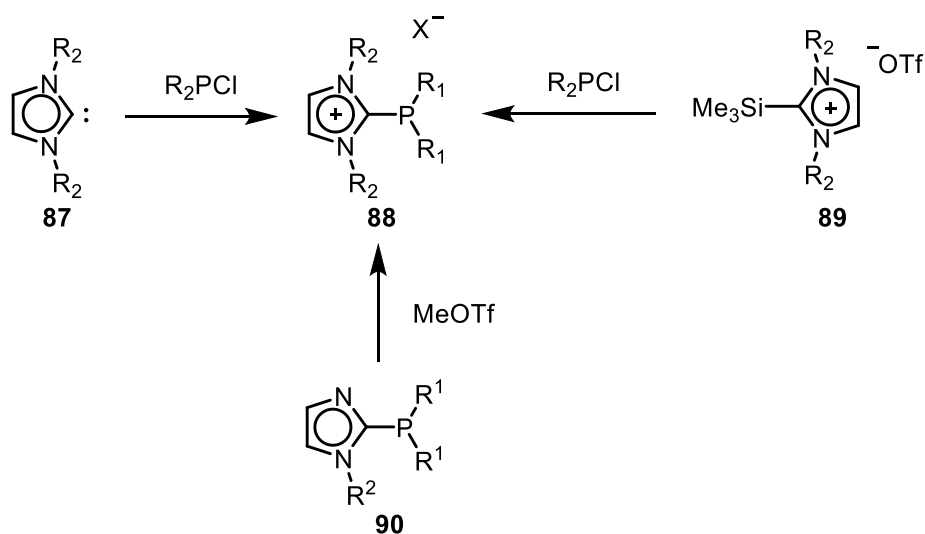
Scheme 35: Overview of possible syntheses for cationic imidazoliophosphines.

An exemplary application of the carbene route is the synthesis of the TADDOL-based cationic phosphonite ligands used for the synthesis of helicenes by González-Fernadández *et al.*

(Scheme 36). The cationic phosphonite is reacted with an IMes-carbene, yielding the desired ligand, which can then be coordinated to gold.
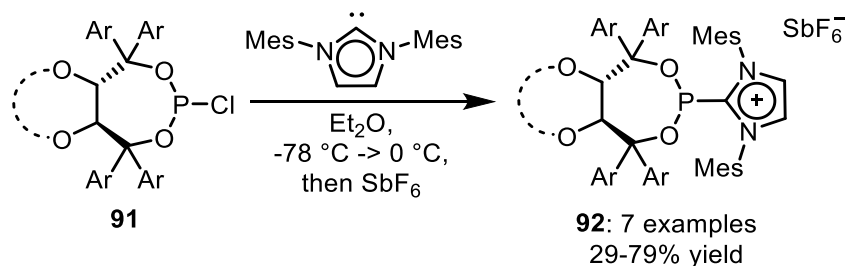
Scheme 36: Synthesis of TADDOL-based cationic phosphonite.

Although the approach via carbenes proved to be very successful for the synthesis of cationic phosphines, for some of the desired structures it was not possible to generate the desired carbene or the carbene did not react with the phosphine in the desired selectivity.

To overcome this issue, our group developed the direct condensation of Vilsmeier-type salts with secondary phosphines to generate cationic phosphines (Scheme 37). This approach led to a variety of cationic phosphines, bearing imdazolium-,[66] pyridinium,[67] cyclopropenium[68] and non-cyclic amines as cationic groups. While the reaction proceeds for electron-rich phosphines readily by heating, strong bases like nBuLi or KH are needed to assist with the deprotonation in the case of electron withdrawing phosphines such as bis-(3,5-bis(trifluoromethyl)phenyl)phosphine. By using primary phosphines as starting materials for this kind of reactions, dicationic phosphines can be synthesized.[69]
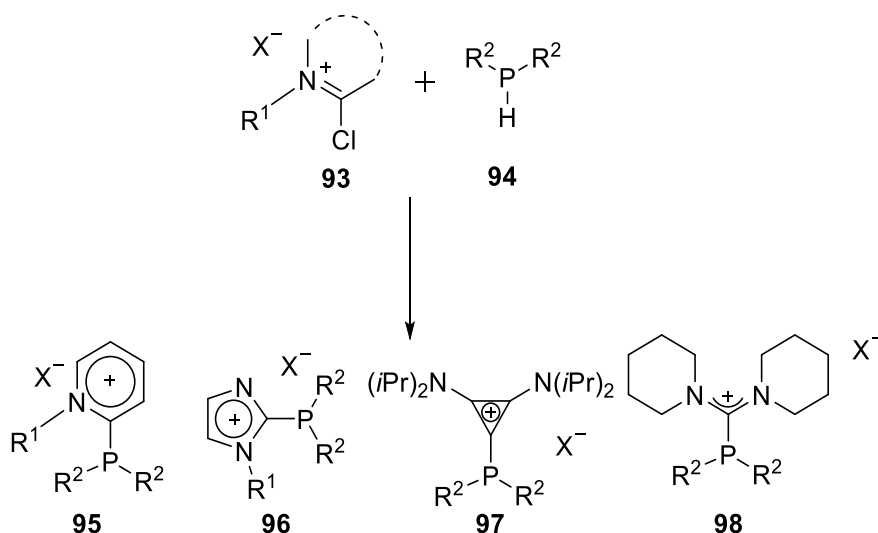
Scheme 37: Modular synthesis of cationic phosphines.

One example for such a synthesis are the pyridiniophosphines, synthesized by Tinnermann *et al.* (Scheme 38). In contrast to reactions with carbenes, the positive charge is not generated in the step where the chloro-phosphine is added, but a secondary phosphine is added to an already charged substrate. Two equivalents of the phosphine are used as it is

not only the substrate, but also functions as the base in the reaction, thereby improving the yield.
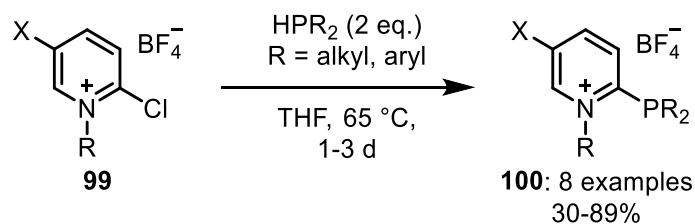
Scheme 38: Synthesis of pyridiniophosphines.

An example for the use of a primary phosphine resulting in a dicationic phosphine is the synthesis of the dicationic chelating phosphines by Gu *et al.* (Scheme 39). The general mechanism is similar to the synthesis of the monocationic substrates, however a stronger base is needed and the reaction is more sensitive due to the use of primary phosphines.
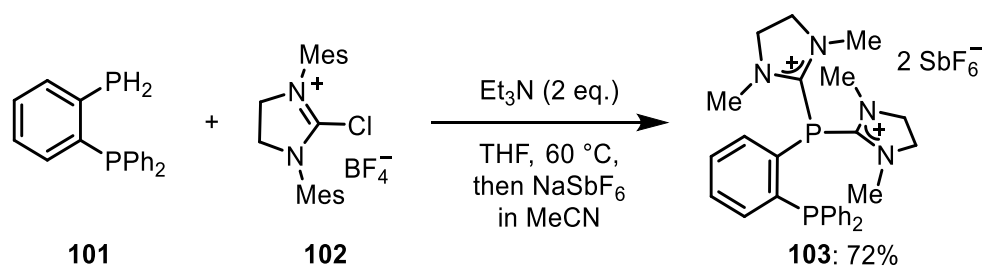
Scheme 39: Synthesis of dicationic chelating phosphines.

Tricationic phosphines can be synthesized by addition of either silylimidazolium salts to PCl_3 or cyclopropenium chloride salts to $P(SiMe_3)_3$ (Scheme 40). A direct reaction of a free carbene with a very electrophilic phosphorus source (for example PCl_3) does not work, as the reaction is quite vulnerable to the steric bulk of the carbenes employed, leading to unfavored outcomes of the reaction, for example the reduction products being obtained.[5]
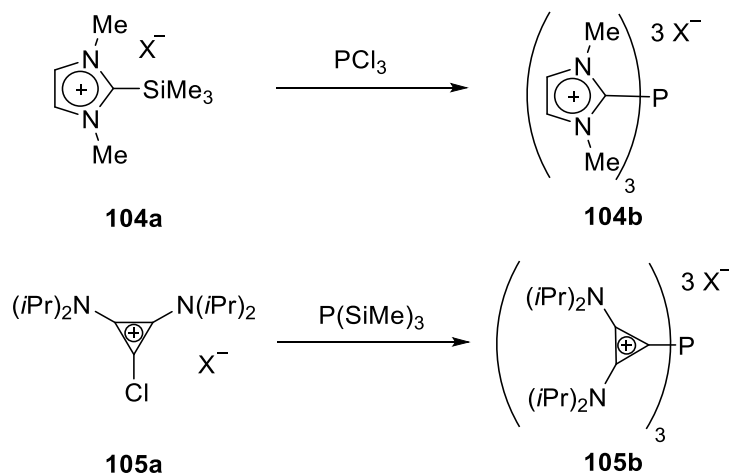
Scheme 40: Modular synthesis of tricationic phosphines.

The introduction of substituents on the cationic parts is normally quite easy, but in some cases more elaborate methods have to be used. One such case is the pyridinium phosphine **100**. For the introduction of simple alkyl-chains at the nitrogen, strong alkylating agents like Meerwein-type salts are sufficient,[67] but if functionalized aryl groups like dimethoxybenzene need to be introduced, more complex synthetic procedures have to be used. Marset *et al.* used in this case the copper-catalyzed arylation of 2-hydroxypyridines[70] while the Alcarazo group employed the Zincke reaction to exchange the substituents of an dinitrobenzene-substituted pyridine (Scheme 41).[71,72]
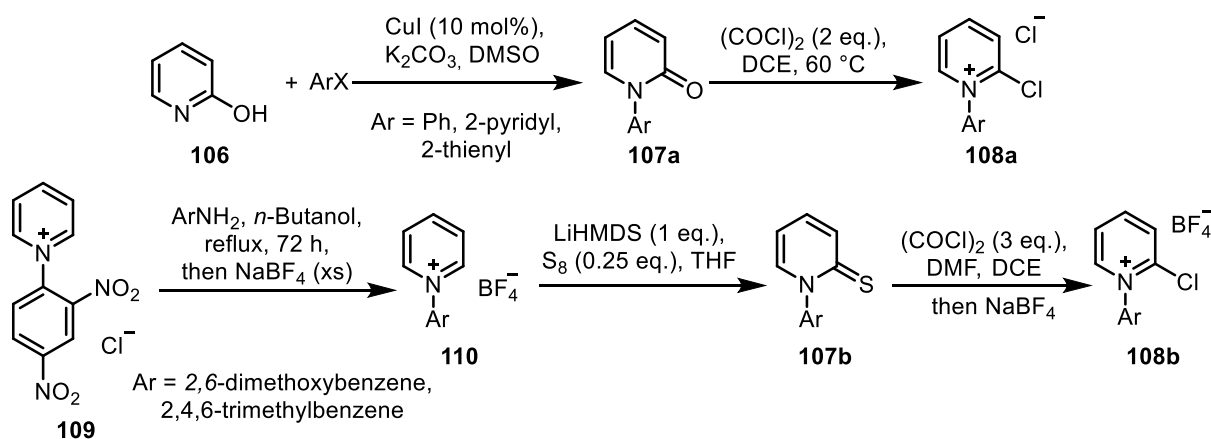
Scheme 41: *N*-aryl-substituent introduction by Marset *et al.* (top) and Tinnermann *et al.*

1.4.2 Carbenes

As shown in Scheme 35, the addition of a carbene to chlorophosphine is a reliable way of synthesizing $\alpha-$cationic phosphines. As this is also the method used later in this thesis, I will briefly go into the properties and history of carbenes.

Carbenes are carbon-containing molecules with an electron sextet on a carbon, thus having an electron deficiency leading to very high reactivity.[73] In contrast to phosphines, carbenes are good σ- and π-donors and only very weak π-acceptors. Because of their reactivity, they were elusive as isolated species for a long time, despite often considered to be intermediate species in reactions described long ago, for example by Curtius and Buchner[74], Staudinger[75] and Doering (Scheme 42).[76] The works of Doering and Staudinger notably feature dichlorocarbene, which is a well-known intermediate in organic chemistry and easy to obtain, as it can be generated from chloroform and a strong base.
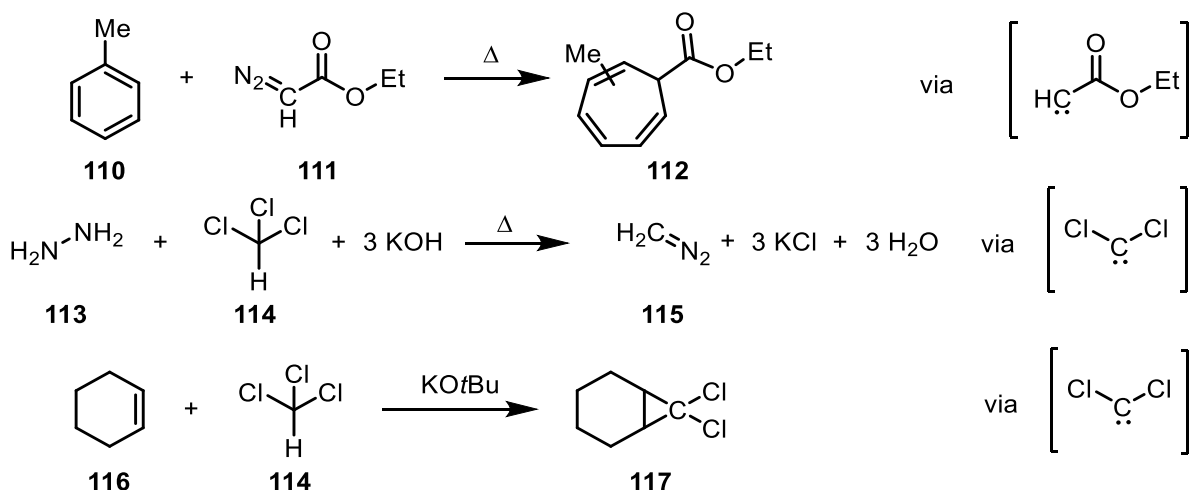
Scheme 42: Early reactions with carbene intermediates by Curtius and Buchner (top), Staudinger (middle) and Doering (bottom).

Although many metal complexes of carbenes have been published throughout the nineteen hundreds, for example by Chugaev[77], Fischer[78] and Öfele[79], the isolation and characterization of a free carbene remained elusive.

Breslow[80] and Wanzlick[81] then proposed that a carbene can be stabilized by being in the center of a thiazolium- or imdazolium-moiety via mesomeric structures (Scheme 43), but still only carbene adducts could be isolated, not the free carbene.[82] This however paved the way for the research of N-heterocyclic carbenes (NHC), which would yield a variety isolated free carbenes.
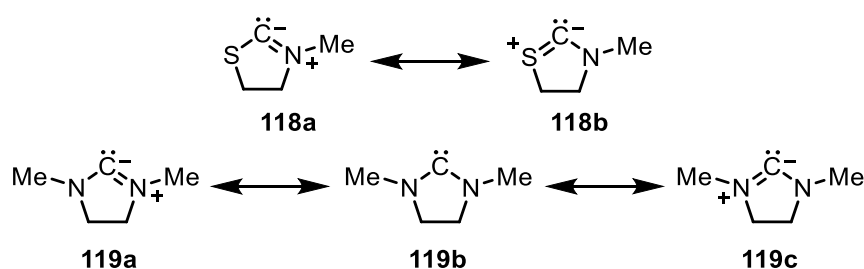
Scheme 43: Stabilization of thiazolium- and imidazolium carbenes, as proposed by Breslow (top) and Wanzlick.

The first isolated carbene were finally reported by the Bertrand group, who could synthesize and isolate a phosphino-silyl carbene.[83] Shortly later the Arduengo group published the synthesis and isolation of an NHC, and they were also able to provide a crystal structure, thus proving the connectivity (Scheme 44).[84]
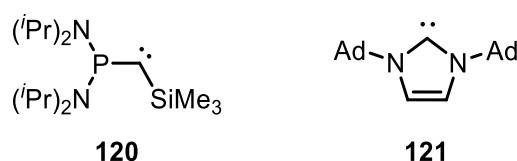
Scheme 44: First isolated carbenes by Bertrand and Arduengo.

The Bertrand group did subsequently synthesize more carbenes of different types (Scheme 45), notably the cyclopropenylidenes[85] **122** and the cyclic(alkyl)(amino)carbenes (CAAC, **123**).[86] In a CAAC, one of the nitrogen centers present in a NHC is replaced by a carbon.
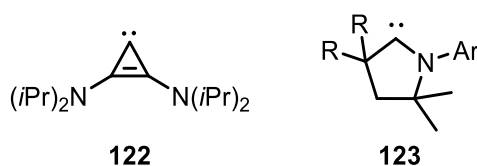
Scheme 45: Cyclopropenylidene and CAAC synthesized by the Bertrand group.

As the nitrogen is electron-withdrawing and π-donating, but a carbon is σ-donating and not π-donating, the resulting CAAC is in comparison to an NHC more nucleophilic, but also more electrophilic.[87] This is supported by the calculation of the HOMO-LUMO-gap performed by the Bertrand group (Figure 11). When comparing the five-membered NHC and five-membered CAAC, the LUMO decreases from 0.70 eV to 0.06 eV, while the HOMO increases from -5.62 eV to -5.20 eV. This results in a much smaller HOMO-LUMO gap for the CAAC, being only 5.26 eV, while the NHC has 6.32 eV. When comparing NHCs and CAACs with their ring-expanded homologues, the energy of the LUMO does not change very much, being in a range of 0.17 eV for NHCs and 0.08 eV for the CAACs, but the HOMO seems to be more affected by change of geometry around the carbene center, as the energy changes by 0.47 eV for the NHCs and 0.38 eV for the CAACs.[88]
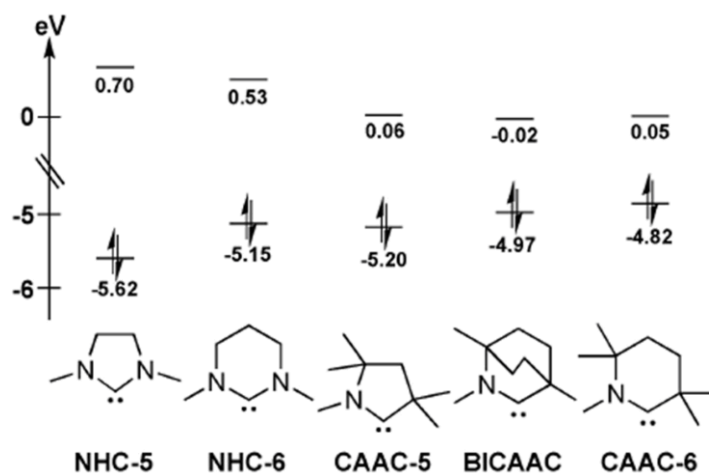
Figure 11: Calculated HOMO-LUMO-gap of selected carbenes at the B3LYP/def2-TZVPP level. Figure taken out of Weinstein *et al., J. Am. Chem. Soc.* **2018**, *140*, 9255-9260.

Besides the electronic factors, the exchange of a trivalent for a tetravalent atom also changes the sterical properties of the ligand, as the carbon is able to carry one additional substituent. This allows to make the carbene sterically much more encumbered as for example a single adamantyl could be directly adjacent to the carbene[89] and not only in β-position like with Arduengo´s NHC.

Because of their already mentioned good donor-qualities, carbene ligands are often used in catalysis. The most prominent examples include the 2nd generation Grubbs[90]- (**124**) and the Hoveyda-Grubbs[91] catalyst (**125**).
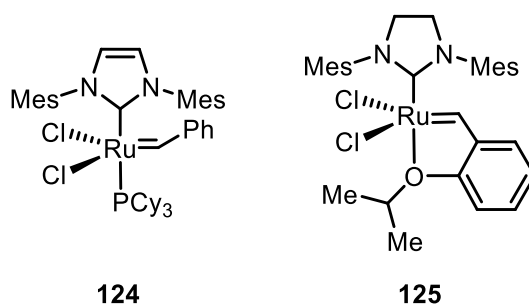
Scheme 46: 2nd-generation Grubbs (left) and Hoveyda-Grubbs catalyst.

The applications of carbenes in this thesis however is not the direct coordination with metals, but their addition to chlorophospholes, substituting the chloride and yielding cationic phospholes with chloride as anion (Scheme 47).
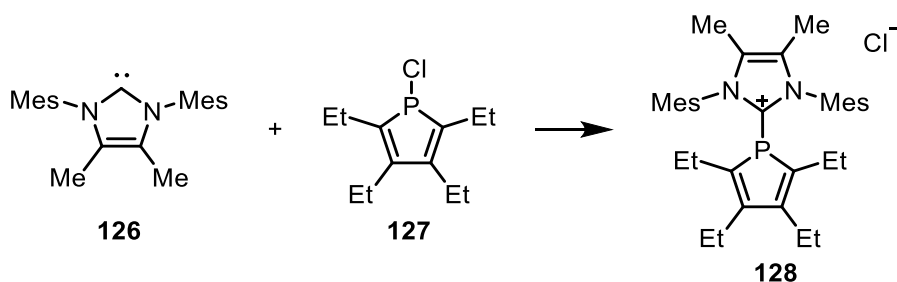
Scheme 47: Schematic synthesis of cationic phospholes from carbenes.

1.4.3 Applications of cationic phosphines

If not used because of their physical properties, cationic phosphines find applications mostly as ligands in metal catalysis, although sometimes reactions can also be directly catalyzed by them or their derivatives, as they are highly lewis acidic themselves.

One example of a cationic phosphines derivative directly catalyzing a reaction is the hydrosilylation of alkenes and alkynes with the quaternary cationic phosphonium salt **130**, published by the Stephan group in 2014 (Scheme 48). With just 2% catalyst loading using triethylsilane as reagent in deuterated DCM at 45 °C, isolated yields between 77% and 96% could be achieved.[92]
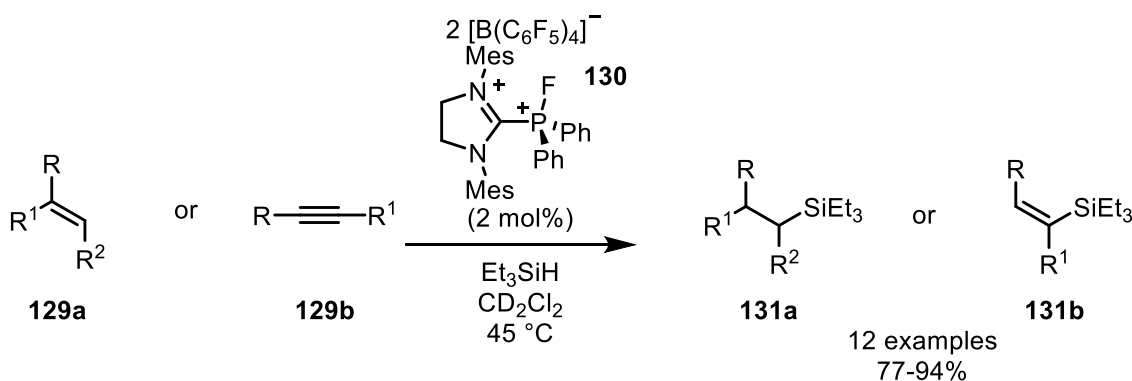
Scheme 48: Direct cationic phosphine-catalyzed hydrosilylation of alkenes and alkynes.[92]

Cationic phosphines were also tested as ligands in reactions where uncharged phosphines were already well established. As an example, the group of Knochel used imidazolium-phosphine **134** in a classic Negishi coupling[93], achieving high yields with reaction times less than 5 h at room temperature (Scheme 49). The reaction was performed in a biphasic solution, the classical solvents of toluene and/or THF were accompanied by an ionic liquid, 1-butyl-2,3-dimethylimidazolium tetrafluoroborate ([bdmim][BF$_4$]). The ionic liquid was not only intended to ensure the solubility of the cationic metal complex, but to fixate the catalyst and thereby allow the recycling of the precious palladium.[94]
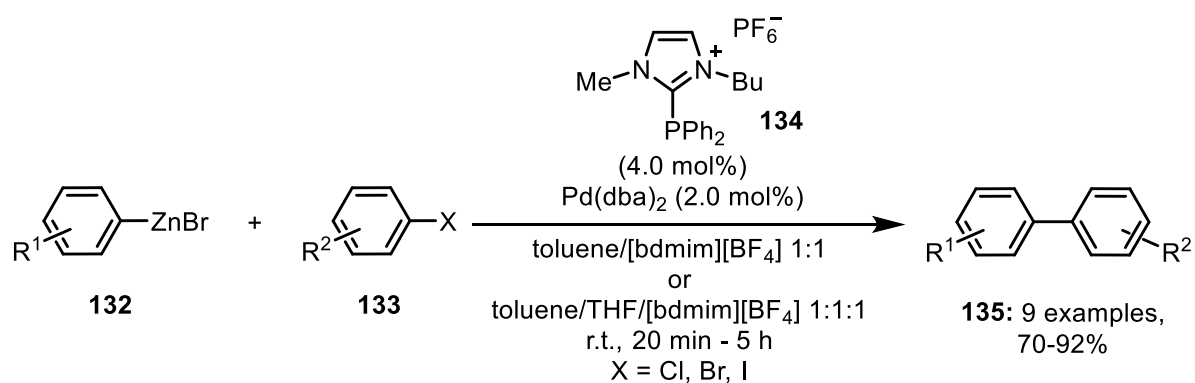
Scheme 49: Negishi coupling with cationic phosphines as ligands.

One of the applications our group has studied is the Au-catalyzed synthesis of helicenes. These reactions usually involve the hydroarylation of a triple bond (Scheme 50). As products of these reactions can have different regioisomers and enantiomers, control over these products via catalyst design is needed. This can be achieved by incorporating already chiral backbones like TADDOLs and BINOLs into the catalysts. One of the newest examples consists of the enantioselective synthesis of penta-helicenes through hydroarylation by a BINOL-based Au-catalyst. The BINOL-backbone **141**, similar to the TADDOL-backbone (**137**) induces the chirality, while the cationic part of the molecule enhances the reactivity.[95] This increased reactivity allows lower temperatures, which also benefits the enantioselectivity. This approach was first applied in the synthesis of [6]-carbohelicenes[96] and later expanded to [4]-[97] and [5]-helicenes.[98]
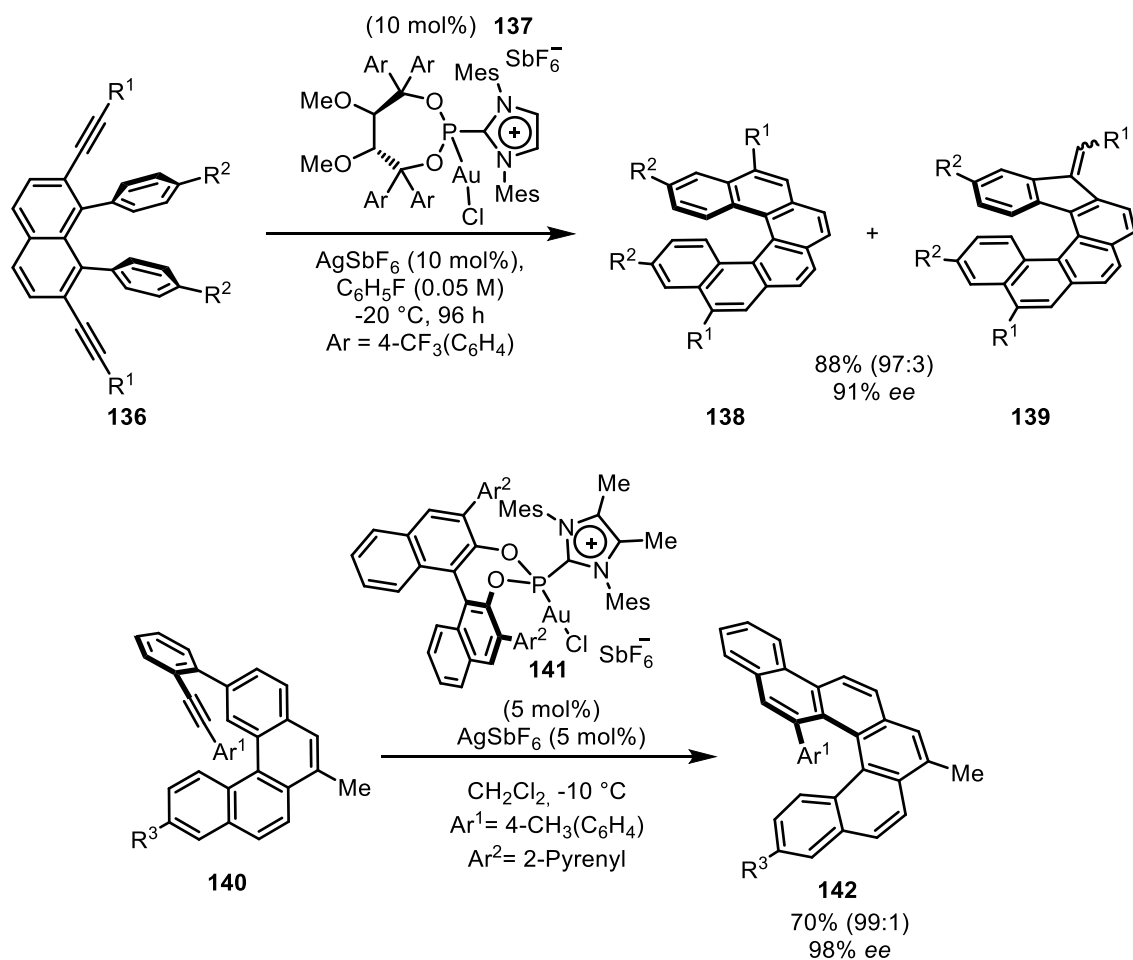
Scheme 50: Gold catalyzed synthesis of 6- and 5-carbohelicenes with chiral TADDOLs (top) and BINOLs (bottom).

While the configuration of the helicenes is fixed after the hydroarylation, more flexible systems can also be prepared. This is shown by the atroposelective synthesis of binaphthalene-2,3'-diols (Scheme 51). The high reactivity of the cationic catalysts allows for working at low reaction temperatures (-30 °C) which is in the case of atropoisomers especially interesting, as not only the initial enantiomeric excess is high, but also the racemization threshold is not met.[99]
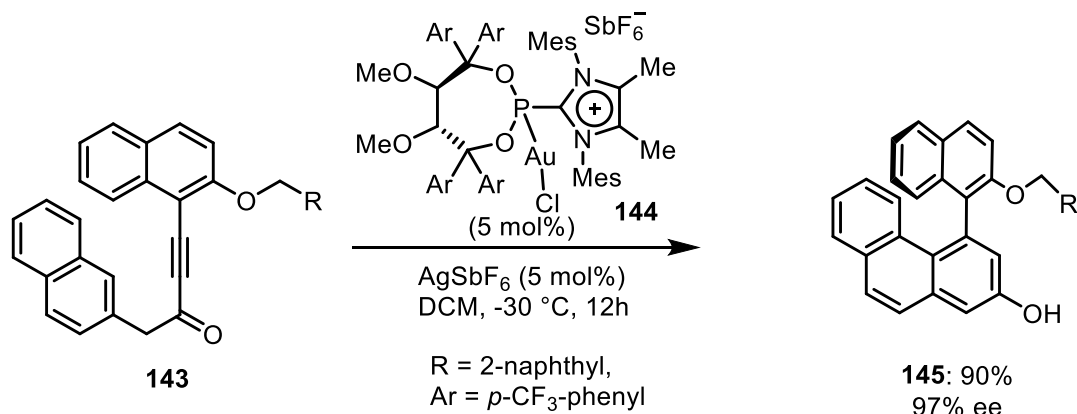
Scheme 51: Gold catalyzed atropo-selective synthesis of binaphthalen-diols.

In addition to these special applications, cationic phosphines as ligands show a general increase in reactivity if the rate determining step of the reaction is lowered in energy by stronger π-accepting metals. An example is shown in the gold catalyzed hydroarylation of biphenyl-alkyne **146** into phenanthrene **147** (Scheme 54). While the normal phosphine ligand leads to extremely low conversion after 10 minutes, the phosphite ligand shows roughly ten percent conversion. With the extremely electron poor dicationic phosphine ligand, the reaction has already reached maximal conversion after ten minutes.[69]
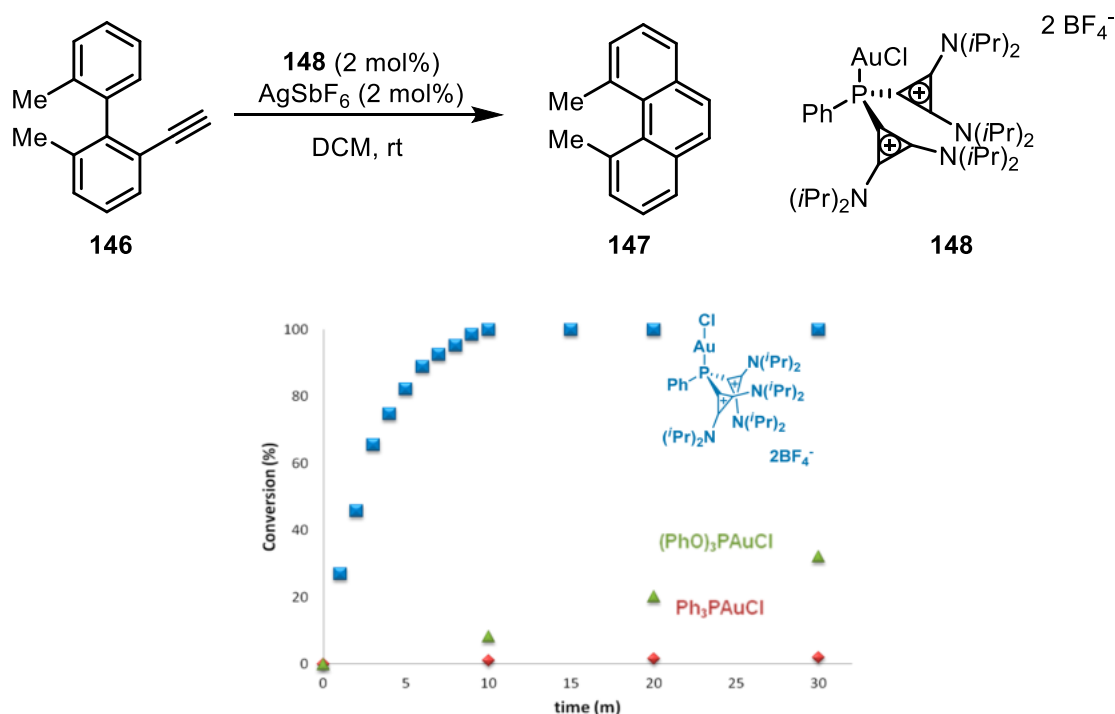
Scheme 52: Gold catalyzed hydroarylation and kinetic study. Scheme taken out of Carreras *et al.*, *J. Am. Chem. Soc.* **2013**, *135*, 18815.

With a similar substrate, the catalyst also shows a different regioselectivity than more electron-donating ligands (Scheme 55). While the dicationic gold-catalyst **148** strongly favors the 6-*endo*-dig-cyclization, the proportion of the 7-*exo*-dig product **151** increases when more electron-donating ligands (**3** and **1**) are used.[69]

148: 98:2
AuCl/**3**: 40:60
AuCl/**1**: 25:75
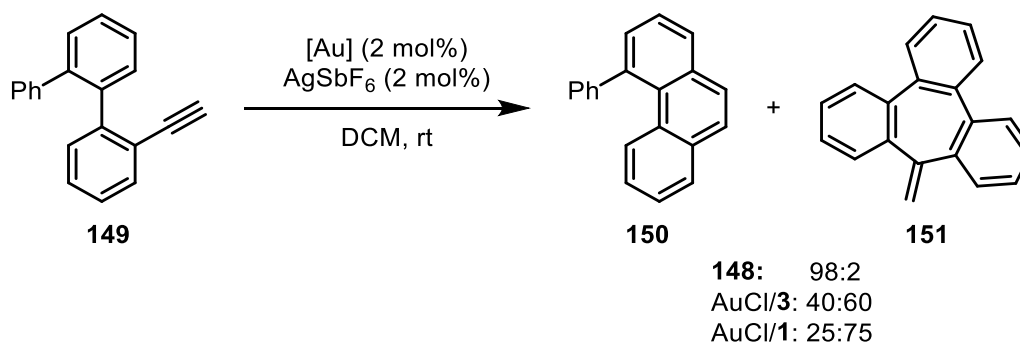
Scheme 53: Electronic effect of different ligands on the gold catalyzed hydroarylation.

Even when much simpler catalysts like acids can do a hydroarylation, more complex catalyst can lead to another product. This has for example been shown by Sprenger *et al.* in 2020 (Scheme 56). The example shows that the gold center is more than just a "very large proton" as it is often jokingly referred to. While the use of a proton source often leads to an anthracene derivate or a mixture, the use of the cationic gold catalyst produces selectively the cycloheptatrienes. It should be noted however, that the substituents on the substrate also affect the selectivity. The position most vulnerable to change is the substituent at the alkyne. A less bulky substituent, for example a hydrogen, leads to very high selectivity for the anthracene-product with both catalysts.[100]
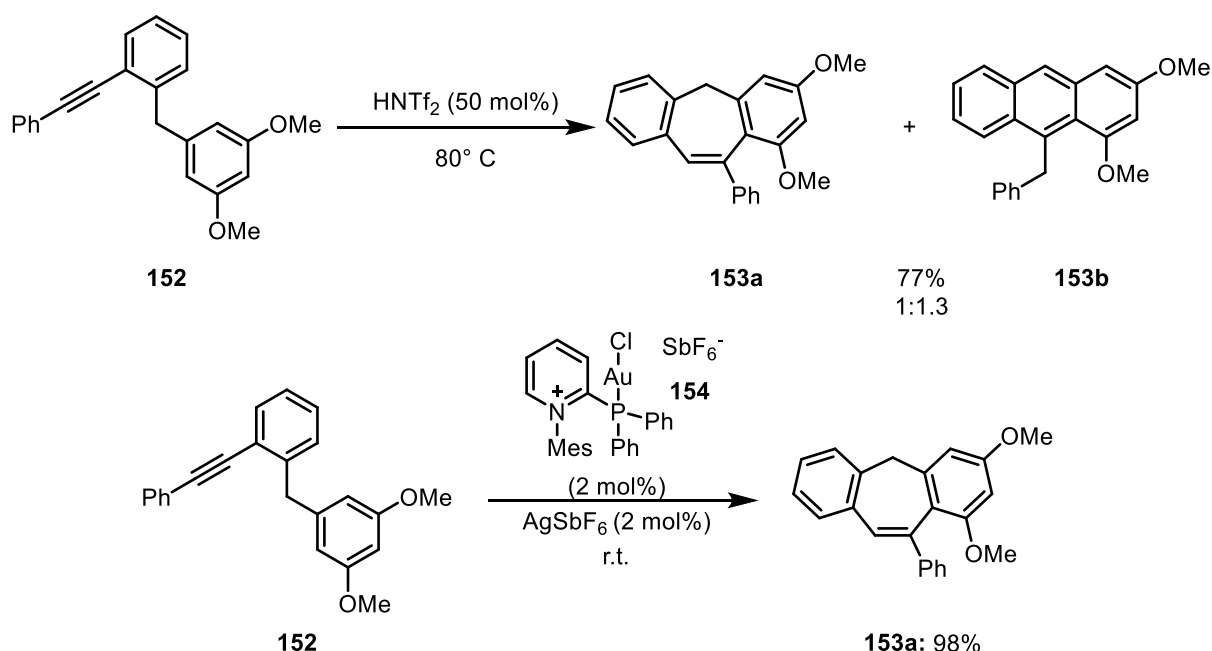
Scheme 54: Gold catalyzed hydroarylations and product distribution in the synthesis of cycloheptatrienes and anthracen.

Cationic phosphines show not only great results in the activation of triple, but also in double bonds, as demonstrated in the hydroarylation of dienes with dicationic chelating phosphines (Scheme 52, **103**). In contrast to most of the other cases, where either platinum or gold was used, in this case rhodium was the metal of choice. In this case not only simple substrates like indoles could be used, but also more sophisticated like substituted benzenes and azulene.[101]
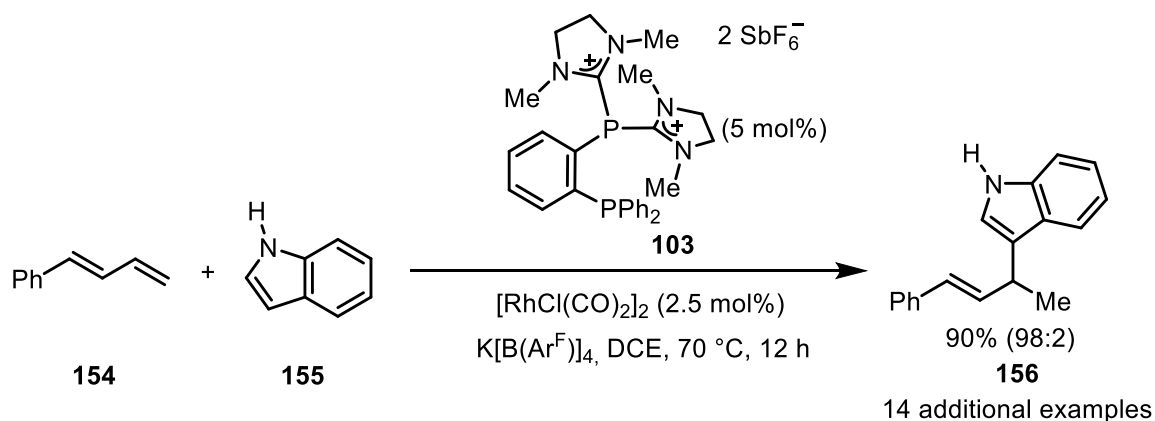
Scheme 55: Rhodium-catalyzed hydroarylation of dienes.

The work on the dicationic chelating phosphines was continued leading to one of the most recent examples of the applications of cationic phosphines in catalysis in our group: the dimerization of norbornadiene into heptacyclotetradecane-cages (HCTD) (Scheme 53). In this reaction, the dicationic rhodium-complex **160** with a dicationic chelating phosphine catalyzes the first step of the dimerization, leading to the norbornadiene-dimers **158**, that are not yet closed to a cage. Subsequent addition of an Brønsted acid then achieves the final product.[102] These cages are interesting because of their structural similarity to adamantane, another cage-like molecule only consisting of carbon and hydrogen. As adamantane derivatives have applications in material science and is also part of a few therapeutic drugs, the synthesis of a surrogate is interesting and was further explored by our group.[103]
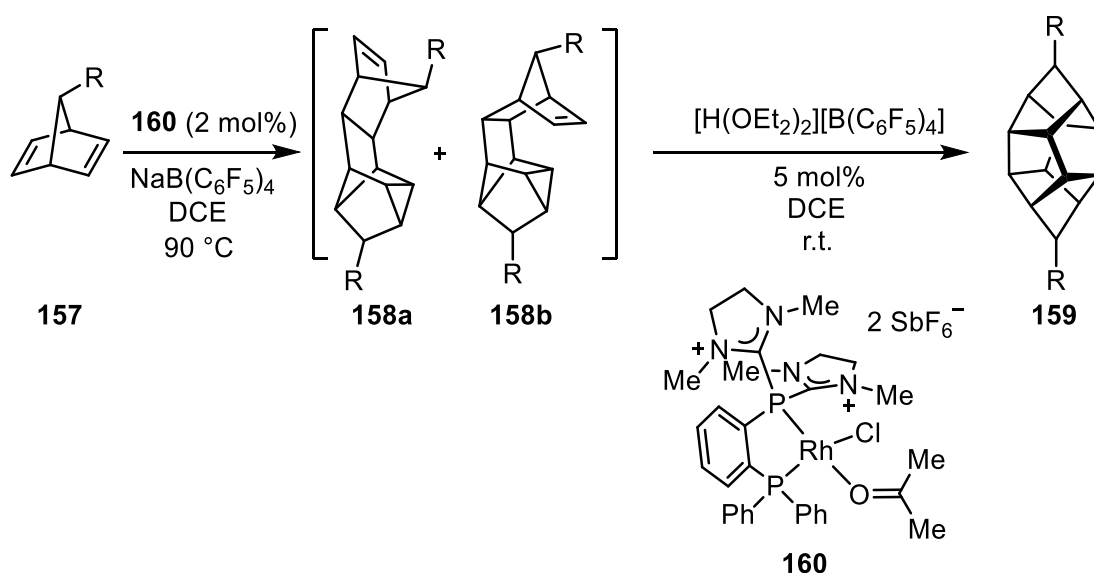
Scheme 56: Rhodium-catalyzed synthesis of HCTD-cages.

2. Project Aims

This PhD-thesis consists of two different projects.

In the first project, our objective is to find further applications for the ligands and catalysts developed by Alcarazo and Tinnermann. Tinnermann *et al.* developed cationic phosphines based on a pyridinium core. The pyridinium was modified on the nitrogen with differently substituted aryl-groups. Also, the phosphorus can either bear phenyl- or cyclohexyl groups besides the cationic group. As the synthesis of these ligands and initial catalytic reactions were already discussed in the thesis of Tinnermann[71], this thesis´ aim is to find additional applications. To help with the search for new applications, the electronic properties of the cationic phosphines will be determined.

The second and bigger project´s aim is the synthesis and application of phosphole-based cationic phosphines. Until now, the Alcarazo group has focused extensively on the substitution of the rests in generic phosphine-complexes PR_3 with one or more cationic groups. In some cases, the usual substituents were substituted by groups which allow the incorporation of chiral information. This dissertation will focus on the substitution of two of the generic rests with one phosphole moiety. As a phosphole should be more electron deficient than a phosphine, the exchange towards a phosphole should help to prepare an even more electron deficient ligand. The aim is to prepare a library of cationic phospholes and to determine their electronic and steric properties. Then their coordination chemistry to metals will be investigated and, if this proves successful, they will be applied in catalysis. Their prowess in catalysis will also be compared with other cationic and normal phosphines.

3. Results and discussion

3.1 Applications for cationic biaryl phosphines

3.1.1 Introduction

Hendrik Tinnermann and Christian Wille developed the synthesis of cationic biaryl phosphines (Scheme 57).[71,72] From pyridine **161** and 2,4-dinitrocholorobenzene **162** the cationic salt **163** is generated. The Zincke-reaction[104] then allows to change the extremely electron poor aryl-substituent for a more electron rich one. The pyridinium is then deprotonated and oxidized with sulfur leading to molecule **165**. The sulfur is then substituted with chloride, reinstating the aromaticity on the pyridinium. The obtained structure **166** resembles a Vilsmeier-type salt and can be turned in to the desired phosphine complex **167** by addition of a secondary phosphine. The addition of a metal salt to the phosphine, for example AuCl(SMe2), yields the corresponding metal complex **168**.
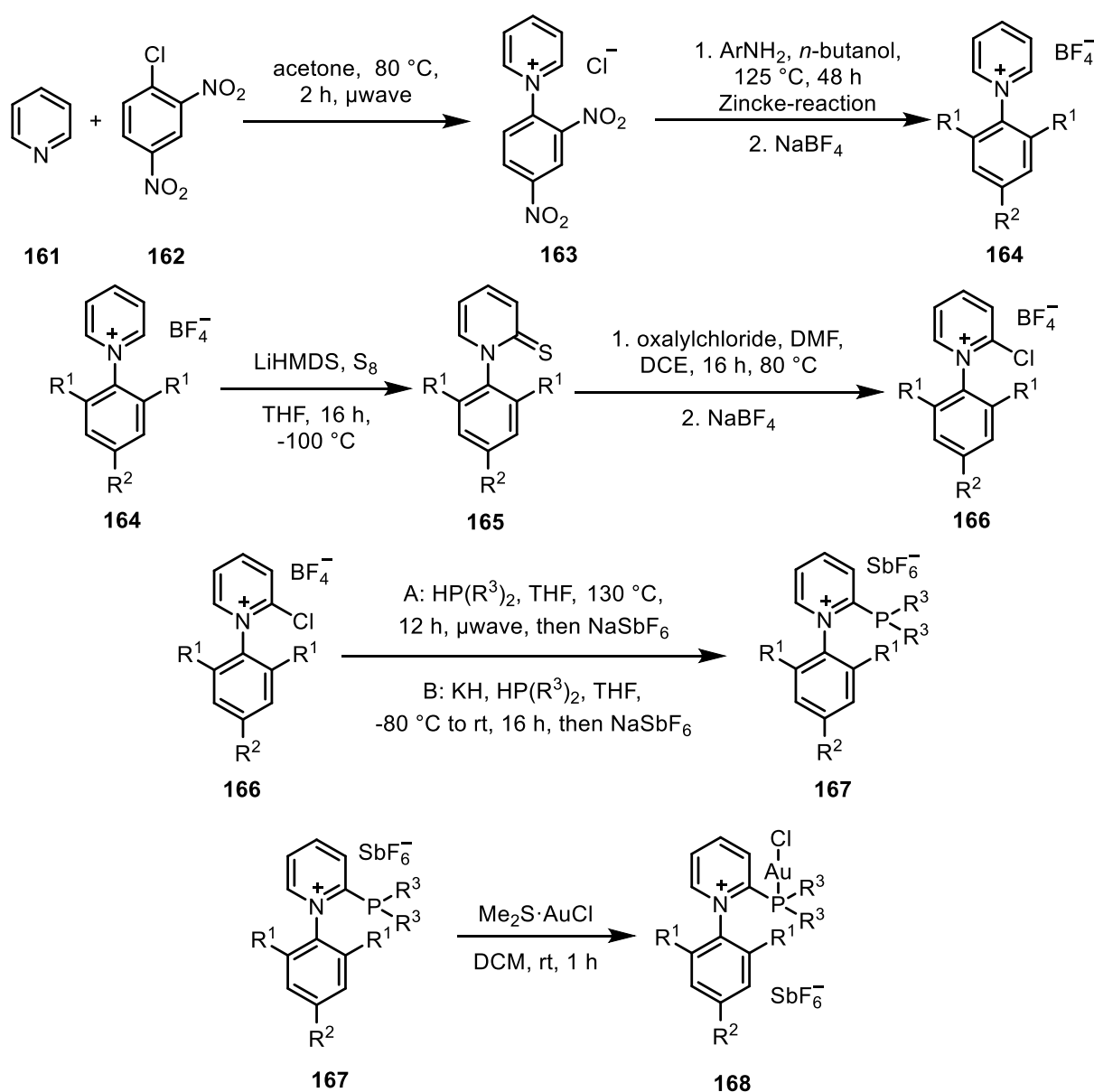
Scheme 57: Synthesis of cationic biarylphosphines.

This synthesis yielded a total of 8 different ligands (Scheme 58). The ligands differ on two positions: the substituents on the nitrogen and the phosphorus. On the nitrogen, substituted aryls of different structure were introduced: mesityl, 2,6-di(isopropyl)phenyl and 2,6-dimethoxyphenyl. While the former two have similar electronic qualities but different steric bulk, the latter one is electron richer. The phosphorus bears two ligands, either phenyl, cyclohexyl or 3,5-di(trifluoro)-phenyl. The last one withdraws even more electron density from the phosphorus. Noteworthy are the similarities between ligand **169d** and **169h** and the commercially available phosphine ligands SPhos und XPhos, although the latter one misses the isopropyl in the *para*-position.
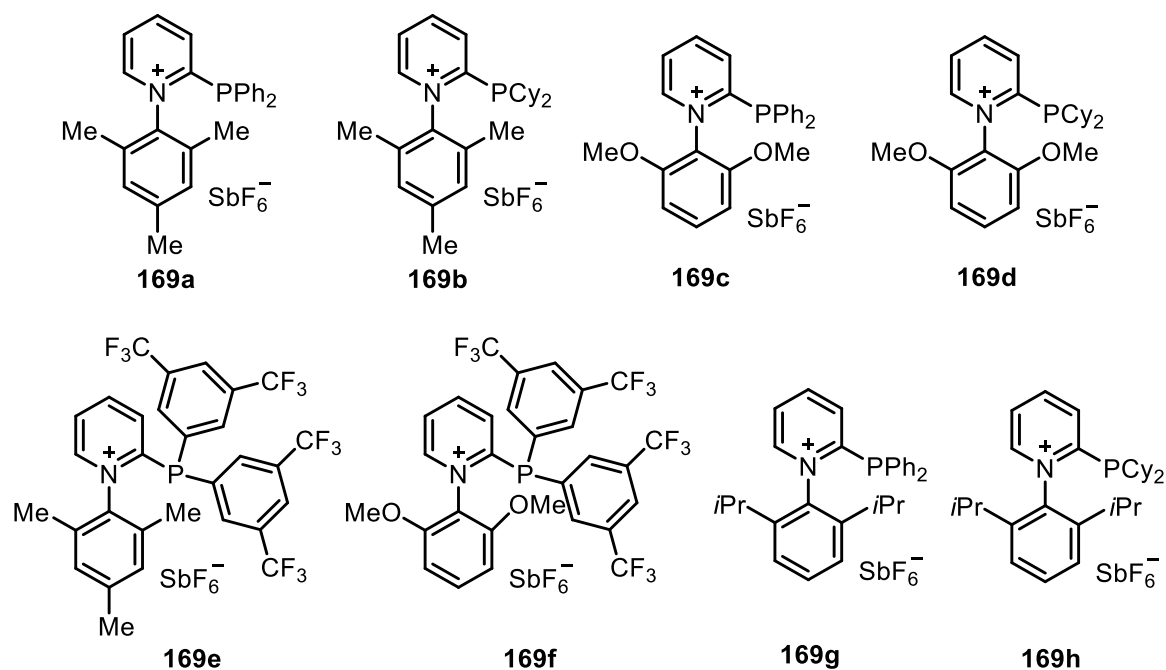
Scheme 58: Cationic biarylphosphines.

The ligands **169g** and **169h** could not be converted into the corresponding gold complexes, as the reaction was unclean, probably because of the weak σ-bonding of the ligand and the high steric bulk, yielding a total of six different gold-complexes (Scheme 59).

170a: R = Ph, R_1 = R_2 = Me
170b: R = Cy, R_1 = R_2 = Me
170c: R = Ph, R_1 = OMe, R_2 = H
170d: R = Cy, R_1 = OMe, R_2 = H
170e: R = 3,5-di(CF_3)C_6H_3, R_1 = R_2 = Me
170f: R = 3,5-di(CF_3)C_6H_3, R_1 = OMe, R_2 = H
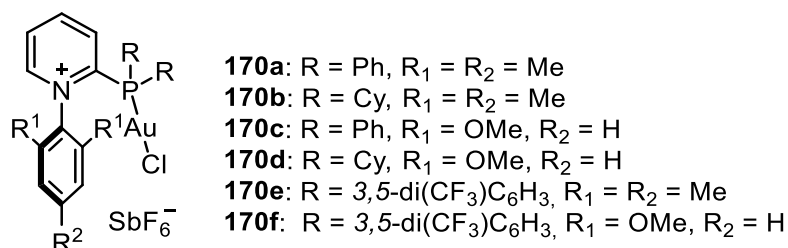
Scheme 59: Cationic pyridiniophosphine gold complexes.

3.1.2 Electronic properties

With the synthesis, characterization, steric evaluation and initial catalytic applications done by Tinnermann[71], the initial task was to evaluate the electronic properties of the ligands. For this the Tolman electronic parameter should be measured or calculated. As the synthesis of Ni-complexes with similar cationic ligands failed due to the low stability of the resulting complex, and the synthesis of rhodium complexes analogue to Vaska´s one lead to deformation of the ideal square planar structure of the complex due to the steric demands of the ligands, we used the model complex usually used by the Nolan group instead (Scheme 60). They have prepared Iridium-CO-complexes of bulky diarylphosphines like XPhos and were able to measure the corresponding stretching frequencies. From these stretching frequencies, the TEP could easily be calculated.[105]
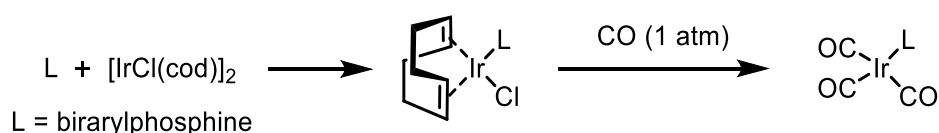
Scheme 60: General synthesis by Nolan for iridium complex suitable for TEP-evaluation.

However, the presence of a pyridine instead of a benzene in the upper ring led to a different outcome in the first reaction step. Although the coordination of the ligand took place, compound **171** could not be isolated in clean form. Instead, the reaction proceeded with a C-H insertion of the iridium into the *meta*-C-H bond of the pyridinium, leading to structure **172** with a four-membered ring (Scheme 61).
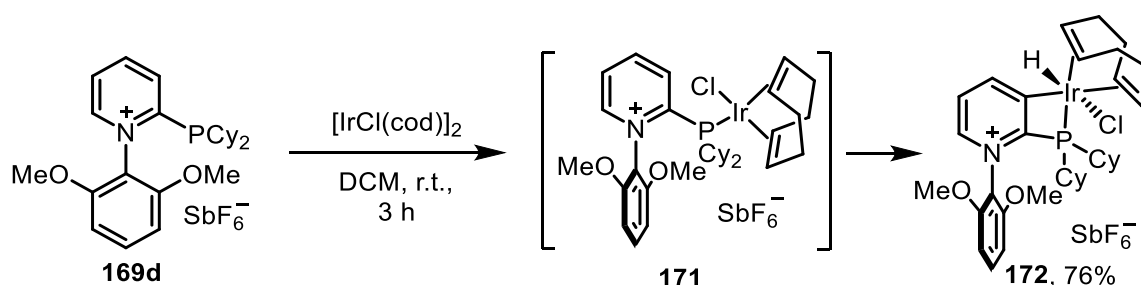
Scheme 61: Synthesis of four membered iridacycle **172**.

The ^{1}H-NMR spectrum of structure **172** clearly shows the hydride present at the iridium at -14.81 ppm. The connectivity could be proven by X-ray analysis, which is shown in Figure 12.
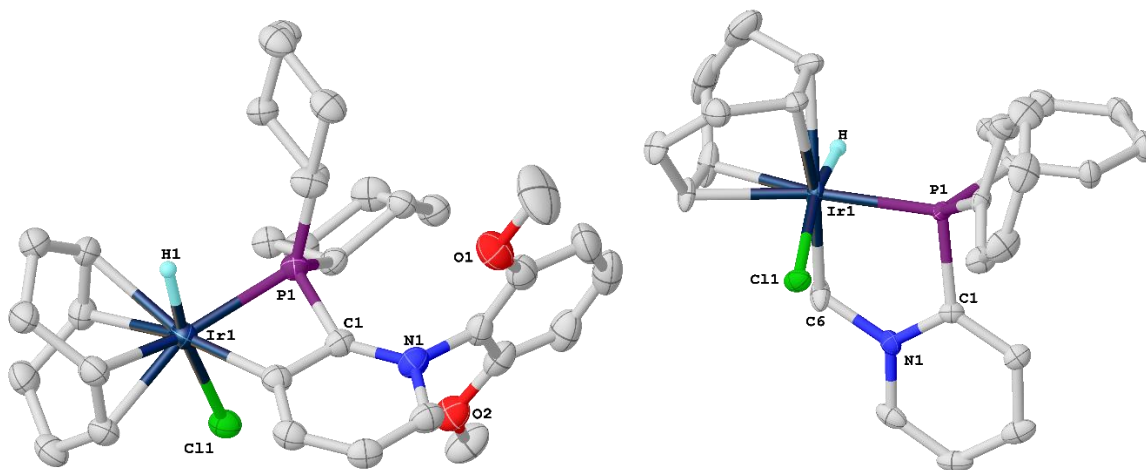
Figure 12: Molecular structures of **172** and **174**. Hydrogen atoms except the hydride and anions are omitted for clarity. Anisotropic displacement parameters are shown at 50% probability level.

Intrigued by this reactivity, we checked another ligand in this reaction. The choice fell upon compound **173**.[67] This compound has phenyls instead of cyclohexyls as substituents on the phosphorus, but more importantly, only has a methyl group as substituent on the nitrogen and not an aryl. With this starting material, the iridium can either form a four-membered ring as in the example above, or a five-membered ring, if the C-H activation happens on the methyl group instead. Comparing these two possibilities, the five-membered ring should be more stable, as the ring strain is reduced. And indeed, with this ligand a five membered ring was formed as the only product (Scheme 62). For this compound the hydride was found at -15.37 ppm in the ^{1}H-NMR. The different geometry around the phosphorus greatly influences the chemical shift in the ^{31}P-NMR. While in molecule **172** the phosphorus signal was found at -6.79 ppm (Ir1-P1-C1 angle: 81.76°), it shifted by nearly 40 ppm to 32.27 ppm (Ir1-P1-C1 angle: 101.21°) in compound **174**, farther than expected due to the change of substituents from cyclohexyl to phenyl on the phosphorus. Interestingly, the hydrogen atoms on the carbon C6 bridging the iridium and the nitrogen have two distinct signals at room temperature, indicating a rigid conformation.
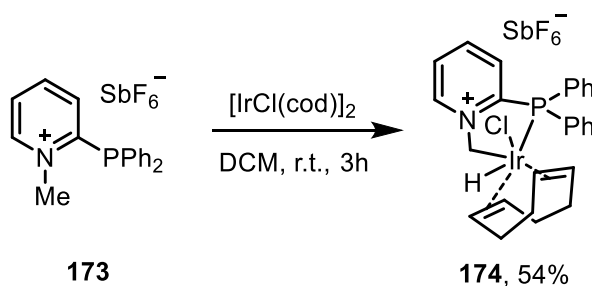
Scheme 62: Synthesis of the five membered iridacycle.

Although these results were very interesting, it prevented us from obtaining the electronic values via IR-measurements. For this reason, we used voltammetry instead. Table 2 shows the obtained results by squared-wave voltammetry. The values are in the same range as the standard phosphite **2** and in the same range as the alkyl-substituted compound **173**. Also the

ligands follow the expected behavior, with the phenyl-substituted phosphines (**169a** and **169g**) being slightly more electron-withdrawing then their cyclohexyl-substituted counterparts (**169b** and **169h**). A difference between the mesityl- (Entries 3 and 4) and the di(isopropyl)phenyl-substituted pyridiniums (Entries 5 and 6) could also be observed. Most likely because of their stronger +*I* effect, the substitution with isopropyl makes the whole ligand less electron withdrawing, with the two isopropyls outcompeting the three methyl groups of the mesityl in this regard. Sadly, we were not able to obtain the oxidation potentials for the four ligands with either methoxy or trifluoromethyl substituents, as their cyclic and squarewave voltammograms did not show a clear oxidation peak.

Table 2: Electrochemical oxidation potentials of selected ligands. Referenced against Fc/Fc$^+$.

Entry	Ligand	E_p(ox) /V
1	**2**	1.287
2	**173** (BF$_4$ as anion)	1.285
3	**169a**	1.302
4	**169b**	1.271
5	**169g**	1.287
6	**169h**	1.225

For molecules **169c** and **169d** the supposed oxidation peak was only visible as a small shoulder, so no exact maximum could be defined. In the case of **169e** and **169f**, which should have the highest oxidation potentials, the first visible oxidation in the CV and SWV was the oxidation of the solvent (DCM), where the oxidation peaks of the tested molecules have no chance of standing out from.

3.1.3 Catalytic experiments

With the electronic properties determined, the in next task was to find new catalytic applications for the corresponding gold complexes **170a-f**. The main obstacle in this regard was not to achieve reactivity but to tune the reactivity in a reasonable fashion. Often the system proved to be to reactive leading to mixtures or decomposition. In some cases the silver salt needed for activation of the catalyst was enough to promote the reaction, resulting in unselective behavior.

The first reaction looked at was the synthesis of oxazoles as described by Teci *et al.*[106] and Hashmi *et al.*[107]
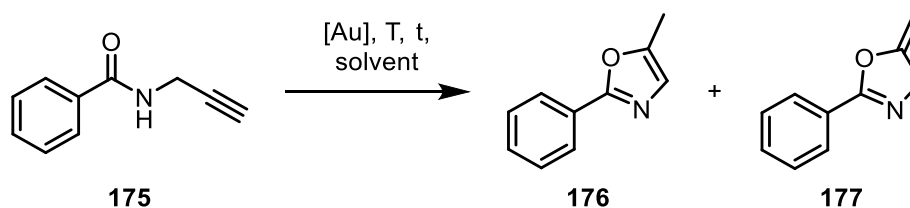
Scheme 63: Synthesis of oxazole by gold catalysis.

For this reaction, usually gold(III)-catalyst are employed. With simple AuCl$_3$ product **176** could be achieved in excellent yields (Table 3, Entry 1).[107] Teci *et al.* then tried the reaction with their NHC Au^I and Au^{III}-catalysts (Scheme 64). Catalysts **178** produced only very poor conversions, while catalysts **179** produced product mixtures (Table 3, entries 2 and 3). This can be explained considering the electronic properties. Au^{III} is quite electron deficient and while the additional chlorides in AuCl$_3$ enhances this behavior, a NHC-ligand diminishes it. The Au^I-complex is more electron rich, thus resulting in the bad conversion. As our catalysts are extremely electron poor for Au^I-catalysts, they may be able to yield higher conversions in this reaction in contrast to other Au^I-catalysts tested, hence we chose this reaction as the first benchmark.

178a: Saturated
178b: Unsaturated

179a: Saturated
179b: Unsaturated
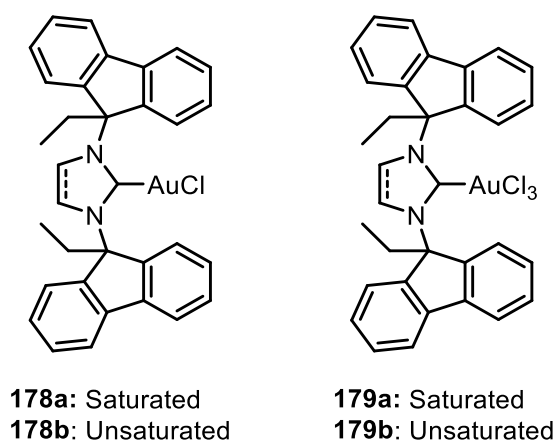
Scheme 64: NHC-gold-complexes.

Although our catalysts were indeed superior to the previously employed Au(I)-catalyst, yielding product **177** in excellent yields and good selectivities, the same is true for the standard AuClPPh$_3$-catalyst (Table 3, Entry 13). As our catalysts are more difficult to prepare and therefore more expensive, it is not cost-efficient to employ them in this synthesis. Entries 7 and 8 show that gold is needed for the reaction to proceed, as the reaction does not work with AgSbF$_6$ or triflic acid alone. Our catalysts were able to produce compound **177** in under 3 hours, while the other catalyst did not achieve complete conversion even after 24 h. We could match the low catalyst loadings reported in the literature of 2 mol% and even reduce them to 1.5 mol% (Entries 9 and 10). Catalyst loadings of 1% were also tried in this reaction, but the results were not reliable and varied over the different experiments. With the simple AuClPPh$_3$-catalyst, reaction with catalyst loadings of 1 mol% provided reproducible results (table 3, entry 14).

Table 3: Results of the catalytic synthesis of oxazoles.

| Entry	Catalyst (mol%)	T / °C	t / h	Ratio		Conversion %
				176	177	
1	AuCl$_3$ (2)[a]	20	12	99	1	95
2	179a (2)[b]	20	24	42	58	76
3	179b (2)[b]	20	24	5	95	68
4	170b (5)	20	3	1	99	91
5	170a (5)	20	3	2	98	>99
6	170a (2)	20	3	1	99	>99
7	- (5)[c]	20	3	-	-	-
8	Triflic acid (5)	20	3	-	-	-
9	170a (1.5)	20	3	1	99	97
10	170d (1.5)	20	3	1	99	>99
11	AuCl/P(C$_6$F$_5$)$_3$ (5)	20	3	3	97	>99
12	AuClPPh$_3$ (5)	20	3	1	99	>99
13	AuClPPh$_3$ (2)	20	3	1	99	>99
14	AuClPPh$_3$ (1)	20	3	2	98	91
15	170a (5)	50 (DCE)	5	79	21	>99
16	AuClPPh$_3$ (5)	50 (DCE)	5	30	70	>99
17	-[d]	50 (DCE)	5	1	99	>99

Conversion, yields and ratio determined by ^{1}H-NMR. [a] comparison with reaction reported by Hashmi *et al.*[107] [b] comparison with reaction reported by Teci *et al.*[106] [c] only AgSbF$_6$, no catalyst [d] pure **177** was used in the reaction, without any catalyst or silver salt.

As the next step, the effect of a higher temperature was investigated. This resulted in a positive outcome, leading up to 79% yield of **176** at 50 °C in DCE (table 3, entry 15). But also here AuClPPh$_3$ showed a similar behavior, resulting in 30% yield of **176**. On reason for the low yield of **176** could lie in the short reaction time, as Hashmi *et al.* showed in their kinetic study that **177** was quickly formed, up to a concentration of 80% after just 20 minutes, and then slowly converted to **176** over a longer period of time.[107] As Entry 17 shows that there was almost no conversion of **177** into **176** by simply heating, there has to be an additional effect of the catalyst on this process. At this point this project was stopped, as we failed to outcompete considerably cheaper catalysts in terms of yield and selectivity.

As this project was not successful another attempt was undertaken to test the catalyst in other interesting reported reactions. For example the type of reaction shown in Scheme 65, which can yield, depending on the catalyst and the reaction conditions, four different products.[108]

The reaction with PtCl$_4$ at 60 °C in ethanol yields the isoquinoline **182a** as the main product, while the addition of a simple base, in this case Na$_2$CO$_3$, in ethanol at 60 °C leads to isoindole **182b**. Au^I-catalysts yield the oxygen-containing heterocycles. In case of sterically demanding ligands like XPhos isochromene **181a** is obtained, while with very electron-deficient ligands, the isobenzofurane **181b** is obtained as major product, although small amount of isochromene can be found as well.
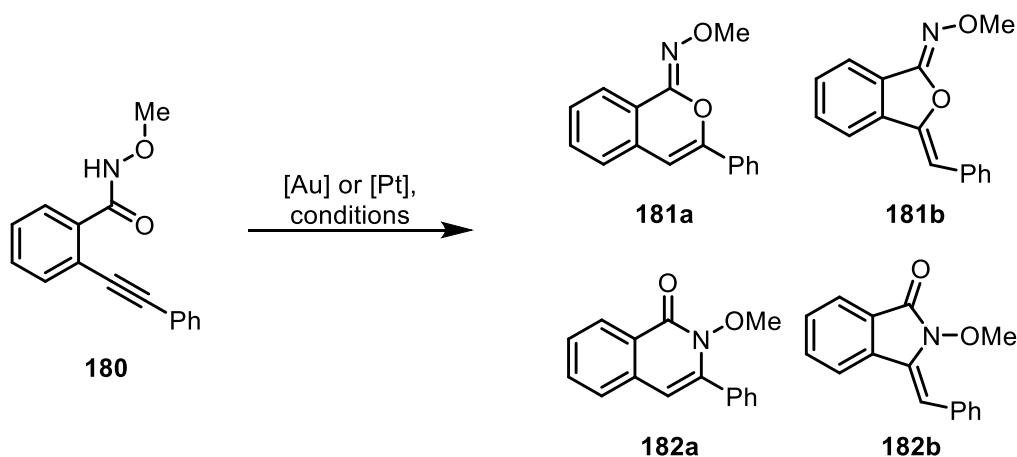
Scheme 65: Gold and platinum catalyzed synthesis of different 5- and 6-membered O- and N-heterocycles from one single starting material.

The benchmark for our results are the two most selective results regarding gold catalysis from the aforementioned paper.[108] Using XPhosAuNTf$_2$ as catalyst at room temperature for 8 h in DCE they were able to obtain **181a** in 91% yield with no major side product. For the obtainment of **181b** the best system proved to be (2,4-di-tert-butylphenoxy)$_3$PAuOTf in ethylbenzene at room temperature for 8 h. They were able to obtain 84% yield of **181b**, but with **181a** as a side product with 11% yield.

Scheme 66 shows a comparison of XPhos **183** with cationic **169**. They are quite similar, but most prominently, **169b** misses the increased steric bulk of the isopropyl groups. From an electronic point of view, our ligand should be more similar to the phosphite employed in the reaction favoring **181b**. As the authors argued the product distribution is directly influenced by steric and electronic properties, using our catalysts might be a way to determine which effect is dominant over the other.
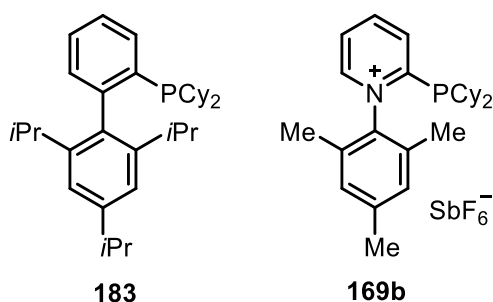
Scheme 66: Comparison of different ligands.

The results showed indeed that our catalyst combined to values of both the previously employed catalysts from the reference, as product mixtures were obtained.

Table 4: Results of the catalytic synthesis of isochromenes and isobenzofuranes.
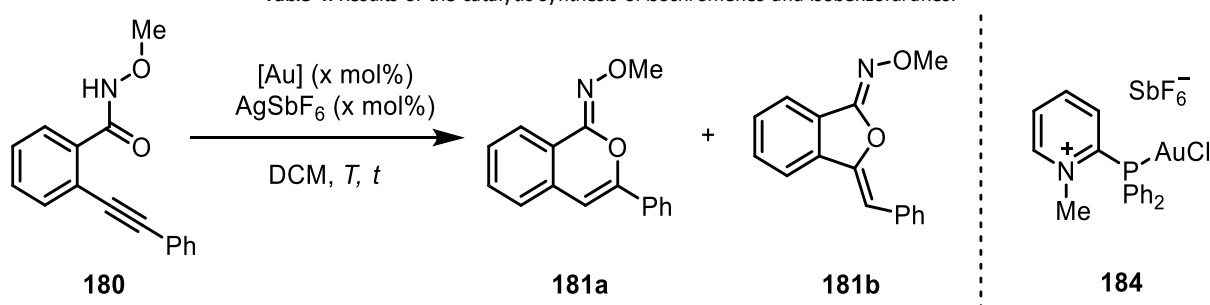
| Entry	Catalyst (x mol%)	T / °C	t / min	Yield of 181a[a]	Yield of 181b[a]
1	170a (5)	20	10	68	32
2	170a (5)	20	5	69	31
3	170a (2.5)	20	5	71	29
4	170d (2.5)	20	5	71	29
5	170e (2.5)	20	5	79	21
6	170c (2.5)	20	5	70	30
7	170a (5)[b]	20	5	55	45
8	170a (2.5)	0	7	45	29
9	170a (2.5)	0	60	58	42
10	170a (2.5)	-20	300	58	42
11	170a (2.5)	-78	300	-	-
12	184 (2.5)	20	5	84	16

[a] yield determined by ^{1}H-NMR referenced against a standard; [b] dichlorobenzene was used as solvent.

The first observation was a tendency of our catalysts to lead to mixtures, but also to prefer **181a**, the product preferred in the reaction with the sterically demanding biaryl-phosphines. This suggests sterics might play a bigger role than electronic properties. This is supported by the fact that catalysts **170a**, **170c** and **170d** all yield similar ratios, despite being electronically different. An outliner is **170e**, which is more electron poor, but increases the amount of **181a** even further (Table 4, Entry 5). The influence of the solvent was also briefly investigated. When using an aromatic solvent like dichlorobenzene instead of DCM, the ratio shifted to 55:45. Similar ratios were obtained when the temperature was lowered, but no difference other than an increased reaction time could be seen when comparing the reaction at 0 °C and -20 °C. At -78 °C only the starting material could be reisolated.

With this inconclusive results in hand, we decided to test the previously prepared catalyst **184**[67] in this reaction, which did not have a biaryl structure like **170**, but still has similar electronic properties. Interestingly, this shifted the ratio even more towards **181a**, which contradicts the hypothesis by Ding *et al.*[108] of electron poorer ligands favoring **181b**. As a conclusion, our cationic phosphines showed reactivities in this reaction, which greatly deviated from classical phosphines.

As a last attempt in this project it was tried to coordinate the ligands to other coinage metals, as this would lead up to new interesting catalysts, which are also cheaper to prepare and could be used in different reactions than the gold complexes (Scheme 67).
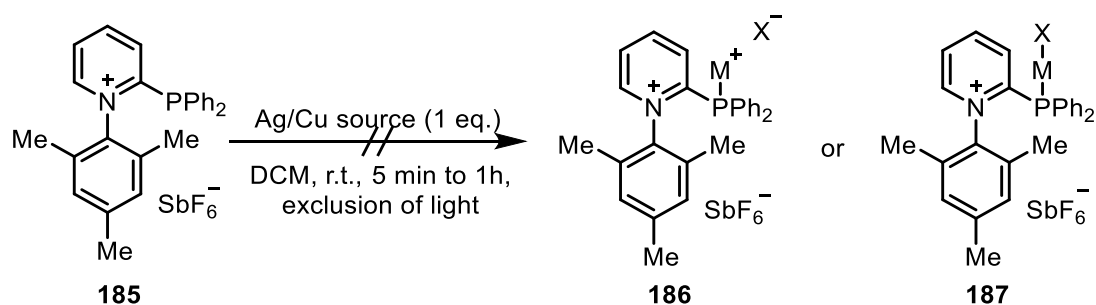
Although many different reaction conditions and silver sources (e.g. $AgSbF_6$, $AgBF_4$, AgCl, AgOTf) were tried, no synthetic useful amounts of the desired complexes could be obtained. The reactions were set up under the exclusion of light and analyzed by NMR under inert conditions, but the ^{31}P-NMR never showed promising signals, only starting material and small amounts of decomposition products. In one of the reactions with AgOTf, a promising mass-to-charge ratio was detected by HR-MS, but also in this case the amount was so small, that the peak of this species could not be seen in the ^{31}P-NMR-spectrum.

The same was true for the tests with copper, using $CuBr(SMe_2)$ as a more refined metal source. Although an analogue of the commonly used gold source $AuCl(SMe_2)$, for copper no metal complexes could be obtained.

The possible reason for the failings of the other coinage metals in coordination to our ligands may lie in their less pronounced affinity for phosphorus, resulting in a weaker metal-ligand bond and unstable complexes. A possible solution may be the introduction of another coordination site in reasonable geometry to the coordinated metal-to-be, to achieve a chelating effect and more stable complexes. But this was not investigated further, bringing this project to an end.

3.1.4 Summary
As a short summary, we were able to obtain the electronic properties for some of the cationic biaryl-phosphines synthesized previously in our group. The coordination to iridium led to interesting results regarding the intramolecular C-H-activation of our ligands by iridium. We also checked our metal complexes in two different catalytic experiments, but this did not result in the desired outcome.
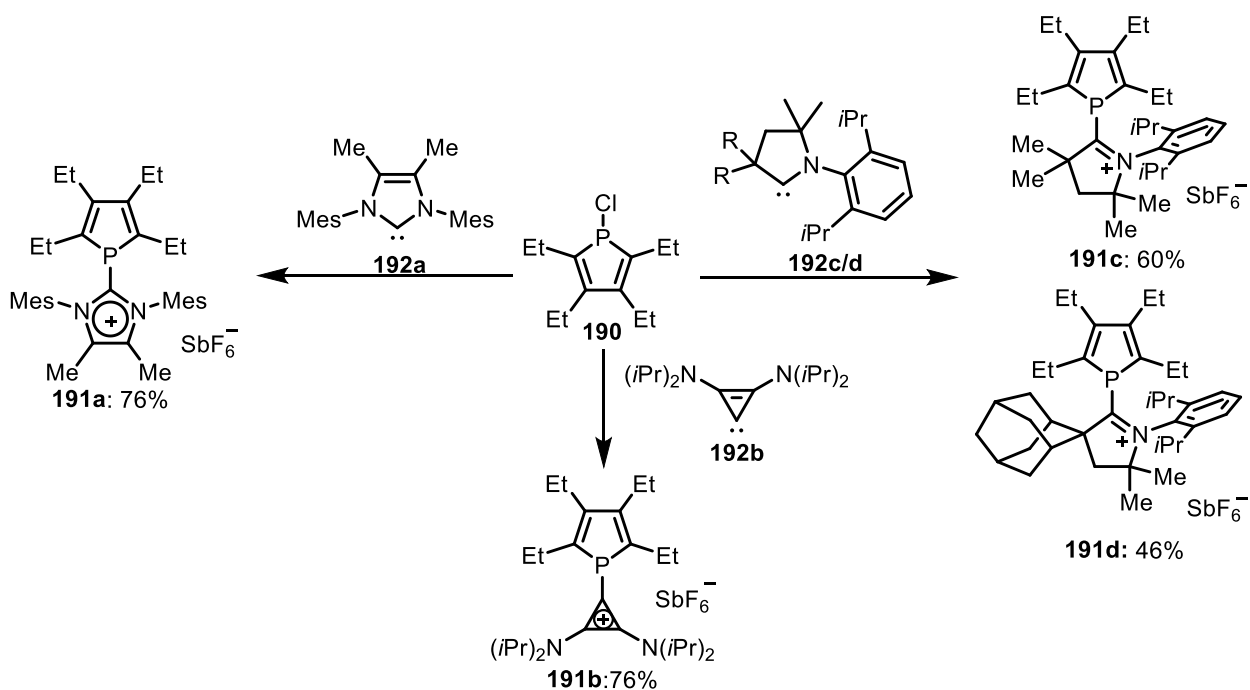
3.2 Cationic phospholes

3.2.1 Synthesis

For the reason stated in chapter 1.2 we wanted to change the substituent on the phosphorus of two aryls or alkyl groups to a phosphole, thereby exchanging two substituents for one connected ring while maintaining the cationic charge in α-position. The phospholes were synthesized by the method developed by Fagan and Nugent.[24] The phosphole could be synthesized in decent yields over two steps from commercially available starting materials. Although most alkynes would work in this reactions, 3-hexyne was chosen as it is symmetrical and only leads to small ethyl-substituents on the final phosphole, but its boiling point of 81 °C makes it easier to work with than 2-butyne with a boiling point of only 27 °C. To synthesize chlorophosphole **190**, two equivalents of the alkyne **188** were inserted into zirconocene dichloride, yielding the zirconocyle **189** in good yields. The zirconocene moiety was then exchanged for phosphorus by the addition of PCl_3, yielding the desired compound **190** as yellow oil. As the ^{1}H-NMR showed additional signals, the product was purified by Kugelrohr-distillation and stored under inert gas.
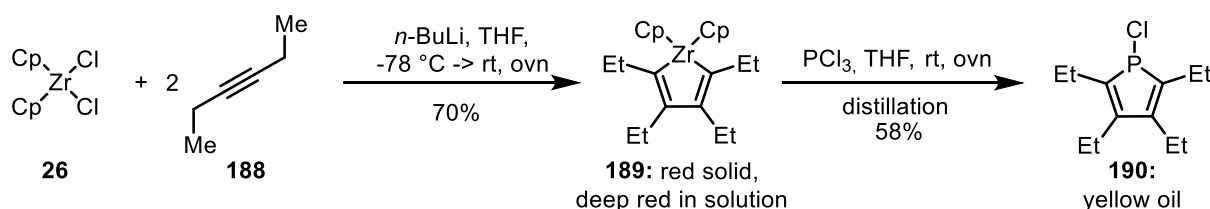
Scheme 68: Synthesis of chlorophosphole.

The chlorophosphole could then be converted into the cationic phosphole by adding the corresponding isolated carbenes at -78 °C (Scheme 69). The used carbenes, 1,2-(diisopropylamino) cyclopropenyl-1-ylidene, 4,5-di(Me)IMes and two cAACs with different steric demands, are all well known in literature. To change the counterion from chloride to hexafluoroantimonate dry $NaSbF_6$ was added. The $NaSbF_6$ could be added at any time after the addition of the free carbene and as long as it was properly dried, no effect on the yield could be seen. To purify the products, the supernatant was filtered of and the residue washed with pentane. The solid was then dissolved in DCM and filtered to remove the inorganic salts. The solvent was subsequently removed *in vacuo* to yield the corresponding products as white (**191a**), off-white (**191b**), yellow (**191c**) or orange (**191d**) crystalline solids. The yield range between good with 76% for **191a** and **191b** to acceptable with 46% for **191d**. The reason for the in comparison poorer yields for **191c** and **191d** stemmed from the fact that the workup did not yield clean product, but a mixture with a small amount of the reprotonated carbene which was used in the reaction. Although we thoroughly tried to remove any possible proton source from the reaction, we were still unable to obtain a clean product without further purification.

Scheme 69: Synthesis of cationic phospholes.

The proton source in question is not likely to be water, because under the same reaction conditions, only the reaction to **191c** and **191d** showed this behavior, while **191a** and **191b** were still obtained clean. As a result, we assume the proton source could only be deprotonated by **192c** and **192d** and not the weaker bases **191a** and **191b**. However **191c** and **191d** can be purified by column chromatography, as they are stable under air and on the column. **191a** and **191c** were further tested for stability towards air and could be kept on air for a month without showing signs of decomposition; storing them under inert conditions for longer periods of time is anyway advised. The syntheses for **191a-c** can be scaled up to gram scale, tested up to 1.24 g of product in the case of **191c**, but at the cost of a slightly decreased yield. All ligands could be crystallized easily from DCM/pentane or DCM/Et$_2$O to yield crystals suitable for X-ray diffraction. Their molecular structures are shown in Figure 13.

For our newly synthesized structures, the sum of angles around the phosphorus showed with values between 302.65° and 311.15° in all cases a strong pyramidalization of the phosphorus, hinting to the presence of an active lone pair available for coordination. The degree of pyramidalization is also considerably influenced by the steric bulk. For example **191c** and **191d** are on the opposite ends of the scale for the tested ligands, although they both share the CAAC backbone and should have similar acceptor properties. The P1-C13 distances range between 1.806 and 1.894 Å, showing in comparison a shorter phosphole-carbene bond for the cyclopropenium and IMes-backbones and a longer bond for the two CAAC-variants. The P1-C1 and P1-C4 bond lengths differ little between the different molecules and are all within the 1.80-1.82 Å range. This differs massively from the C-C-bond distances within the phosphole (for **191c**: C1-C2: 1.365(9); C2-C3: 1.471(9); C3-C4: 1.354(9)), strongly suggesting an extremely weak, if not complete lack of aromaticity in the phosphole

ring. This is further supported by the displacement of the phosphorus atom out of the plane defined by the butadiene moiety.

Table 5: Important bond lengths and sum of angles around the phosphorus for **191a-d.**

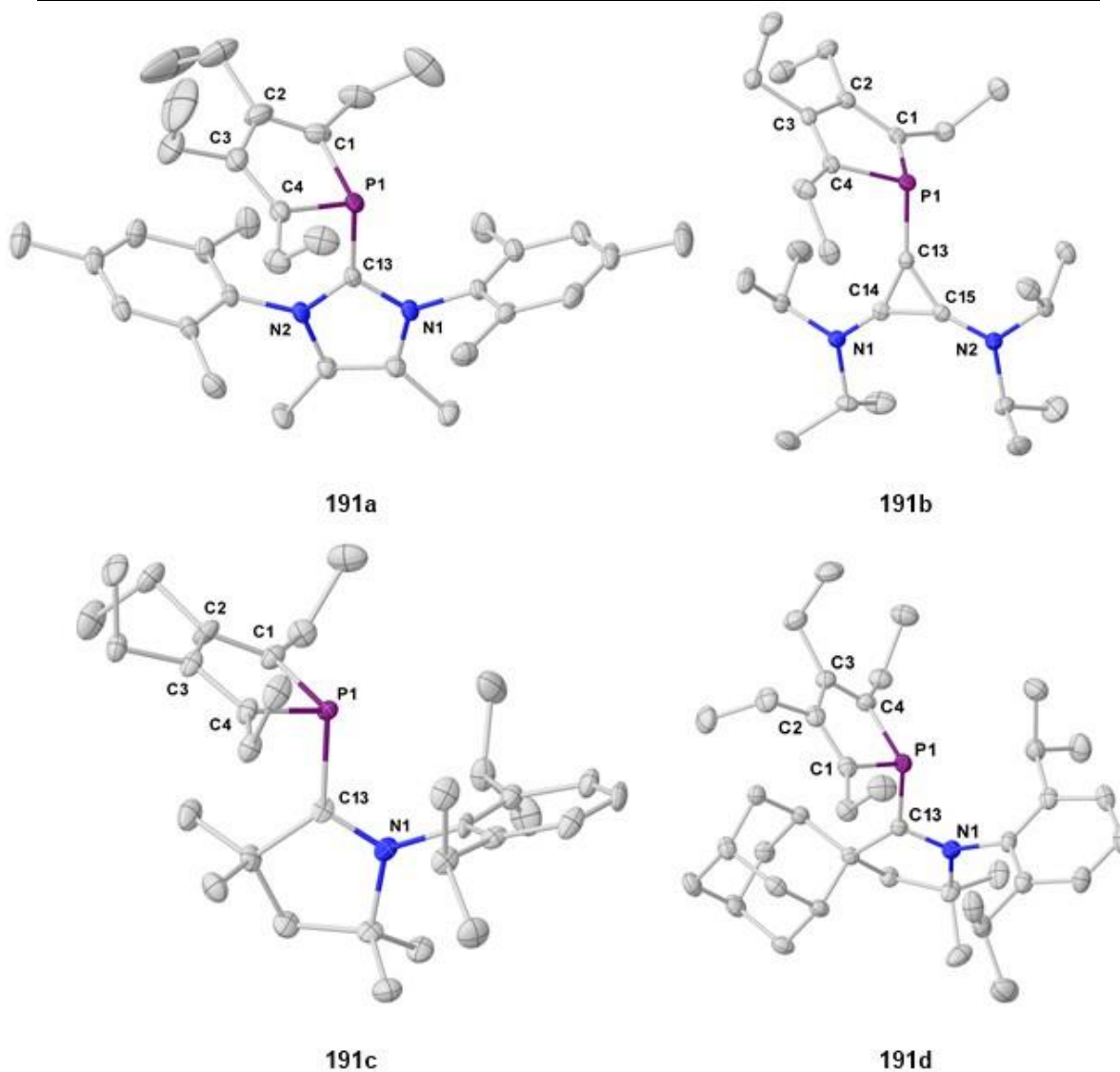| Compound	d(P1-C1) [Å]	d(P1-C4) [Å]	d(P1-C13) [Å]	pyramidalization [°]
191a	1.8048(16)	1.8013(15)	1.8275(14)	302.65
191b	1.798(2)	1.801(2)	1.806(2)	304.45
191c	1.805(7)	1.816(7)	1.867(6)	294.92
191d	1.808(2)	1.807(2)	1.894(2)	311.15

Figure 13: Molecular structures of **191a-d**. Hydrogen atoms and anions are omitted for clarity. Anisotropic displacement parameters are shown at 50% probability level.

The effect of adding a cationic rest can also be seen in the ^{31}P-NMR. While **190** is defined by a chemical shift of 3.0 ppm, **191a** (-38.3 ppm), **191b** (-41.0 ppm) and **191c** (-16.0 ppm) have a significantly upfield shift. **191d** (0.8 ppm) has a shift similar to **190**, but this may be attributed to the different geometry induced by large adamantly rest, as the ^{31}P-NMR shift is known to be strongly influenced by the geometry of the P-atom.

3.2.2 Stereoelectronic properties of cationic phospholes

With the new ligands in hand, we tried the obtain their electronic and steric properties. First it was tried to obtain the rhodium-CO complexes by reaction of the ligands with [RhCl(CO)$_2$]$_2$. This only worked with ligand **191b**, which is the sterically least demanding one, yielding molecule **193**. For **191a** and **191c** no conversion could be seen and the starting material was recovered.
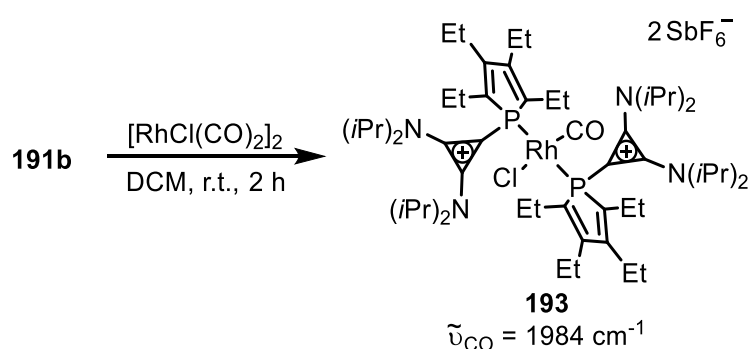
$$\tilde{\upsilon}_{CO} = 1984 \text{ cm}^{-1}$$

Scheme 70: Synthesis of the rhodium-CO complex **193**.

With 1984 cm^{-1} the stretching frequency showed similar values as depicted for the cationic pyridinio-phosphines synthesized in our group. The rhodium complex with **173** as a ligand has a stretching frequency of 1996 cm^{-1}.[71] As already known complexes with sterically demanding substituents often deviated from the desired square-planar geometry, and the molecular structure of this complex could be obtained (Figure 14), its geometry was checked. The P1-Rh1-P2 angle was the expected linear 180°, while the P1-Rh1-C1 angle with 90.15° only showed a small deviation from the desired angle of 90°. The P1-Rh1-Cl1 angle with 94.64° and the Cl1-Rh1-C1 angle with 174.01° showed however, that P1, P2, Cl1 and C1 do not all lie in the same plane, C1 displaces by roughly 6°. Although this deviation is rather small, it should be taken into consideration when comparing the stretching frequency with less bulky systems.
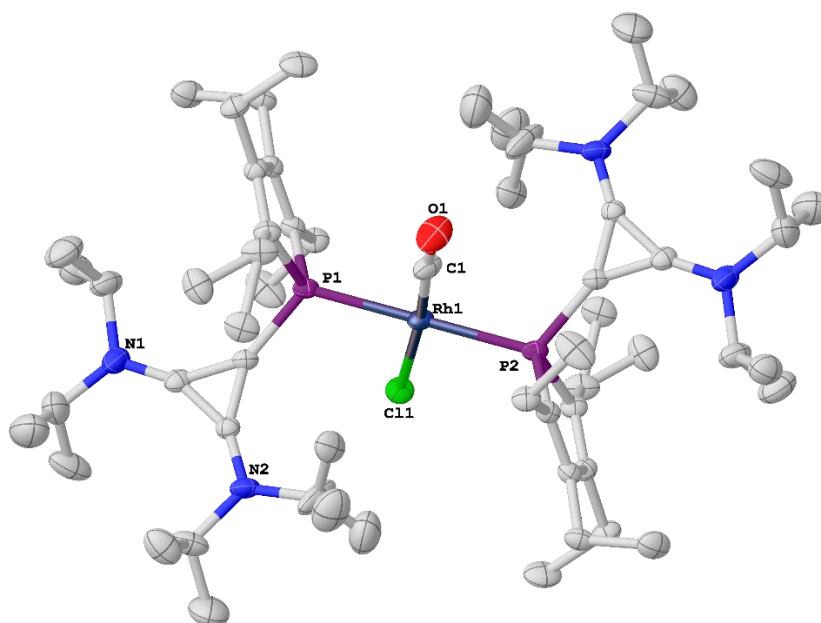
Figure 14: Molecular structures of **193**. Hydrogen atoms and anions are omitted for clarity. Anisotropic displacement parameters are shown at 50% probability level.

As the measurement of CO-stretching frequency did only work for one of our molecules, we tried to obtain the electronical values by oxidizing the compounds with selenium and measure the ^{77}Se-^{31}P-coupling constant of the resulting doublet in the ^{31}P-NMR spectrum. But also in this case only ligand **191b** yielded a satisfactory result, albeit with a low yield of only 34% (Scheme 71).
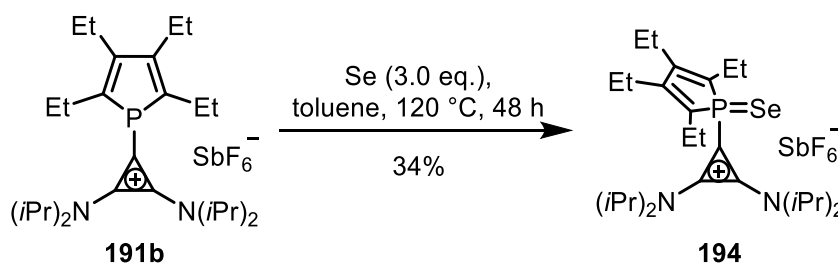
Scheme 70: Synthesis of the selenium-complex **194**.

The reaction was also tried with **191a** and **191c** as starting material under similar conditions, but no product could be found. For temperatures up to 150 °C there was no conversion, while temperatures above resulted in the complete decomposition of the starting material after 17 h. The reactions were monitored throughout the reaction time, but at no point the desired product could be observed, only the process of decomposition could be seen. Although no selenium complexes could be obtained for these two ligands, this already hints at their poor electron donor properties. As it is easier to oxidize an electron-richer atom, it can be assumed that **191a** and **191c** have less electron density on the phosphorus and should be more electron withdrawing than **191b**. We expect steric factors not to have a strong influence. Complex **194** shows in the ^{31}P-NMR a coupling constant of 763 Hz. This is a value close to complex **195** (766 Hz)[109], a triarylphosphine which is clearly more electron-

withdrawing than PPh₃ (732 Hz)[109] due to the introduction of trifluoromethylgroups in the para-positions. But as already discussed in the chapter 1.4, the coupling constant is not unaffected by steric factors and this should be taken into account when directly comparing these values.

195
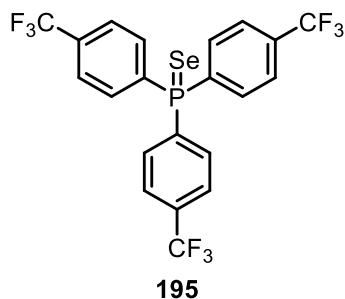
Scheme 71: Selenium-complex triarylphosphine [*p*-(CF₃)C₆H₄)]₃PSe, serving as reference for the Se-P-coupling constant.

This left cyclic voltammetry as the last option for the experimental determination of the electronic values. By SWV and referenced against Fc/Fc⁺, the oxidation potentials of the ligands **191a** (1.32 V), **191b** (1.18 V) and **191c** (1.46 V) could be determined. Compared with the biaryl-phosphines (Table 2), **191b** has a value close to **169h**, the least electron-withdrawing one, while **191a** slightly exceeds **169a** and the classical phosphite **2**, while **191c** surpasses their values by far, indicating that we were able to obtain an even more electron-withdrawing phosphine with the phosphole approach than previously with the pyridinio biaryl-phosphines.

The cyclic voltammetry experiments performed alongside the squared wave measurements revealed for **191c** and **191d** a reversible reduction at -1.512 V (**191c**) and -1.306 V (**191d**). This can be attributed to the presence of the CAAC-fragment, as **191a** and **191b** do not show them, ruling out the phosphole structure as the sole reason for the presence of these reversible processes. This result hinted at the stability of an α-radical phosphole, thus we tried to synthesize the corresponding radical by one-electron reduction through the addition of KC₈, which yielded the desired radical in poor but reproducible yields. The formation of the radical also resulted in a well observable color change from yellow to very dark green in solution and black as a solid.

191c → **196**: 30%
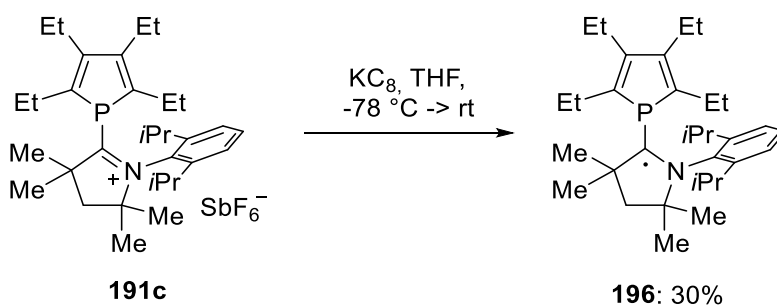
Scheme 72: Synthesis of the radical complex.

The radical could be successfully characterized by EPR-spectroscopy and X-ray diffraction. The EPR-spectrum shows a multiplet with a *g*-factor of 2.0028 and small and similar in size hyperfine coupling constants to both the phosphorus (a_P = 5.36 G) and nitrogen (a_N = 5.62 G) nuclei. In the molecular structure, differences between the radical and the cation can be found, as both the P1-C13 and C13-N1 bond lengths change considerably. While the C13-P1-bond in the radical (1.7976(9) Å) is shorter than in the cation (1.867(6) Å), the C13-N1 bond is with 1.3960(11) Å longer in the radical **196** than in **191c** with 1.309(8) Å. The reason of the shortening of the C-N-Bond in the radical most likely resulted by the weakening of the π-bond, as the added electron in the radical partly populates the C-N π*-orbital. The shorter P1-C13 bond of the radical most likely stems from the partial delocalization of the unpaired electron into a molecular orbital made up of p-orbitals of N1, C13 and the phosphole ring, as similar effects were observed for the radical phosphines developed previously by our group[110] and for systems reported by the Bertrand group, where a CAAC was added to a pyridine.[111]
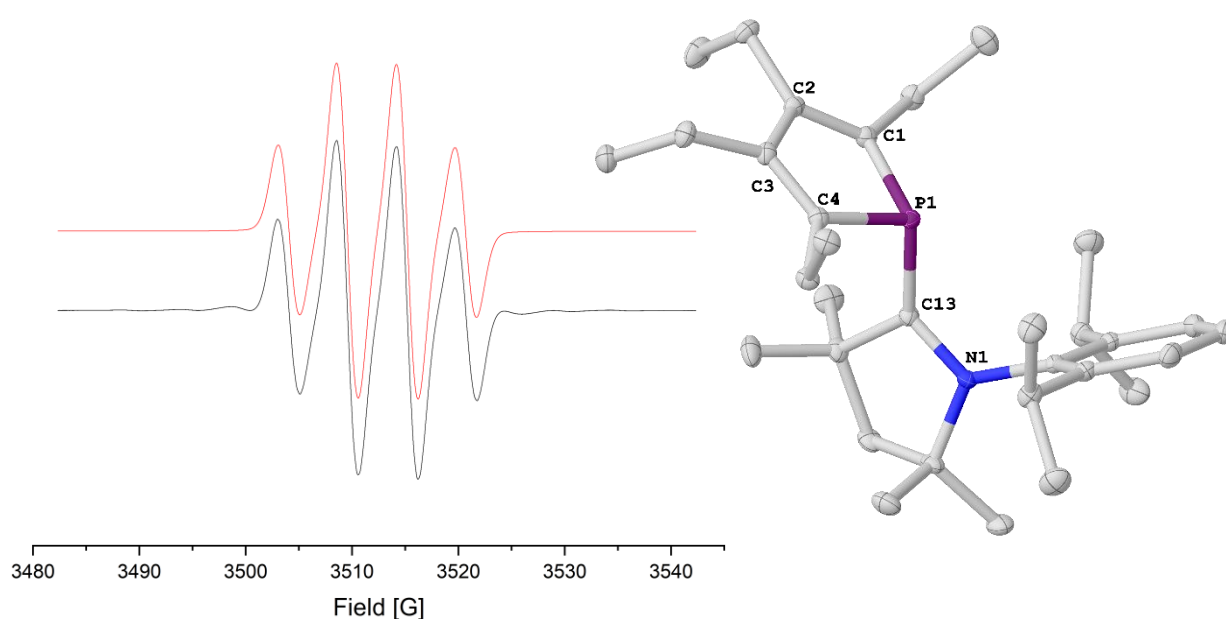

Figure 15: Calculated (red) and measured (black) EPR-spectra and molecular structure (right) of **196**. Hydrogen atoms were removed for clarity. Anisotropic displacement parameters are shown at 50% probability level.

For **196**, Dr. Christopher Golz also performed DFT calculations at the UB3LYP-D3/def2-TZVP//UTPSS/def2-TZVP level[112] resulting in a quantitative picture of the spin distribution. The plots of the localized Mulliken spin densities and the singly occupied molecular orbitals (SOMO) show the unpaired electron density to be mostly localized at the former carbene-atom, with an unpaired spin density of about 68%. Ca. 21% of the spin density can be found at the nitrogen atom, while the rest in scattered across the molecule, with the residual spin density at the phosphorus being less than 1%.
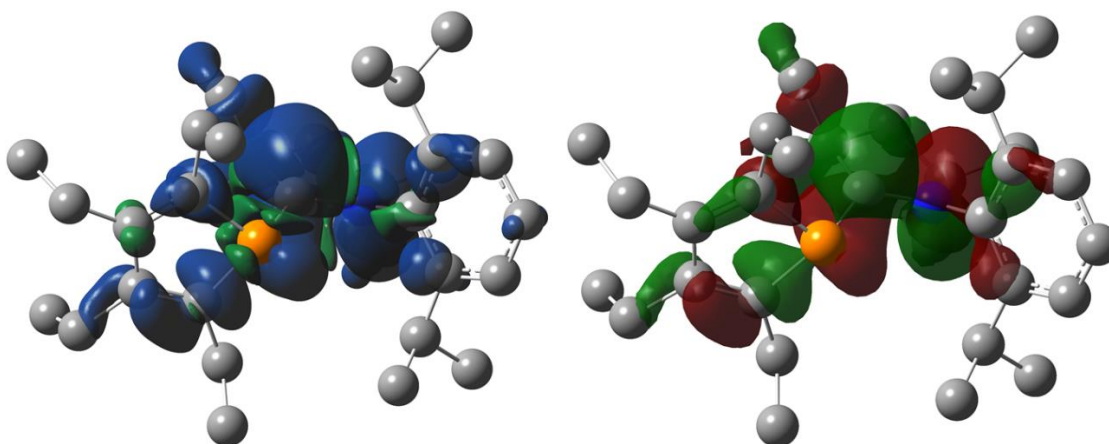
Figure 16: Calculated spin densities of **196** (left) and SOMO plot (right) at the UB3LYP-D3/def2-TZVP level. Total spin density drawn at an isosurface value of 0.0005 and SOMO drawn at 0.025.

3.2.3 Buried volume determination

To analyse the steric properties, we calculated the buried volume using the molecular structures of the gold-complexes with **191a-d** as ligands. The buried volume was estimated in a sphere with a diameter of 3.5 Å, the hydrogen atoms were omitted for the calculation. **191b** has by far the smallest buried volume with just 40.8%. This is unsurprising, as the N(iPr)$_2$-substituents on the cyclopropenium point outwards from the center and are also quite flexible. Also no side of the active center is particularly shielded.
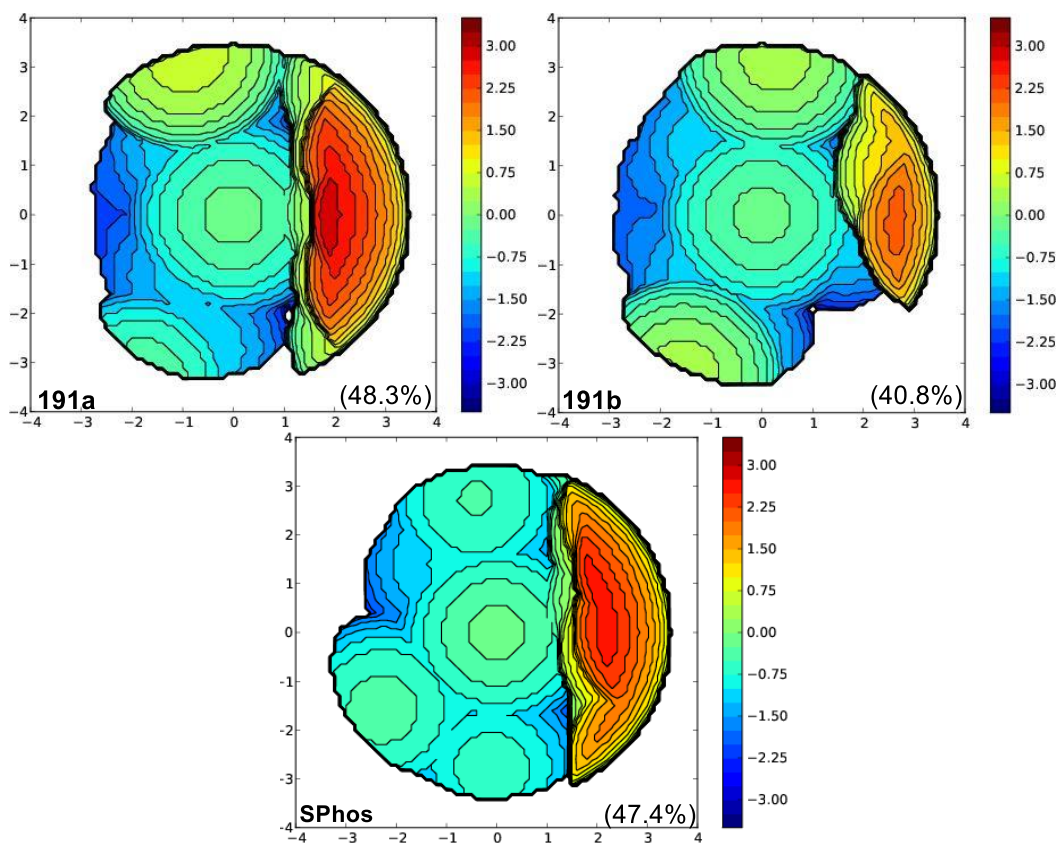

Figure 17: Topographic steric maps for **191a**, **191b** and SPhos.

The buried volume of **191a** is, with 48.3%, considerably higher. The imidazolium-structure is far more rigid with one of the mesityl substituents shielding the center. This can be seen clearly in Figure 17 as the space right to the center is nearly completely occupied. This is also a feature the Buckwald-type ligands like SPhos, which buried volume is also shown in Figure 17. The center remains well accessible from the left and bottom.

Next in line is the simple CAAC-ligand **191c** with a buried volume of 52.9%. In comparison with **191a**, the effects of the *i*Pr groups in contrast to the methyl groups can be clearly seen, as the shielding right to the center may not be as pronounced but extends much further to the top and bottom. Unsurprisingly, the phosphole with the AdCAAC **191d** has with 56.2% the highest buried volume. The shielded areas remain the same as with **191c**, but it can be seen that the shielding to the left is slightly more pronounced.
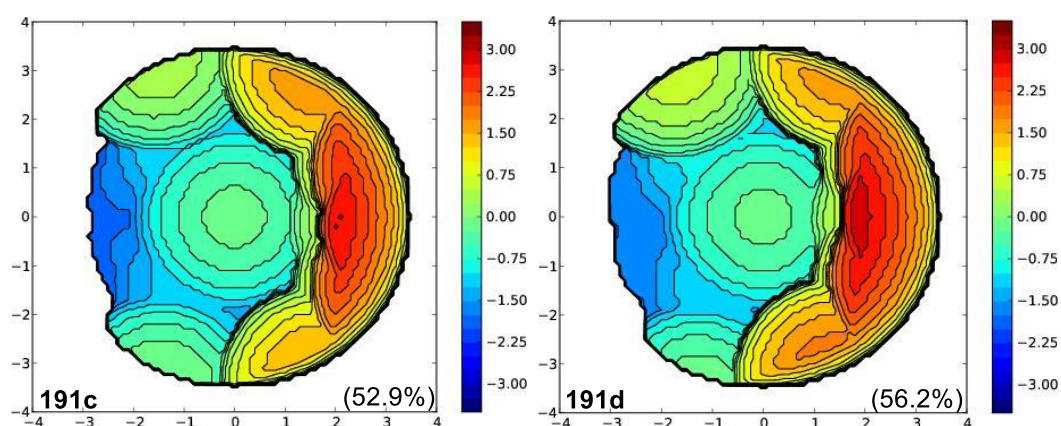

**Figure 18:** Topographic steric maps for **191c** and **191d**.

3.2.4 Oxidation reactions

To obtain references for NMR-spectroscopy and as starting material for further reactions, we deliberately oxidized the ligands **191a**, **191b** and **191c** by addition of hydrogen peroxide. In all three cases the product could be obtained in reasonable to good yields. To reduce the possibility of side reactions, we used hydrogen peroxide, a rather weak oxidation reagent and low temperatures. The product was usually obtained clean after dilution with water and extraction with DCM but it can also be easily purified by crystallisation (DCM/Et$_2$O) or column chromatography (DCM/MeOH 40:1).
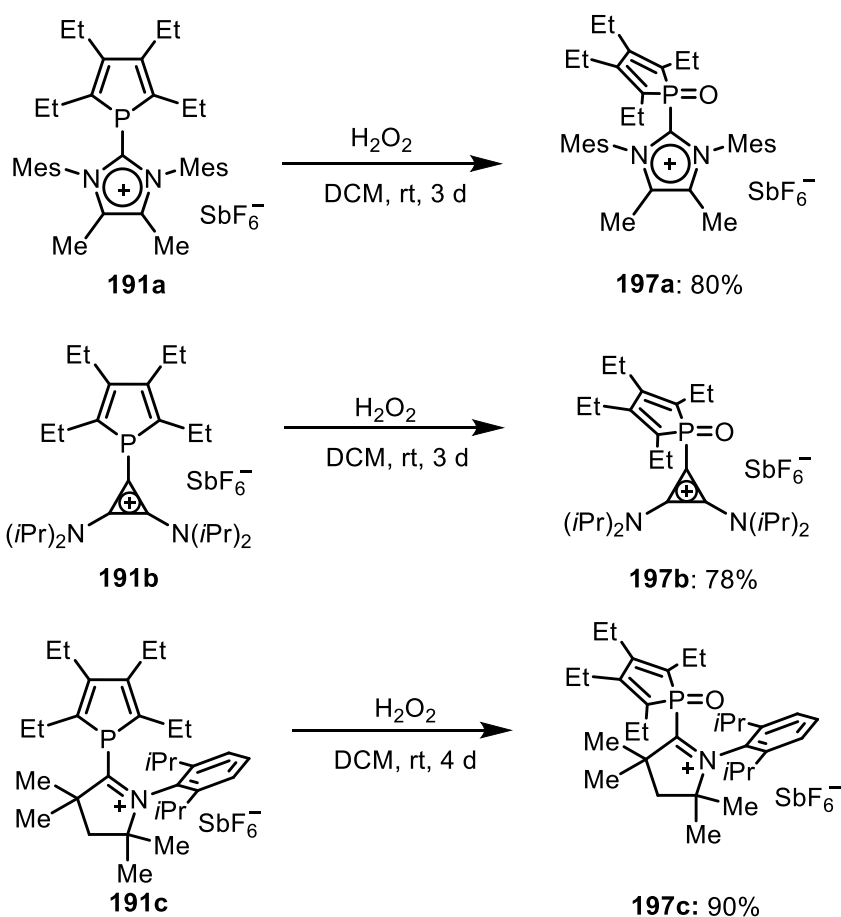
Scheme 73: Synthesis of oxidized phosphole complexes.

The crystallization of **197a** and **197c** yielded single crystals suitable for X-ray analysis. The P-C-distances are still close to the value of the unoxidized structures, but a slight decrease in the P-C-bonds in the phosphole an increase of the P1-C13 bond length was found. The bond distances of the P1-O1 differ greatly. In the more electron withdrawing **197c**, the bond length is with 1.4806(13) Å more than 0.22 Å larger than in **197a** (1.245(14) Å).
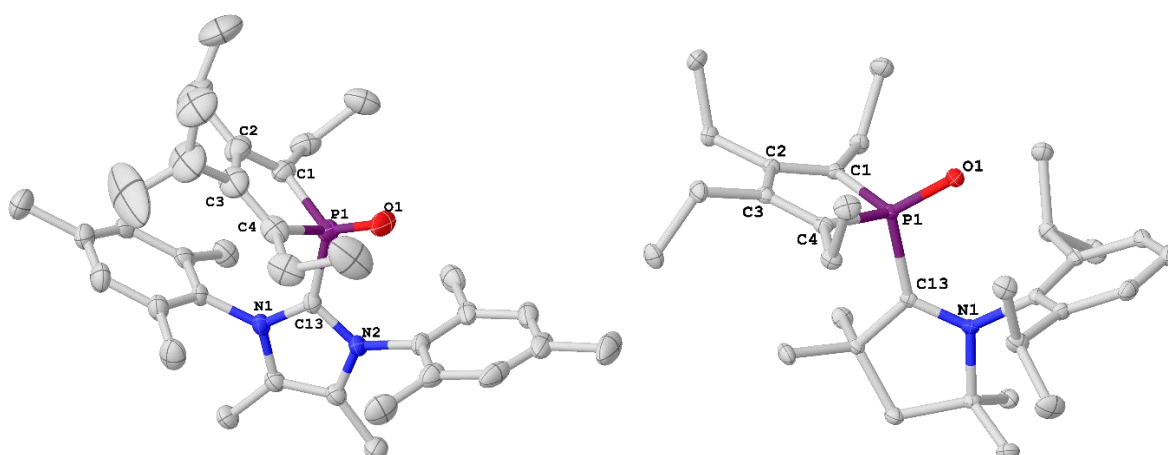
Compound	d(P1-C1) [Å]	d(P1-C4) [Å]	d(P1-C13) [Å]	d(P1-O1) [Å]
197a	1.799(2)	1.795(3)	1.831(2)	1.245(14)
197c	1.7947(12)	1.7975(18)	1.8812(18)	1.4806(13)

Figure 19: Molecular structures and table with important bond distances of **197a** (left) and **197c**. Hydrogen atoms and anions are omitted for clarity. Anisotropic displacement parameters are shown at 50% probability level.

One of the follow-up reactions tried was the activation of the oxygen with Tf_2O, following a procedure published by the Wiegand group for carbodiphosphoranes.[113] The triflate could then be exchanged for different nucleophiles, possibly resulting in a variety of new molecules. We also hoped to obtain the selenium complexes of the corresponding molecules by adding a nucleophiles selenium source like $Se(TMS)_2$. This however did not work. Upon treating **191a** with triflic acid in MeCN at room temperature for 12 h, only a complex mixture of products was obtained.

Besides the classical oxidation, it was also tested how compound **191a** would react with XeF_2. This strong fluorinating agent should be able to oxidize the cationic phosphine to its P^V-analogue (Scheme 74). Indeed, promising new peaks could be found in the ^{31}P- and ^{19}F-NMR spectra, but unfortunately a mixture of a least 3 different compounds was obtained and could not be separated. Multiple attempts of crystallization were unsuccessful.
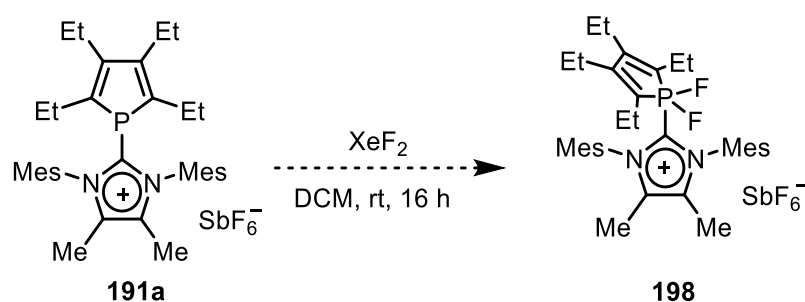
**Scheme 74:** Attempted fluorination of **191a**.

3.2.5 Diels Alder-reactions

At this point, we also tried to alter the complete phosphole structure. The first reaction that came to our minds was the Diels-Alder reaction, since phospholes should easily react as a diene in this reaction. As dienophiles, three candidates were tested: the commercially available diethyl acetylendicarboxylate **199**, the pyrrole-dione derivative **200**, which can be synthesized in two steps from commercially available starting materials[114] and is known to engage in Diels-Alder reactions with electron-poor phosphines[115] and benzyne **201**, which was prepared *in situ* due to its high reactivity.
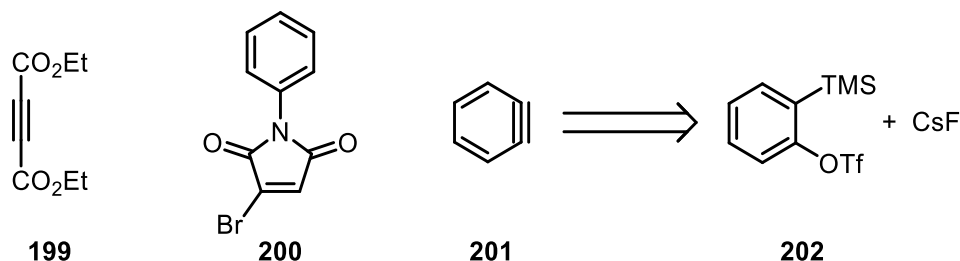
Scheme 75: Dienophiles for Diels-Alder reactions.

From these three dienophiles, only **201** was reacting with **191c**. With **199** and **200** there was no conversion at all, even when heating the reaction mixture to 160 °C in dichlorobenzene or mesitylene and stirring for 14 hours. We assume that **199** is not reactive enough and although **200** was reacting in Diels-Alder reactions at 130 °C in the literature, our phosphole is considerably electron-poorer and more sterically encumbered. In sharp contrast, **201** reacted already at room temperature with **191c**. Scheme 76 shows the reaction yielding molecule **203**, where not only the desired Diels-Alder-reaction has taken place, but an additional equivalent of benzyne was also inserted into the former CAAC-phosphole bridge. Initially the reaction was tried with less than 2 equivalents of the benzyne, which led to a mixture containing **191c**, **203** and another compound, which we believe to be the Diels-Alder product without the insertion. The unknown compound could not be separated from **203** by all purification methods tried. We tried to optimize the reaction towards this unidentified product, but in all cases only inseparable mixtures with **203** could be obtained. We then optimized the reaction towards **203** which was easy possible by increasing the amount of benzyne, resulting in full conversion if 4 equivalents of the benzyne-precursor were used.
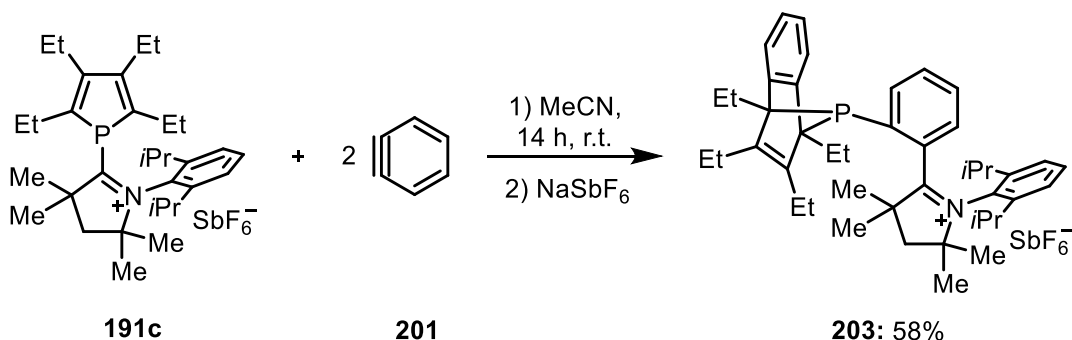
Scheme 76: Diels-Alder reaction and insertion with benzyne.

Because of the high amounts of CsF used in the reaction, usually twice the equivalents of **202**, the fluoride partially substituted the hexafluroantimonate as counterion. To counteract this, additional amounts of NaSbF$_6$ were added after the reaction. Interestingly, if complexes with both counterions are present in reasonable quantities, they can be separated from one another by column chromatography.
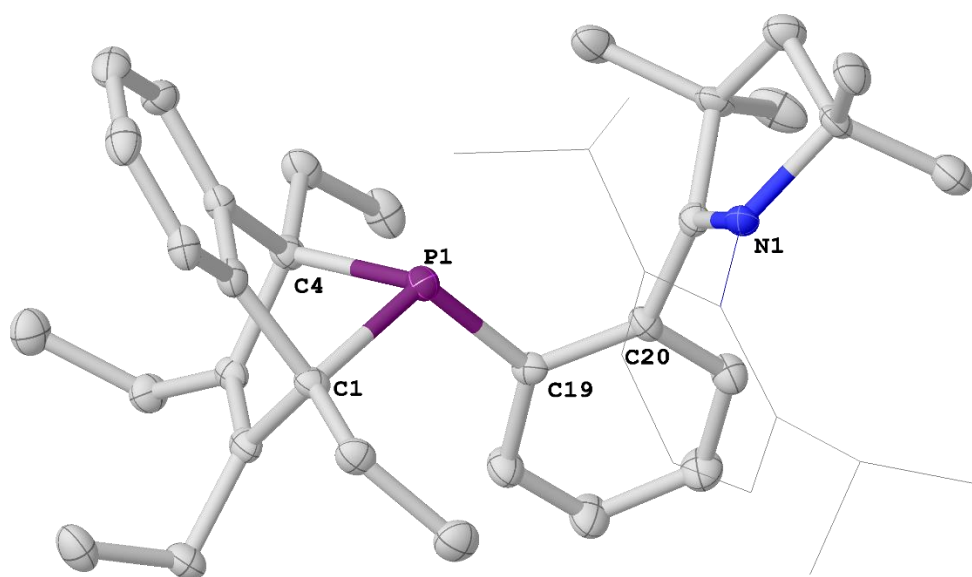

Figure 20: Molecular structure of **203**. Hydrogen atoms and anions are omitted for clarity. Diisopropylphenyl substituent displayed as capped sticks for clarity. Anisotropic displacement parameters are shown at 50% probability level.

Figure 20 shows the molecular structure of **203**. Compared to the starting material **191c**, the C1-P1 and C4-P1 bond distances increased to 1.903(5) and 1.913(5) Å, respectively. The sum of angles around phosphorus with 301.72° still emphasizes the presence of a lone pair on the phosphorus available for coordination. Due to steric reasons the success of coordination attempts seemed questionable and when tried, the compounds decomposed.

As a major drawback for this interesting reactivity, molecule **191c** seems to be only one forming a stable compound like **203**. With **191a**, **191b** and **191d** we were not able to obtain a stable compound when reacting it with benzyne. This is especially unpleasant for **191d**, as we mainly synthesized it hoping the increased steric bulk of the adamantyl-rest would prevent the insertion of the benzyne from happening. Interestingly, we were able to identify small amounts of molecule **204** in all the unsuccessful reactions. **204** could also be observed slowly appearing in solutions of **203** after several days had passed.
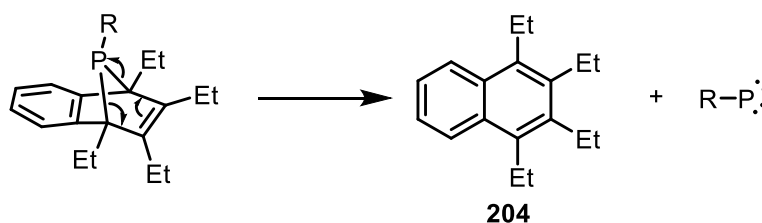

Scheme 77: 1,2,3,4-Tetraehtylnaphtalene formed by fragmentation.

With **204** being one fragmentation product, a phosphinidene should, in theory, form in the same reaction. It was tried to trap the phosphinidine by addition of 1,3-cyclohexadiene as demonstrated by the Cummins group[116], but this was unsuccessful. The presence of **204** indicates, that with **191a**, **191b** and **191d** the Diels-Alder-reaction took place as well, but the resulting complexes were prone to fragmentation.

3.2.6 Coordination chemistry

For all four phospholes, the gold complexes could easily be prepared by reaction with AuCl(SMe$_2$) in DCM at room temperature for three hours. The gold complexes were obtained in good (78%, **205b**, **205d**) to excellent yields (95%, **205a**).
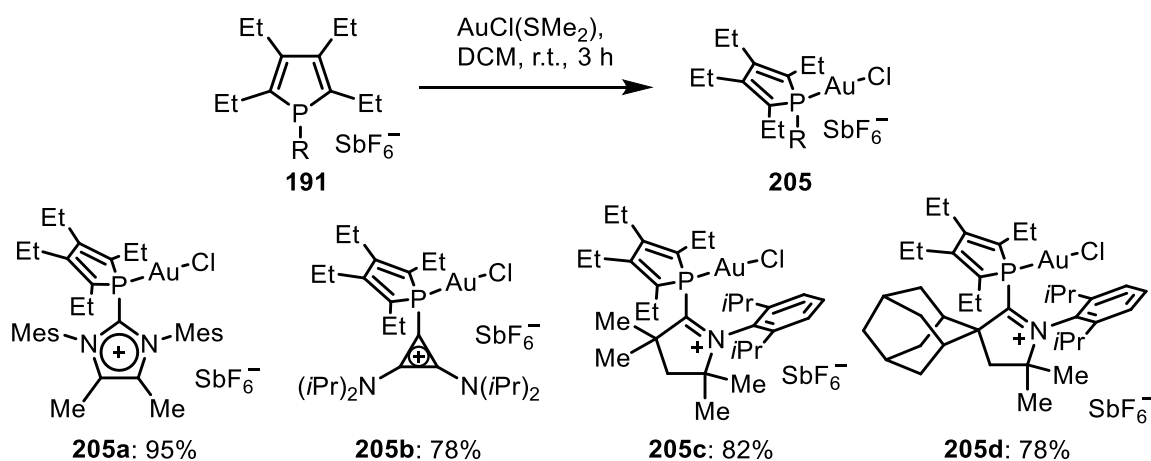
Scheme 78: Synthesis of the gold complexes.

205a-d could easily be crystallized from DCM/Et$_2$O and analyzed by X-ray diffraction. The molecular structures are shown in Figure 21 and the most interesting distances and angles in Table 6.

Table 6: Important bond lengths and sum of angles in the gold complexes **205a-d**.

Compound	d(P1-C1) [Å]	d(P1-C4) [Å]	d(P1-Au1) [Å]	d(Au1-C$_{ipso}$Aryl) [Å]	P1-Au1-Cl1 angle [°]
205a	1.795(4)	1.798(4)	2.2283(9)	3.0949(35)	175.06
205b	1.788(11)	1.794(12)	2.233(3)	-	176.49
205c	1.792(2)	1.792(2)	2.2151(6)	3.1691(22)	173.17
205d	1.803(3)	1.797(2)	2.2283(9)	2.9757(32)	174.36

When comparing the bond lengths in the phosphole moiety between the ligands **191** and the gold complexes **205**, there is hardly any difference, suggesting that the coordination of the gold to the phosphorus has little to no effect on the bonding situation inside the phosphole. The P1-Au1 bond lengths are all very similar and with values between 2.21 and 2.23 Å in the same range as neutral phosphines, for example dialkybiarylphosphine complexes.[117] In all cases, the P1-Au1-Cl1 deviates slightly from the expected angle of 180°, with **205b** being the closest the linearity with an angle of 176.49°. One reason for the higher

deviation of the other three ligands is their ability to engage in a weak intramolecular interaction between the gold and the C_{ipso} of the aryl ring in their backbone. This contact is the shortest for **205d**, as the steric influence of the adamantly in the backbone pushes the aryl ring closer to the center, but in all cases the distance is well below the sum of the van-der-Waals radii of gold and carbon with 3.360 Å.
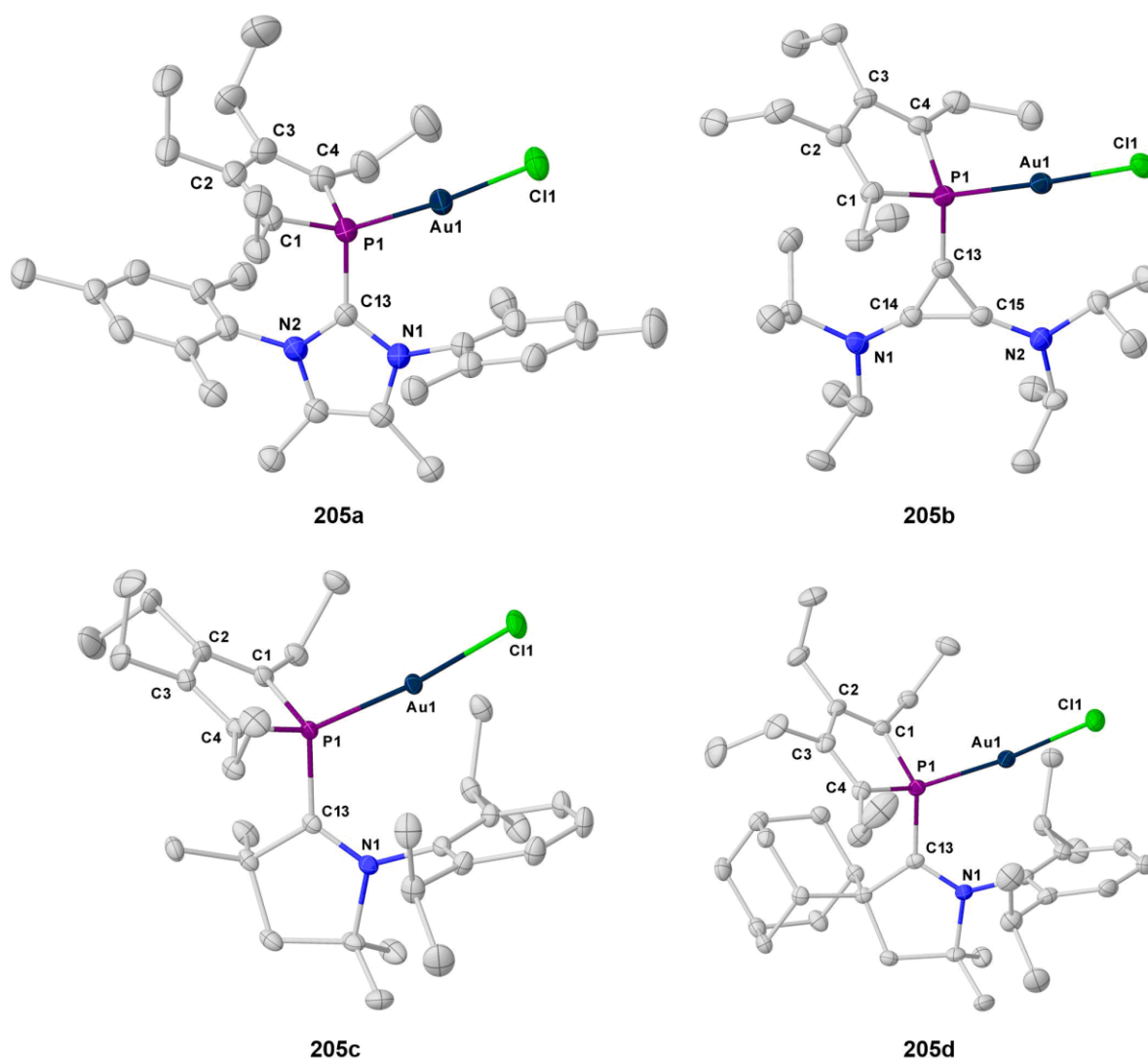

205a

205b

205c

205d

Figure 21: Molecular structures of **205a-d**. Hydrogen atoms and anions are omitted for clarity. Anisotropic displacement parameters are shown at 50% probability level.

Besides the coordination to gold, we also tried to coordinate palladium to our ligands, as the use of gold limits us mostly to π-acid catalysis. Although not many examples are known of palladium complexes with strong π-accepting ligands, some were previously synthesized by our group[71] using the palladium amino biphenyl precursor **206**. Ligand **191a** was chosen as its structure resembles roughly the typical Buckwald-ligands like SPhos. Buckwald´s group had great success coordinating their biaryphosphines to this Pd-complex and then using it in catalysis.[118] As the aminobiphenyl is quickly eliminated at higher temperatures, the reaction and work-up was performed at -20 °C. As workup, the solvent was removed, DCM was added and the solution filtered. Removal of the solvent yielded a brownish solid. The reaction

yielded an inseparable mixture, that could not be further purified by crystallization or filtration.
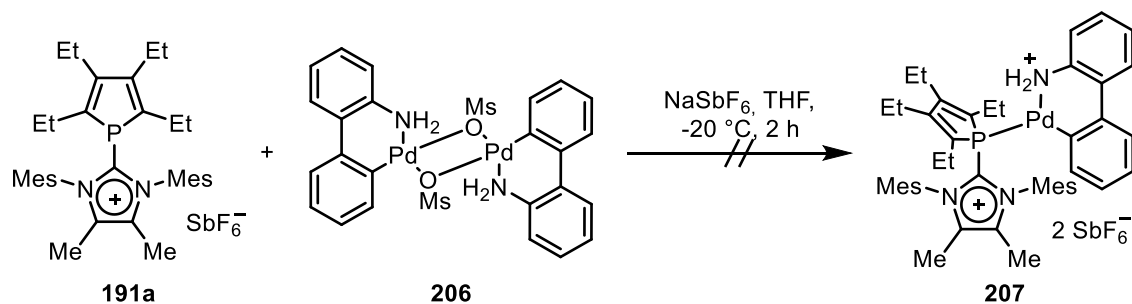
Scheme 79: Attempted synthesis of the palladium complexes.

3.2.7 Catalytic applications

To test our new gold catalysts and to compare them with neutral and other cationic phosphines, we chose the hydroarylation of sulfide **208** into thiepine **209** as the test reaction.[100] The reaction proceeds via activation of the triple bond by the gold center, followed by a *7-endo*-dig cyclisation, leading to the 7-membered ring in compound **209**. The reaction conditions can be seen in Scheme 80. The reaction was directly done in a Young-NMR tube, so the mixture was homogeneous but not stirred. The first NMR-spectrum was measured 10 minutes after initiating the reaction with the addition of AgSbF$_6$ and then every 5 min another spectrum would be measured. Besides our catalyst **205a-c**, three more were tested. The neutral phosphole **210**, the phosphite **211** and the cationic phosphine **212,** which resembles **205b** but has the standard diphenylphosphine moiety instead of a phosphole.
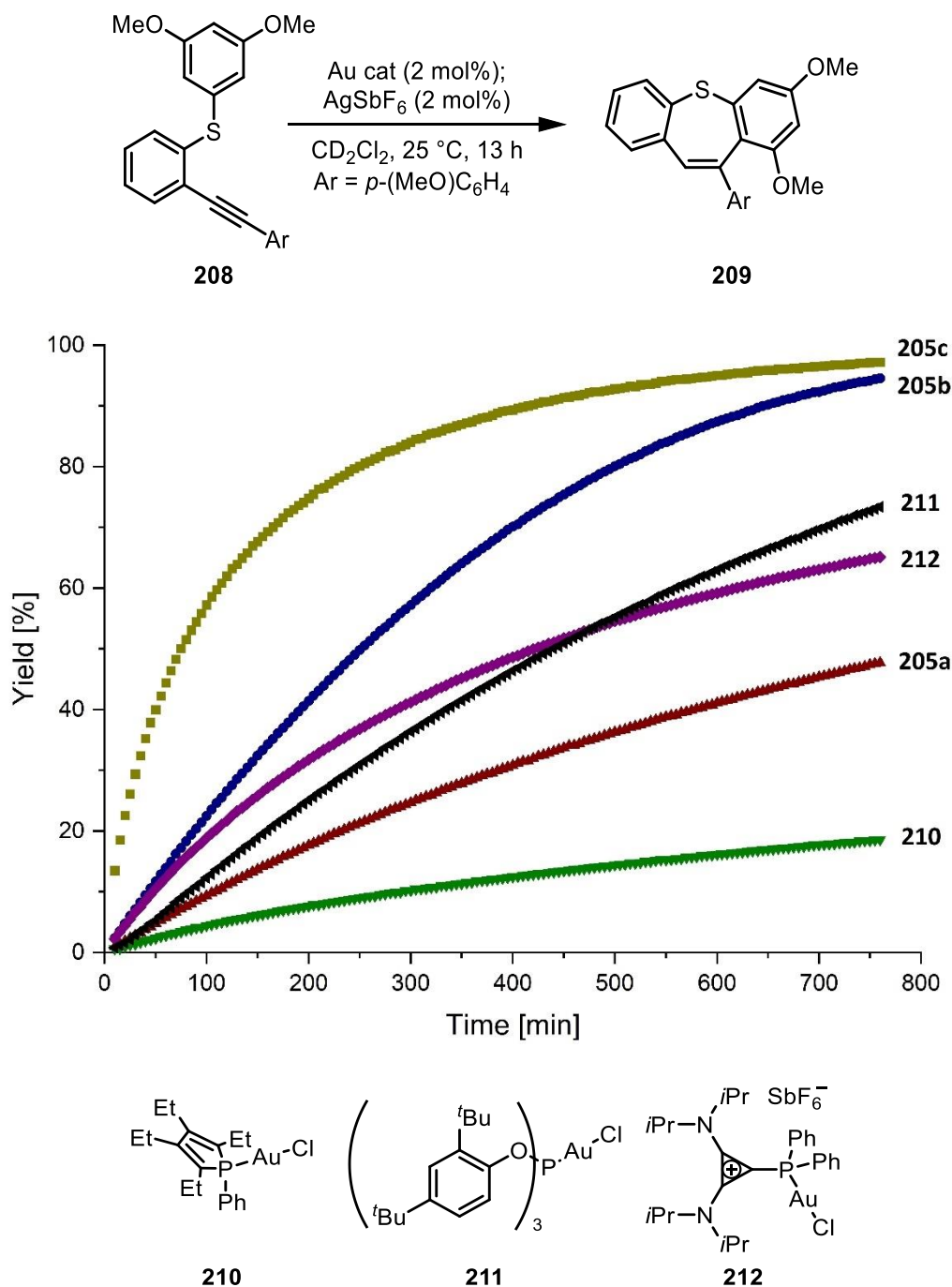
Figure 22: Ligand effect on the gold-catalyzed hydroarylation of sulfide **208** to thiepine **209**. Yield measured by ^{1}H-NMR. The kinetic experiment for **205c** was performed by K. Sprenger.

As expected, **210** showed the worst results, as compared to the phosphites and cationic complexes, it is the weakest π-acceptor. The strongest π-acceptor **205c** was also the most reactive one, achieving yields close to 55% already after 100 minutes, more than twice the yield obtained by any other ligand. **205b** was the second-best catalyst and the only one besides **205c** to achieve more than 90% yield during the time of the experiment. By comparison of **205b** with **212** the influence of the phosphole on the reactivity and stability can be assumed. While the difference in reactivity is very small at the start the curve then flattens much faster for **212**, indicating that the phosphole has a positive effect on the

lifetime of the catalytic species. This results in a more than twice the yield at the end of the experiment. The sterically demanding phosphite **211** showed a performance between **205b** and **212**; while the initial reaction rate is not nearly as high as the one of **212**, the resulting catalytic active species seems to be more stable. Thus it overtakes **212** in terms of yield after 480 minutes. A surprise was the rather poor performance of **205a**. In terms of electronical values, the catalyst should show a performance between **205b** and **205c**, but actually ranks as the second worst. The reason for this might lie in the IMes moiety, as it imposes steric shielding to two sides via the mesityl-substituents, not only towards on side like the CAAC in **205c**. Although the second mesitylene in **205a** is relatively far away from the active center, a large substrate like **208** could still be influenced by it, especially as both **208** and **205a** have several aryl rings that could participate in π–π-interactions. **211**, which is also quite bulky, is far more flexible than the rigid **205a** and π–interactions are less likely, as the *tert*-butyl groups directly attached to the rings might sterically interfere.

Having proved the capabilities of our ligands in terms of pure reactivity, we then tried to find a system where selectivity is an issue. In this regard we focused on the Au-catalyzed cyclisation of alkenyl-*N*-tosylanilines **213** into dihydroquinolines **216** and **217**.[119]
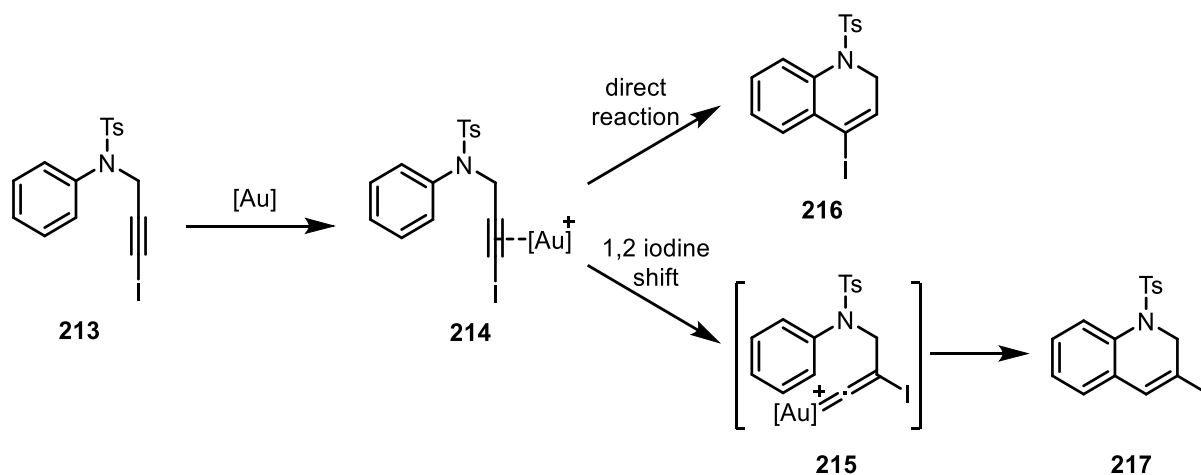

Scheme 80: Different reaction-pathways in the synthesis of dihydroquinolines.

After activation of the triple bond by the Au-catalyst (**214**), depending on the nature of the ligands, two reaction pathways could take place. If the ligands on the gold are strong π-acceptors, the triple bond is strongly activated and the direct reaction to **216** would proceed. In absence of good π-acceptors and with good σ-donors an 1,2-iodine shift would first take place, leading to the intermediate **215**, the gold vinylidene species.[120] This ultimately yields **217**, with the iodine in the 3-position.

In Table 7 we compared the results of our catalysts with the results of a previous publication[119]. As assumed, good σ-donating ligands like the NHC present in **218** strongly favored the formation of **217** (Entries 2 and 8), leading to an excellent selectivity of over 99:1 in favor of **217** when slightly electron poor anilines are used. As expected, the ratio changed towards **216** if electron withdrawing ligands like the phosphites in **211** were used. The ratio is also affected by the electronic properties of the substrate. The best ratio towards **216** was

achieved with 78:22 if the substituents on the aniline are electron donating, like the keto-group in **213c** (Entry 10). The ratio dropped to 58:42 when **213a** was employed (Entry 1) and even became favorable towards **217** for the chloroaniline **213b** (31:69, Entry 7).

213a; R = H
213b; R = Cl
213c; R = C(O)Me
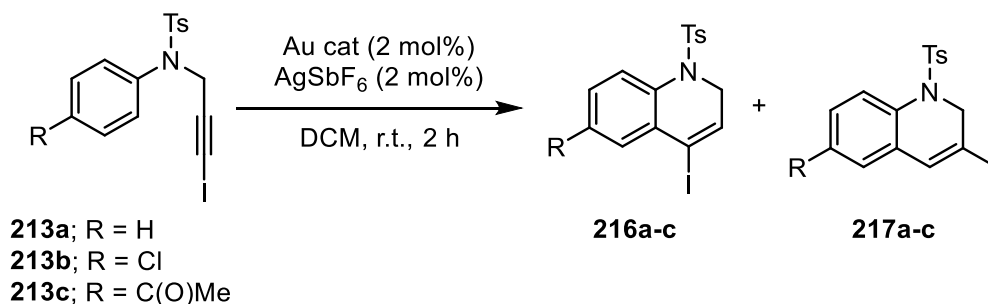
Entry	Substrate	Au cat.	Conv (%)[b]	216:217 ratio[c]
1[a]	213a	211	(64)	58:42
2[a]	213a	218	(85)	7:93
3	213a	205a	>95	75:25
4	213a	205b	>95	56:44
5	213a	205c	>95 (80)	97:3
6	213a	212	>95	59:41
7[a]	213b	211	(79)	31:69
8[a]	213b	218	(80)	<1:99<
9	213b	205c	>95 (79)	97:3
10[a]	213c	211	67	78:22
11	213c	205c	>95(95)	99:1
12	213a	-[d]	-	-

[a] Results from reference 119; [b] Conversions determined from crude reaction mixtures by ^{1}H-NMR, the value in parenthesis indicate isolated yields; [c] the isomeric ratios were determined by ^{1}H-NMR; [d] only AgSbF$_6$ was added.

218
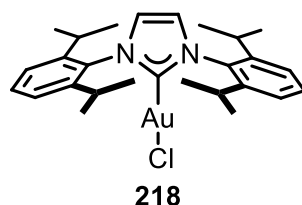
To benchmark our ligands, we chose the unsubstituted starting material **213a**. The ratio followed the expected trend, being close to equal for **205b** with 56:44, improving to 75:25 for **205a** and achieving a remarkable ratio of 97:3 for the complex with the best acceptor ligand **205c** (Entries 3-5). We also tried **212** in this reaction (Entry 6), to check if the influence of the phosphole by comparison with **205b**. In contrast to the kinetic experiment, no significant difference could be found, as the ratio of **212** is with 59:41 in the margin of error

of the ratio of **205b**. This was expected, as the different results for the kinetic experiments stemmed from the stability of the active species and not from a difference in the initial reaction rate. As the reaction was completed after 2 hours, the different stabilities did not matter.

We then tried our best performing catalyst **205c** with the other two substrates. It performed extremely well in the reaction with **213b**, the most challenging substrate. While the ratio with phosphite precatalyst **212** was still favorable towards **217b**, **205c** was not only able to shift the ratio towards **216b** but achieved a remarkable product distribution of 97:3 (Entry 9). As from **213b** either **216b** or **217b** can be prepared with very good selectivity it can be assumed that while the electronic properties of the substrates also play a role, the properties of the catalyst have the larger effect on the product distribution. As expected, **205c** was also able to achieve an excellent selectivity (99:1 Entry 11) using **213c** as a substrate. Although the product ratios of the all the reaction with precatalyst **205c** (Entries 5, 9, and 11) are similar, the reaction with **213c** is overall cleaner. This resulted in an isolated yield of 95% for **216c**. Besides our standard procedure to deactivate and immobilize the catalyst, filtration over a short pad of silica, no further purification was needed. **216a** and **216b** with isolated yields of 80% and 79%, respectively, had to be purified by column chromatography, explaining the lower isolated yields.

We also used this reaction to show the ability of our catalyst on larger scales and were able to scale up the reaction shown in Entry 5 to gram-scale. Using 1.40 g of **213a** and 64.6 mg of **205c**, we were able to obtain 1.11 g of **216a**, which corresponds to a yield of 79%.

3.2.8 Summary II

To conclude, we able to expand our library of cationic phosphine with the introduction of a new class: cationic phospholes. Cationic phospholes were prepared in a well scalable reaction sequence in good yields, resulting in four compounds with different electronic and steric values, which all are quite stable against moisture and air. Their electronic properties were evaluated by means of electrochemistry and for **191b** we could also obtain the CO-stretching frequency and the P-Se-coupling in the ^{31}P-NMR as additional ways to compare their electronic properties. We were also able to obtain molecular structures by means of X-ray analysis, clarifying the connectivities. This also allowed us to calculate buried volumes and thereby the steric demand of the ligands.

The chemistry of the ligands was explored by experiments regarding their behavior towards oxidations and Diels-Alder reactions, leading to interesting results in the latter case. In the case of **191c**, we were able to obtain a radical by one-electron reduction which we were able to analyze by EPR and X-ray.

We then explored their coordination chemistry and were able to obtain four gold complexes, three of which were tested in catalysis and exhibited great effects in the reactions tested, accelerating the reaction in one case and effectively discriminating between competing reaction pathways in the other.

4. Experimental Section

4.1 General working methods

Unless stated otherwise, all manipulations were carried out under inert atmosphere (nitrogen or argon, use of argon specifically stated) in flame-dried glassware on a Schlenk line or under nitrogen atmosphere in an MBraun UNIlab plus glovebox. Dry and degassed solvents were obtained by distillation over the appropriate drying agents and stored under argon. Alternatively, dry solvents were obtained using an MBraun MB-SPS-7 solvent purification system (THF, diethyl ether, toluene, pentane, dichloromethane, acetonitrile). Flash chromatography was performed on Macherey Nagel 60 (40-63 μm) silica gel. Reactions were controlled by thin-layer chromatography (TLC) analysis, performed using polygram SIL G/UV254 from Macherey Nagel and visualized by UV irradiation (λ = 254 nm), phosphomolybdic acid or iodine stains.

4.2 Starting materials

Unless otherwise stated, all reagents were used as received from commercial suppliers (ABCR, AcrosOrganics, Alfa Aesar, Chempur GmbH, J and K Scientific, Sigma Aldrich, Thermo Fisher Scientific, Tokyo Chemical Industry). Silver hexafluoroantimonate was purchased from Sigma Aldrich and stored in a glovebox. The carbenes (IMes^Me (**192a**)[121], Cyclopropenylidene (**192b**),[85] CAAC (**192c**),[86,122] AdCAAC (**192d**)[88,89]) used were prepared according to literature procedures. 1-chloro-2,3,4,5-tetraethyl-1*H*-phosphole (**190**) was prepared according to literature procedures[123] but additionally purified by Kugelrohr-distillation ($1 \cdot 10^{-3}$ mbar, 100 °C) using argon as inert gas. **213a**, **213b** and **213c** were prepared according to literature procedures.[119,124] **211**[125], **213a**[119], **213b**[119], **213c**[119], **216c**[119], **219**[126] and **220**[68] have been previously reported in literature.

4.3 General analytical methods

NMR: The NMR-spectra were recorded on a Bruker Avance III 300 MHz, Bruker Avance III HD 300 MHz, Bruker Avance III 400, Bruker Avance III HD 400 MHz or Bruker Avance Neo 400 MHz. The kinetic measurements were recorded on a Bruker Avance III HD 400 MHz. ^{1}H and ^{13}C chemical shifts are given in ppm relative to TMS, using the solvent signals as references and converting the chemical shifts to the TMS scale. ^{31}P chemical shifts are given in ppm relative to H_3PO_4 (external standard). The chemical shift is depicted in parts per million (ppm), and the coupling constants (*J*) in Hertz (Hz). Solvents for NMR spectroscopy were used as received, but stored over 3Å molecular sieves or in a glove box. The CD_2Cl_2 for the kinetic measurements was dried over 4Å molecular sieves and degassed, introduced into a glovebox and filtered before use.

HR-MS: Mass spectrometry analysis was recorded using the following equipment: Bruker Daltronik microTOF (ESI), Bruker Daltronik maXis (ESI) or Jeol AccuTOF (EI).

IR: neat samples were measured on a JASCO FT/IR-4100 or JASCO FT/IR-4600 at room temperature. The stretching frequencies are reported in wavenumbers (cm^{-1}).

X-ray-diffraction: Single crystal structure determination was performed by Dr. Christopher Golz at the University of Göttingen. Experimental setup: Data collection was done on a *Bruker D8 Venture* four-circle-diffractometer from *Bruker AXS GmbH*; detector: *Photon II* from *Bruker AXS GmbH*; X-ray sources: microfocus *IµS* Cu/Mo from *Incoatec GmbH* with mirror optics *HELIOS* and single-hole collimator from *Bruker AXS GmbH*. Used programs: *APEX3 Suite* (v2017.3-0) and therein integrated programs *SAINT* (Integration) und *SADABS* (Absorption correction) from *Bruker AXS GmbH*; structure solution was done with *SHELXT*, refinement with *SHELXS* (Both: G.M. Sheldrick, *Acta Cryst*. **2008,** *A64*, 112-122.); OLEX^2 was used for data finalization (O.V. Dolomanov, L.J. Bourhis, R.J Gildea, J.A.K. Howard, H. Puschmann, *J. Appl. Cryst*. **2009,** *42*, 339-341.). Special Utilities: *SMZ1270* stereomicroscope from *Nikon Metrology GmbH* was used for sample preparation; crystals were mounted on *MicroMounts* or *MicroLoops* from *MiTeGen*; for sensitive samples the *X-TEMP 2 System* was used for picking of crystals (T. Kottke, D. Stalke, *J. Appl. Cryst*. **1993,** *26*, 615-619.); crystals were cooled to given temperature with *Cryostream 800* from *Oxford Cryosystems.*

EPR-measurement: EPR-spectra were measured on a Bruker EMX mikro X-Band EPR from BRUKER Biospin with the Bruker Xenon Software. The spectra were measured in dry and degased toluene at room temperature. Interpretation and calculation was performed with the build in SpinFit Software.

Cyclic voltammetry: Cyclic voltammetry was measured with a VersaSTAT 4 potentiostat from *Princeton Applied Research* using the VersaStudio software (version 2.44.4). A standard three electrodes setup was used with a glassy carbon working electrode, a platinum counter electrode and a gold pseudo-reference electrode. Referencing was performed against $[Fe(Cp)_2]^{0/+}$. As electrolyte, a 0.1 M solution of $^nBu_4NPF_6$ in dry and degassed DCM was used. For square wave voltammetry the measuring range was set from 0 to +2.0 V. The pulse height was set to 25 mV, the step height to 1.2 mV and the frequency to 12 Hz.

5. Synthesis of new compounds
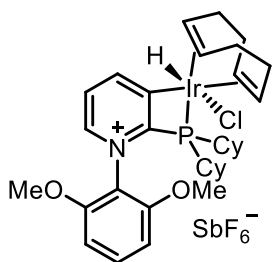
Compound 172: To a mixture of [Ir(cod)Cl]$_2$ (74.6 mg, 0.11 mmol, 1.0 equiv.) and phosphine **169d** (144 mg, 0.22 mmol, 2.0 equiv.) was added DCM (6 mL). The solution was stirred for 3 h at rt, before evaporating the solvent. The residue was washed with Et$_2$O (2 mL) and n-pentane (2 mL), then recrystallized from DCM/Et$_2$O yielding the desired product (165 mg, 0.16 mmol, 76%) as a light brown solid. Product slowly decomposes in solution.

^{1}H NMR (400 MHz, CD$_2$Cl$_2$) δ = 8.01 (ddd, J = 6.1, 2.0, 1.2 Hz, 1H), 7.91 (ddd, J = 7.7, 2.7, 1.3 Hz, 1H), 7.73 (dd, J = 7.7, 6.1 Hz, 1H), 7.63 (t, J = 8.6 Hz, 1H), 6.89 (d, J = 8.7 Hz, 1H), 6.79 (d, J = 8.6 Hz, 1H), 5.36-5.27 (m, 2H(overlap with solvent signal)), 5.03-4.96 (m, 1H), 4.80-4.73 (m, 1H), 3.87 (s, 3H), 3.83 (s, 3H), 3.10-2.99 (m, 1H), 2.92-2.85 (m, 1H), 2.70-2.62 (m, 2H), 2.58-2.48 (m, 2H), 2.43-2.34 (m, 1H), 2.26-2.04 (m, 3H), 1.89-1.77 (m, 5H), 1.70-1.49 (m, 6H(overlap with H$_2$O signal)), 1.34-1.21 (m, 5H), 1.17-1.01 (m, 3H), 0.96-0.82 (m, 1H), -14.81 (d, J = 11.4 Hz, 1H) ppm; ^{13}C{^{1}H} NMR (101 MHz, CD$_2$Cl$_2$) δ = 155.9, 154.5, 146.1 (d, J = 11.1 Hz), 143.4, 134.5, 127.5 (d, J = 1.8 Hz), 118.8 (d, J = 1.1 Hz), 105.4 (d, J = 37.6 Hz), 104.9, 96.8, 88.5 (d, J = 16.1 Hz), 88.0, 83.8 (d, J = 8.7 Hz), 62.8, 57.3, 56.7, 35.9 (d, J = 2.1 Hz), 32.8 (d, J = 22.4 Hz), 32.3, 31.7 (d, J = 16.2 Hz), 30.9, 30.9, 30.4 (d, J = 5.4 Hz), 30.0 (d, J = 2.5 Hz), 28.6, 28.5, 28.3 (d, J = 6.6 Hz), 28.1, 28.0 (d, J = 7.0 Hz), 26.7 (d, J = 15.1 Hz), 26.3, 26.3 (d, J = 1.9 Hz), 26.1 ppm; ^{31}P NMR (121 MHz, CD$_2$Cl$_2$) δ = -6.79 ppm; m.p: 156 °C (decomposition); IR (neat) $\bar{\nu}$ = 2926, 2848, 1604, 1592, 1484, 1445, 1401, 1306, 1265, 1134, 1020, 1000, 875, 849, 809, 779, 730, 705, 655, 631, 604 cm^{-1}; HRMS *calcd.* for C$_{33}$H$_{47}$ClIrNO$_2$P [M-SbF$_6$]$^+$: 748.2655; *found*: 748.2649.
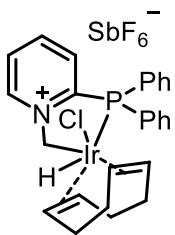
Compound 174: To a mixture of [Ir(cod)Cl]$_2$ (131 mg, 0.19 mmol, 1.0 equiv.) and phosphine **173** (200 mg, 0.39 mmol, 1.0 equiv.) was added DCM (10 mL). The solution was stirred for 1 h at rt, before evaporating the solvent. The residue was washed with Et$_2$O (3 mL) then recrystallized from DCM/Et$_2$O yielding the desired product (180 mg, 0.21 mmol, 54%) as a white solid. Product slowly decomposes in solution.

^{1}H NMR (400 MHz, CD$_2$Cl$_2$) δ = 8.90 (d, J = 6.1, 1H), 8.32 (t, J = 7.8 Hz, 1H), 8.02 (ddd, J = 7.9, 4.1, 0.9 Hz, 1H), 7.92-7.85 (m, 3H), 7.68-7.59 (m, 4H), 7.56-7.45 (m, 4H), 5.72 (d, J = 12.6 Hz, 1H), 5.39-5.33 (m, 1H), 5.12 (dd, J = 12.8, 3.3 Hz, 1H), 4.95 (t, J = 8.0 Hz, 1H), 4.89-4.83 (m, 1H), 4.11 (td, J = 8.2, 4.1 Hz, 1H), 2.98-2.89 (m, 1H), 2.75-2.53 (m, 4H), 2.51-2.40 (m, 2H), 2.30-2.22 (m, 1H), -15.37 (d, J = 10.6 Hz, 1H) ppm; ^{13}C{^{1}H} NMR (101 MHz, CD$_2$Cl$_2$) δ = 156.0, 155.4, 148.3 (d, J = 5.9 Hz), 143.8 (d, J = 4.0 Hz), 133.9 (d, J = 12.3 Hz), 133.77, 133.75, 133.74 (d, J = 10.3 Hz), 133.0 (d, J = 2.9 Hz), 132.7 (d, J = 4.0 Hz), 130.5 (d, J = 11.4 Hz), 129.5 (d, J = 1.8 Hz), 129.3 (d, J = 11.7 Hz), 128.1, 127.5, 124.7, 124.1, 99.3 (d, J = 16.9 Hz), 93.7 (d, J = 9.5 Hz), 92.1, 84.3, 52.1 (d, J = 5.1 Hz), 34.5 (d, J = 2.7 Hz), 32.1, 29.5 (d, J = 2.6 Hz), 28.9 (d, J = 3.7 Hz) ppm; ^{31}P NMR (121 MHz, CD$_2$Cl$_2$) δ = 32.27 ppm; m.p: 198 °C (decomposition); IR (neat) $\overline{v}$ = 2889, 2247, 1603, 1491, 1482, 1434, 1414, 1340, 1313, 1292, 1187, 1156, 1118, 1097, 1076, 1053, 1027, 998, 859, 831, 812, 792, 775, 754, 748, 717, 707, 697, 690, 651 cm^{-1}; HRMS *calcd.* for C$_{26}$H$_{29}$ClIrNP [M-SbF$_6$]$^+$: 614.1342; *found*: 614.1343.

General scheme for the synthesis of cationic phospholes
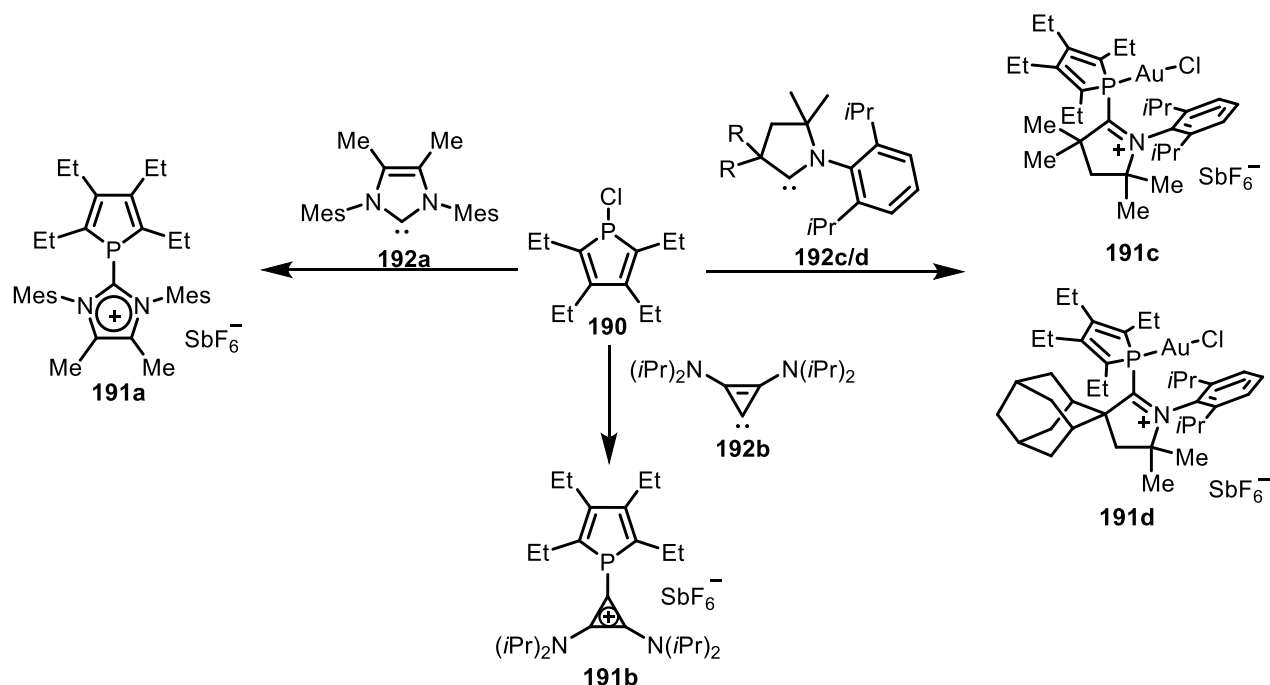
General procedure A (GPA) for the synthesis of the cationic phospholes 191

For these reactions argon was used as inert gas. The free carbene (1.0 eq.) was dissolved in Et$_2$O (1.5 mL/mmol) and slowly added at -78 °C to a solution of **190** (1.1 eq.) in Et$_2$O (2 mL per 0.1 mL of **190**). The resulting mixture was stirred for 2 h at -78 °C. Dry NaSbF$_6$ (3.0 eq.)

was added and the mixture stirred overnight, warming up to room temperature. The supernatant was filtered off by cannula and the residue washed with pentane (2 mL/mmol). The residue was shortly dried under vacuum, dissolved in DCM (2 mL/mmol) and filtered to remove the inorganic salts. The solvent was removed *in vacuo* to yield the desired product as a solid. If unclean (only observed for **191c** and **191d**) the product can be purified by column chromatography on air (DCM/MeOH 40:1). The products are stable on column and air (tested up to one month) but should be stored under inert conditions over longer periods of time. Crystals suitable for X-Ray diffraction can be obtained by crystallization from DCM/pentane or DCM/Et$_2$O.
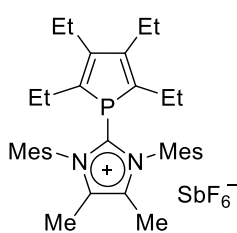
Compound 191a: Prepared from **192a** (400 mg, 1.20 mmol, 1.0 eq.), chlorophosphole **190** (305 mg, 1.32 mmol, 1.1 eq.) and NaSbF$_6$ (0.93 g, 3.60 mmol, 3.0 eq) following GP**A**. Colorless solid (695 mg, 0.91 mmol, 76%). When the reaction was performed at a scale 1.5 times as large (600 mg of **192a**), the yield was 71% (980 mg, 1.28 mmol).

^{1}H NMR (400 MHz, CD$_2$Cl$_2$) δ = 7.05 (s, 4H), 2.58-2.45 (m, 2H), 2.36 (s, 6H), 2.15-1.93 (m, 6H), 2.05 (s, 6H), 2.02 (s, 12H), 0.94 (t, J = 7.4 Hz, 6H), 0.84 (t, J = 7.6 Hz, 6H) ppm; ^{13}C{^{1}H} NMR (101 MHz, CD$_2$Cl$_2$) δ = 154.3 (d, J = 13.5 Hz), 142.3, 136.2 (d, J = 1.4 Hz), 134.8, 130.3, 23.2 (d, J = 19.6 Hz), 21.5, 21.4, 18.4 (d, J = 6.9 Hz), 18.2 (d, J = 0.8 Hz), 14.6 (d, J = 3.4 Hz), 9.7 ppm; ^{31}P{^{1}H} NMR (162 MHz, CD$_2$Cl$_2$) δ = -38.3 ppm; m.p: 246-248 °C; IR (neat) $\bar{v}$ = 2966, 2931, 2870, 1628, 1608, 1481, 1448, 1406, 1383, 1305, 1232, 1111, 1052, 1015, 863, 794, 739, 654 cm^{-1}; HRMS *calcd.* for C$_{35}$H$_{48}$N$_2$P [M-SbF$_6$]$^+$: 527.3550; *found*: 527.3543.
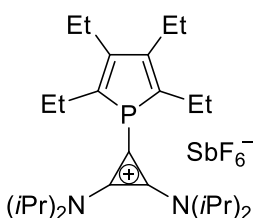
Compound 191b: Prepared from **192b** (320 mg, 1.35 mmol, 1.0 eq.), chlorophosphole **190** (344 mg, 1.49 mmol) and NaSbF$_6$ (1.05 g, 4.06 mmol, 3.0 eq.) following GP**A**. Off-white solid (668 mg, 1.00 mmol, 74%). When the reaction was performed at a larger scale (500 mg, 2.10 mmol of **192b**), the yield of **191** was 68% (950 mg, 1.42 mmol).

^{1}H NMR (400 MHz, CD$_2$Cl$_2$) δ = 4.28-3.48 (m, 4H) 2.68-2.54 (m, 2H), 2.51-2.27 (m, 6H), 1.67-1.15 (m, 24H), 1.10 (t, J = 7.6 Hz, 6H), 1.08 (t, J = 7.7 Hz, 6H) ppm (the two triplets appear as one quartet); ^{13}C{^{1}H} NMR (101 MHz, CD$_2$Cl$_2$) δ = 154.8 (d, J = 12.9 Hz), 139.8, 103.2, 102.4, 22.1 (d, J = 18.5 Hz), 21.6 (d, J = 3.3 Hz), 21.4 (broad s), 16.9 (d, J = 6.5 Hz), 14.9 (d, J = 3.4 Hz)

ppm; $^{31}P\{^1H\}$ NMR (162 MHz, CD$_2$Cl$_2$) δ = -41.0 ppm; m.p: 203-205 °C; IR (neat) $\overline{v}$ = 2965, 2933, 2871, 1859, 1558, 1410, 1374, 1352, 1211, 1157, 1140, 1048, 1018, 892, 653, 632 cm^{-1}; HRMS *calcd.* for C$_{27}$H$_{48}$N$_2$P [M-SbF$_6$]$^+$: 431.3550; *found*: 431.3553.
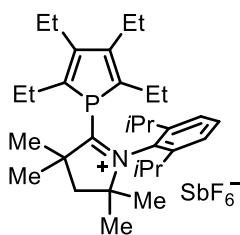
Compound 191c: Prepared from **192c** (385 mg, 1.34 mmol, 1.0 eq.), chlorophosphole **190** (340 mg, 1.47 mmol) and NaSbF$_6$ (1.04 g, 4.02 mmol, 3.0 eq.) following GP**A**. Yellow solid (580 mg, 0.81 mmol, 60%). When the reaction was performed at a larger scale, (840 mg, 2.94 mmol of **192c**) the yield of **191c** was 59**%** (1.24 g, 1.73 mmol).

^1H NMR (400 MHz, CDCl$_3$) δ = 7.60 (t, *J* = 7.8 Hz, 1H), 7.44 (d, *J* = 7.8 Hz, 2H), 2.85-2.61 (m, 4H), 2.55-2.45 (m, 4H), 2.36 (s, 2H), 2.25-2.15 (m, 2H), 1.46 (d, *J* = 6.4 Hz, 6H), 1.42-1.39 (m, 12H), 1.31 (d, *J* = 6.6 Hz, 6H), 1.15 (t, *J* = 7.6 Hz, 6H), 1.07 (t, *J* = 7.4 Hz, 6H) ppm; $^{13}C\{^1H\}$ NMR (101 MHz, CDCl$_3$) δ = 213.7 (d, *J* = 63.0 Hz), 158.6 (d, *J* = 12.1 Hz), 144.5, 137.9 (d, *J* = 7.3 Hz), 131.9, 130.3 (d, *J* = 4.9 Hz), 125.9, 88.3 (d, *J* = 1.3 Hz), 57.8 (d, *J* = 7.5 Hz), 50.5, 30.7, 30.4, 29.2, 28.9 (d, *J* = 3.4 Hz), 23.9, 22.3 (d, *J* = 18.1 Hz), 21.6 (d, *J* = 3.1 Hz), 17.3 14.1 (d, *J* = 3.7 Hz) ppm; $^{31}P\{^1H\}$ NMR (162 MHz, CDCl$_3$) δ = -16.0 ppm; m.p: 225-227 °C; IR (neat) $\overline{v}$ = 2974, 2935, 2874, 1522, 1461, 1389, 1375, 1366, 1339, 1198, 1132, 1109, 1053, 918, 907, 806, 752, 740, 726, 655 cm^{-1}; HRMS *calcd.* for C$_{32}$H$_{51}$NP [M-SbF$_6$]$^+$: 480.3754; *found*: 480.3754.
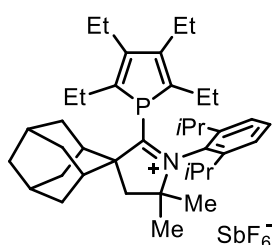
Compound 191d: Prepared from **192d** (76 mg, 200 μmol) chlorophosphole **190** (51 mg, 220 μmol) and NaSbF$_6$ (155 mg, 600 μmol, 3.0 eq.) following GP**A**. Orange solid (75 mg, 93 μmol, 46%).

^1H NMR (400 MHz, CD$_2$Cl$_2$) δ = 7.62 (t, *J* = 7.8 Hz, 1H), 7.46 (d, *J* = 7.9 Hz, 2H), 2.78-2.57 (m, 6H), 2.52-2.42 (m, 4H), 2.35-2.24 (m, 2H), 2.13-2.08 (m, 4H), 1.94 (s, 1 H), 1.83-1.69 (m, 5H), 1.64-1.61 (m, 2H), 1.51 (s, 2H), 1.46 (s, 6H), 1.43 (d, *J* = 6.6 Hz, 6H), 1.29 (d, *J* = 6.6 Hz, 6H), 1.11 (t, *J* = 7.7 Hz, 12H) ppm; $^{13}C\{^1H\}$ NMR (101 MHz, CD$_2$Cl$_2$) δ = 223.9 (d, *J* = 81.7 Hz), 157.0 (d, *J* = 18.2 Hz), 144.7 (d, *J* = 1.8 Hz), 137.9 (d, *J* = 10.5 Hz), 132.3, 132.2, 126.5, 82.3, 69.4 (d, *J* = 9.1 Hz), 47.1 (d, *J* = 1.5 Hz), 38.1, 37.8, 34.6, 34.1, 30.4, 30.3 (d, *J* = 1.5 Hz), 27.9 (d, *J* = 4.7 Hz), 26.7, 26.3, 24.1, 23.0 (d, *J* = 17.8 Hz), 22.0 (d, *J* = 3.3 Hz), 16.9 (d, *J* = 2.9 Hz), 14.1 (d, *J* = 5.1 Hz) ppm; $^{31}P\{^1H\}$ NMR (162 MHz,

CD$_2$Cl$_2$) δ = 0.78 ppm; m.p: 218-220 °C; IR (neat) $\bar{v}$ = 2971, 2895, 2882, 1470, 1453, 1388, 1375, 1336, 1307, 1264, 1249, 1147, 1130, 1098, 1050, 1026, 993, 955, 930, 897, 868, 811, 784, 777, 713, 651, 608 cm^{-1}; HRMS *calcd.* for C$_{39}$H$_{59}$NP [M-SbF$_6$]$^+$: 572.4380; *found*: 572.4380.
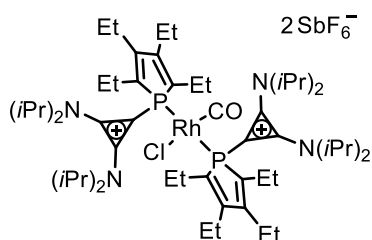
Compound 193: Argon was used as inert gas. A schlenk was charged with **191b** (70 mg, 105 µmol, 1.0 eq.) and [RhCl(CO)$_2$]$_2$ (10 mg, 26.2 µmol, 0.25 eq.), then DCM (1.5 mL) was added. The mixture was stirred for 2 h. The solvent was removed *in vacuo* and the residue washed with pentane (2 x 2 mL) yielding the desired product as off-white solid (41 mg, 27 µmol, 52%). Crystals suitable for X-Ray diffraction were obtained by crystallization from DCM/pentane.

^{1}H NMR (400 MHz, CD$_2$Cl$_2$) δ = 4.45-4.10 (m, 8H) 2.77-2.58 (m, 8H), 2.55-2.42 (m, 8H), 1.42-1.28 (m, 48H), 1.22 (t, *J* = 7.5 Hz, 12H), 1.14 (t, *J* = 7.6 Hz, 12H) ppm; ^{13}C{^{1}H} NMR (101 MHz, CD$_2$Cl$_2$) δ = 156.1 (t, *J* = 9.7 Hz), 139.2 (t, *J* = 1.4 Hz), 135.5 (t, *J* = 22.1 Hz), 98.0, 22.4, 22.1 (t, *J* = 7.1 Hz),, 21.9 (broad s), 21.9 (t, *J* = 5.3 Hz), 21.6, 21.1, 19.8, 16.5, 14.6 ppm; the signals of the CO could not be found; ^{31}P{^{1}H} NMR (162 MHz, CD$_2$Cl$_2$) δ = 7.53 (d, *J* = 123.8 Hz) ppm; m.p: <120 °C (decomposition); IR (neat) $\bar{v}$ = 2973, 2937, 2876, 1984, 1855, 1548, 1455, 1377, 1355, 1202, 1181, 1146, 1114, 1032, 1009, 977, 678, 654 cm^{-1}; HRMS *calcd.* for C$_{27}$H$_{48}$N$_2$PRhClCO [M-C$_{27}$H$_{48}$N$_2$PSb$_2$F$_{12}$]$^+$: 597.2242; *found*: 597.2242.
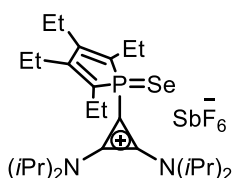
Compound 194: A pressure-schlenk was charged with **191b** (29 mg, 43.4 µmol, 1.0 eq) and selenium (10.3 mg, 130 µmol, 3.0 eq.), then Toluene (8 mL) was added. The mixture was stirred for 48 h at 120 °C. The mixture was filtered through cotton wool to remove the excess selenium. The solvent was removed *in vacuo*. Column chromatography (DCM/^{t}BuOMe 10:1) yielded the desired product as brown solid (11 mg, 14.7 µmol, 34%). Even after several purification attempts, small amounts of the starting material **191b** were still present.

^{1}H NMR (400 MHz, CDCl$_3$) δ = 4.33-414 (m, 4H), 2.75-2.58 (m, 2H), 2.55-2.34 (m, 6H), 1.42 (d, *J* = 6.1 Hz, 24H), 1.24 (t, *J* = 7.6 Hz, 6H), 1.15 (t, *J* = 7.6 Hz, 6H) ppm; ^{13}C{^{1}H} NMR (101 MHz, CDCl$_3$) δ = 153.9 (d, *J* = 26.2 Hz), 134.4, 133.6 (d, *J* = 57.0 Hz), 95.4, 95.1, 21.7, 21.2, 21.1

(broad s), 21.0, 15.2 (d, $J = 1.4$ Hz), 14.2 (d, $J = 2.3$ Hz) ppm; $^{31}P\{^1H\}$ NMR (162 MHz, CD$_2$Cl$_2$) δ = 14.1, 14.1 (d, J_{PSe} = 763 Hz) ppm; IR (neat) $\overline{v}$ = 2974, 2936, 2874, 1857, 1556, 1456, 1378, 1355, 1203, 1182, 1147, 1036, 1009, 912, 893, 732, 679, 652 cm^{-1}; HRMS *calcd.* for C$_{27}$H$_{48}$N$_2$PSe [M-SbF$_6$]$^+$: 511.2716; *found*: 511.2731.
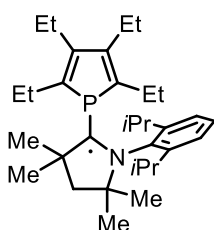
Compound **196**: Argon was used as inert gas. A Schleck was charged with **191c** (50 mg, 70 µmol, 1.00 eq.) and KC$_8$ (10 mg, 70 µmol, 1.00 eq.), then THF (2 mL) was slowly added at -78 °C. The reaction was allowed to warm to room temperature and stirred for 1 h, resulting in a color change from yellow to dark green. The solvent was removed *in vacuo* and the residue dissolved in pentane (2.5 mL) and filtered via cannula. The solvent was removed *in vacuo* to yield the desired product (10 mg, 21 µmol, 30%) as black solid. Crystals suitable for X-Ray diffraction could be obtained from pentane by cooling down a saturated solution to -20 °C. The EPR-spectrum was recorded in toluene. As the compound is very sensitive, it was only characterized by EPR and X-ray diffraction.

General procedure B (GPB) for oxidation of cationic phospholes

Under air a flask was charged with the **191** and DCM (10 mL) then H$_2$O$_2$ (30% in H$_2$O, 1 mL) was added and the solution stirred for 3 days at rt (4 days for CAAC). The reactions mixture was diluted with H$_2$O and extracted with DCM (3 x 15 mL). The solvent was removed *in vacuo*. If needed, the products can be purified by column chromatography (DCM/MeOH 40:1).
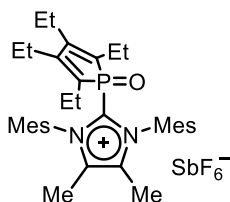
Compound **197a**: Prepared from phosphole **191a** (100 mg, 131 µmol) and H$_2$O$_2$ (35 wt% in H$_2$O, 0.2 mL) following GP**B**. White solid (82 mg, 105 µmol, 80%).

^1H NMR (300 MHz, CD$_2$Cl$_2$) δ = 7.06 (s, 4H), 2.53-2.31 (m, 2H), 2.37 (s, 6H), 2.24-2.04 (m, 4H), 2.02 (s, 12H), 2.01 (s, 6H), 1.82-1.69 (m, 2H), 1.07 (t, $J = 7.5$ Hz, 6H), 0.97 (t, $J = 7.7$ Hz, 6H) ppm; $^{13}C\{^1H\}$ NMR (101 MHz, CD$_2$Cl$_2$) δ = 157.3 (d, $J = 32.7$ Hz), 141.9, 134.4, 134.1 (d, $J = 2.2$ Hz), 130.5, 130.1, 129.9, 128.9, 21.31, 21.29 (d, $J = 10.9$ Hz), 20.8 (d, $J = 17.4$ Hz), 17.8, 14.3 (d, $J = 0.8$ Hz), 13.8 (d, $J = 2.4$ Hz), 9.4 ppm; $^{31}P\{^1H\}$ NMR (121 MHz, CD$_2$Cl$_2$) δ = 34.5 ppm; m.p: 173-175 °C; IR (neat) $\overline{v}$ = 2977, 2932, 2875, 1630, 1607, 1560,

1455, 1403, 1381, 1287, 1214, 1040, 856, 790, 731, 655 cm^{-1}; HRMS *calcd.* for C$_{35}$H$_{48}$N$_2$OP [M-SbF$_6$]$^+$: 543.3499; *found*: 543.3500.
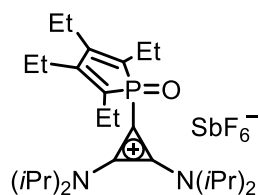
Compound 197b: Prepared from phosphole **191b** (100 mg, 150 µmol) and H$_2$O$_2$ (35 wt% in H$_2$O, 0.2 mL) following GP**B**. Offwhite solid (80 mg, 117 µmol, 78%).

^{1}H NMR (300 MHz, CD$_2$Cl$_2$) δ = 4.18-3.82 (m, 4H) 2.62-2.27 (m, 8H), 1.42-1.33 (m, 24H), 1.15 (t, *J* = 7.4 Hz, 6H), 1.12 (t, *J* = 7.4 Hz, 6H) ppm (the two triplets appear as one quartet); ^{13}C{^{1}H} NMR (75 MHz, CD$_2$Cl$_2$) δ = 155.5 (d, *J* = 31.5 Hz), 131.9, 130.5 100.7, 99.8, 21.4 (broad s), 20.9, 20.8, 20.6, 19.6 (d, *J* = 10.6 Hz), 14.1 (d, *J* = 2.6 Hz), 13.9 (d, *J* = 1.9 Hz) ppm; ^{31}P{^{1}H} NMR (121 MHz, CD$_2$Cl$_2$) δ = 27.9 ppm; m.p: 215-217 °C; IR (neat) $\overline{v}$ = 2976, 2938, 2877, 1870, 1561, 1460, 1377, 1360, 1230, 1204, 1145, 1042, 1012, 893, 739, 681, 653 cm^{-1}; HRMS *calcd.* for C$_{27}$H$_{48}$N$_2$OP [M-SbF$_6$]$^+$: 447.3499; *found*: 447.3499.
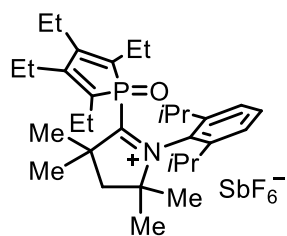
Compound 197c: Prepared from phosphole **191c** (100 mg, 140 µmol) and H$_2$O$_2$ (35 wt% in H$_2$O, 0.2 mL) following GP**B**. Yellow solid (92 mg, 126 µmol, 90%).

^{1}H NMR (400 MHz, CD$_2$Cl$_2$) δ = 7.56 (t, *J* = 7.8 Hz, 1H), 7.40 (d, *J* = 7.8 Hz, 2H), 2.68-2.57 (m, 4H), 2.54-2.49 (m, 4H), 2.37 (s, 2H), 2.34-2.24 (m, 2H), 1.53 (s, 6H), 1.45 (d, *J* = 6.4 Hz, 6H), 1.42 (s, 6H), 1.35 (d, *J* = 6.7 Hz, 6H), 1.21 (t, *J* = 7.7 Hz, 6H), 1.13 (t, *J* = 7.5 Hz, 6H) ppm; ^{13}C{^{1}H} NMR (101 MHz, CD$_2$Cl$_2$) δ = 202.9 (d, *J* = 25.9 Hz), 160.8 (d, *J* = 31.5 Hz), 143.8, 132.1, 131.2, 131.1, 125.8, 87.1 (d, *J* = 4.5 Hz), 53.5, 50.5 (d, *J* = 3.6 Hz), 30.9 (d, *J* = 13.1 Hz), 29.1, 28.4, 23.9, 21.2 (d, *J* = 16.7 Hz), 19.9 (d, *J* = 11.3 Hz), 15.9, 13.5 (d, *J* = 2.5 Hz) ppm; ^{31}P{^{1}H} NMR (162 MHz, CD$_3$Cl) δ = 37.0 ppm; m.p: 258 °C (decomposition); IR (neat) $\overline{v}$ = 2972, 2937, 2880, 1542, 1468, 1376, 1216, 1057, 809, 778, 715, 653 cm^{-1}; HRMS *calcd.* for C$_{32}$H$_{51}$NOP [M-SbF$_6$]$^+$: 496.3703; *found*: 496.3703.
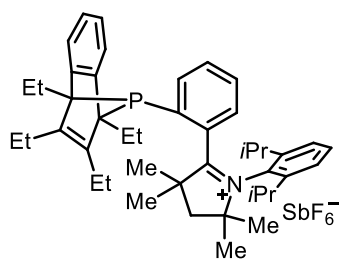
Compound 203: A schlenk was charged with **191c** (200 mg, 279 µmol, 1.00 eq.) and CsF (340 mg, 2.23 mmol, 8.00 eq.), then MeCN (12 mL) was added. Then 2-(Trimethylsilyl)phenyl trifluoro-methanesulfonate (0.27 mL, 1.12 mmol, 4.00 eq.) was added and the mixture stirred for 14 h at room temperature. NaSbF$_6$ (1.15 g, 4.46 mmol, 16.0 eq.) was added and the mixture stirred for 3 h at room

temperature. The solvent was removed *in vacuo* and the residue dissolved in DCM (15 mL) and filtered via cannula. The solvent was removed *in vacuo* and the residue purified by column chromatography (DCM/MeOH 40:1) to yield the desired product (140 mg, 161 μmol, 58%) as yellow solid. Crystals suitable for X-Ray diffraction were obtained by crystallization from DCM/pentane.

^{1}H NMR: (400 MHz, CD$_2$Cl$_2$) δ = 8.80 (d, *J* = 8.1 Hz, 1H), 7.69 (t, *J* = 7.7 Hz, 1H), 7.48 (t, *J* = 7.8 Hz, 1H), 7.41 (t, *J* = 7.6 Hz, 1H), 7.39 – 7.30 (m, 2H), 7.17 – 7.11 (m, 2H), 7.03 (m, 3H), 2.62-2.06 (m, 12H), 1.86 (s, 3H), 1.62-1.61 (m, 3H), 1.56 (s, 3H), 1.50 (s, 3H), 1.23-1.17 (m, 6H), 0.99 (d, *J* = 5.6 Hz, 3H), 0.74-0.63 (m, 9H), 0.32 (d, *J* = 6.0 Hz, 3H), -0.22 (t, *J* = 7.1 Hz, 3H) ppm; ^{13}C{H} NMR: (101 MHz, CD$_2$Cl$_2$) δ = 205.6, 150.9 (t, *J* = 23.9 Hz), 149.9, 148.6, 147.1, 144.6, 140.0 (d, *J* = 53.0 Hz), 134.9 (d, *J* = 40.5 Hz), 132.4, 131.7, 130.9, 130.4 (d, *J* = 1.2 Hz), 130.3, 128.9 (d, *J* = 10.2 Hz), 128.1, 127.5, 125.5, 124.4, 119.8 (d, *J* = 49.7 Hz), 86.9, 65.1 (dd, *J* = 32.0, 12.3 Hz), 54.9, 47.9, 34.2 (d, *J* = 18.8 Hz), 33.4, 30.4 (d, *J* = 22.6 Hz), 29.7 (d, *J* = 17.5 Hz), 28.7 (d, *J* = 6.3 Hz), 28.0, 27.5, 27.2 (d, *J* = 22.8 Hz), 26.3, 26.2, 25.5, 22.9, 21.7 (d, *J* = 7.4 Hz), 21.5, 21.4 (d, *J* = 5.8 Hz), 21.2, 14.1 (d, *J* = 4.8 Hz), 13.8, 13.2 ppm; ^{31}P{^{1}H} NMR (162 MHz, CD$_2$Cl$_2$) δ = 130.1 ppm; m.p: 175-177 °C (decomposition); IR: (neat, cm^{-1}) ṽ = 2966, 2930, 2870, 1548, 1457, 1377, 1179, 1122, 1097, 1003, 927, 809, 798, 753, 745, 652; HRMS: *calcd. m/z* for C$_{44}$H$_{59}$NP [M-SbF$_6$]$^+$: 632.4380; *found*: 632.4376.

General Procedure C (GPC) for the synthesis of cationic phosphole gold complexes 205
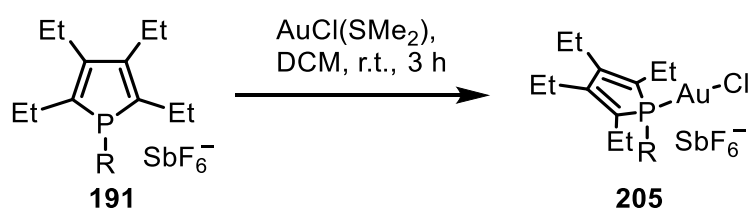
A schlenk was charged with AuCl(SMe$_2$) (1 equiv.) and the corresponding phosphole **191** (1 eq.), then DCM (10 mL/mmol) was added and the solution stirred for 3 h at room temperature. After stirring for 3 h the solvent was removed *in vacuo.* The resulting solid was washed with Et$_2$O (1 x 20 mL/mmol) and *n*-pentane (2 x 20 mL/mmol). Crystals suitable for X-Ray diffraction can be obtained by crystallization from DCM/pentane or DCM/Et$_2$O.
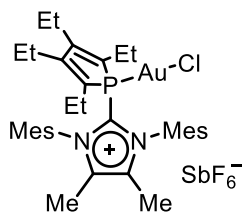
Compound **205a**: Prepared from phosphole **191a** (79.0 mg, 103 μmol. 1.0 eq) and AuCl(SMe₂) (30.5 mg, 103 μmol. 1.0 eq) following GP**C**. White solid (98.0 mg, 98.4 μmol, 95%).

¹H NMR (400 MHz, CD₂Cl₂) δ = 7.13 (s, 4H), 2.71-2.57 (m, 2H), 2.43 (s, 6H), 2.21-2.10 (m, 4H), 2.08 (s, 6H), 2.01 (s, 12H), 1.98-1.91 (m, 2H), 1.33 (t, J = 7.4 Hz, 6H), 0.95 (t, J = 7.6 Hz, 6H) ppm; ¹³C{¹H} NMR (101 MHz, CD₂Cl₂) δ = 159.4 (d, J = 21.7 Hz), 144.0, 136.7, 134.8, 131.1, 130.4 (d, J = 57.5 Hz), 129.0, 22.2 (d, J = 28.6 Hz), 22.1, 21.7, 19.2 (d, J = 2.4 Hz), 18.2, 14.0 (d, J = 1.5 Hz), 10.1 ppm; ³¹P{¹H} NMR (162 MHz, CD₂Cl₂) δ = -2.15 ppm; m.p: 268 °C (decomposition); IR (neat) $\bar{v}$ = 2962, 2928, 2867, 1621, 1608, 1538, 1449, 1399, 1380, 1287, 1260, 1223, 1094, 1047, 1015, 856, 794, 654, 623 cm⁻¹; HRMS *calcd.* for C₃₅H₄₈AuClN₂P [M-SbF₆]⁺: 759.2904; *found*: 759.2904.
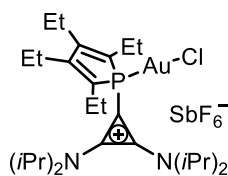
Compound **205b**: Prepared from phosphole **191b** (100 mg, 150 μmol, 1.0 eq.) and AuCl(SMe₂) (44.1 mg, 150 μmol, 1.0 eq.) following GP**C**. White solid (105 mg, 117 μmol, 78%).

¹H NMR (400 MHz, CD₂Cl₂) δ = 4.21-3.75 (m, 4H) 2.78-2.64 (m, 2H), 2.57-2.36 (m, 6H), 1.75-1.34 (m, 24H), 1.32 (t, J = 7.5 Hz, 6H), 1.14 (t, J = 7.6 Hz, 6H) ppm; ¹³C{¹H} NMR (101 MHz, CD₂Cl₂) δ = 158.2 (d, J = 21.4 Hz), 139.4 (d, J = 7.3 Hz), 132.8 (d, J = 57.0 Hz), 93.2 (d, J = 2.4 Hz), 92.8 (d, J = 2.3 Hz), 22.0, 21.9, 21.5 (broad s), 20.9 (d, J = 14.8 Hz), 17.0 (d, J = 3.6 Hz), 14.4 (d, J = 1.5 Hz) ppm; ³¹P{¹H} NMR (162 MHz, CD₂Cl₂) δ = -2.19 ppm; m.p: 228 °C (decomposition); IR (neat) $\bar{v}$ = 2974, 2940, 2878, 1869, 1570, 1457, 1377, 1362, 1203, 1182, 1145, 1041, 1011, 956, 895, 749, 687, 655 cm⁻¹; HRMS *calcd.* for C₂₇H₄₈AuClN₂P [M-SbF₆]⁺: 663.2904; *found*: 663.2909.
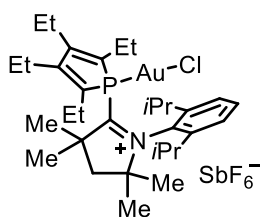
Compound **205c**: Prepared from phosphole **191c** (55.0 mg, 76.8 μmol, 1.0 eq.) and AuCl(SMe₂) (22.6 mg, 76.8 μmol, 1.0 eq.) following GP**C**. Yellow solid (59.7 mg, 62.9 μmol, 82%).

¹H NMR (400 MHz, CD₂Cl₂) δ = 7.80 (t, J = 7.9 Hz, 1H), 7.53 (d, J = 7.9 Hz, 2H), 2.92-2.76 (m, 2H), 2.65-2.50 (m, 6H), 2.45 (s, 2H), 2.27-2.15 (m, 2H), 1.61 (d, J = 6.7 Hz, 6H), 1.53 (s, 12H), 1.46 (d, J = 6.3 Hz, 6H), 1.29 (t, J = 7.4 Hz, 6H), 1.22 (t, J = 7.6 Hz, 6H) ppm; ¹³C{¹H} NMR (101 MHz, CD₂Cl₂) δ = 202.2 (d, J = 5.0 Hz), 163.0 (d,

$J = 20.0$ Hz), 144.2, 133.5, 132.1 (d, $J = 50.9$ Hz), 131.4 (d, $J = 5.7$ Hz), 127.6, 88.5 (d, $J = 1.8$ Hz), 57.7 (d, $J = 2.9$ Hz), 50.9 (d, $J = 1.9$ Hz), 31.1, 30.6, 29.7, 29.5, 25.0, 22.3 (d, $J = 11.8$ Hz), 21.4 (d, $J = 15.0$ Hz), 17.9, 13.5 (d, $J = 1.3$ Hz) ppm; ^{31}P{^{1}H} NMR (162 MHz, CDCl$_3$) $\delta = 15.4$ ppm; m.p: 236-238 °C (decomposition); IR (neat) $\bar{v} = 2971, 2936, 2875, 1530,$ 1458, 1392, 1376, 1339, 1195, 1124, 1104, 1054, 1029, 804, 755, 654, 607 cm^{-1}; HRMS *calcd.* for C$_{32}$H$_{51}$AuClNP [M-SbF$_6$]$^+$: 712.3108; *found*: 712.3104.
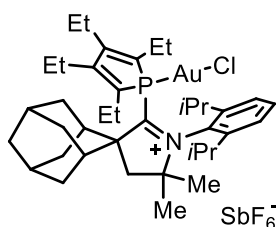
Compound **205d**: Prepared from phosphole **191d** (20 mg, 24.7 µmol, 1.0 eq.) and Me$_2$S•AuCl (7.3 mg, 24.7 µmol, 1.0 eq.) following GP**C**. Yellow solid (20.1 mg, 19.3 µmol, 78%).

^{1}H NMR (300 MHz, CD$_2$Cl$_2$) δ = 7.81 (t, $J = 7.9$ Hz, 1H), 7.52 (d, $J = 7.9$ Hz, 2H), 2.88-2.65 (m, 5H), 2.60-2.44 (m, 6H), 2.38-2.23 (m, 3H), 2.18 (s, 3H), 2.00 (s, 1 H), 1.87 (s, 1H), 1.82-1.77 (m, 6H), 1.70 (s, 1H), 1.63 (d, $J = 6.6$ Hz, 6H), 1.52 (s, 6H), 1.45 (d, $J = 6.3$ Hz, 6H), 1.37 (t, $J = 7.4$ Hz, 6H), 1.19 (t, $J = 7.6$ Hz, 6H) ppm; ^{13}C{^{1}H} NMR (101 MHz, CD$_2$Cl$_2$) δ = 207.8 (d, $J = 8.7$ Hz), 161.4 (d, $J = 22.5$ Hz), 143.9, 133.9 (d, $J = 5.7$ Hz) 133.5, 132.5 (d, $J = 48.0$ Hz), 127.7, 86.7 (d, $J = 2.2$ Hz), 71.9, 54.2, 48.6 (d, $J = 2.5$ Hz), 38.0, 37.5, 34.9, 34.7, 30.9, 30.3, 29.6, 26.5, 25.6, 25.1, 22.6 (d, $J = 12.7$ Hz), 21.8 (d, $J = 14.9$ Hz), 17.4 (d, $J = 1.7$ Hz), 13.6 ppm; ^{31}P{^{1}H} NMR (162 MHz, CD$_2$Cl$_2$) δ = 26.3 ppm; m.p: 220 °C (decomposition); IR (neat) $\bar{v}$ = 2968, 2897, 1464, 1455, 1389, 1377, 1335, 1308, 1263, 1247, 1225, 1191, 1145, 1128, 1098, 1052, 990, 954, 927, 860, 807, 773, 705, 659, 650, 609 cm^{-1}; HRMS *calcd.* for C$_{39}$H$_{59}$AuClNP [M-SbF$_6$]$^+$: 804.3734; *found*: 804.3737.
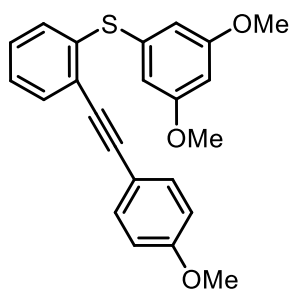
Compound **208**: Adapting a literature procedure,[127] a schlenk was charged with (3,5-dimethoxyphenyl)(2-iodophenyl)sulfane (580 mg, 1.56 mmol, 1.0 eq.), PdCl$_2$(PPh$_3$)$_2$ (54.7 mg, 77.9 µmol, 5mol%) and CuI (29.7 mg, 155.8 µmol, 10mol%), then Et$_3$N (10 mL) was added. The reaction mixture was degassed for 15 min using argon. 4-ethynylanisole (309 mg, 2.34 mmol, 1.5 eq.) was added drop wise and the reaction mixture stirred for 14 h at room temperature. The reaction mixture was filtered through a short plug of celite, using DCM as eluent. The reaction mixture was diluted with water (10 mL) and extracted with EtOAc (3 x 10 mL). The combined organic phases were washed with sat. aq. NH$_4$Cl-solution (2 x 10 mL), water (2 x 10 mL) and dried over Na$_2$SO$_4$.

The solvent was removed *in vacuo*. Column chromatography (*n*-pentane/EtOAc 10:1) yielded the desired product (530 mg, 1.41 mmol, 90%) as white solid.

^{1}H NMR (300 MHz, CDCl$_3$): δ = 7.53 − 7.49 (m, 1H), 7.48 − 7.42 (m, 2H), 7.21 − 7.10 (m, 3H), 6.91 − 6.82 (m, 2H), 6.63 (d, *J* = 2.3 Hz, 2H), 6.42 (t, *J* = 2.3 Hz, 1H), 3.83 (s, 3H), 3.75 (s, 6H) ppm. ^{13}C{^{1}H} NMR (101 MHz, CDCl$_3$): δ = 161.3, 159.9, 139.3, 135.7, 133.3, 132.5, 129.3, 128.6, 126.3, 123.7, 115.4, 114.1, 110.5, 100.7, 95.9, 86.1, 55.6, 55.5 ppm. IR (neat) $\overline{v}$ = 3060, 3005, 2957, 2934, 2832, 2210, 1596, 1579, 1508, 1448, 1433, 1416, 1335, 1283, 1249, 1204, 1174, 1157, 1106, 1066, 1041, 1024, 988, 929, 869, 834, 818, 785, 761,719, 683, 620, 534 cm^{-1}; HRMS *calcd.* for C$_{23}$H$_{21}$O$_3$S [M+H]$^+$: 377.1206; *found*: 377.1213.
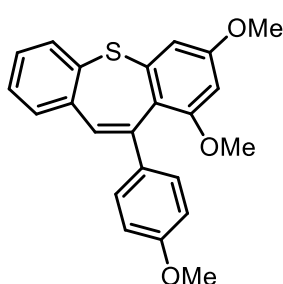
1,3-dimethoxy-11-(4-methoxyphenyl)dibenzo[*b,f*]thiepine (209): Argon was used as inert gas. A schlenk was charged with **208** (376.5 mg, 1.00 mmol, 1.0 eq.) and **205c** (19.0 mg, 20 µmol, 2mol%). The schlenk was evacuated and filled with argon (three cycles), then DCM (16 mL) was added. AgSbF$_6$ (6.87 mg, 20 µmol, 2mol%) was added as a 0.05 M solution in DCM and the reaction mixture stirred for 15 h at room temperature. The reaction mixture was filtered through a short plug of silica, using DCM as eluent. The solvent was removed *in vacuo*. Column chromatography (*n*-pentane/EtOAc 3:1) yielded the desired product (348 mg, 0.92 mmol, 92%) as white solid.

^{1}H NMR (400 MHz, CDCl$_3$) δ = 7.50 (dd, *J* = 7.7, 1.3 Hz, 1H), 7.38-7.34 (m, 1H), 7.32 (broad s, 1H), 7.29-7.25 (m, 3H), 7.20 (td, *J* = 7.5, 1.6 Hz, 1H), 6.86-6.82 (m, 2H), 6.81 (d, *J* = 2.4 Hz, 1H), 6.35 (d, *J* = 2.8 Hz, 1H), 3.82 (s, 3H), 3.82 (s, 3H), 3.35 (s, 3H) ppm; ^{13}C{^{1}H} NMR (101 MHz, CDCl$_3$) δ = 160.9, 159.0, 158.8, 143.8, 141.9, 140.8, 137.22, 137.17, 132.3, 130.7, 129.1, 128.2, 127.0, 127.4, 123.0, 113.5, 108.5, 100.5, 55.8, 55.6, 55.4 ppm; IR (neat) $\overline{v}$ = 2997, 2960, 2927, 2832, 1608, 1589, 1555, 1507, 1472, 1456, 1429, 1399, 1356, 1312, 1299, 1277, 1234, 1213, 1182, 1162, 1128, 1103, 1039, 960, 946, 933, 908, 887, 869, 857, 840, 821, 786, 769, 752, 740, 671, 636, 632, 620, 601 cm^{-1}; HRMS *calcd.* for C$_{23}$H$_{21}$O$_3$S [M+H]$^+$: 377.1206; *found*: 377.1208.

Preparation of gold catalysts 9 and 10 for the kinetic experiments
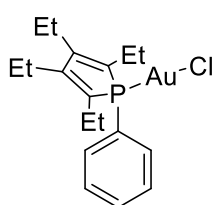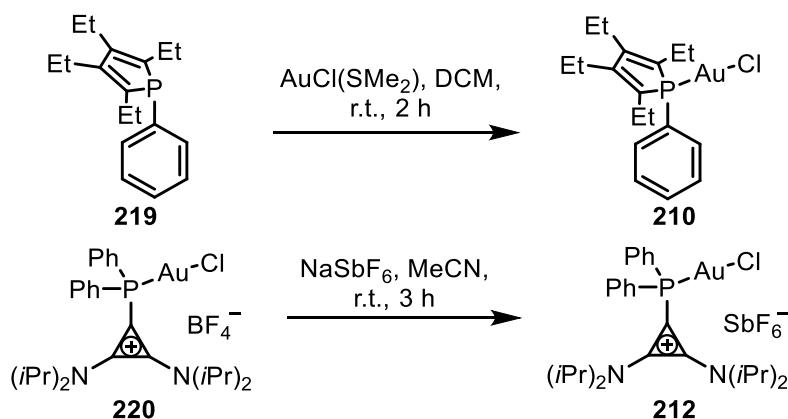
2,3,4,5-tetraethyl-1-phenyl-1*H*-phospholegold(I)-chloride (210): A schlenk was charged with phosphole **219** (35 mg, 128 μmol, 1.0 eq.) and AuCl(SMe$_2$) (42.0 mg, 128 μmol, 1.0 eq.), then DCM (1.5 mL) was added. The solution was stirred for 2 h at room temperature. The solvent was removed *in vacuo* and the residue dissolved in pentane (5 mL) and filtered. Crystallization by slow evaporation from pentane at room temperature yielded the desired product (43 mg, 85 μmol, 66%) as colorless crystals.

^{1}H NMR (300 MHz, CDCl$_3$) δ = 7.57-7.45 (m, 3H), 7.43-7.37 (m, 2H), 2.62-2.37 (m, 6H), 2.27-2.10 (m, 2H), 1.14 (t, *J* = 7.6 Hz, 6H), 1.10 (t, *J* = 7.6 Hz, 6H) ppm; ^{13}C{^{1}H} NMR (101 MHz, CDCl$_3$) δ = 153.9 (d, *J* = 17.8 Hz), 136.0 (d, *J* = 56.7 Hz), 134.2 (d, *J* = 13.8 Hz), 132.3 (d, *J* = 2.5 Hz), 129.4 (d, *J* = 12.0 Hz), 125.7 (d, *J* = 57.0 Hz), 21.0 (d, *J* = 11.6 Hz), 20.3 (d, *J* = 15.3 Hz), 16.2 (d, *J* = 3.6 Hz), 14.6 (d, *J* = 2.2 Hz) ppm; ^{31}P{^{1}H} NMR (162 MHz, CDCl$_3$) δ = 34.0 ppm; m.p: 140 °C (decomposition); IR (neat) $\bar{v}$ = 2960, 2930, 2869, 1547, 1473, 1455, 1434, 1376, 1306, 1172, 1099, 1063, 1046, 1022, 997, 960, 892, 820, 749, 709, 693, 670, 631, 619 cm^{-1}; HRMS *calcd.* for C$_{18}$H$_{25}$AuClPNa [M+Na]$^+$: 527.0940; *found*: 527.0935.
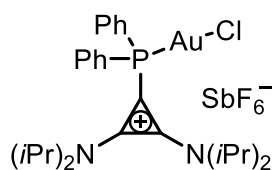
Compound **212:** A schlenk was charged with **220** (100 mg, 135 μmol, 1.0 eq.) and NaSbF$_6$ (105 mg, 405 μmol, 3.0 eq.). The solids were schlenked (three cycles). MeCN (5 mL) was added and the mixture stirred for 3 h at room temperature. The solvent was removed *in*

vacuo and the residue dried under high vacuum. The residue was dissolved in DCM (6 mL) and filtered to separate the inorganic salts. The solvent was removed *in vacuo* to yield the desired product (98 mg, 110 µmol, 82%) as white solid.

^{1}H NMR (400 MHz, CD_2Cl_2) δ = 7.97-7.87 (m, 4H), 7.73-7.63 (m, 6H), 4.14 (sep, *J* = 7.0 Hz, 2H), 3.46 (sep, *J* = 7.0 Hz, 2H), 1.40 (d, *J* = 7.0 Hz, 12H), 1.04 (d, *J* = 7.0 Hz, 12H) ppm; ^{13}C{^{1}H} NMR (101 MHz, CD_2Cl_2) δ = 138.0 (d, *J* = 7.3 Hz), 135.4 (d, *J* = 16.1 Hz), 134.5 (d, *J* = 2.6 Hz), 130.8 (d, *J* = 13.1 Hz), 124.9 (d, *J* = 66.8 Hz), 21.6, 21.5 ppm; ^{31}P{^{1}H} NMR (162 MHz, CD_2Cl_2) δ = 17.2 ppm; m.p: 190 °C (decomposition); IR (neat) $\overline{v}$ = 2979, 1871, 1569, 1471, 1438, 1375, 1354, 1182, 1151, 1139, 1116, 1103, 1030, 999, 895, 751, 717, 703, 693, 656, 630, 614 cm^{-1}; HRMS *calcd.* for $C_{27}H_{38}AuClN_2P$ [M-SbF$_6$]$^+$: 653.2121; *found*: 653.2129.
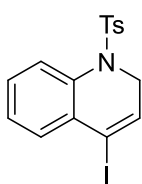
4-iodo-1-tosyl-1,2-dihydroquinoline (216a): A schlenk was charged with **213a** (102 mg, 248 µmol, 1.0 eq) and **205c** (4.7 mg, 4.95 µmol, 2 mol%), then DCM (8 mL) was added. AgSbF$_6$ (1.7 mg, 4.95 µmol, 2 mol%, as 0.01 M solution in DCM) was added and the mixture stirred for 2 h at room temperature. The mixture was filtered through a short pad of silica using Et$_2$O as eluent. The solvent was removed *in vacuo*. Column chromatography (hexanes/EtOAc 10:1) yielded the desired product as yellowish oil (82 mg, 199 µmol, 80%) which turns slowly into a yellow solid. Product needs to be stored under inert conditions. To show synthetic applicability, the reaction was repeated on large scale using **213a** (1.40 g, 3.40 mmol), **205c** (64.6 mg, 68.1 µmol, 2mol%) and AgSbF$_6$ (23.4 mg, 68.1 µmol, 2mol%) in DCM (40 mL). This reaction afforded 1.11 g (2.70 mmol, 79%) of the desired product after column chromatography.

^{1}H NMR (300 MHz, CDCl$_3$) δ = 7.59 (dd, *J* = 7.8, 1.0 Hz, 1H), 7.37-7.30 (m, 1H), 7.27-7.22 (m, 4H), 7.11 (d, *J* = 8.5 Hz, 2H), 6.18 (t, *J* = 4.6 Hz, 1H), 4.33 (d, *J* = 4.6 Hz, 2H), 2.36 (s, 3H) ppm; ^{13}C{^{1}H} NMR (101 MHz, CDCl$_3$) δ = 144.1, 135.5, 135.0, 134.9, 131.0, 130.5, 129.6, 129.5, 127.6, 127.5, 127.4, 93.7, 47.4, 21.7 ppm; IR (neat) $\overline{v}$ = 3062, 2918, 2886, 2845, 1599, 1472, 1449, 1350, 1334, 1306, 1293, 1276, 1183, 1159, 1119, 1088, 1070, 1039, 1039, 1024, 1017, 1007, 907, 898, 833, 810, 760, 732, 705, 680, 651 cm^{-1}; HRMS *calcd.* for $C_{16}H_{15}INO_2S$ [M+H]$^+$: 411.9863; *found*: 411.9851.
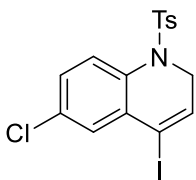
6-chloro-4-iodo-1-tosyl-1,2-dihydroquinoline (216b): A schlenk was charged with **213b** (48 mg, 108 µmol, 1.0 eq) and **205c** (5.1 mg, 5.38 µmol, 5 mol%), then DCM (4 mL) was added. AgSbF$_6$ (1.8 mg, 5.38 µmol, 5 mol%, as 0.01 M solution in DCM) was added and the mixture stirred for 2 h at room temperature. The mixture was filtered through a short pad of silica using Et$_2$O as eluent. The solvent was removed *in vacuo*. Column chromatography yielded the desired product as yellow solid (38 mg, 85.3 µmol, 79%). Product needs to be stored under inert conditions. The reaction was repeated on larger scale using **213b** (500 mg, 1.12 mmol), **205c** (53.2 mg, 56.1 µmol, 5 mol%) and AgSbF$_6$ (19.3 mg, 56.1 µmol, 5 mol%) in DCM (20 mL) yielding 408 mg (0.91 mmol, 82%) of the desired product after column chromatography.

^{1}H NMR (300 MHz, CDCl$_3$) δ = 7.57-7.53 (m, 1H), 7.32-7.27 (m, 3H), 7.25-7.24 (m, 1H), 7.15 (d, J = 8.5 Hz, 2H), 6.22 (t, J = 4.6 Hz, 1H), 4.33 (d, J = 4.6 Hz, 2H), 2.38 (s, 3H) ppm; ^{13}C{^{1}H} NMR (101 MHz, CDCl$_3$) δ = 144.0, 136.2, 134.9, 133.5, 133.2, 132.0, 130.9, 129.7, 129.4, 129.0, 127.3, 91.9, 48.1, 22.2 ppm; IR (neat) $\overline{v}$ = 3058, 2919, 2904, 2857, 1640, 1595, 1576, 1556, 1492, 1480, 1467, 1401, 1352, 1333, 1306, 1289, 1275, 1218, 1209, 1180, 1161, 1135, 1119, 1088, 1063, 1025, 1008, 965, 951, 914, 870, 848, 830, 814, 799, 775, 732, 705, 687, 660, 626, 606 cm^{-1}; HRMS *calcd.* for C$_{16}$H$_{14}$ClINO$_2$S [M+H]$^+$: 445.9473; *found*: 445.9469.

5.1. Setup for optimization reactions and kinetic experiments
Setup for the kinetic experiments
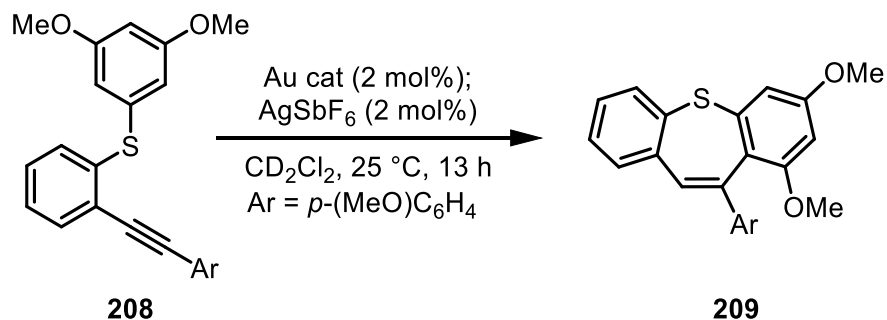
The calculated amount of catalyst **205, 210, 211** or **212** (0.5 μmol, 2 mol%) and starting material **208** (9.41 mg, 25.0 μmol, 1.0 eq.) were weighted into a GC-vial and transferred into a glovebox. In the glovebox, a 0.05 M solution of $AgSbF_6$ in CD_2Cl_2 was prepared. The catalyst and **208** were dissolved in 0.4 mL CD_2Cl_2 and the solution transferred into a Young-NMR-tube. The GC-vial was rinsed with additional 0.15 mL of CD_2Cl_2 which was also transferred into the NMR-tube. Finally with a Hamilton-syringe, the $AgSbF_6$-solution (0.5 μmol, 2 mol%) was added and the Young-NMR-tube closed. The tube was shaken to ensure mixing of the reaction mixture. The Young-NMR-tube was taken out of the glovebox and transferred into an NMR-spectrometer, where it was properly attuned and shimmed. 10 minutes after addition of the $AgSbF_6$-solution, the first ^{1}H-NMR-spectrum (16 scans) was recorded. For the next 12.5 h, an NMR-spectrum was recorded every five minutes. To determine the conversion the signals at 3.81-3.74 ppm (starting material, theoretical integral of six) and 3.43-3.35 ppm (product, theoretical integral of three) were integrated and compared.

General procedure D (GPD) for the optimization reactions
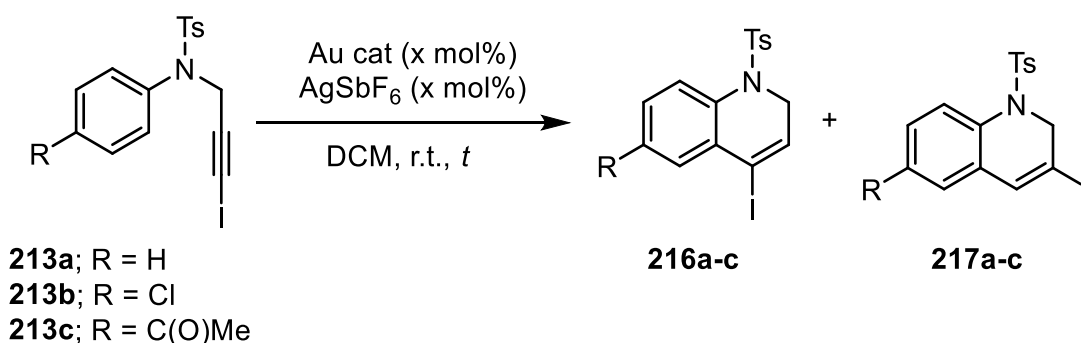
213a; R = H
213b; R = Cl
213c; R = C(O)Me

To a dried Schlenk equipped with magnetic stirrer starting material **213** (100 µmol, 1 eq.) and the gold pre-catalyst **205** was added. The solids were schlenked (three cycles) and DCM (2 ml) was added. AgSbF$_6$ (0.05 M or 0.01 M solution in DCM) was finally added and the reaction stirred at room temperature for the indicated time. The reaction mixture was filtered through a short plug of silica, using Et$_2$O as eluent. The solvent was removed *in vacuo* and the mixture analyzed by ^{1}H-NMR to determine the product ratios.

General procedure E (GPE) for the optimization reactions with low amounts of catalyst (>3 mg)

To a dried Schlenk equipped with magnetic stirrer starting material **213** (100 µmol, 1 eq.) was added. The solid was schlenked (three cycles). In a glovebox, a stock solution of the gold-precatalyst **205** in DCM was prepared. The gold pre-catalyst was added as a solution in DCM (2 ml). AgSbF$_6$ (0.05 M or 0.01 M solution in DCM) was finally added and the reaction stirred at room temperature for the indicated time. The reaction mixture was filtered through a short plug of silica, using Et$_2$O as eluent. The solvent was removed *in vacuo* and the mixture analyzed by ^{1}H-NMR to determine the product ratios.

Table 8: Complete optimization table for synthesis of dihydroquinolines

Entry	Substrate	Catalyst	Loading / mol%	Time / h	Conversion[a] / %	Ratio[b] 216/217
1	213a	205c	5	18	>95%	97/3
2	213b	205c	5	18	>95%	96/4
3	213b	205c	3	18	57	97/3
4	213a	205c	3	18	>95%	97/3
5	213a	205c	2	18	>95%	97/3
6	213a	205c	2	7	>95%	97/3
7	213a	205	2	4	>95%	98/2
8	213a	205c	2	2	>95%	97/3
9	213a	205a	2	2	>95%	75/25
10	213a	205b	2	2	>95%	56/44
11	213a	212	2	2	>95%	59/41
12	213c	205c	5	18	>95%	>99/1
13	213c	205c	2	2	>95%	99/1
14	213b	205c	5	2	>95%	97/3
15[c]	213a	-	2	2	0	-

[a] conversion determined by NMR; [b] selectivity determined by NMR. For **216,** the triplet (J = 4.6 Hz) around 6.20 ppm is used. **217** is identified by the signal around 6.90 ppm ((d, J = 2.4 Hz), appears as a broad singlet if not properly resolved).[4] As both signals have a theoretical integral of 1, the ratio is directly determined by comparison of the integrals. [c] only $AgSbF_6$ was added.

6. References

[1] a) A. F. Hollemann, E. Wiberg, N. Wiberg, *Lehrbuch der Anorganischen Chemie*, Walter de Gruyter, Berlin, **2007**; b) E. I. Musina, A. S. Balueva, A. A. Karasik, *Organophosphorus Chem.* **2019**, *48*, 1.

[2] C. Janiak, H.-J. Meyer, D. Gudat, R. Alsfasser, *Riedel - Moderne Anorganische Chemie*, Walter de Gruyter, Berlin, **2012**.

[3] J. A. Osborn, F. H. Jardine, J. F. Young, G. Wilkinson, *J. Chem. Soc. (A)* **1966**, 1711.

[4] N. Miyaura, A. Suzuki, *J.C.S. Chem. Comm.* **1979**, 866.

[5] M. Alcarazo, *Acc. Chem. Res.* **2016**, *49*, 1797.

[6] W. Keim, *Angew. Chem. Int. Ed.* **2013**, *52*, 12492.

[7] C. W. Kohkpaintner, R. W. Fischer, B. Cornils, *Appl. Catal., A* **2001**, *221*, 219.

[8] M. Hissler, C. Lescop, R. Réau, *C. R. Chimie* **2008**, *11*, 628.

[9] F. Mathey, *Chem. Rev.* **1988**, *88*, 429.

[10] E. Deschamps, L. Ricard, F. Mathey, *Angew. Chem. Int. Ed.* **1994**, *33*, 1158.

[11] W. Egan, R. Tang, G. Zon, K. Mislow, *J. Am. Chem. Soc.* **1971**, *93*, 6205.

[12] S. Pelzer, K. Wichmann, R. Wesendrup, P. Schwerdtfeger, *J. Phys. Chem. A* **2002**, *106*, 6387.

[13] I. Alkorta, K. Zborowski, J. Elguero, *Struct. Chem.* **2006**, *17*, 13.

[14] D. Delaere, A. Dransfeld, M. T. Nguyen, L. G. Vanquickenborne, *J. Org. Chem.* **2000**, *65*, 2631.

[15] E. H. Braye, W. Hübel, *Chem. Ind. (London)* **1959**, 1250.

[16] F. C. Leavitt, T. A. Manuel, F. Johnson, *J. Am. Chem. Soc.* **1959**, *81*, 3163.

[17] W. B. McCormack, *Org. Synth.* **1963**, *43*, 73.

[18] L. D. Quin, J. G. Bryson, *J. Am. Chem. Soc.* **1967**, *89*, 5984.

[19] C. Charrier, H. Bonnard, G. de Lauzon, F. Mathey, *J. Am. Chem. Soc.* **1983**, *105*, 6871.

[20] C. Charrier, F. Mathey, *Tetrahedron Lett.* **1987**, *28*, 5025.

[21] E. H. Braye, I. Caplier, R. Saussez, *Tetrahedron* **1971**, *27*, 5523.

[22] G. Märkl, R. Potthast, *Angew. Chem. Int. Ed.* **1967**, *6*, 86.

[23] M. Ogasawara, A. Ito, K. Yoshida, T. Hayashi, *Organometallics* **2006**, *25*, 2715.

[24] P. J. Fagan, W. A. Nugent, *J. Am. Chem. Soc.* **1988**, *110*, 2310.

[25] P. J. Fagan, W. A. Nugent, *Org. Synth.* **1992**, *70*, 272.

[26] J. Hydrio, M. Gouygou, F. Dallemer, J.-C. Daran, G. G. A. Balavoine, *Tetrahedron: Asymmetry* **2002**, *13*, 1097.

[27] K. Fourmy, D. H. Nguyen, O. Dechy-Cabaret, M. Gouygou, *Catal. Sci. Technol.* **2015**, *5*, 4289.

[28] D. G. Holah, A. N. Hughes, B. C. Hui, *Can. J. Chem* **1972**, *50*, 3714.

[29] a) D. Neibecker, R. Réau, *J. Mol. Catal.* **1989**, *53*, 219; b) D. Neibecker, R. Réau, *J. Mol. Catal.* **1989**, *57*, 153.

[30] D. Neibecker, R. Reau, S. Lecolier, *J. Org. Chem.* **1989**, *54*, 5208.

[31] C. Thoumazet, H. Grützmacher, B. Deschamps, L. Ricard, P. Le Floch, *Eur. J. Inorg. Chem.* **2006**, *2006*, 3911.

[32] G. N. Lewis, *Valence and the structure of atoms and molecules*, The Chemical Catalog Company, New York, **1923**.

[33] R. G. Pearson, *J. Am. Chem. Soc.* **1963**, *85*, 3533.

[34] A. Fürstner, *Chem. Soc. Rev* **2009**, *38*, 3208.

[35] A. Fürstner, P. W. Davies, *Angew. Chem. Int. Ed.* **2007**, *46*, 3410.

[36] A. Fürstner, *Acc. Chem. Res.* **2014**, *47*, 925.

[37] S. Flügge, A. Anoop, R. Goddard, Thiel W, A. Fürstner, *Chem. Eur. J.* **2009**, *15*, 8558.

[38] R. Dorel, A. M. Echavarren, *Chem. Rev.* **2015**, *115*, 9028.

[39] Y. Fukuda, K. Utimoto, H. Nozaki, *Heterocycles* **1987**, *25*, 297.

[40] a) J. Zhang, C.-G. Yang, C. He, *J. Am. Chem. Soc.* **2006**, *128*, 1798; b) X. Han, R. A. Widenhoefer, *Angew. Chem. Int. Ed.* **2006**, *45*, 1747.

[41] A. W. Sromek, M. Rubina, V. Gevorgyan, *J. Am. Chem. Soc.* **2005**, *127*, 10500.

[42] a) A. Fürstner, V. Mamane, *J. Org. Chem.* **2002**, *67*, 6264; b) V. Mamane, P. Hannen, A. Fürstner, *Chem. Eur. J.* **2004**, *10*, 4556.

[43] C. Nieto-Oberhuber, S. López, A. M. Echavarren, *J. Am. Chem. Soc.* **2005**, *127*, 6178.

[44] N. Mézailles, L. Ricard, F. Gagosz, *Org. Lett.* **2005**, *7*, 4133.

[45] S. Sen, F. P. Gabbaï, *Chem. Commun.* **2017**, *53*, 13356.

[46] A. Franchino, À. Martí, S. Nejrotti, A. M. Echavarren, *Chem. Eur. J.* **2021**, *27*, 11989.

[47] P. Mauleón, R. M. Zeldin, A. Z. González, F. D. Toste, *J. Am. Chem. Soc.* **2009**, *131*, 6348.

[48] I. Alonso, B. Trillo, F. López, S. Montserrat, G. Ujaque, L. Castedo, A. Lledós, J. L. Mascareñas, *J. Am. Chem. Soc.* **2009**, *131*, 13020.

[49] D. Benitez, E. Tkatchouk, A. Z. Gonzalez, W. A. Goddard, F. D. Toste, *Org. Lett.* **2009**, *11*, 4798.

[50] L. P. Hammett, *J. Am. Chem. Soc.* **1937**, *59*, 96.

[51] Z. J. Wang, D. Benitez, E. Tkatchouk, W. A. Goddard, F. D. Toste, *J. Am. Chem. Soc.* **2010**, *132*, 13064.

[52] B. Cornils, E. G. Kuntz, *J. Organomet. Chem.* **1995**, *502*, 177.

[53] D. M. Chisholm, J. S. McIndoe, *Dalton Trans.* **2008**, 3933.

[54] M. Alcarazo, *Chem. Eur. J.* **2014**, *20*, 7868.

[55] D. G. Gusev, *Organometallics* **2009**, *28*, 763.

[56] C. A. Tolman, *Chem. Rev.* **1977**, *77*, 313.

[57] C. A. Tolman, *J. Am. Chem. Soc.* **1970**, *92*, 2956.

[58] D. W. Allen, I. W. Nowell, B. F. Taylor, *Dalton Trans.* **1985**, 2505.

[59] A. A. Tolmachev, A. A. Yurchenko, E. S. Kozlov, A. S. Merkulov, M. G. Semenova, A. M. Pinchuk, *Heteroat. Chem.* **1995**, *6*, 419.

[60] I. V. Komarov, M. Y. Kornilov, A. A. Tolmachev, A. A. Yurchenko, E. B. Rusanov, A. N. Chernega, *Tetrahedron* **1995**, *51*, 11271.

[61] N. Kuhn, J. Fahl, D. Bläser, R. Boese, *Z. anorg. allg. Chem.* **1999**, *625*, 729.

[62] N. Kuhn, G. Henkel, M. Göhner, *Z. anorg. allg. Chem.* **1999**, *625*, 1415.

[63] D. J. Brauer, K. W. Kottsieper, C. Liek, O. Stelzer, H. Waffenschmidt, P. Wasserscheid, *J. Org. Chem.* **2001**, *630*, 177.

[64] M. Azouri, J. Andrieu, M. Picquet, P. Richard, B. Hanquet, I. Tkatchenko, *Eur. J. Inorg. Chem.* **2007**, *2007*, 4877.

[65] J. D. Holbrey, W. M. Reichert, I. Tkatchenko, E. Bouajila, O. Walter, I. Tommasi, R. D. Rogers, *Chem. Commun.* **2003**, 28.

[66] E. Haldón, Á. Kozma, H. Tinnermann, L. Gu, R. Goddard, M. Alcarazo, *Dalton Trans.* **2016**, *45*, 1872.

[67] H. Tinnermann, C. Wille, M. Alcarazo, *Angew. Chem. Int. Ed.* **2014**, *53*, 8732.

[68] J. Petuškova, H. Bruns, M. Alcarazo, *Angew. Chem. Int. Ed.* **2011**, *50*, 3799.

[69] J. Carreras, G. Gopakumar, L. Gu, L. Gu, A. Gimeno, P. Linowski, J. Petuškova, W. Thiel, M. Alcarazo, *J. Am. Chem. Soc.* **2013**, *135*, 18815.

[70] X. Marset, A. Khoshnood, L. Sotorríos, E. Gómez-Bengoa, D. A. Alonso, D. J. Ramón, *ChemCatChem* **2017**, *9*, 1269.

[71] H. Tinnermann, *Design, Synthesis and Applications of new cationic ligands of the 15th main group elements*, Georg-August Universität Göttingen, Göttingen, **2017**.

[72] H. Tinnermann, L. D. M. Nicholls, T. Johannsen, C. Wille, C. Golz, R. Goddard, M. Alcarazo, *ACS Catal.* **2018**, *8*, 10457.

[73] D. Bourissou, O. Guerret, F. P. Gabbaï, G. Bertrand, *Chem. Rev.* **2000**, *100*, 39.

[74] E. Buchner, T. Curtius, *Ber. Dtsch. Chem. Ges.* **1885**, *18*, 2377.

[75] H. Staudinger, O. Kupfer, *Ber. Dtsch. Chem. Ges.* **1912**, *45*, 501.

[76] W. v. E. Doering, A. K. Hoffmann, *J. Am. Chem. Soc.* **1954**, *76*, 6162.

[77] L. Tschugajeff, M. Skanawy-Grigorjewa, A. Posnjak, *Z. anorg. allg. Chem.* **1925**, *148*, 37.

[78] E. O. Fischer, A. Maasböl, *Angew. Chem. Int. Ed.* **1964**, *3*, 580.

[79] K. Öfele, *J. Organomet. Chem.* **1968**, *12*, 42.

[80] R. Breslow, *J. Am. Chem. Soc.* **1958**, *80*, 3719.

[81] H.-W. Wanzlick, *Angew. Chem.* **1962**, *74*, 129.

[82] a) H.-J. Schönherr, H.-W. Wanzlick, *Chem. Ber.* **1970**, *103*, 1037; b) H.-J. Schönherr, H.-W. Wanzlick, *Liebigs Ann. Chem.* **1970**, *731*, 176.

[83] A. Igau, H. Grützmacher, A. Baceiredo, G. Bertrand, *J. Am. Chem. Soc.* **1988**, *110*, 6463.

[84] A. J. Arduengo, R. L. Harlow, M. Kline, *J. Am. Chem. Soc.* **1991**, *113*, 363.

[85] V. Lavallo, Y. Canac, B. Donnadieu, W. W. Schoeller, G. Bertrand, *Science* **2006**, *312*, 722.

[86] V. Lavallo, Y. Canac, C. Präsang, B. Donnadieu, G. Bertrand, *Angew. Chem. Int. Ed.* **2005**, *44*, 5705.

[87] D. Martin, M. Melaimi, M. Soleilhavoup, G. Bertrand, *Organometallics* **2011**, *30*, 5304.

[88] C. M. Weinstein, G. P. Junor, D. R. Tolentino, R. Jazzar, M. Melaimi, G. Bertrand, *J. Am. Chem. Soc.* **2018**, *140*, 9255.

[89] V. Lavallo, G. D. Frey, S. Kousar, B. Donnadieu, G. Bertrand, *Proc. Natl. Acad. Sci. USA* **2007**, *104*, 13569.

[90] M. Scholl, T. M. Trnka, J. P. Morgan, R. H. Grubbs, *Tetrahedron Lett.* **1999**, *40*, 2247.

[91] S. B. Garber, J. S. Kingsbury, B. L. Gray, A. H. Hoveyda, *J. Am. Chem. Soc.* **2000**, *122*, 8168.

[92] M. H. Holthausen, M. Mehta, D. W. Stephan, *Angew. Chem. Int. Ed.* **2014**, *53*, 6538.

[93] A. O. King, N. Okukado, E.-I. Negishi, *J.C.S. Chem. Comm.* **1977**, 683.

[94] J. Sirieix, M. Oßberger, B. Betzemeier, P. Knochel, *Synlett* **2000**, *2000*, 1613.

[95] L. D. M. Nicholls, M. Alcarazo, *Chem. Lett.* **2019**, *48*, 1.

[96] a) E. González-Fernández, L. D. M. Nicholls, L. D. Schaaf, C. Farès, C. W. Lehmann, M. Alcarazo, *J. Am. Chem. Soc.* **2017**, *139*, 1428; b) L. D. M. Nicholls, M. Marx, T. Hartung, E. González-Fernández, C. Golz, M. Alcarazo, *ACS Catal.* **2018**, *8*, 6079.

[97] T. Hartung, R. Machleid, M. Simon, C. Golz, M. Alcarazo, *Angew. Chem. Int. Ed.* **2020**, *59*, 5660.

[98] P. Redero, T. Hartung, J. Zhang, L. D. M. Nicholls, G. Zichen, M. Simon, C. Golz, M. Alcarazo, *Angew. Chem. Int. Ed.* **2020**, *59*, 23527.

[99] J. Zhang, M. Simon, C. Golz, M. Alcarazo, *Angew. Chem. Int. Ed.* **2020**, *59*, 5647.

[100] K. Sprenger, C. Golz, M. Alcarazo, *Eur. J. Org. Chem.* **2020**, *2020*, 6245.

[101] L. Gu, L. M. Wolf, A. Zieliński, W. Thiel, M. Alcarazo, *J. Am. Chem. Soc.* **2017**, *139*, 4948.

[102] A. Zieliński, X. Marset, C. Golz, L. M. Wolf, M. Alcarazo, *Angew. Chem. Int. Ed.* **2020**, *59*, 23299.

[103] X. Marset, M. Recort-Fornals, M. Kpante, A. Zieliński, C. Golz, L. M. Wolf, M. Alcarazo, *Adv. Synth. Catal.* **2021**, *363*, 3546.

[104] T. Zincke, *Liebigs Ann. Chem.* **1904**, *330*, 361.

[105] O. Diebolt, G. C. Fortman, H. Clavier, A. M. Z. Slawin, E. C. Escudero-Adán, J. Benet-Buchholz, S. P. Nolan, *Organometallics* **2011**, *30*, 1668.

[106] M. Teci, D. Hueber, P. Pale, L. Toupet, A. Blanc, E. Brenner, D. Matt, *Chem. Eur. J.* **2017**, *23*, 7809.

[107] A. S. K. Hashmi, J. P. Weyrauch, W. Frey, J. W. Bats, *Org. Lett.* **2004**, *6*, 4391.

[108] D. Ding, T. Mou, J. Xue, X. Jiang, *Chem. Commun.* **2017**, *53*, 5279.

[109] D. W. Allen, B. F. Taylor, *Dalton Trans.* **1982**, 51.

[110] L. Gu, Y. Zheng, E. Haldón, R. Goddard, E. Bill, W. Thiel, M. Alcarazo, *Angew. Chem. Int. Ed.* **2017**, *56*, 8790.

[111] S. Styra, M. Melaimi, C. E. Moore, A. L. Rheingold, T. Augenstein, F. Breher, G. Bertrand, *Chem. Eur. J.* **2015**, *21*, 8441.

[112] a) S. Grimme, J. Antony, Ehrlich, S., Krieg, H., *J. Chem. Phys.* **2010**, *132*, 154104; b) F. Weigend, *Phys. Chem. Chem. Phys.* **2006**, *8*, 1057; c) C. Lee, W. Yang, R. G. Parr, *Phys. Rev. B.* **1988**, *37*, 785; d) A. D. Becke, *J. Chem. Phys.* **1993**, *98*, 5648.

[113] S. Yogendra, F. Hennersdorf, A. Bauzá, A. Frontera, R. Fischer, J. J. Weigand, *Chem. Commun.* **2017**, *53*, 2954.

[114] D. Kalia, S. P. Pawar, J. S. Thopate, *Angew. Chem. Int. Ed.* **2017**, *56*, 1885.

[115] L. Wang, R. Ganguly, F. Mathey, *Organometallics* **2014**, *33*, 5614.

[116] W. J. Transue, A. Velian, M. Nava, C. García-Iriepa, M. Temprado, C. C. Cummins, *J. Am. Chem. Soc.* **2017**, *139*, 10822.

[117] D. V. Partyka, T. J. Robilotto, M. Zeller, A. D. Hunter, T. G. Gray, *Organometallics* **2008**, *27*, 28.

[118] P. Ruiz-Castillo, D. G. Blackmond, S. L. Buchwald, *J. Am. Chem. Soc.* **2015**, *137*, 3085.

[119]   P. Morán-Poladura, S. Suárez-Pantiga, M. Piedrafita, E. Rubio, J. M. González, *J. Organomet. Chem.* **2011**, *696*, 12.

[120]   F. Gagosz, *Synthesis* **2019**, *51*, 1087.

[121]   H. Kinuta, M. Tobisu, N. Chatani, *J. Am. Chem. Soc.* **2015**, *137*, 1593.

[122]   R. Jazzar, R. D. Dewhurst, J.-B. Bourg, B. Donnadieu, Y. Canac, G. Bertrand, *Angew. Chem. Int. Ed.* **2007**, *46*, 2899.

[123]   a) M. Westerhausen, C. Gückel, H. Piotrowski, P. Mayer, M. Warchhold, H. Nöth, *Z. anorg. allg. Chem.* **2001**, *627*, 1741; b) P. J. Fagan, W. A. Nugent, J. C. Calabrese, *J. Am. Chem. Soc.* **1994**, *116*, 1880.

[124]   a) J. Cui, L. Meng, X. Chi, Q. Liu, P. Zhao, D.-P. Zhang, L. Chen, X. Li, Y. Dong, H. Liu, *Chem. Commun.* **2019**, *55*, 4355; b) J.-S. Tang, C.-C. Guo, *Synthesis* **2014**, *47*, 108; c) X. Liu, G. Chen, C. Li, P. Liu, *Synlett* **2018**, *29*, 2051.

[125]   A. Ochida, H. Ito, M. Sawamura, *J. Am. Chem. Soc.* **2006**, *128*, 16486.

[126]   C. Qin, X. Xie, G. Wang, X. Jia, Y. Liu, *Tetrahedron Lett.* **2020**, *61*, 151388.

[127]   A. C. Shaikh, D. S. Ranade, P. R. Rajamohanan, P. P. Kulkarni, N. T. Patil, *Angew. Chem. Int. Ed.* **2017**, *56*, 757.

[128]   L. Falivene, Z. Cao, A. Petta, L. Serra, A. Poater, R. Oliva, V. Scarano, L. Cavallo, *Nat. Chem.* **2019**, *11*, 872.

[129]   M. J. Frisch, G. W. Trucks, H. B. Schlegel, G. E. Scuseria, M. A. Robb, J. R. Cheeseman, G. Scalmani, V. Barone, G. A. Petersson, H. Nakatsuji et al., *Gaussian 16, Revision A.03*, D. J. Gaussian, Inc., Wallingford CT, **2016**.

7. Appendix

8. Analytical Data

8.1 NMR-spectra

Compound 172: ^{1}H-NMR (400 MHz, CD$_2$Cl$_2$)
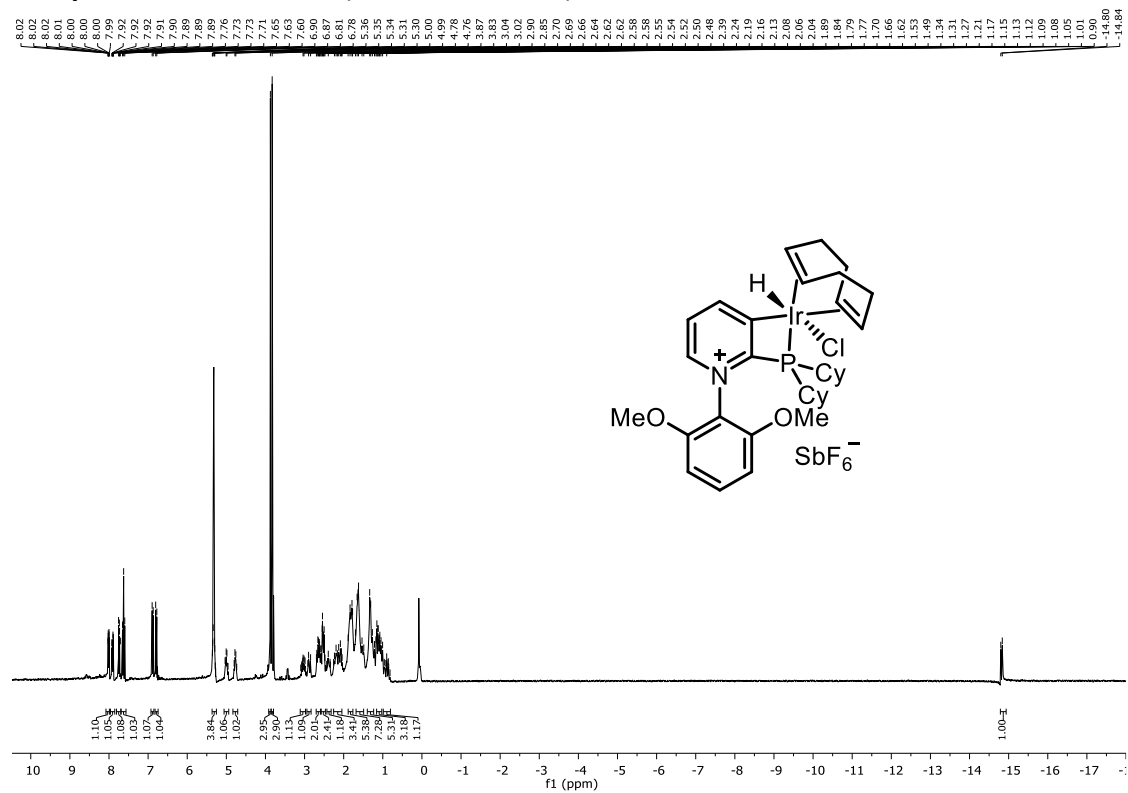
Compound 172: ^{13}C NMR (101 MHz, CD$_2$Cl$_2$)
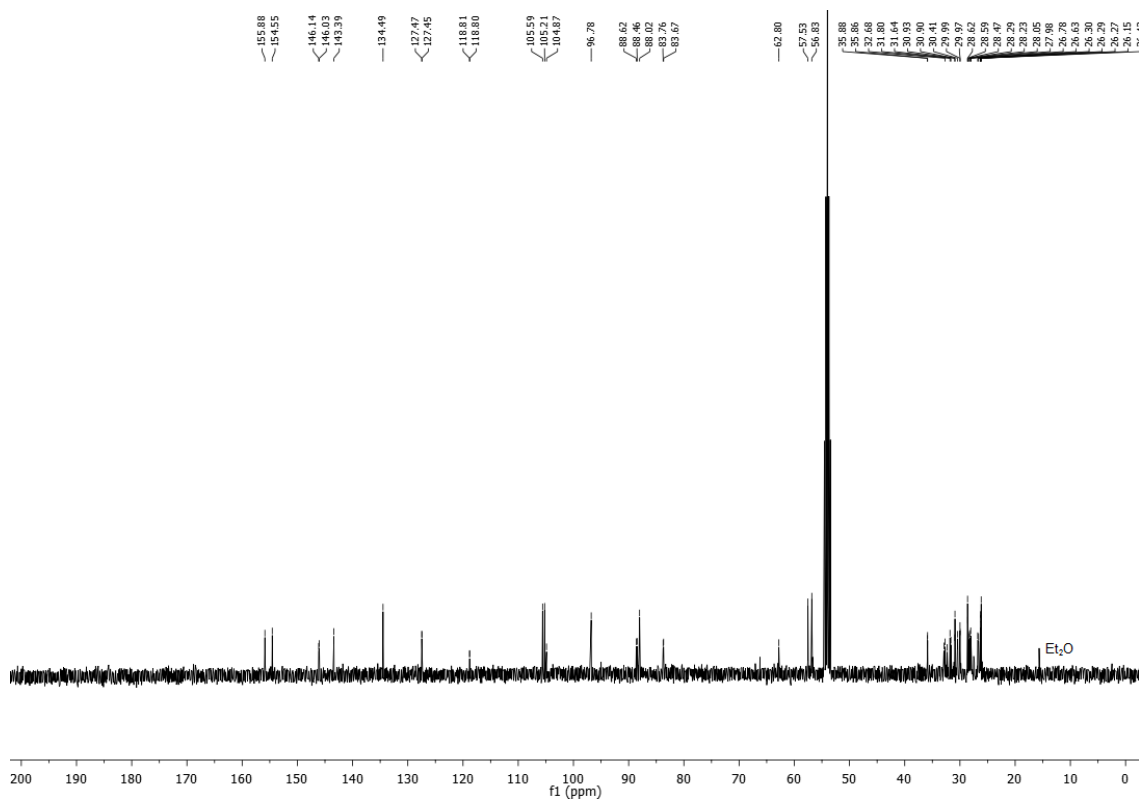
Compound 172: ^{31}P NMR (121 MHz, CD$_2$Cl$_2$)
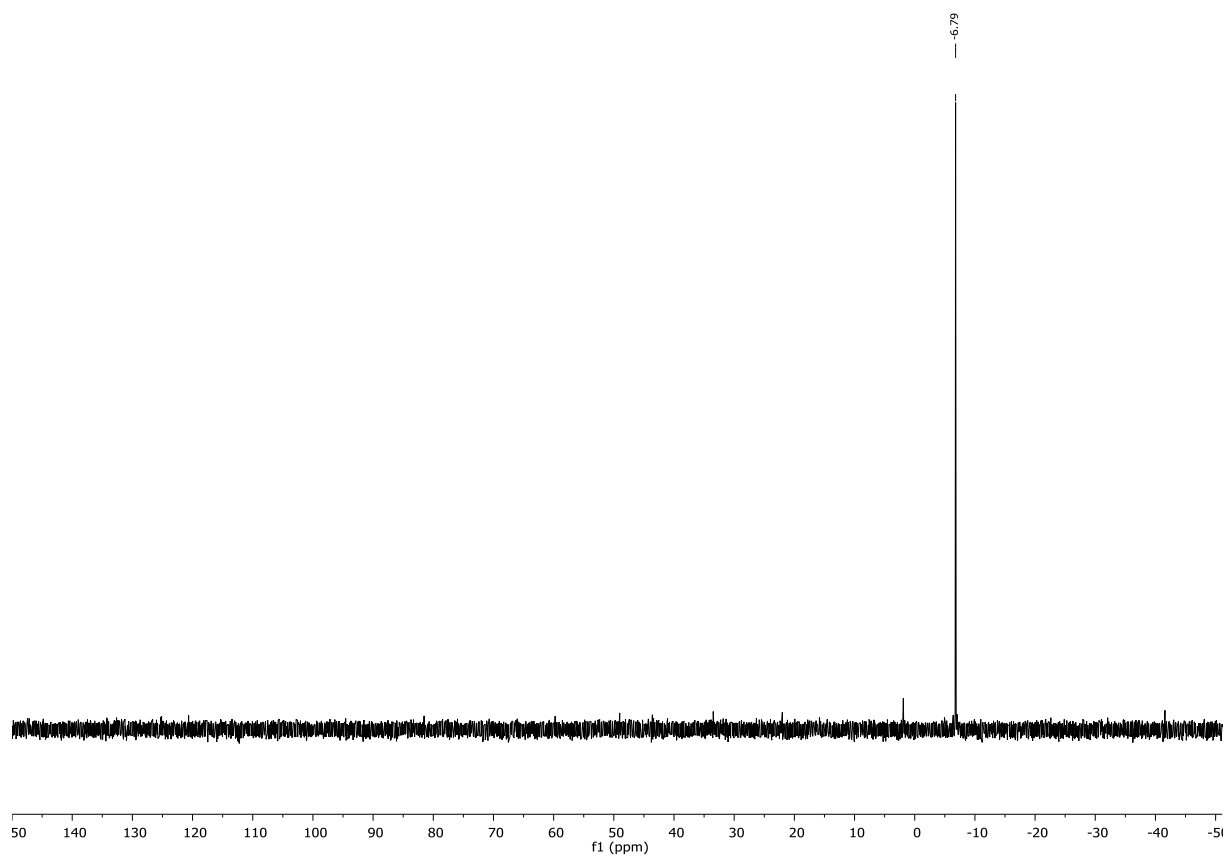
Compound 174: ^{1}H-NMR (400 MHz, CD$_2$Cl$_2$)
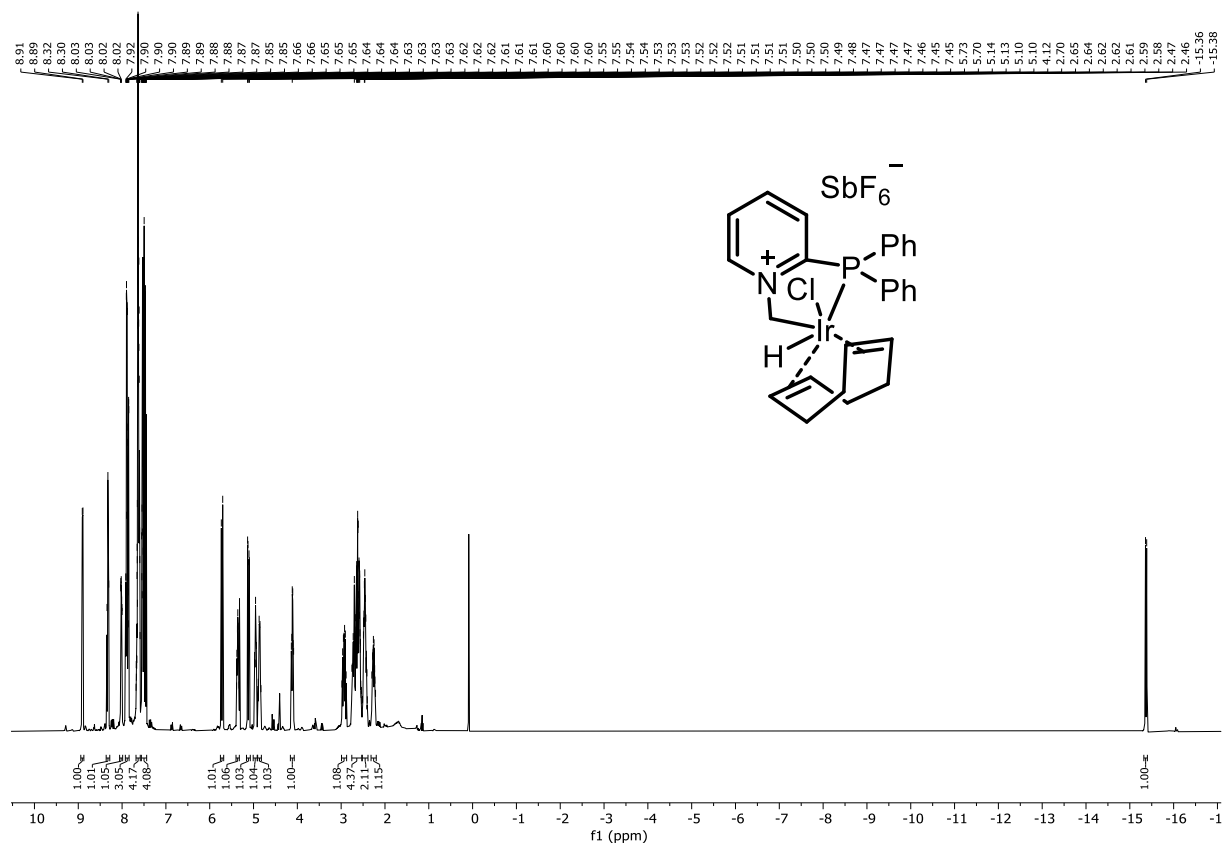
Compound 174: ^{13}C NMR (101 MHz, CD$_2$Cl$_2$)
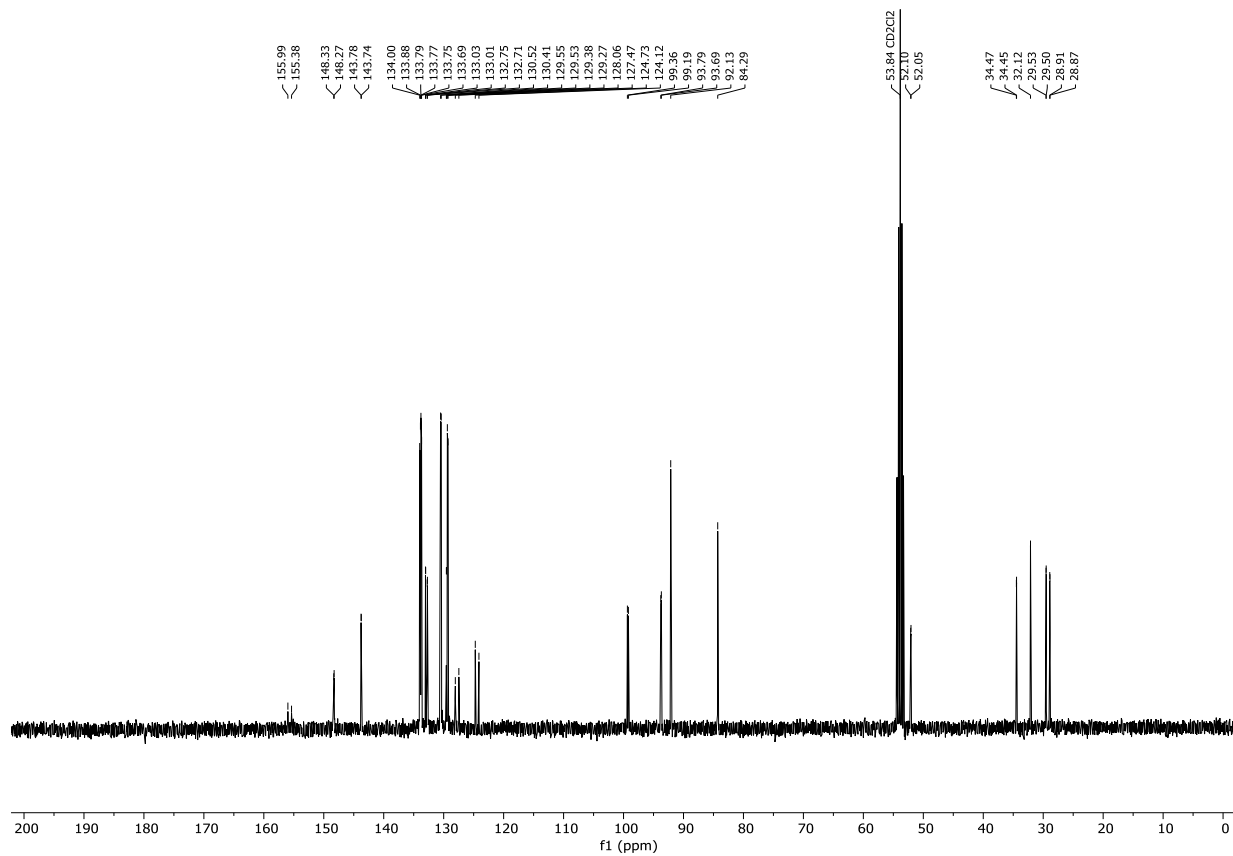
Compound 174: ^{31}P NMR (121 MHz, CD$_2$Cl$_2$)
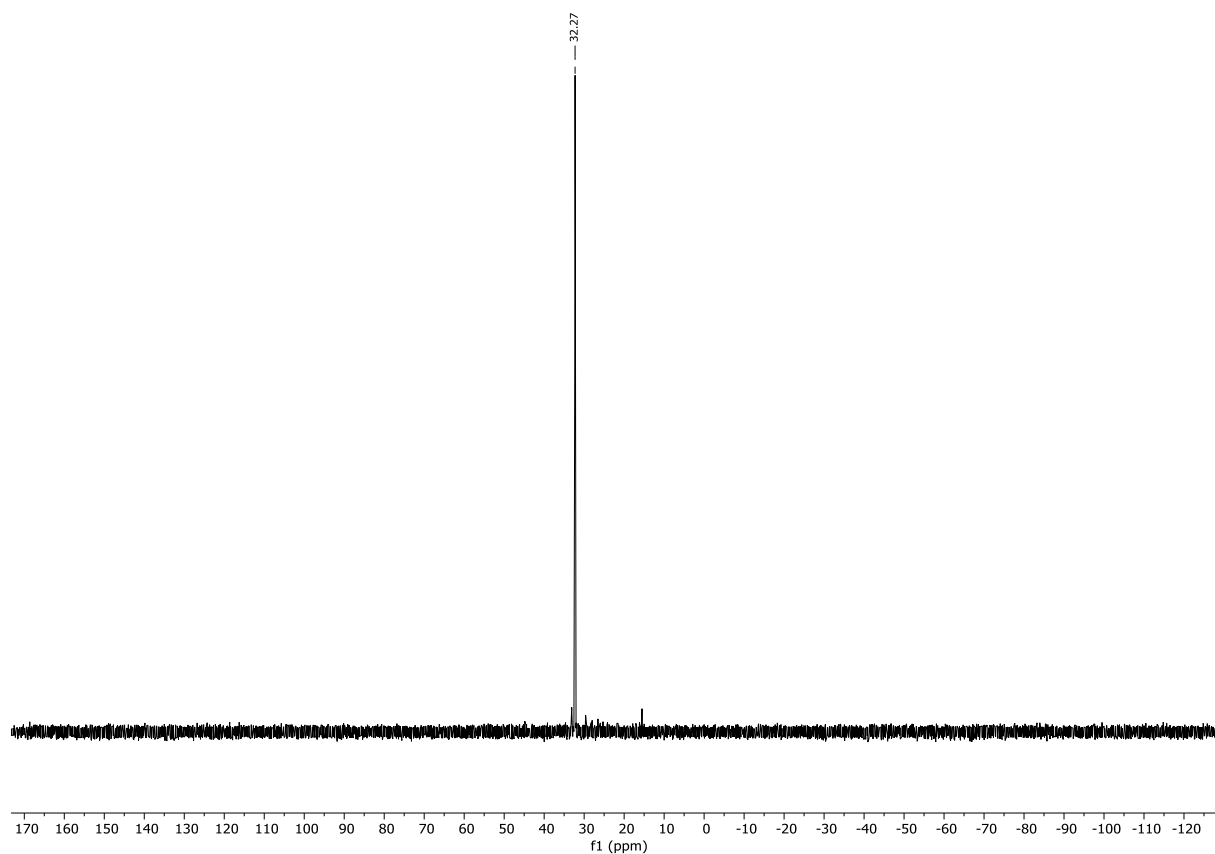
Compound 191a: ^{1}H NMR (400 MHz, CD$_2$Cl$_2$)
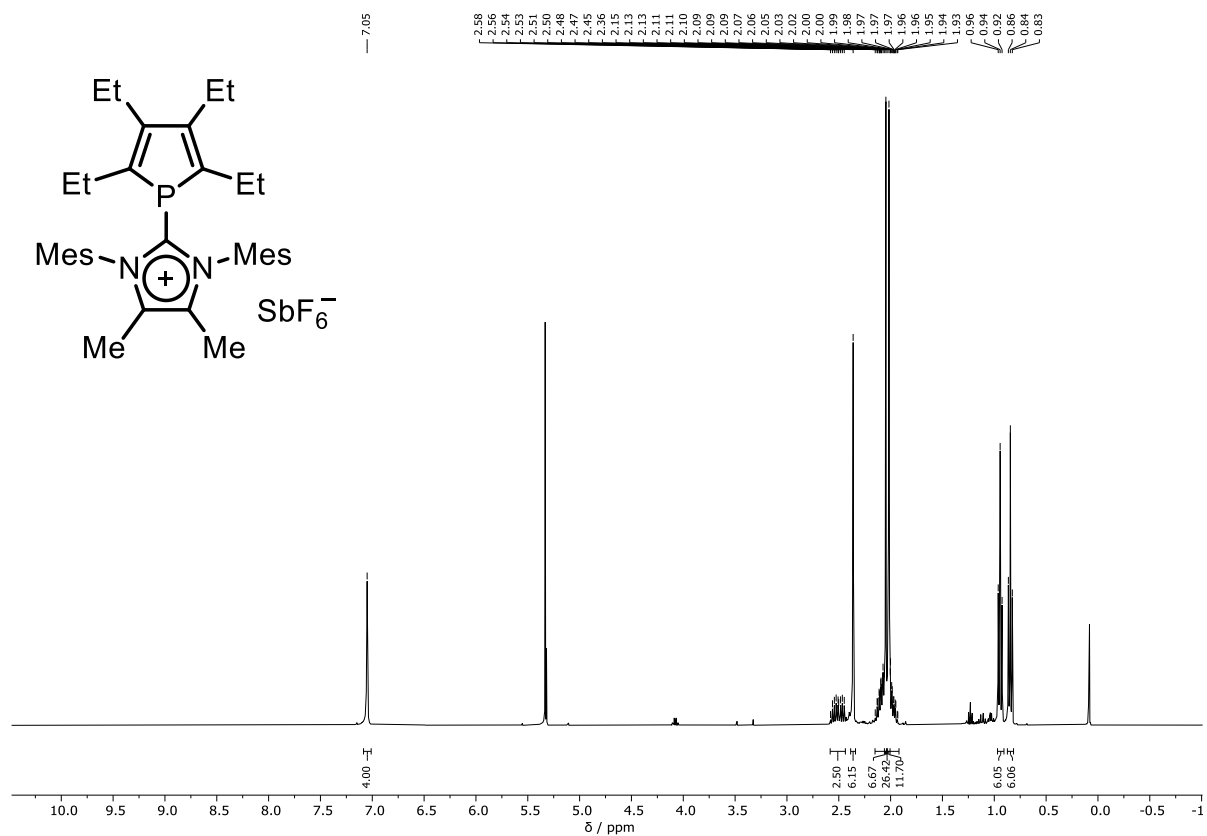
Compound 191a: ^{13}C NMR (101 MHz, CD$_2$Cl$_2$)
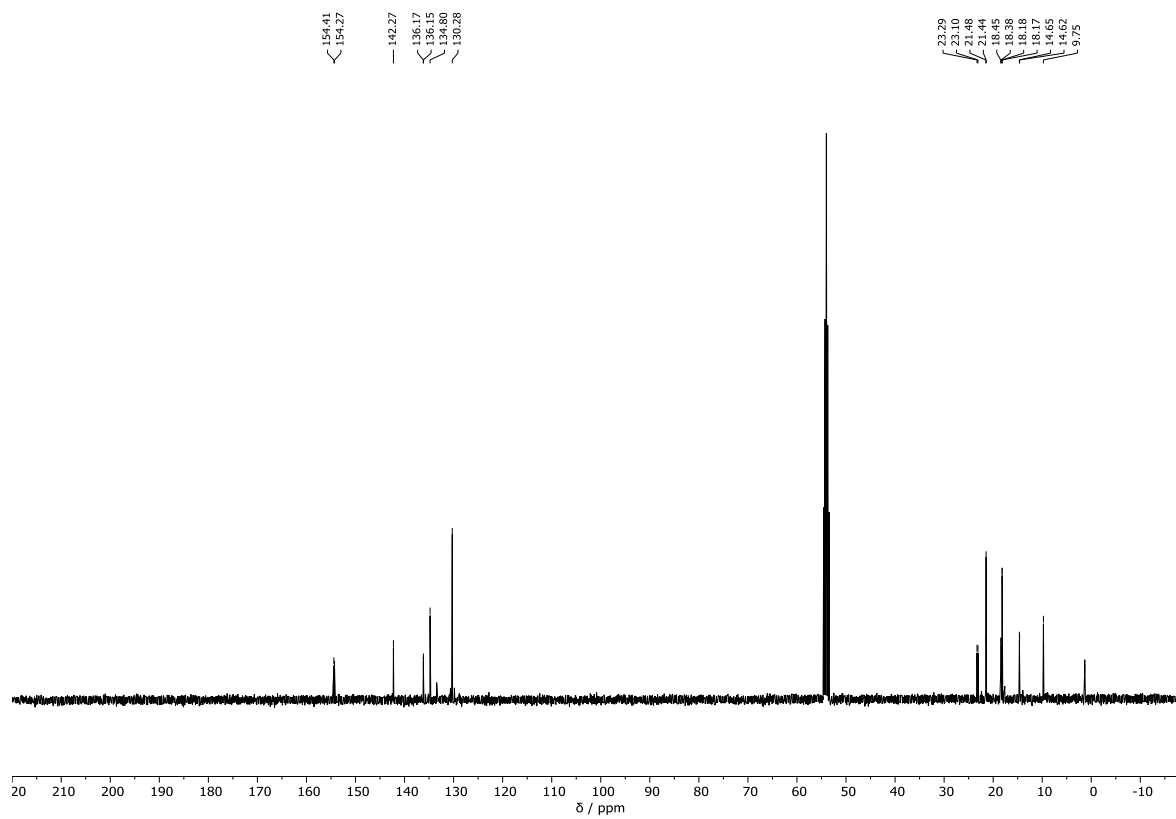
Compound 191a: ^{31}P NMR (162 MHz, CD$_2$Cl$_2$)
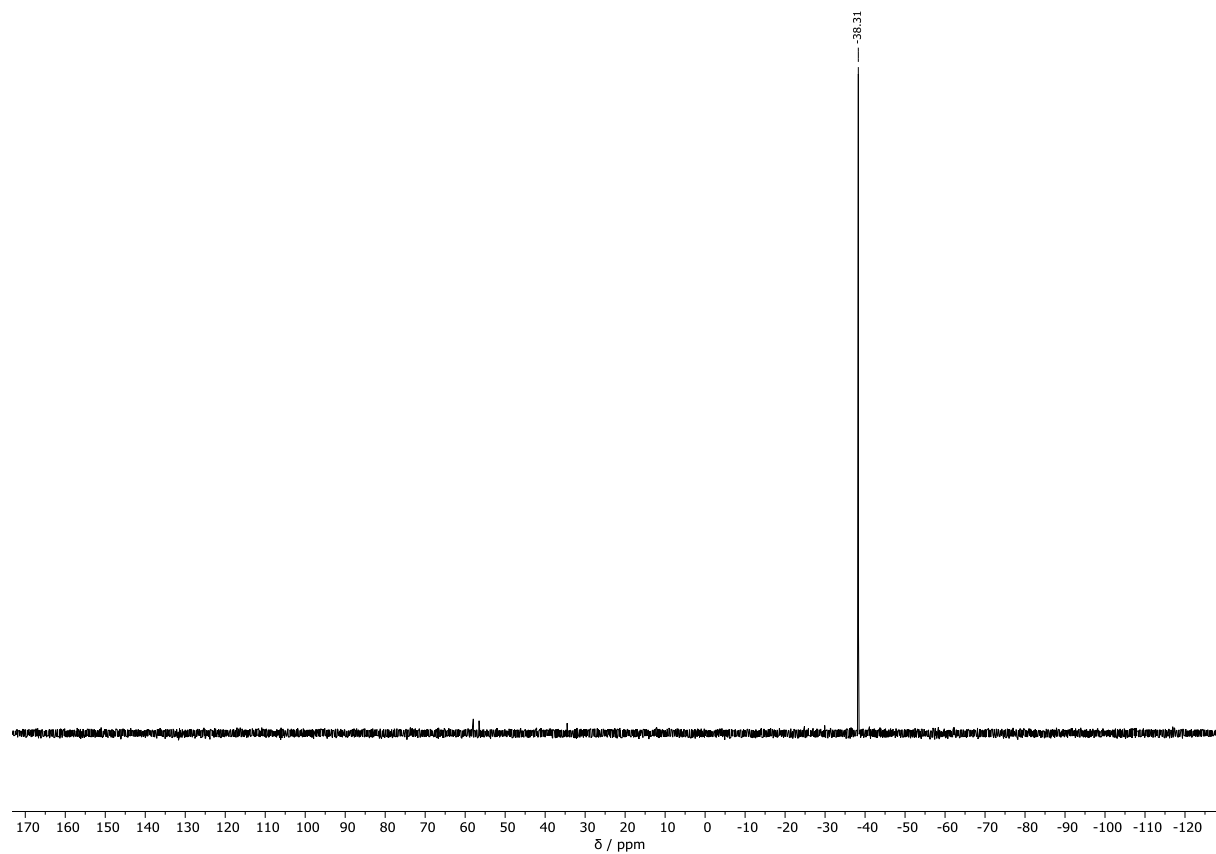
Compound 191b: ^{1}H NMR (400 MHz, CD$_2$Cl$_2$)
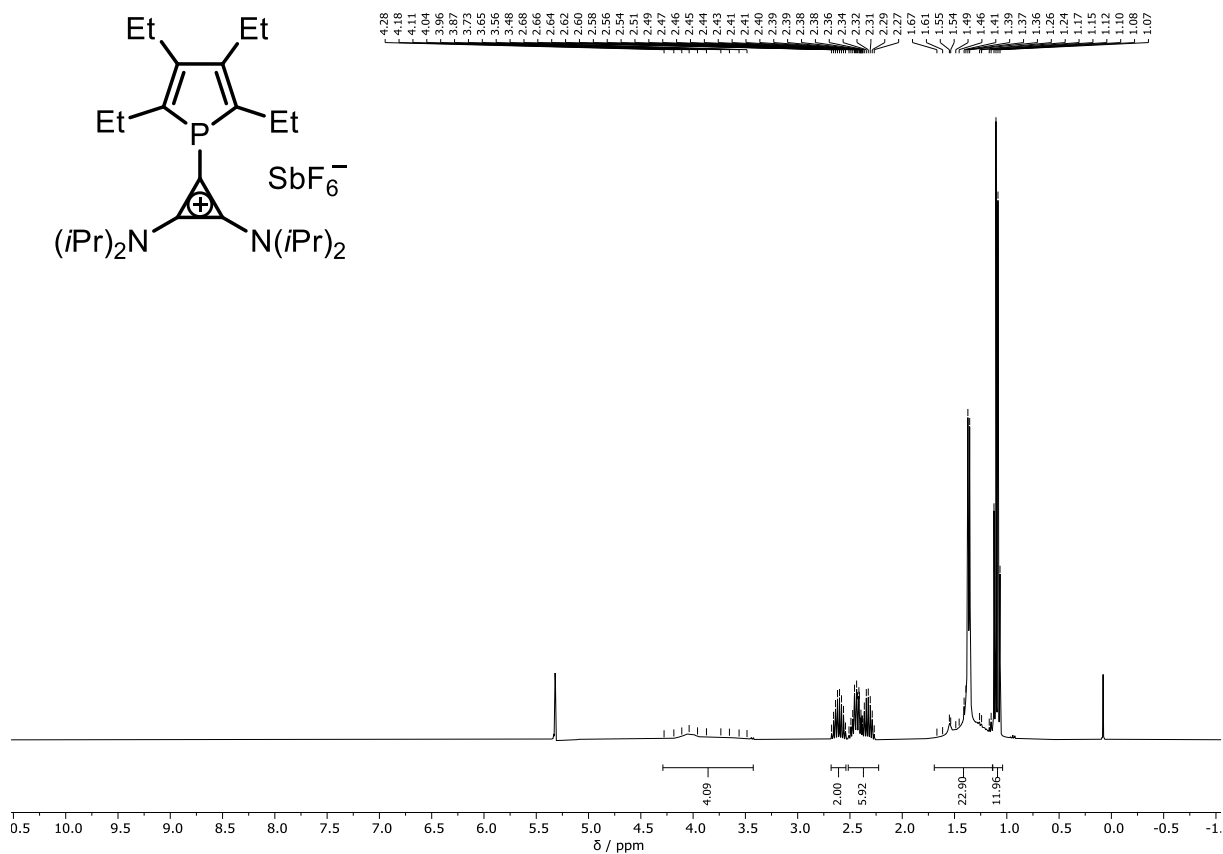
Compound 191b: ^{13}C NMR (101 MHz, CD$_2$Cl$_2$)
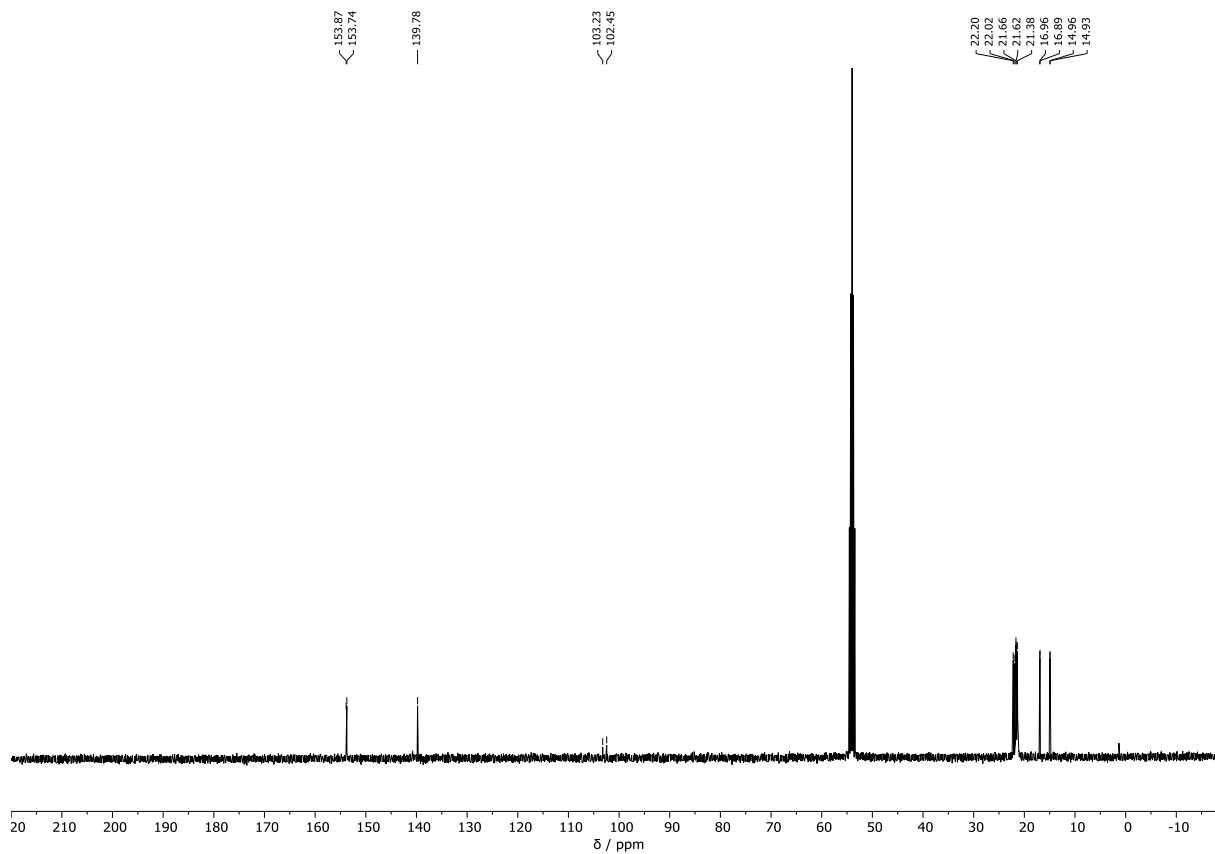
Compound 191b: ^{31}P NMR (162 MHz, CD$_2$Cl$_2$)
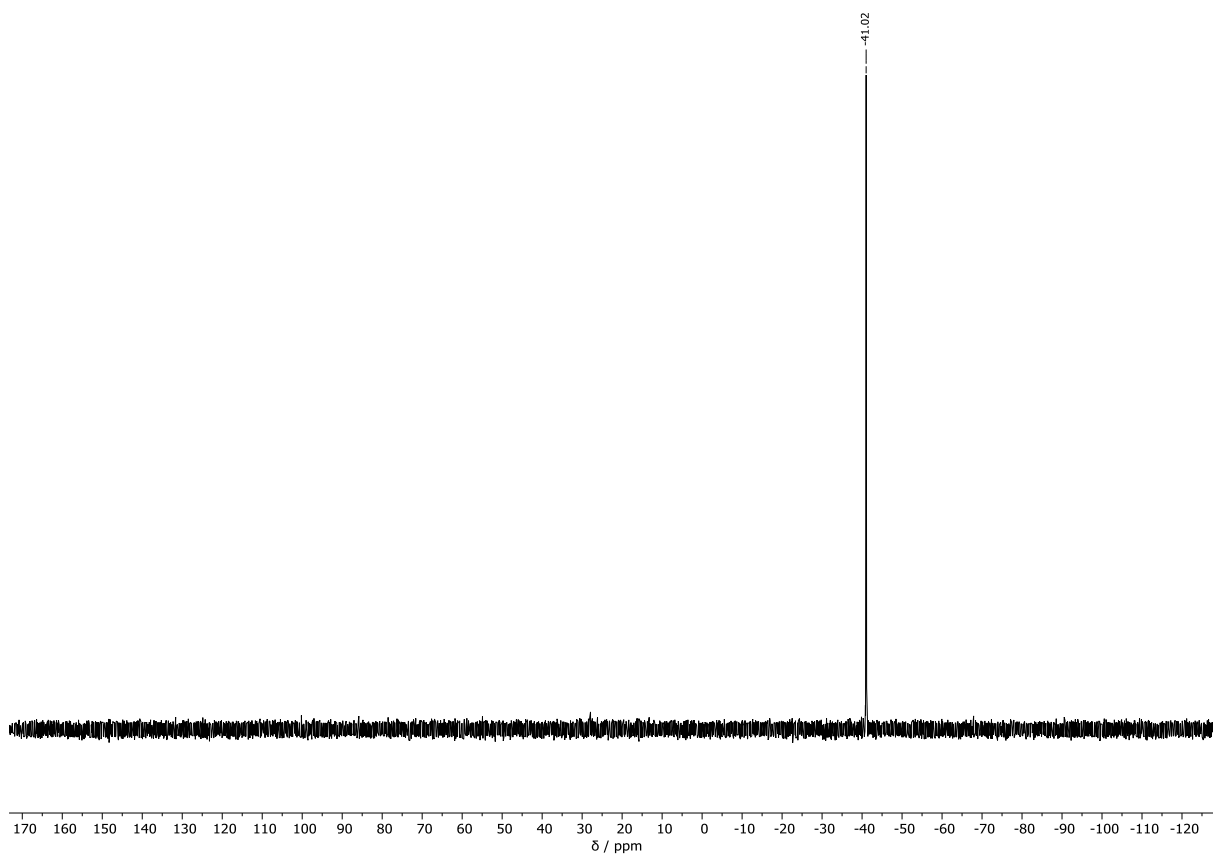
Compound 191c: ^{1}H NMR (400 MHz, CDCl$_3$)
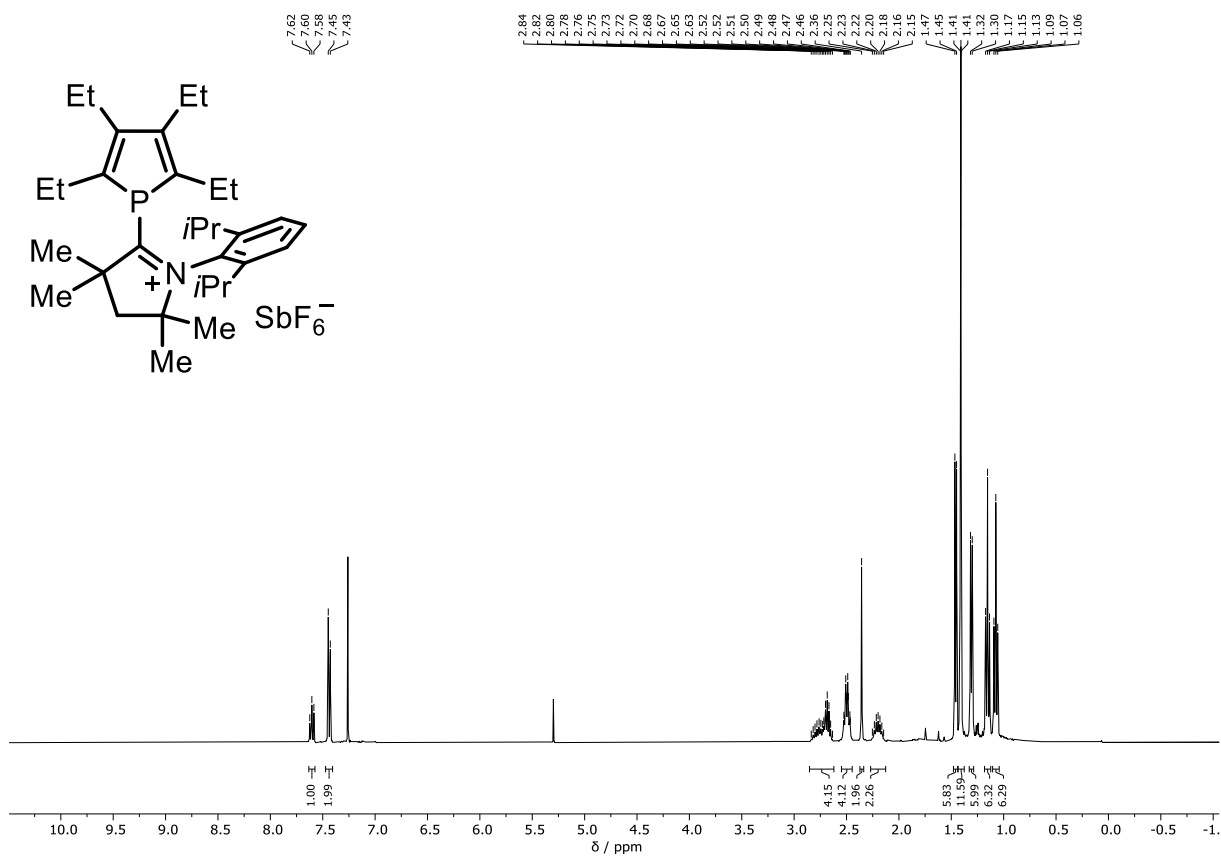
Compound 191c: ^{13}C NMR (101 MHz, CDCl$_3$)

214.01
213.39
158.63
158.51
144.51
137.91
137.83
131.95
130.33
130.28
125.95
84.28
84.27
57.81
57.74
50.48
30.72
30.39
29.19
28.96
28.93
23.93
22.44
22.26
21.63
21.60
17.34
14.09
14.06

δ / ppm
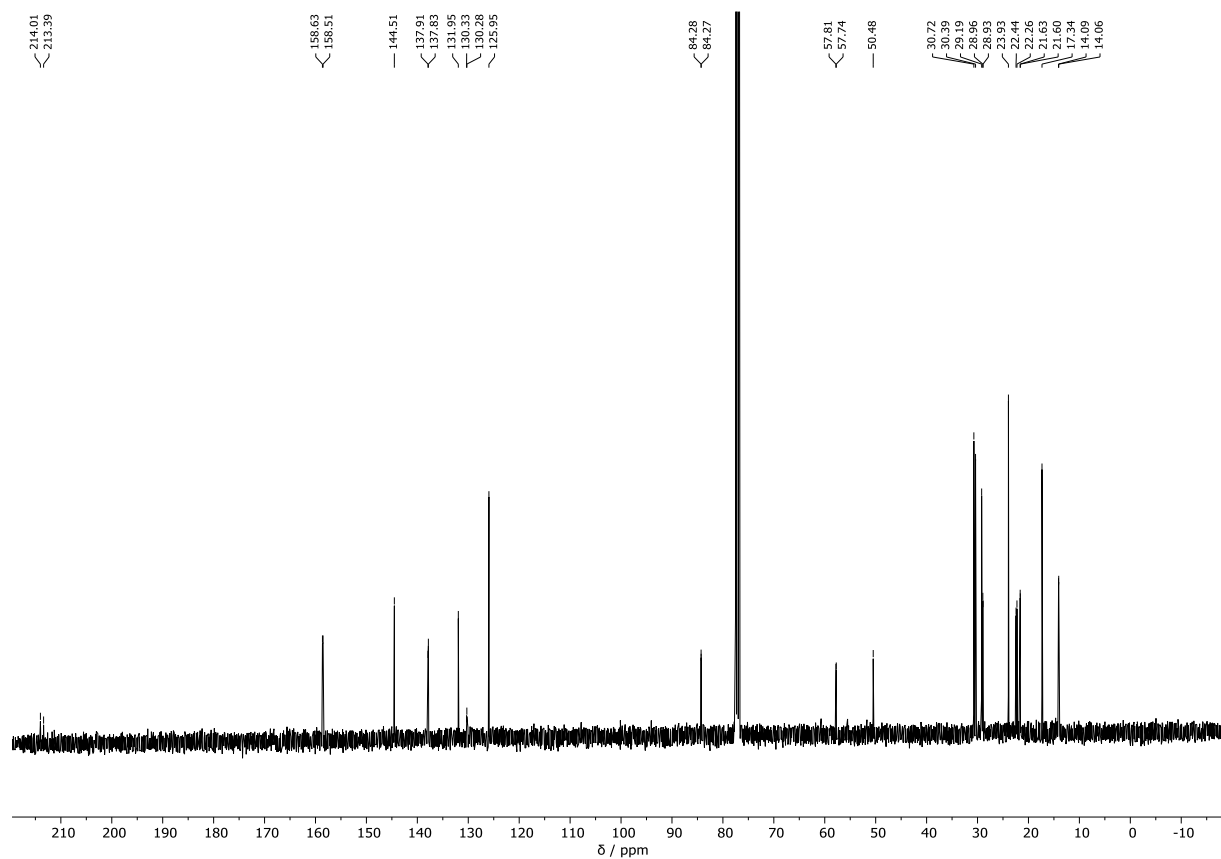
Compound 191c: ^{31}P NMR (162 MHz, CDCl$_3$)

-15.99

δ / ppm
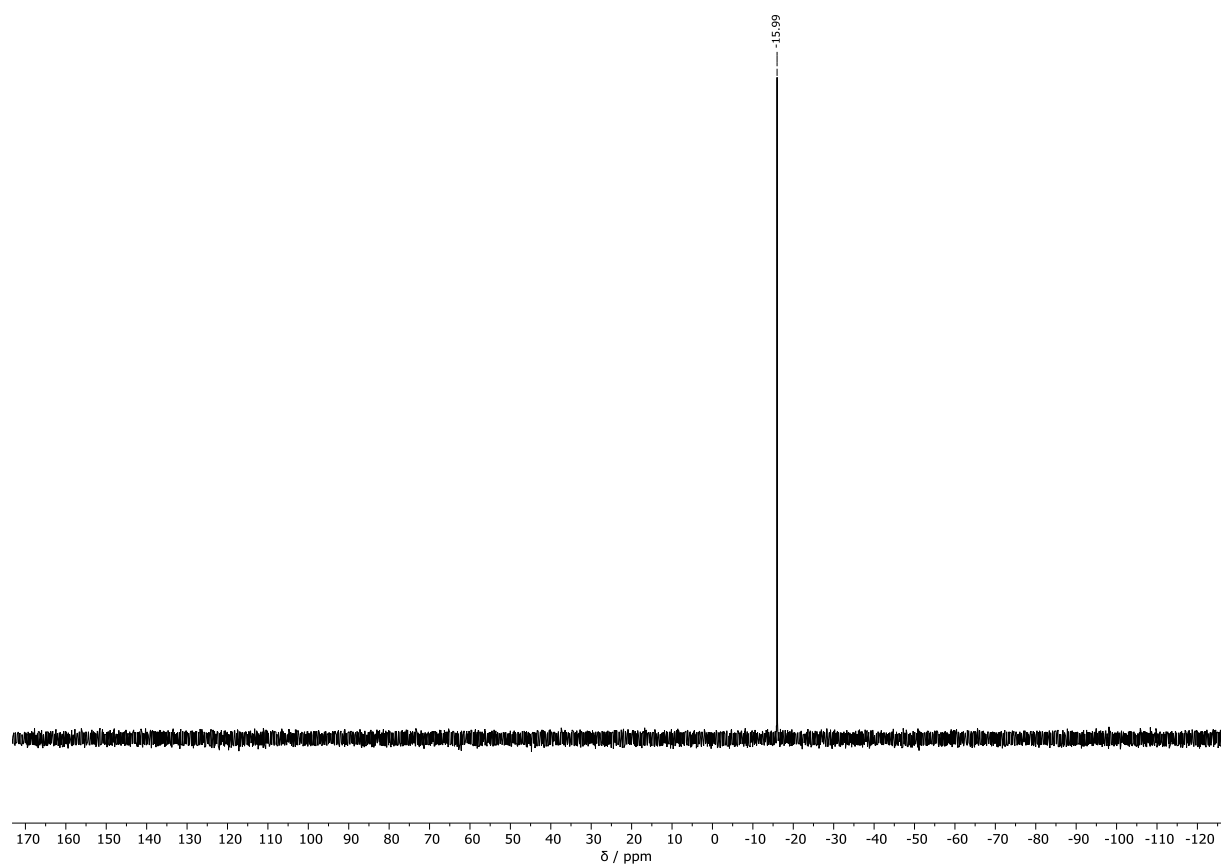
Compound 191d: ^{1}H NMR (400 MHz, CD$_2$Cl$_2$)
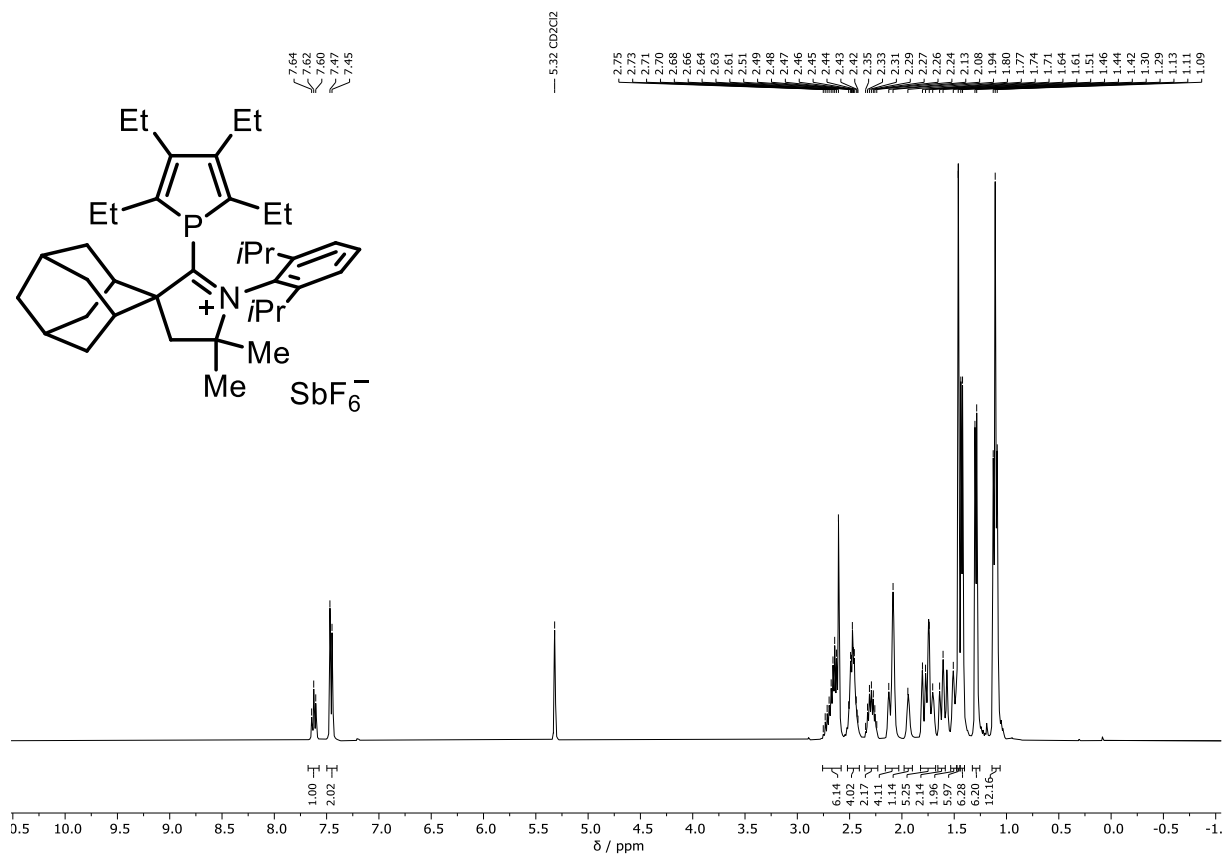
Compound 191d ^{13}C NMR (101 MHz, CD$_2$Cl$_2$)
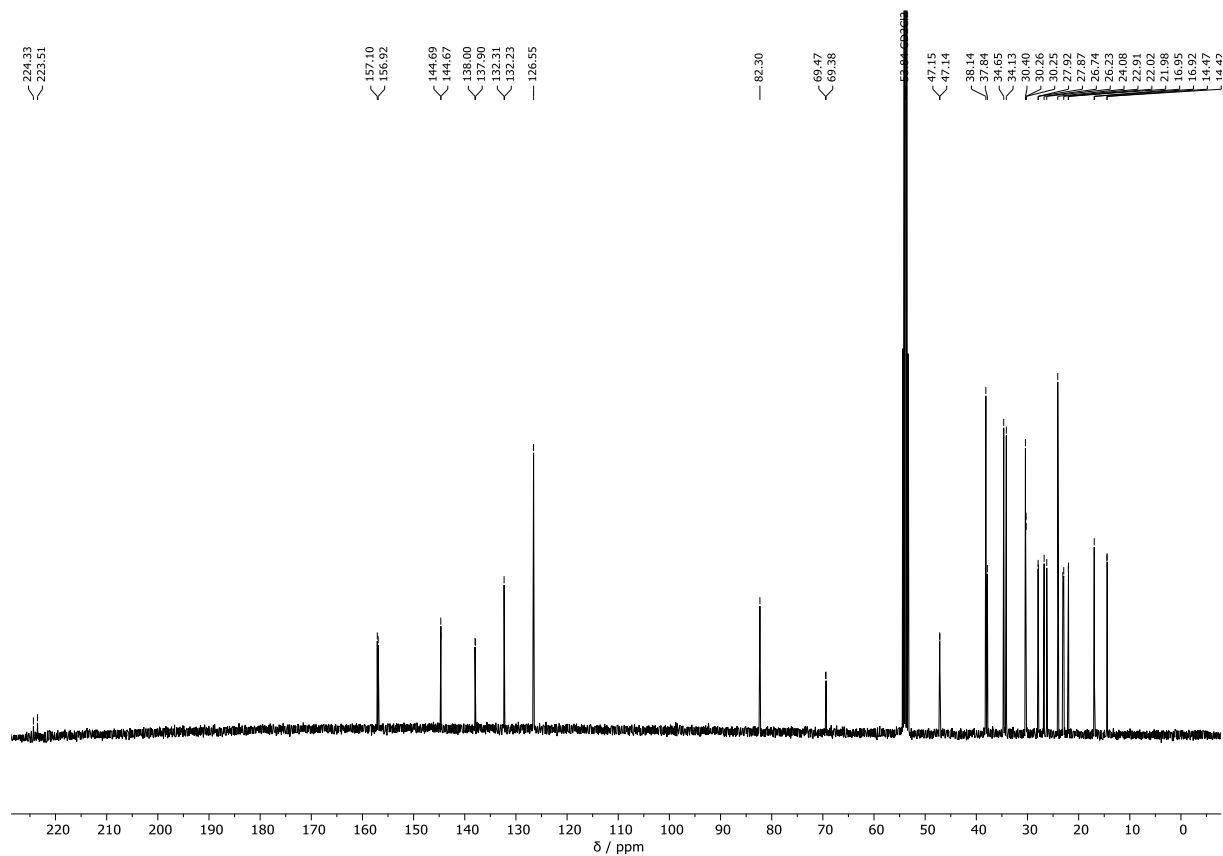
Compound 191d: ^{31}P NMR (162 MHz, CD$_2$Cl$_2$)
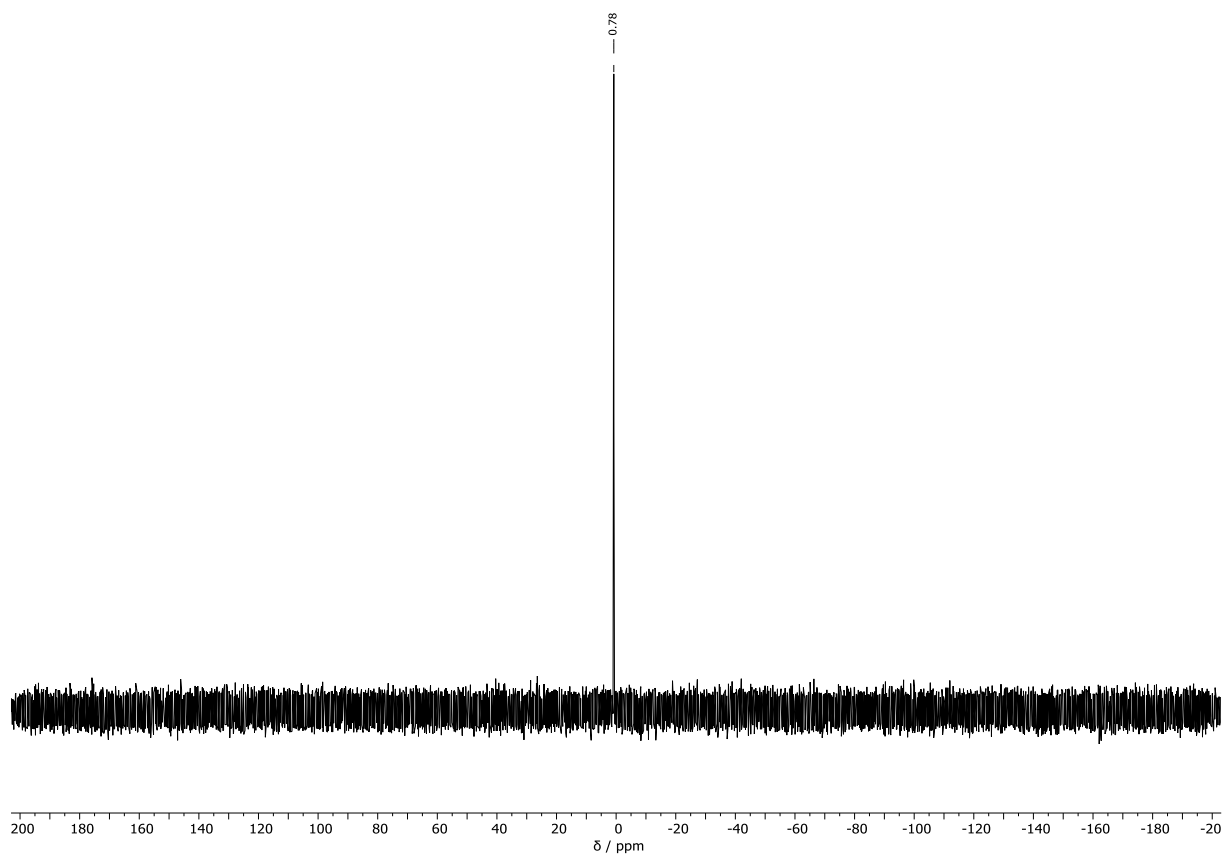
Compound 193: ^{1}H NMR (400 MHz, CD$_2$Cl$_2$)
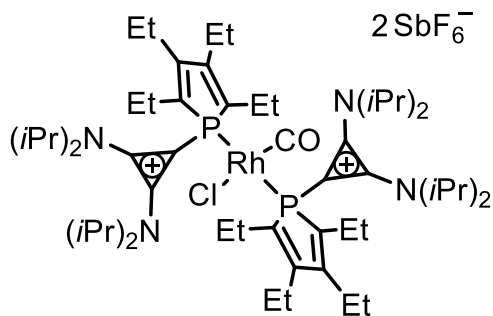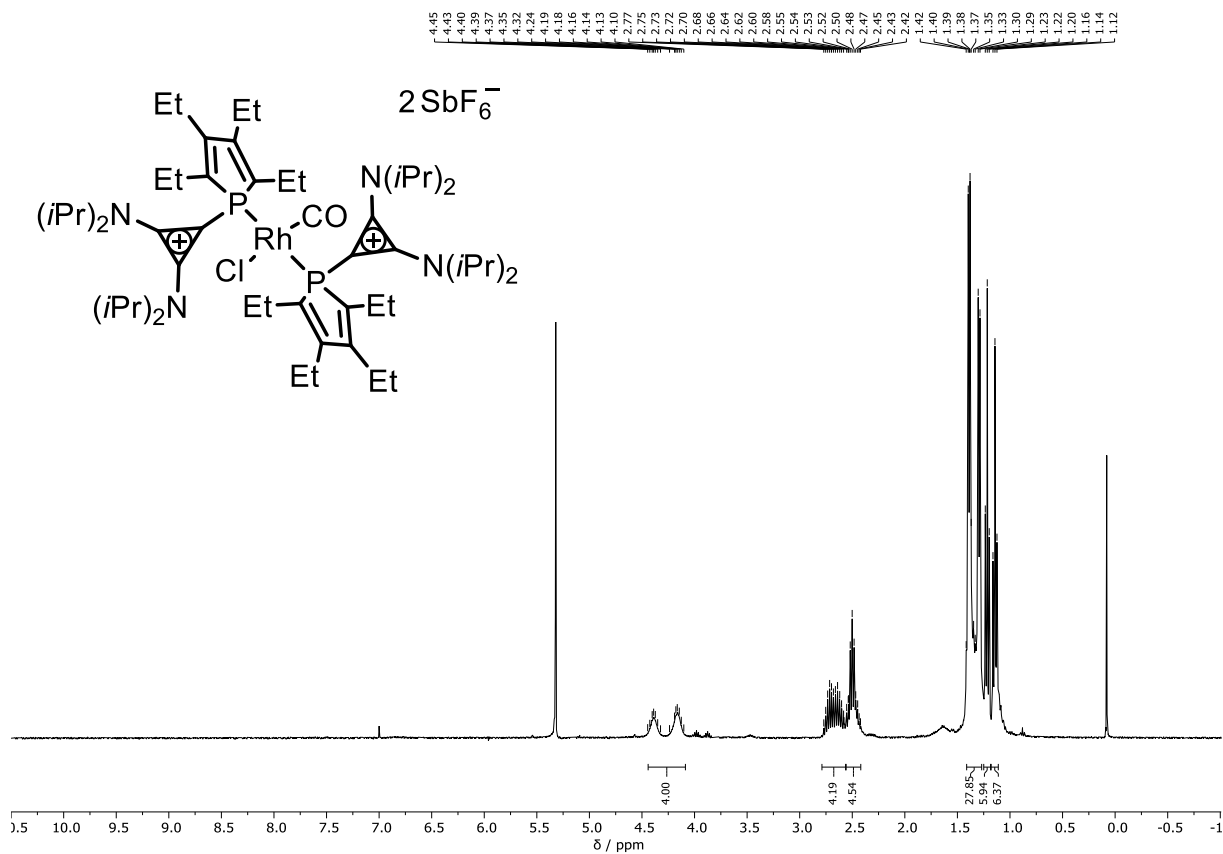
Compound 193: ^{13}C NMR (101 MHz, CD$_2$Cl$_2$)

156.16
156.06
155.97
139.21
139.20
139.18
135.77
135.55
135.33
98.03
22.42
22.14
22.07
22.00
21.95
21.91
21.86
21.80
21.62
21.14
19.80
16.55
14.56

20 210 200 190 180 170 160 150 140 130 120 110 100 90 80 70 60 50 40 30 20 10 0 -10
δ / ppm
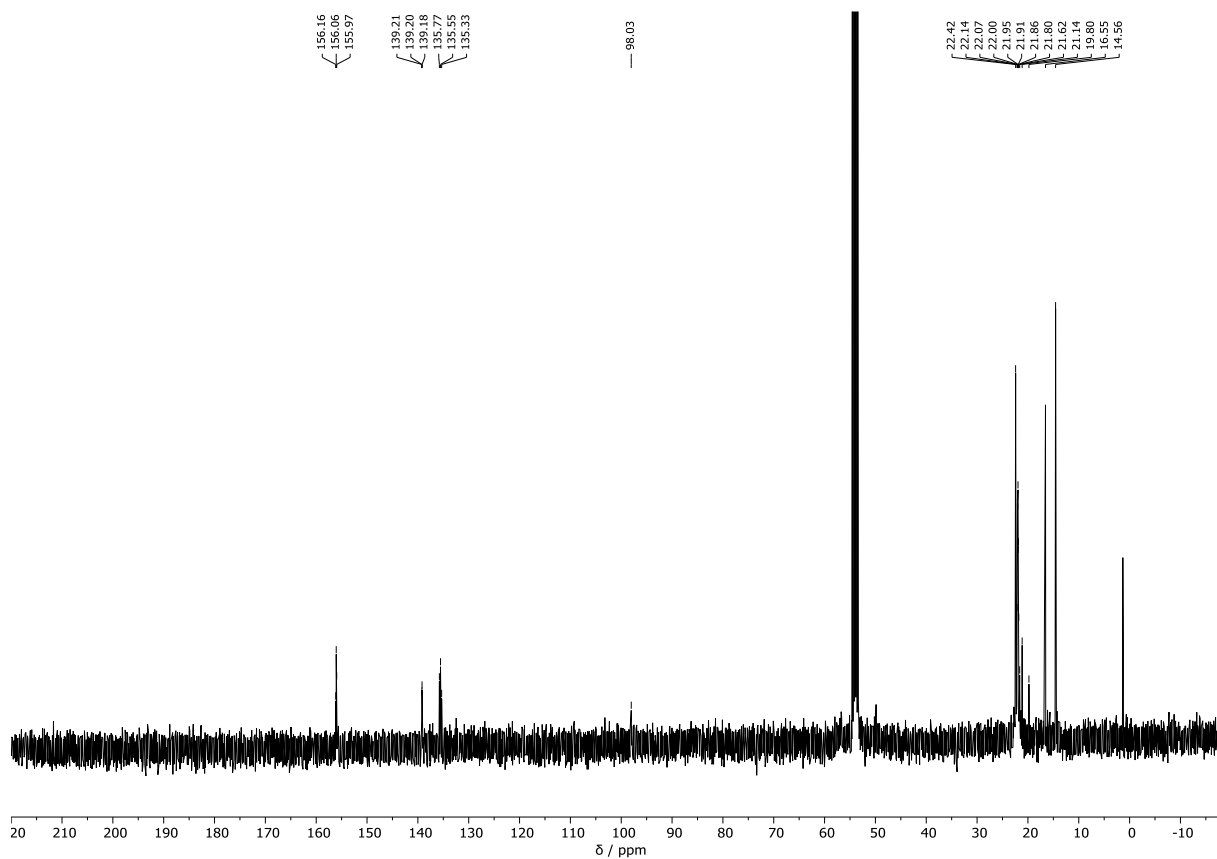
Compound 193: ^{31}P NMR (162 MHz, CD$_2$Cl$_2$)

7.91
7.14

170 160 150 140 130 120 110 100 90 80 70 60 50 40 30 20 10 0 -10 -20 -30 -40 -50 -60 -70 -80 -90 -100 -110 -120
δ / ppm

106
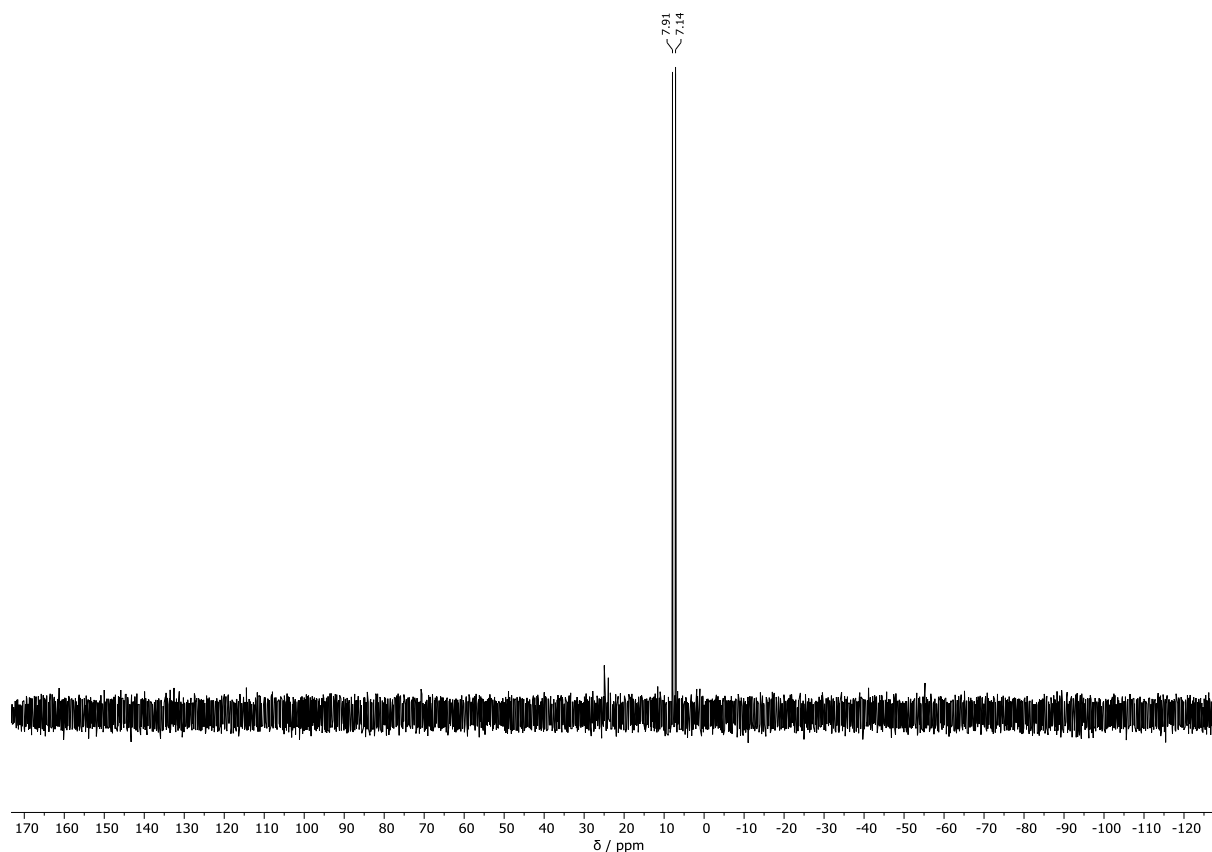
Compound 194: ^{1}H NMR (400 MHz, CDCl$_3$)
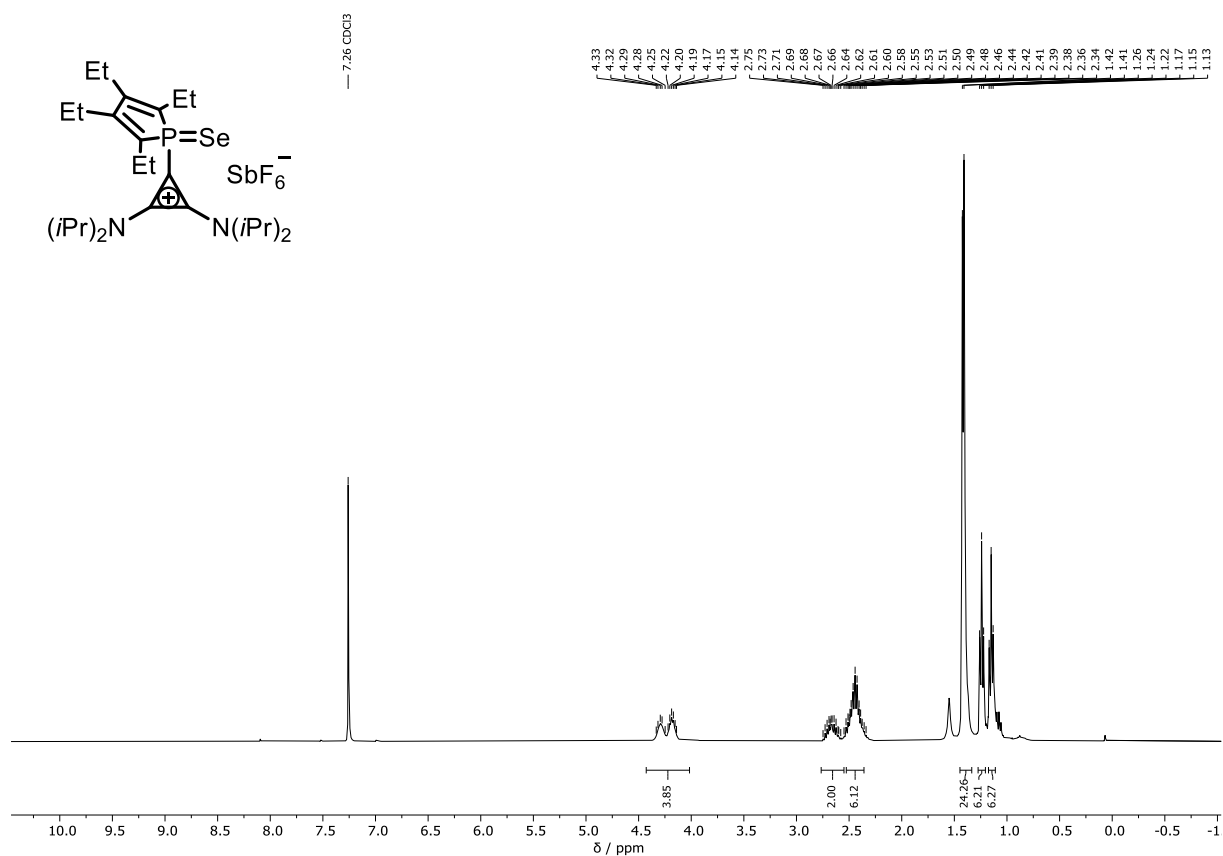
Compound 194: ^{13}C NMR (101 MHz, CDCl$_3$)
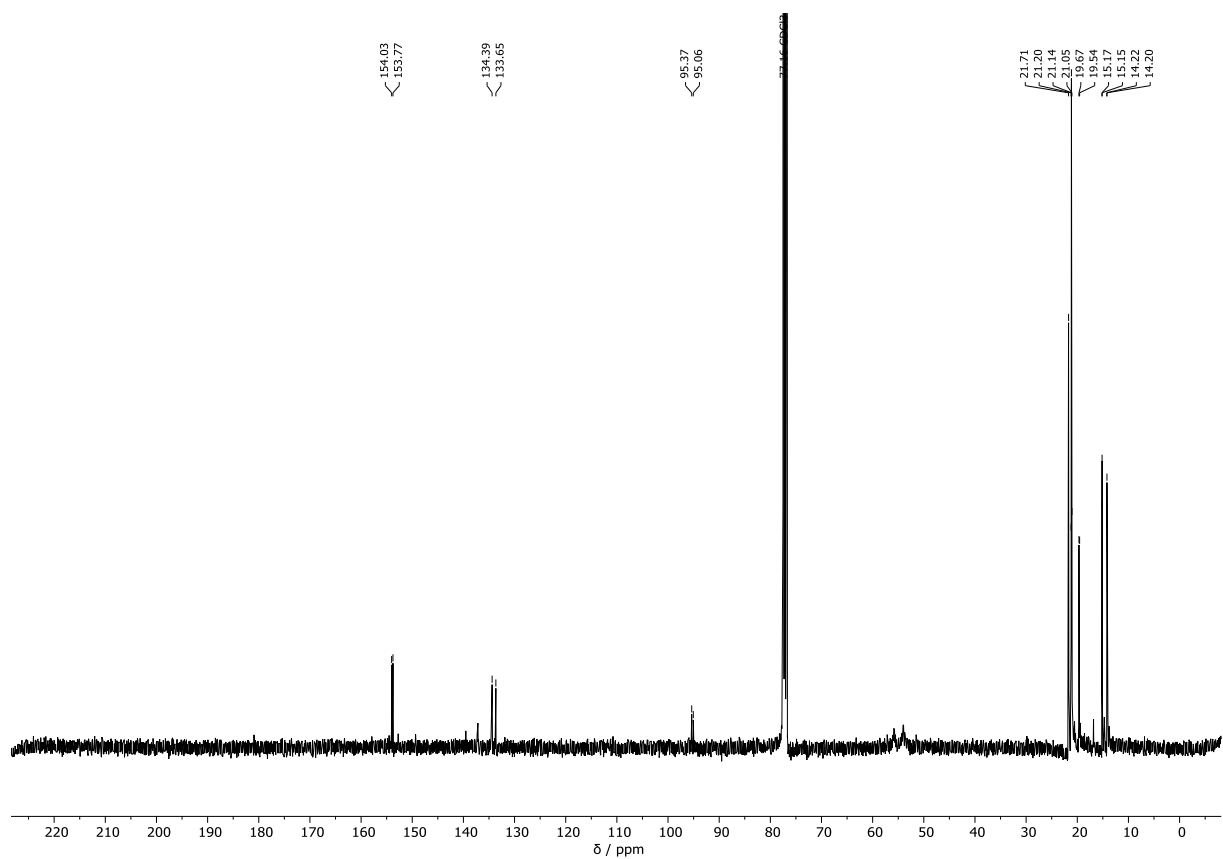
Compound 194: ^{31}P NMR (162 MHz, CDCl$_3$)
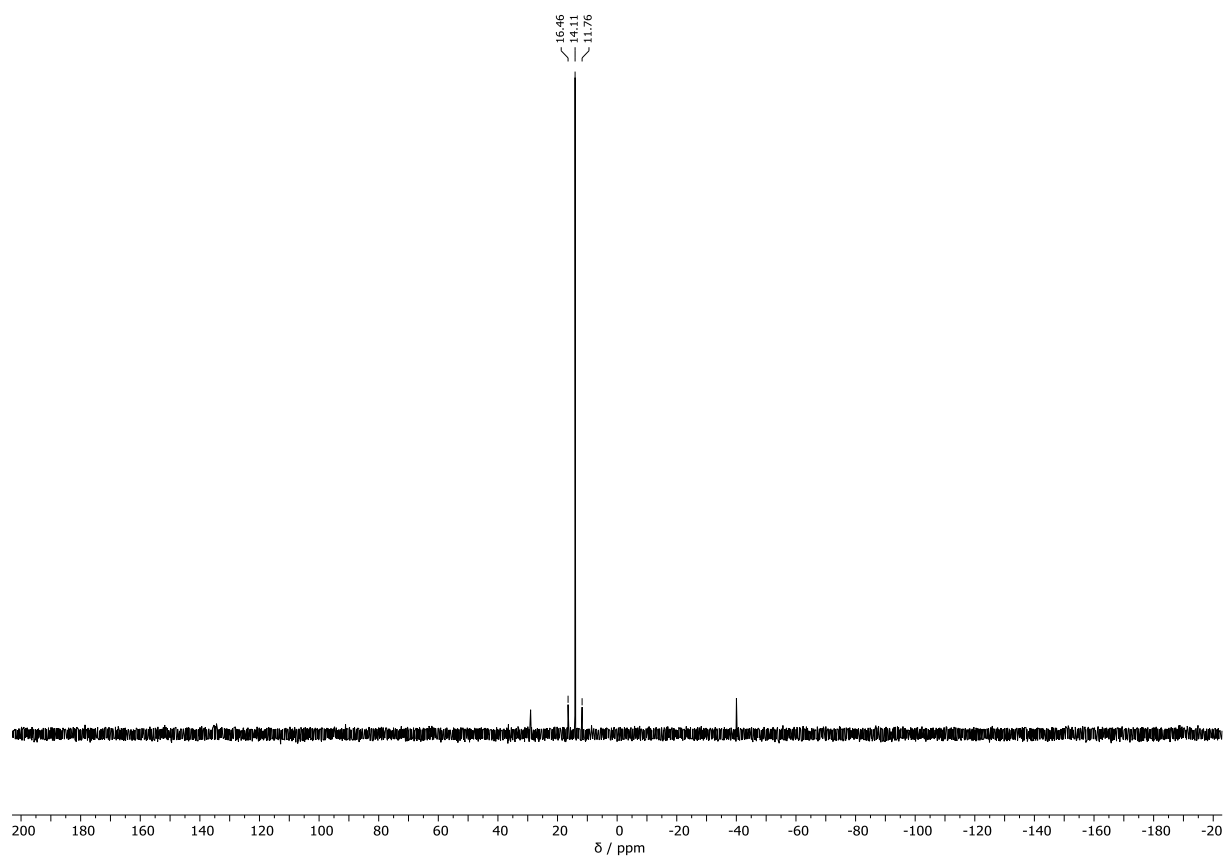
Compound 197a ^{1}H NMR (300 MHz, CD$_2$Cl$_2$)
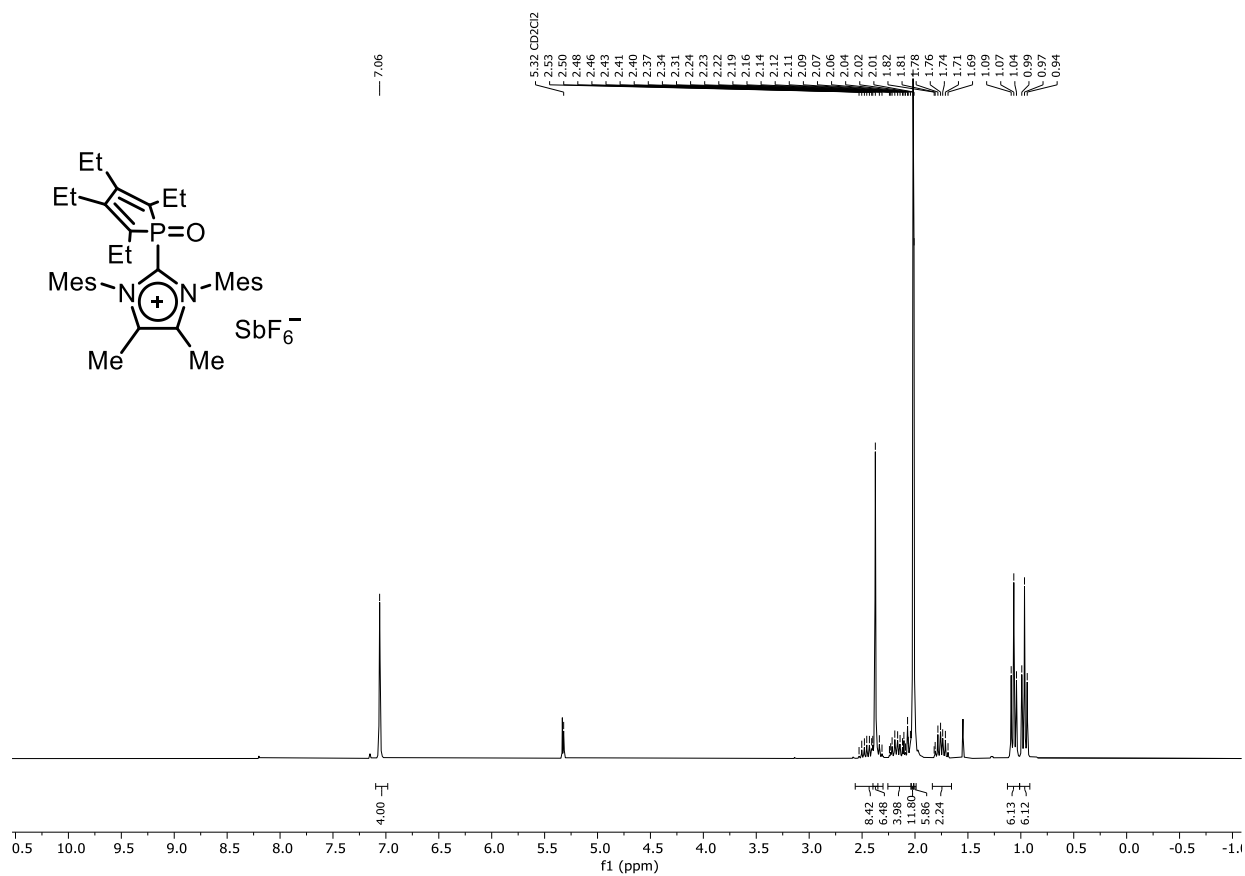
Compound 197a ^{13}C NMR (101 MHz, CD$_2$Cl$_2$)
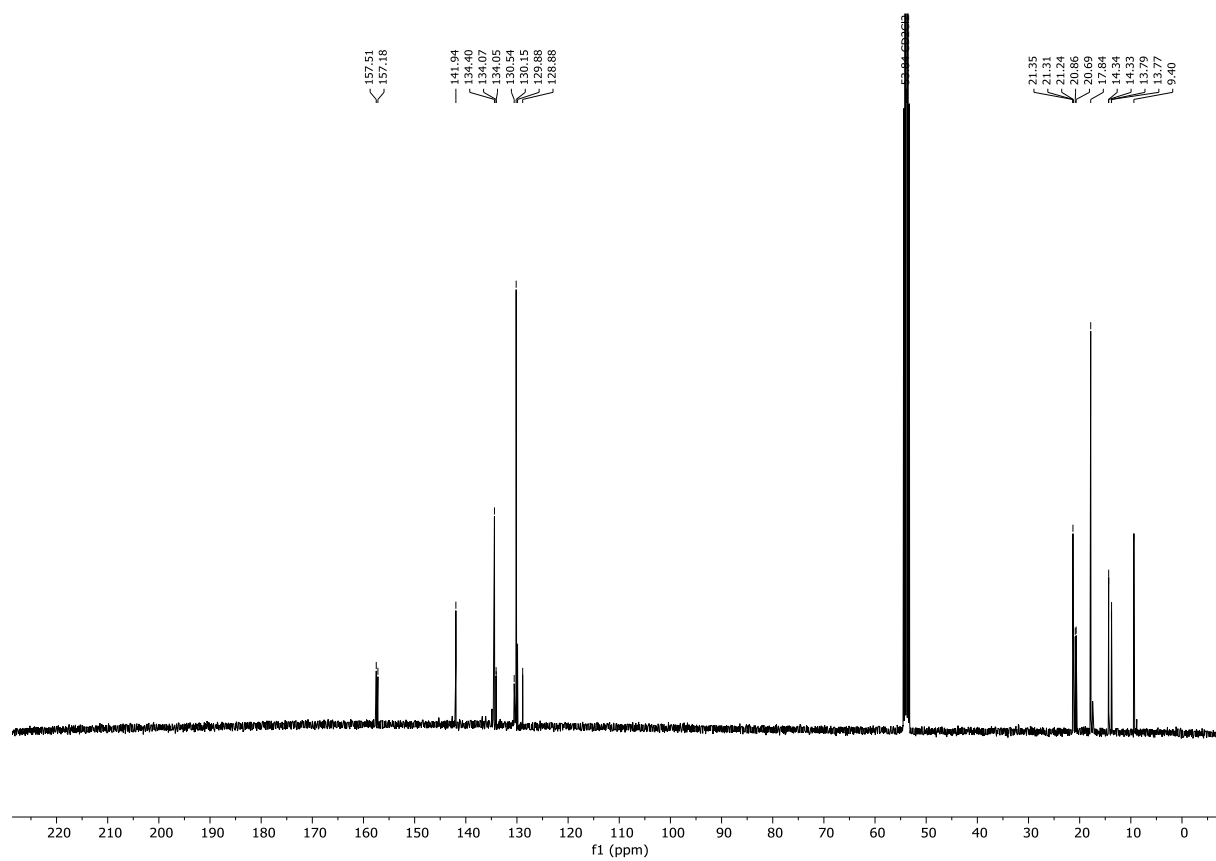
Compound 197a ^{31}P NMR (121 MHz, CD$_2$Cl$_2$)
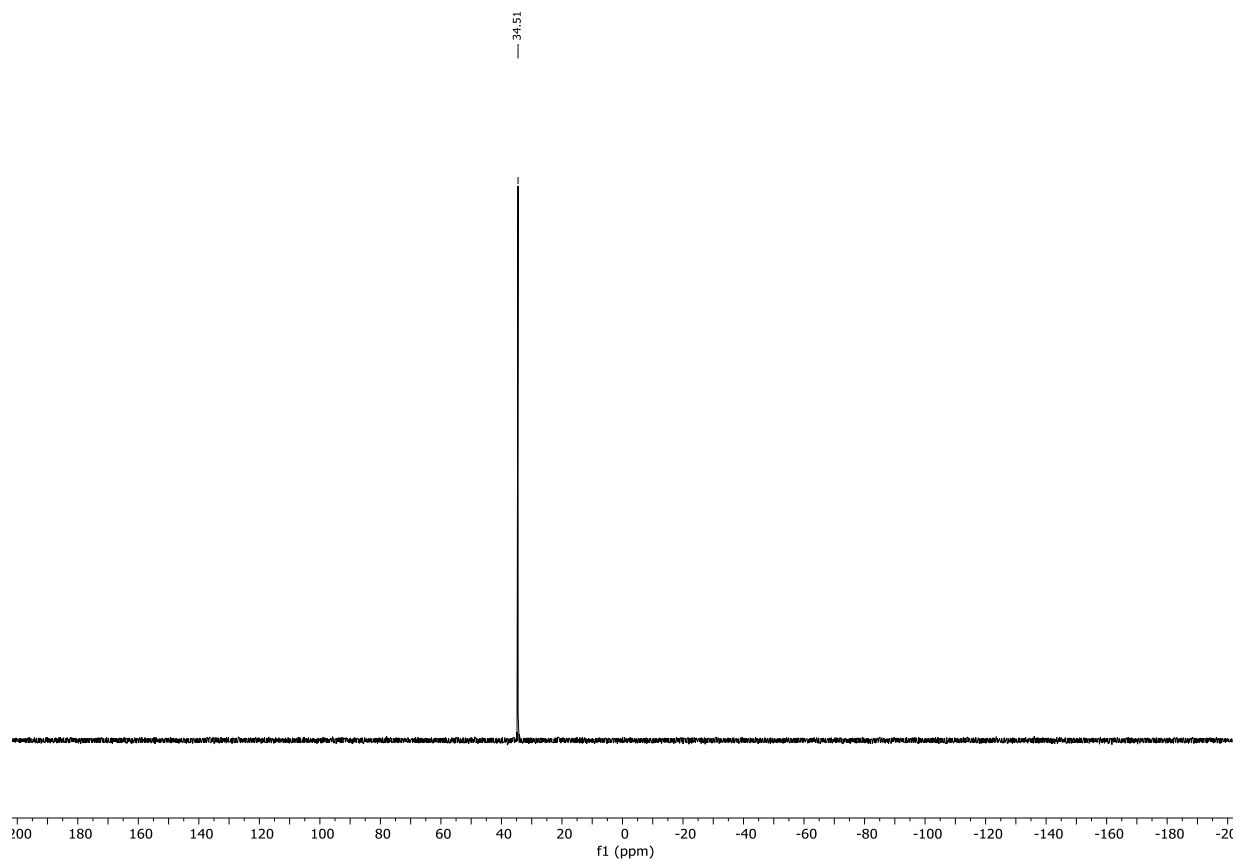
Compound 197b ^{1}H NMR (300 MHz, CD$_2$Cl$_2$)
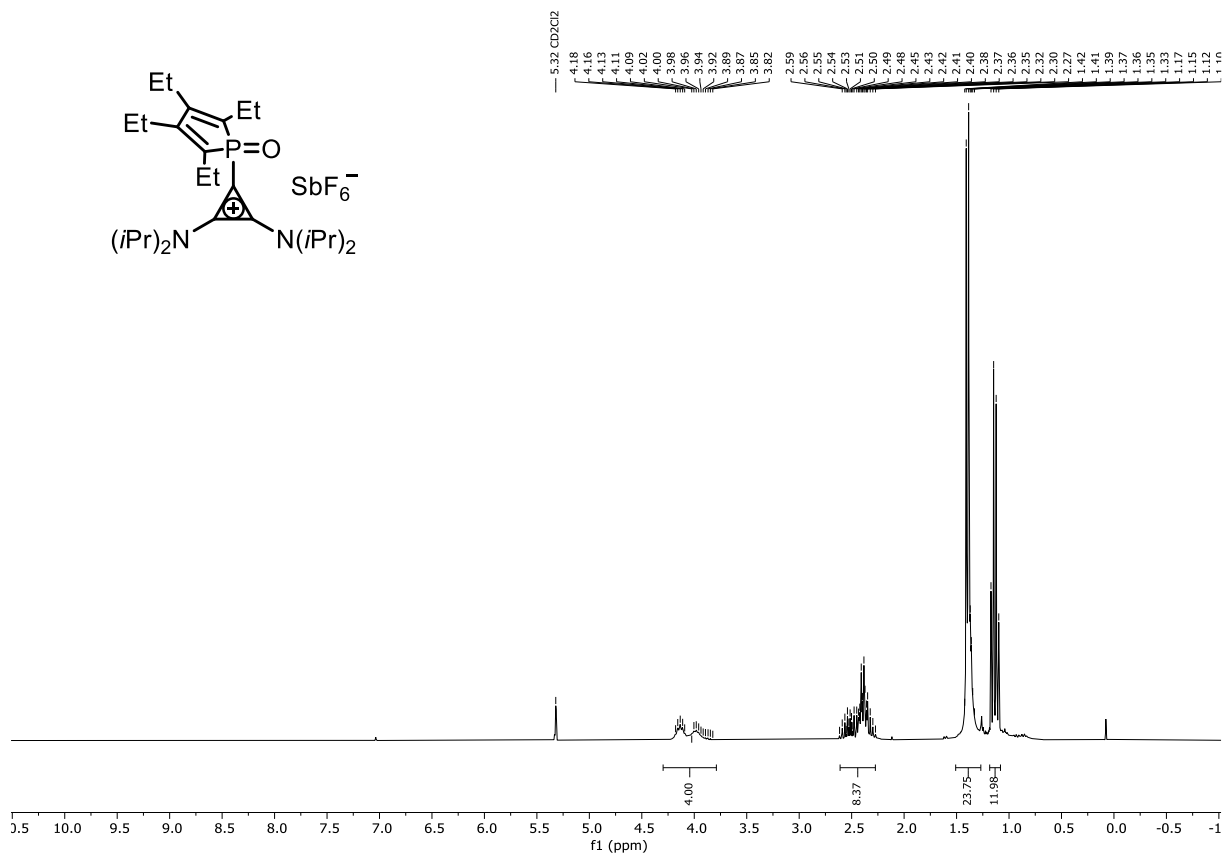
Compound 197b ^{13}C NMR (75 MHz, CD$_2$Cl$_2$)
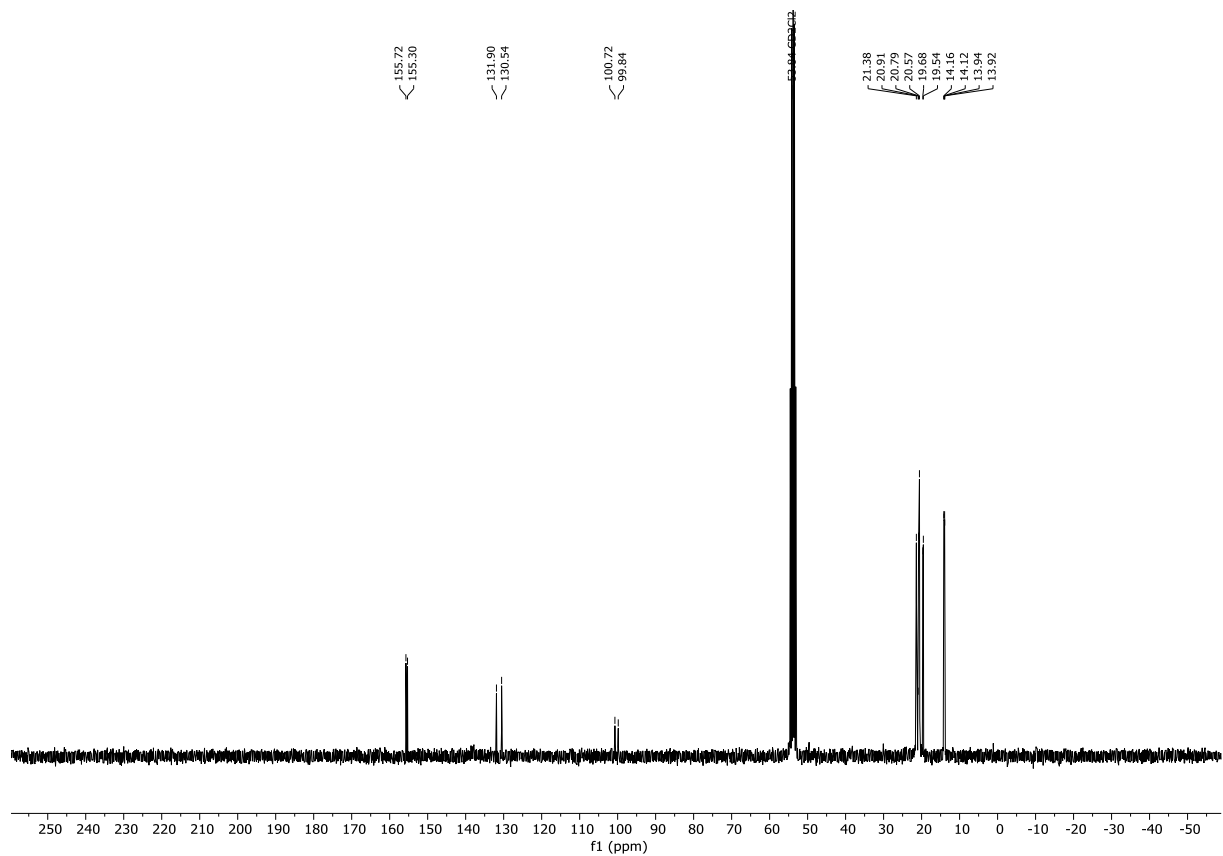
Compound 197b ^{31}P NMR (121 MHz, CD$_2$Cl$_2$)

27.92

200 180 160 140 120 100 80 60 40 20 0 -20 -40 -60 -80 -100 -120 -140 -160 -180 -20
f1 (ppm)
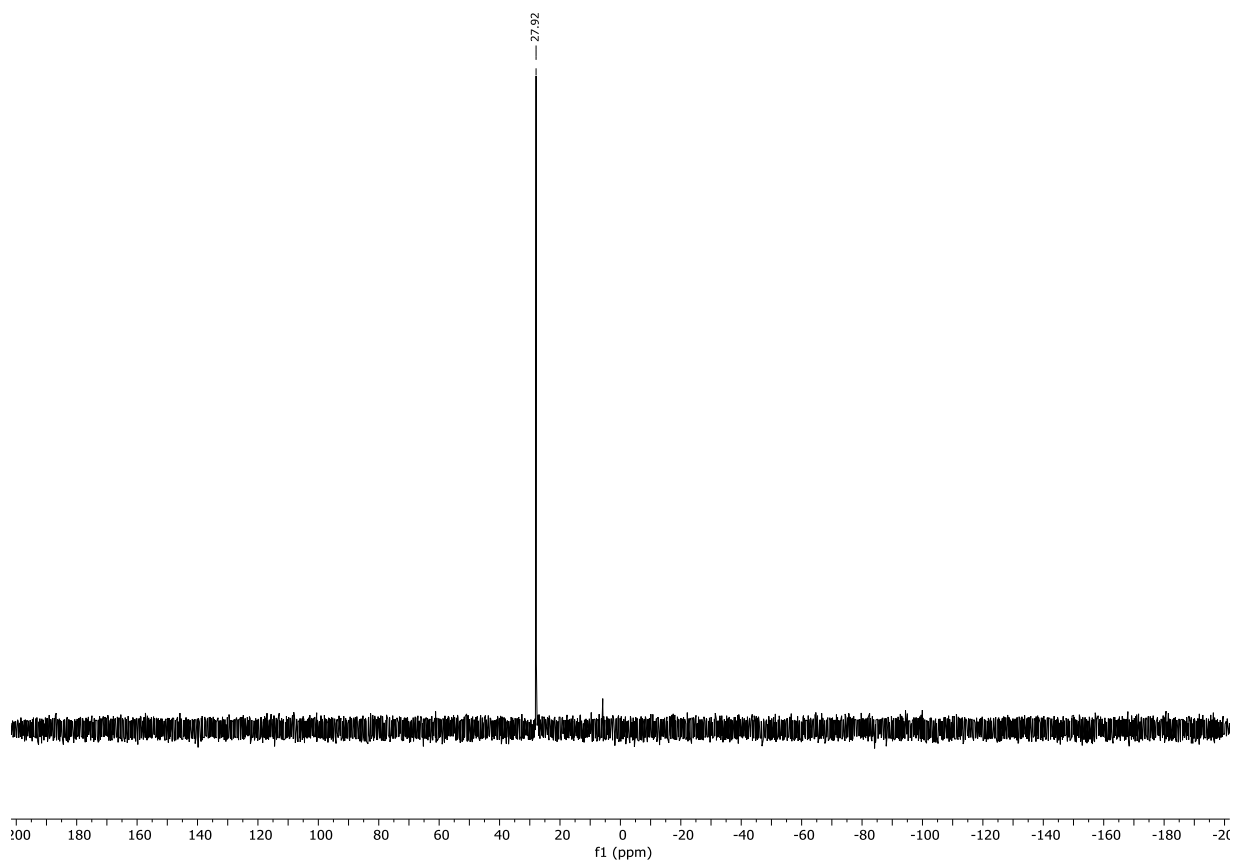
Compound 197c ^{1}H NMR (400 MHz, CD$_2$Cl$_2$)

).5 10.0 9.5 9.0 8.5 8.0 7.5 7.0 6.5 6.0 5.5 5.0 4.5 4.0 3.5 3.0 2.5 2.0 1.5 1.0 0.5 0.0 -0
f1 (ppm)
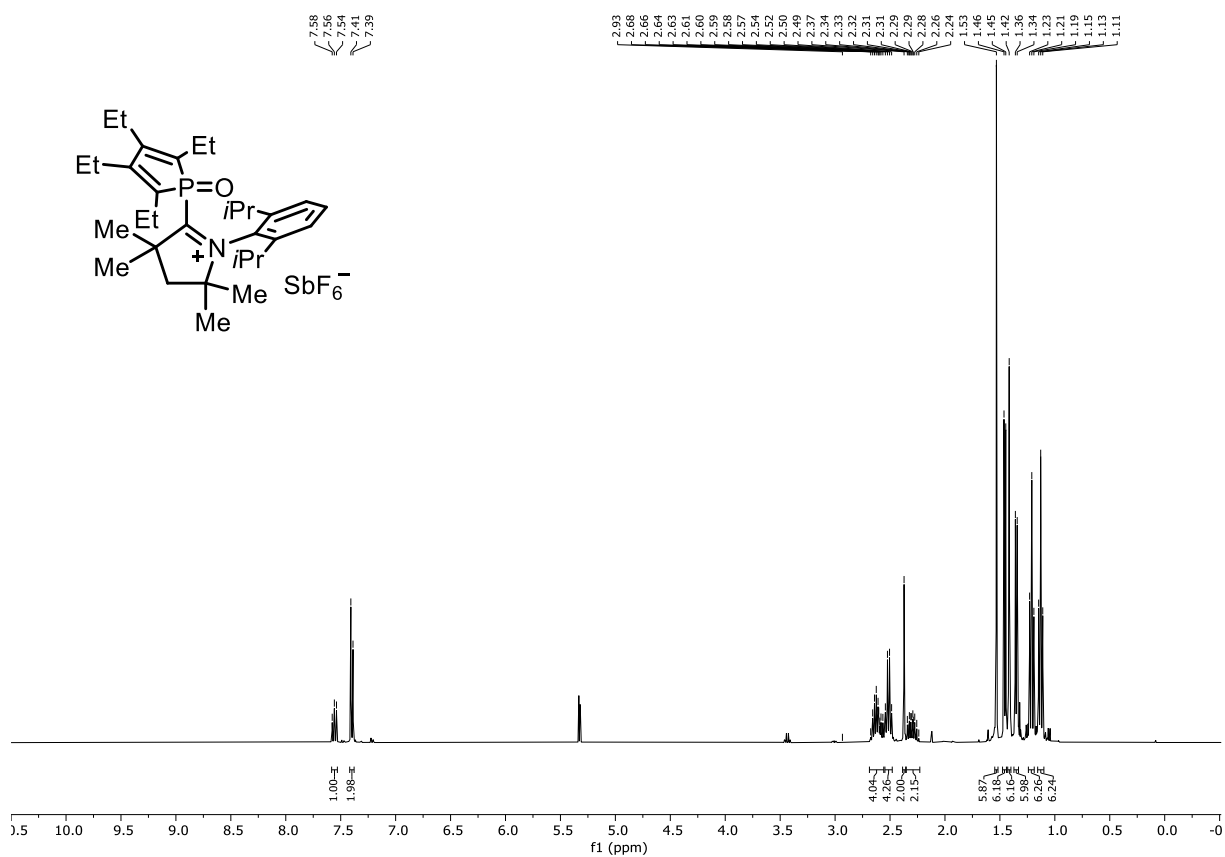
Compound 197c: ^{13}C NMR (101 MHz, CD_2Cl_2)

203.06
202.81
160.94
160.62
143.77
132.07
131.17
131.11
125.76
87.14
87.10
53.84 CD2Cl2
50.54
50.51
30.99
30.86
29.07
28.39
23.87
21.33
21.17
19.99
19.88
15.95
13.47
13.45

f1 (ppm)
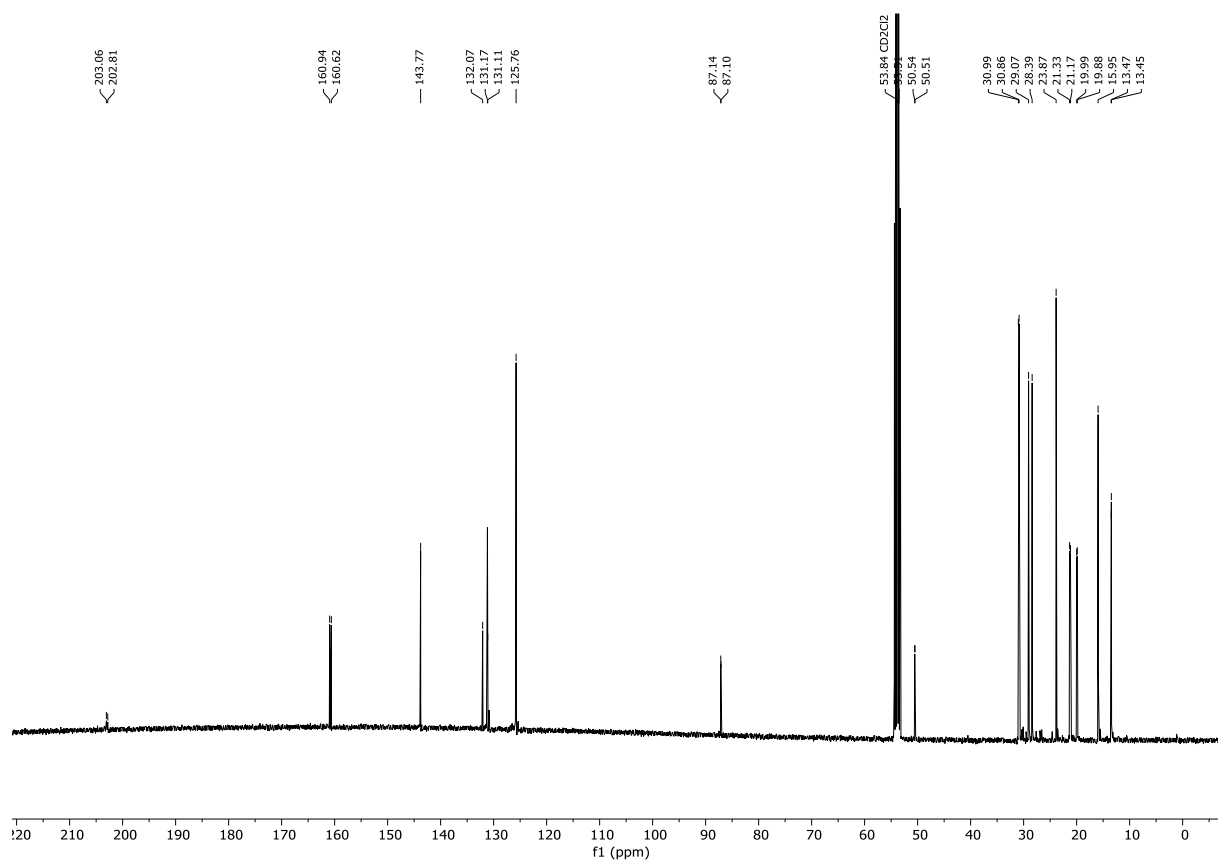
Compound 197c: ^{31}P NMR (162 MHz, CD_2Cl_2)

37.05

f1 (ppm)

112
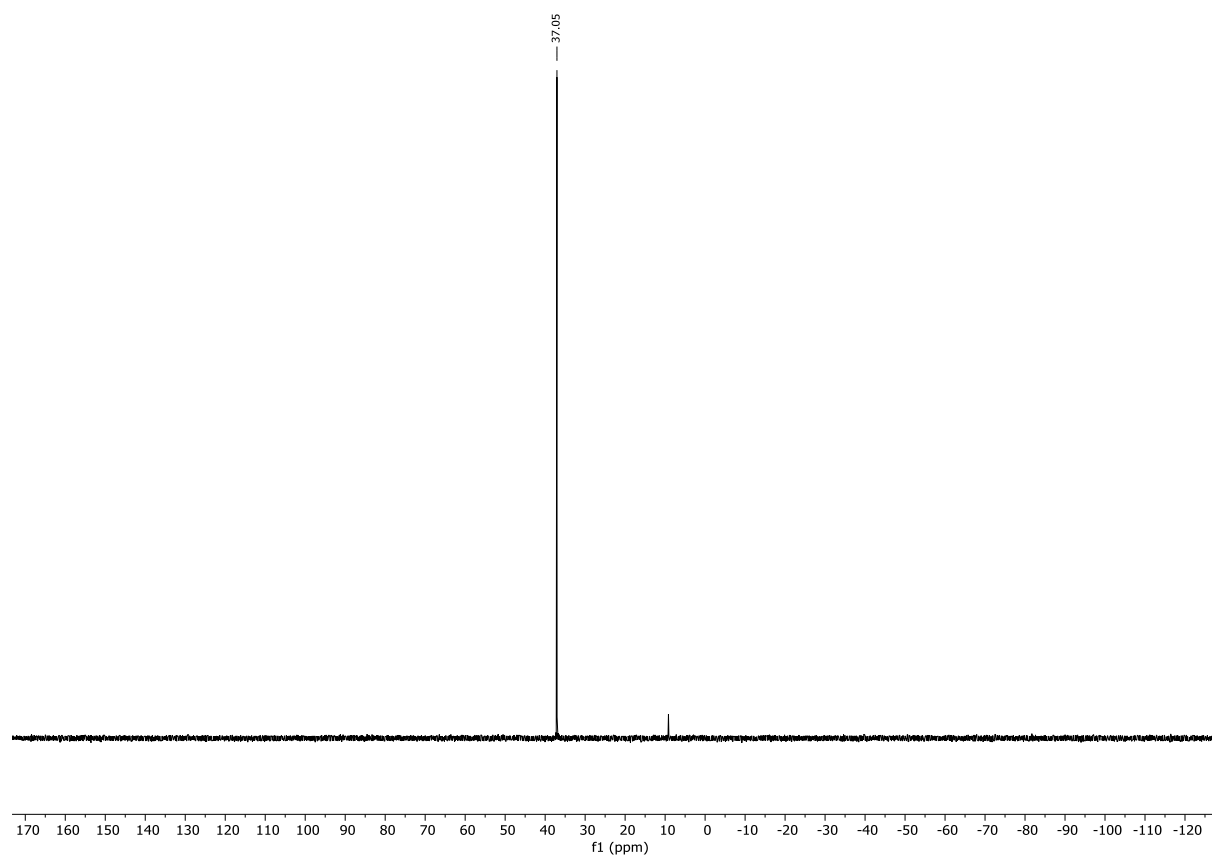
Compound 203: ^{1}H NMR (400 MHz, CD$_2$Cl$_2$)
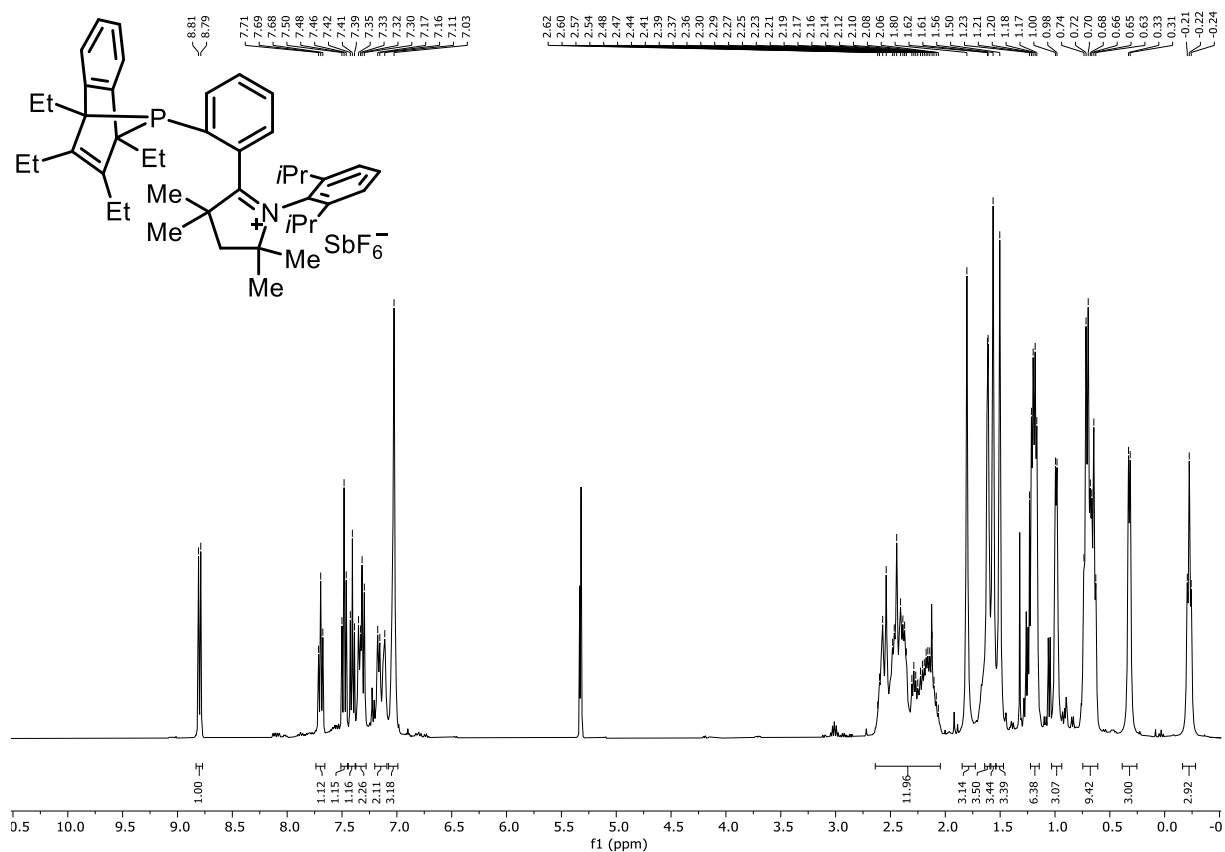
Compound 203: ^{13}C NMR (101 MHz, CD$_2$Cl$_2$)
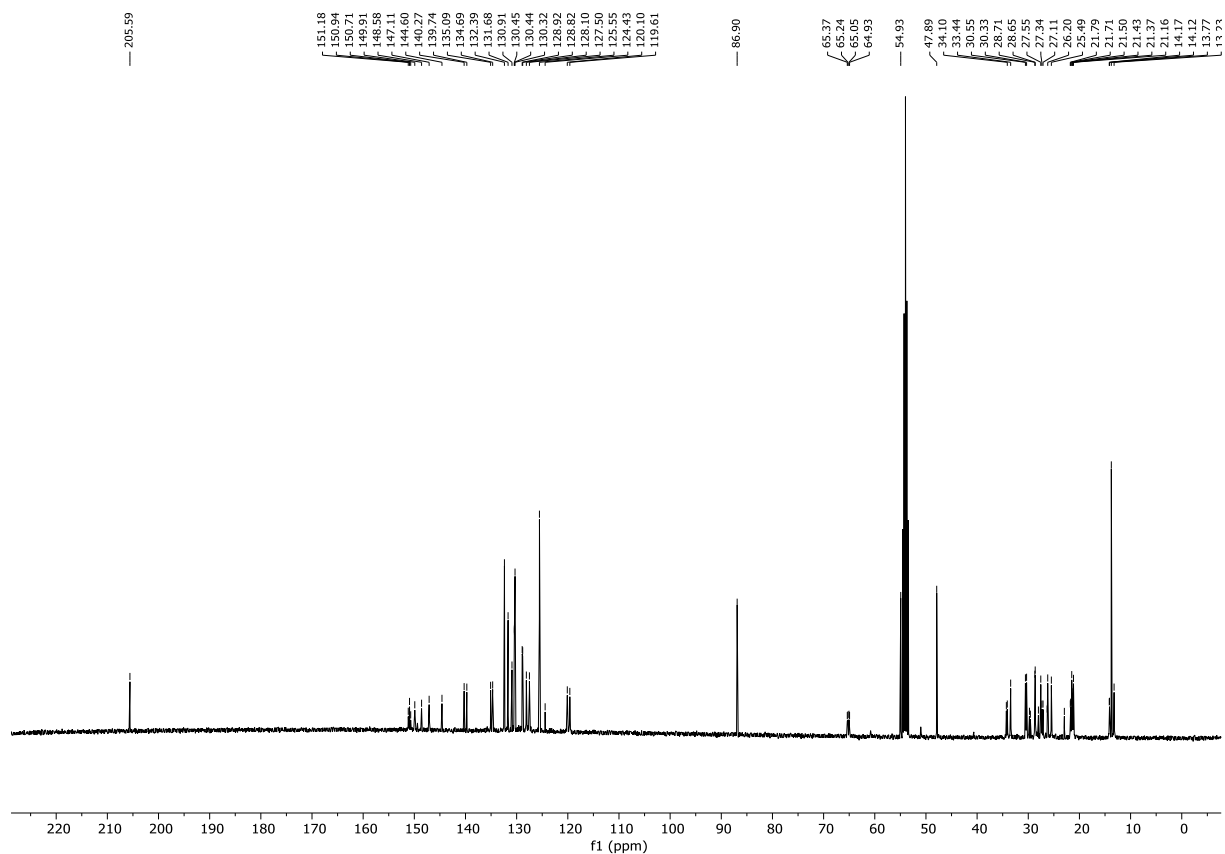
Compound 203: ^{31}P NMR (162 MHz, CD$_2$Cl$_2$)
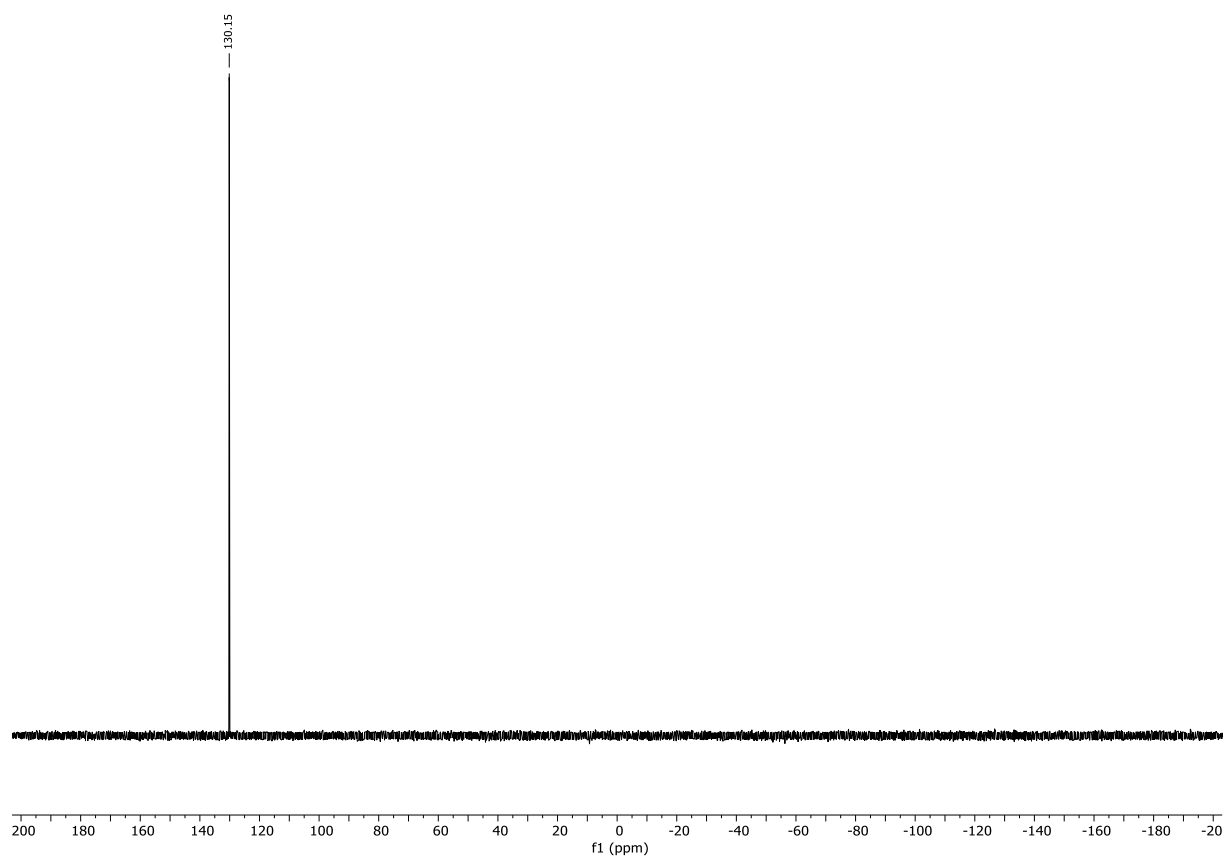
Compound 203: HSQC (400 MHz, CD$_2$Cl$_2$)

114
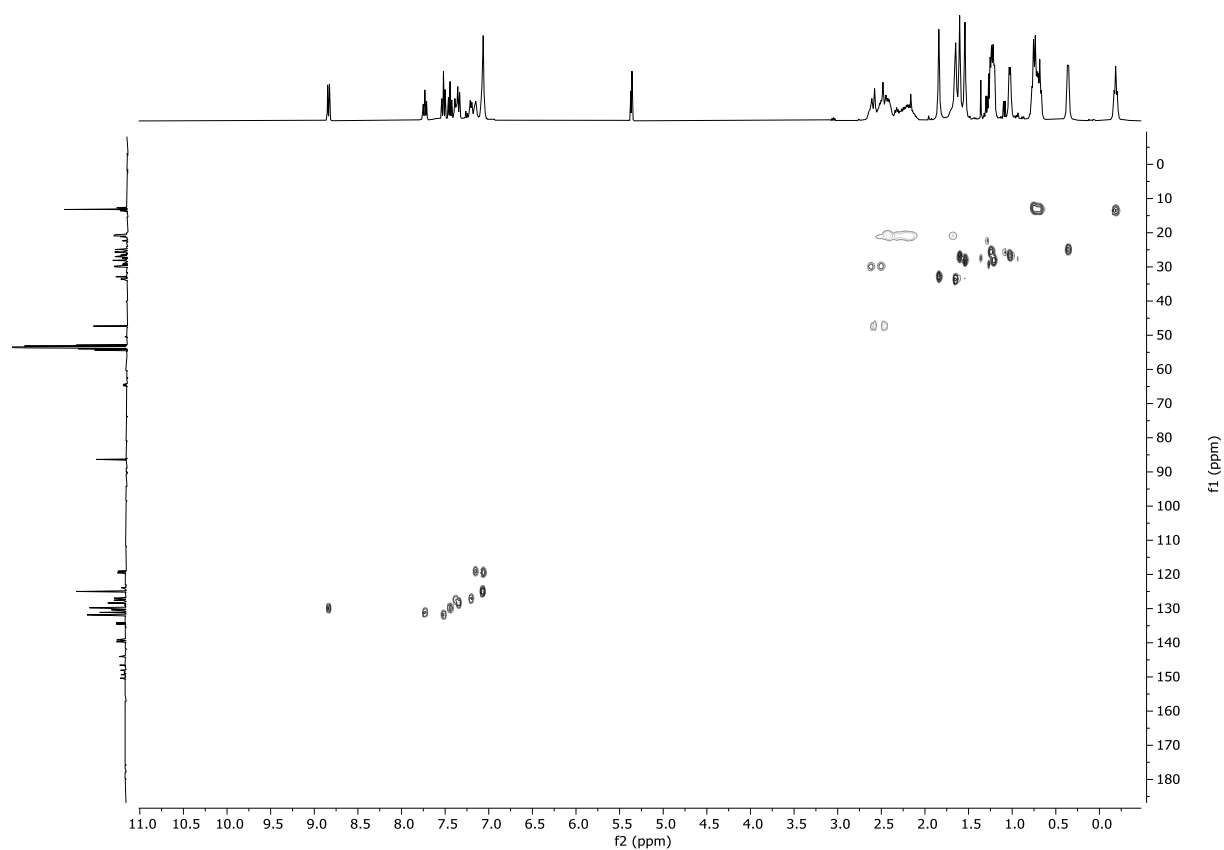
Compound 205a: ^{1}H NMR (400 MHz, CD$_2$Cl$_2$)
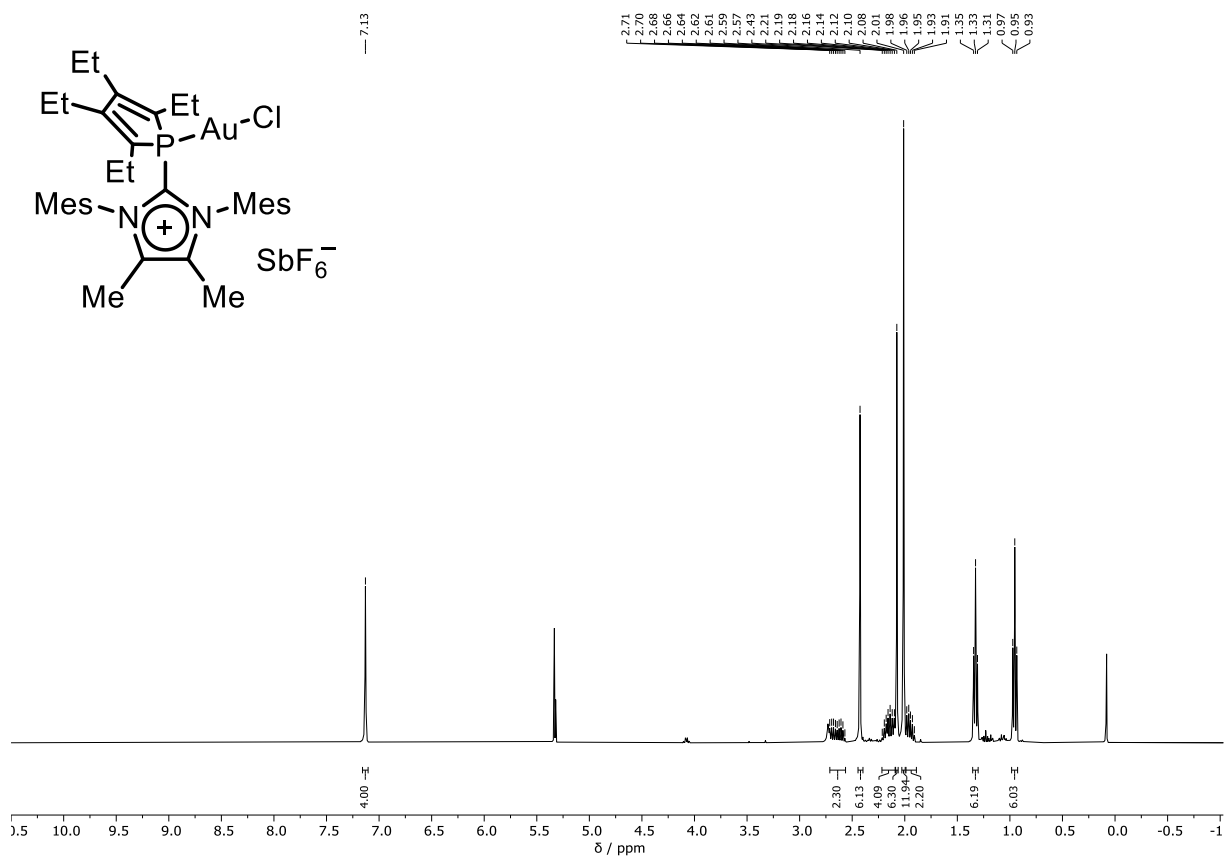
Compound 205a: ^{13}C NMR (101 MHz, CD$_2$Cl$_2$)

115

Compound 205a: ^{31}P NMR (162 MHz, CD_2Cl_2)

δ / ppm

Compound 205b: ^1H NMR (400 MHz, CD_2Cl_2)

δ / ppm
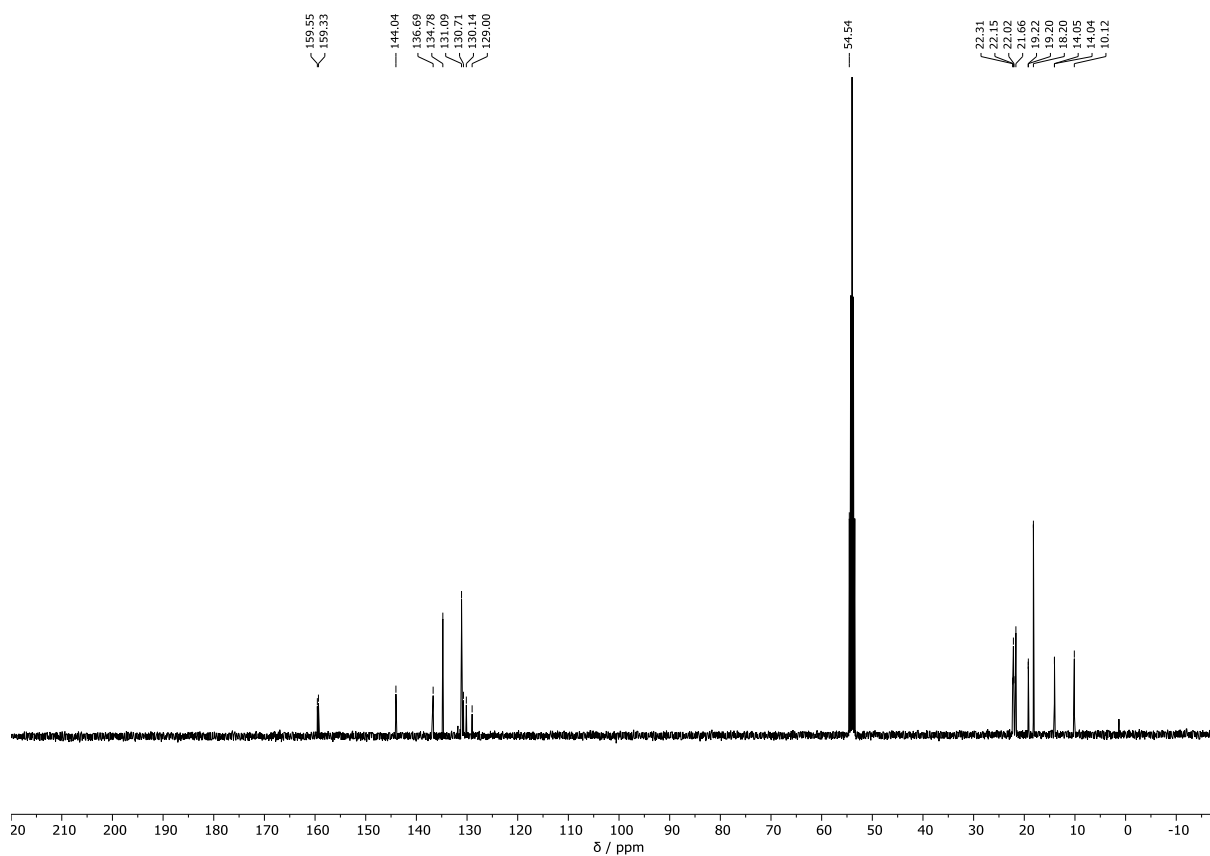
Compound 205b: ^{13}C NMR (101 MHz, CD_2Cl_2)

158.36
158.15
139.47
139.40
133.08
132.52
93.17
93.14
92.85
92.83
22.03
21.90
21.53
21.00
20.86
17.04
17.01
14.41
14.39

20 210 200 190 180 170 160 150 140 130 120 110 100 90 80 70 60 50 40 30 20 10 0 -10

δ / ppm
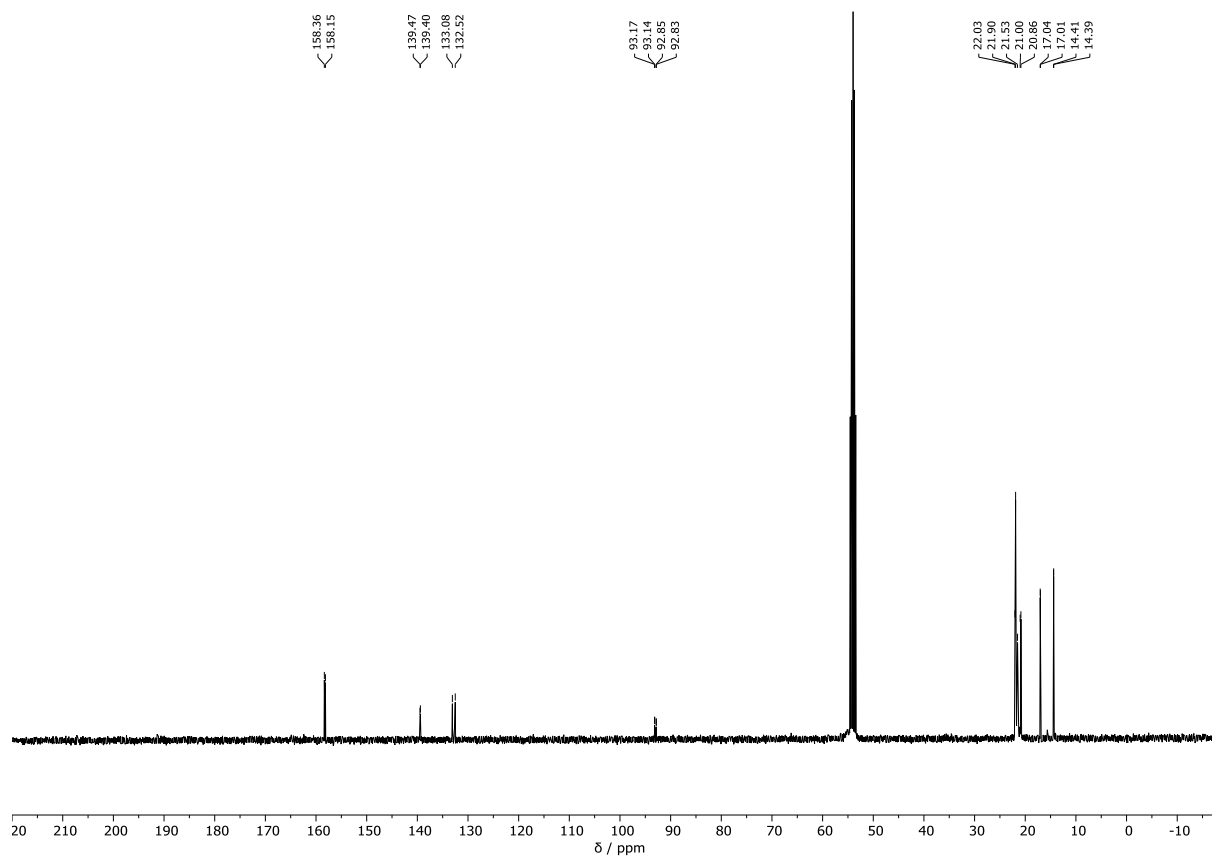
Compound 205b: ^{31}P NMR (162 MHz, CD_2Cl_2)

−2.19

170 160 150 140 130 120 110 100 90 80 70 60 50 40 30 20 10 0 -10 -20 -30 -40 -50 -60 -70 -80 -90 -100 -110 -120

δ / ppm
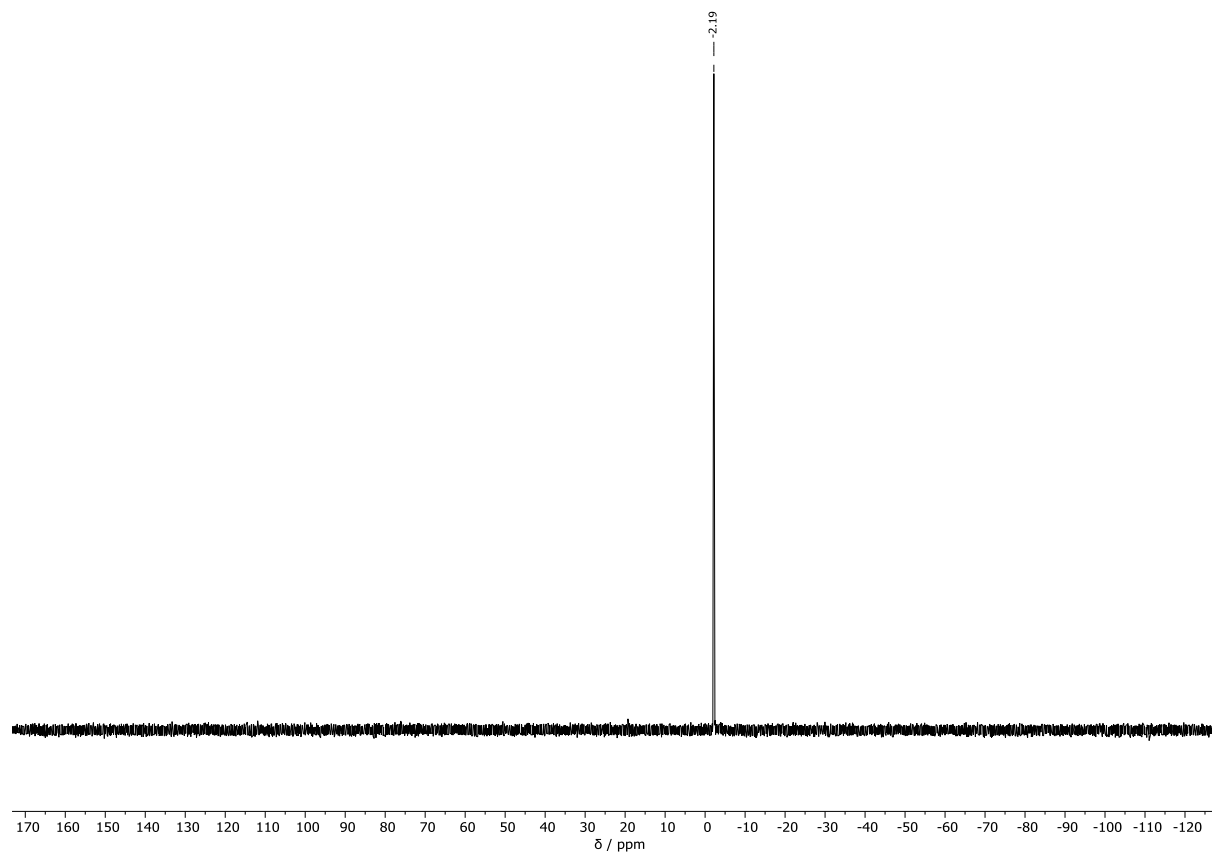
Compound 205c: ^{1}H NMR (400 MHz, CD$_2$Cl$_2$)
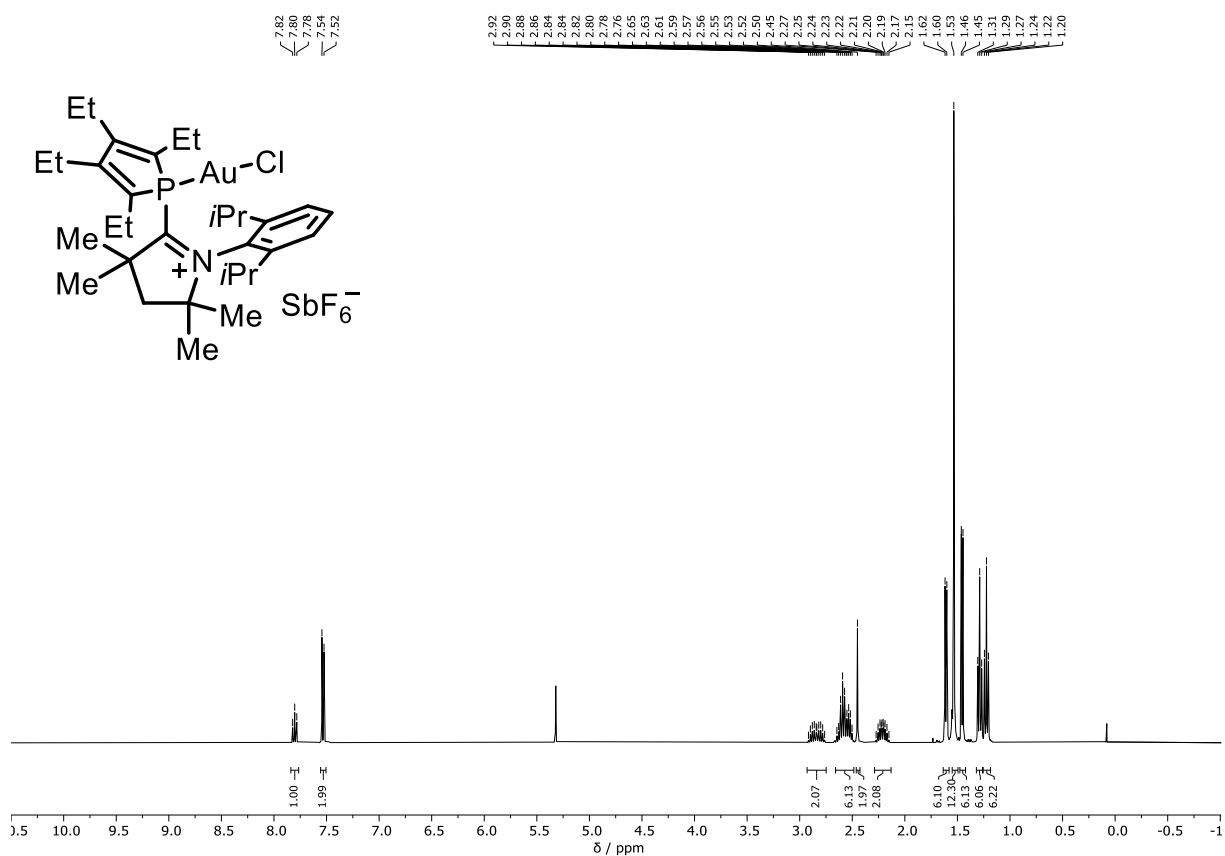
Compound 205c: ^{13}C NMR (101 MHz, CD$_2$Cl$_2$)
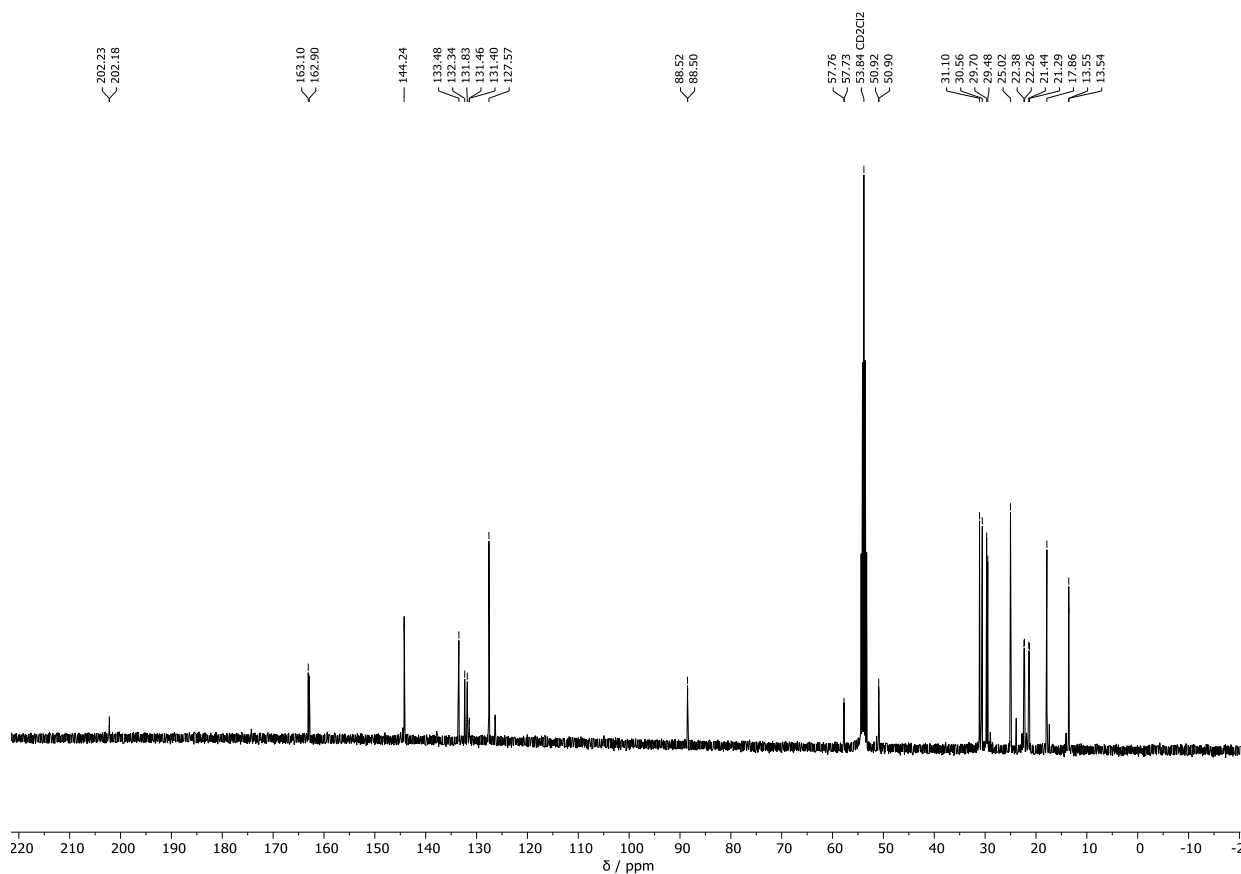
Compound 205c: ^{31}P NMR (162 MHz, CDCl$_3$)
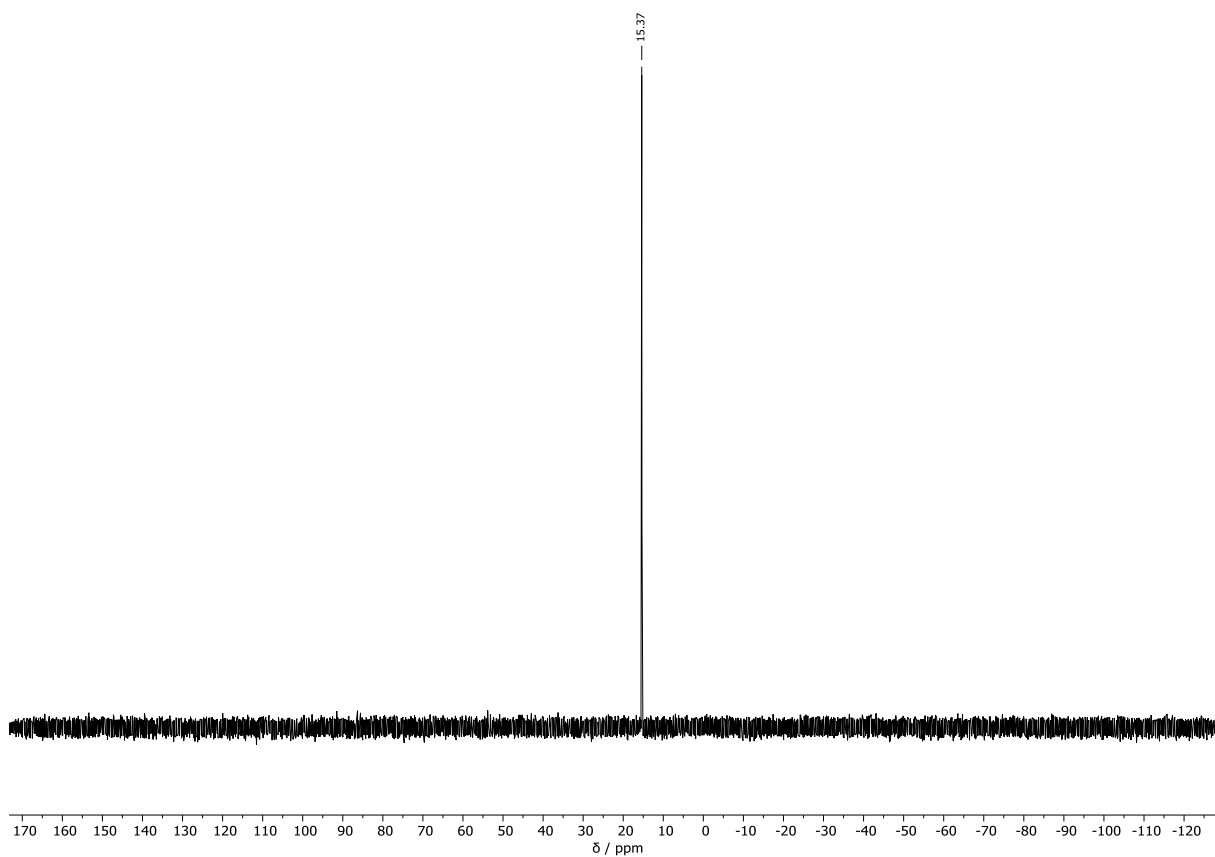
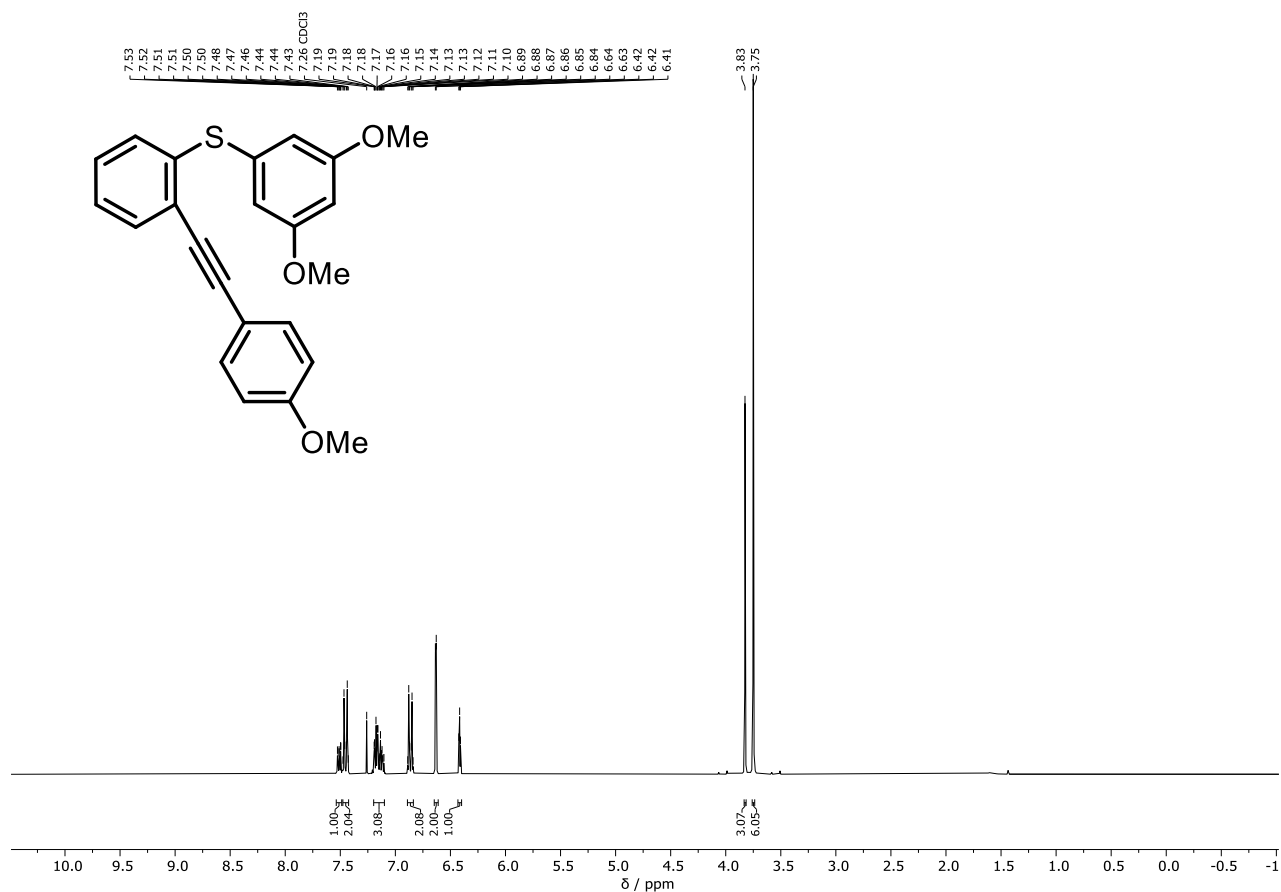
Compound 205d: ^{1}H NMR (300 MHz, CD$_2$Cl$_2$)

119
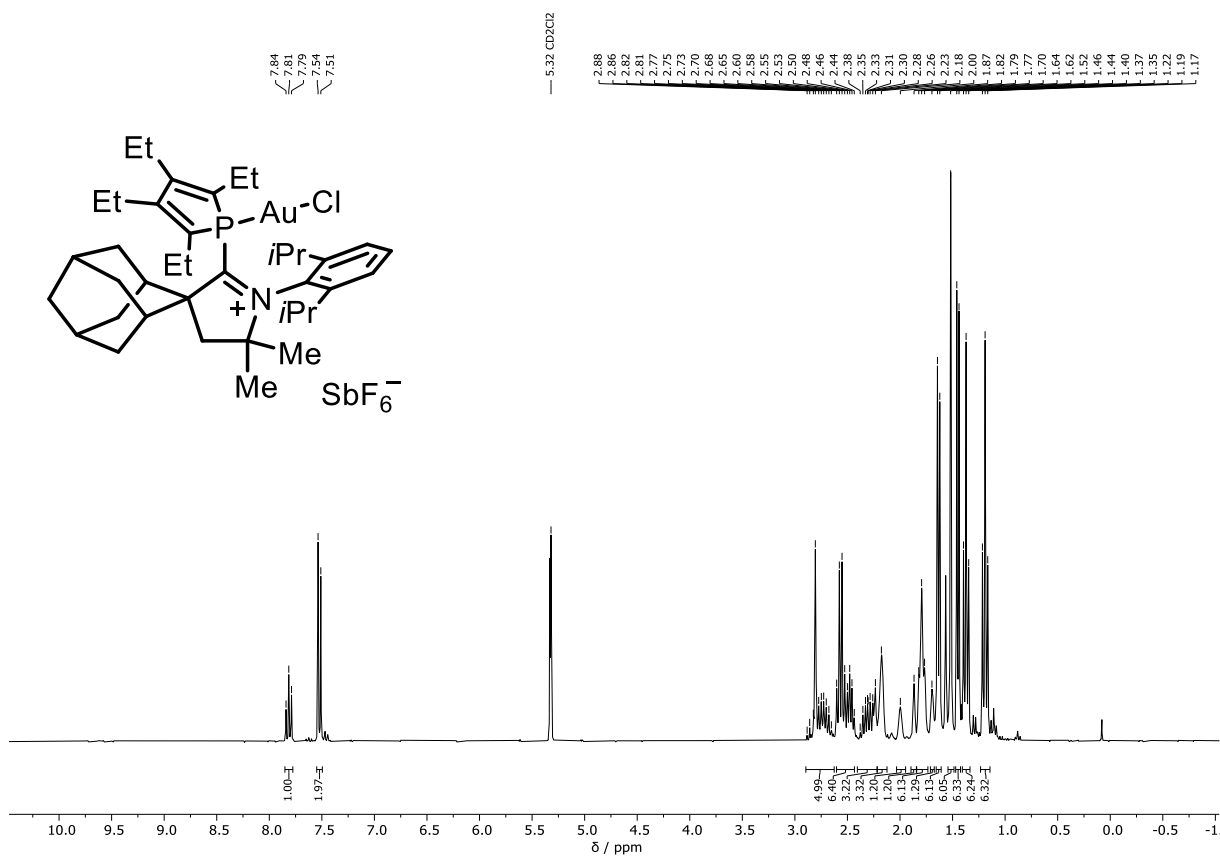
Compound 205d: ^{13}C NMR (101 MHz, CD$_2$Cl$_2$)

207.82, 207.72
161.51, 161.29
143.92
133.92, 133.86, 133.52, 132.74, 132.27, 127.72
86.70, 86.68
71.88
54.24
53.xx CD$_2$Cl$_2$
48.58, 48.56
38.03
37.52
34.87, 34.73
30.88, 30.33
29.65
26.52
25.64, 25.15
22.64, 22.51
21.87, 21.73
17.43, 17.41
13.64
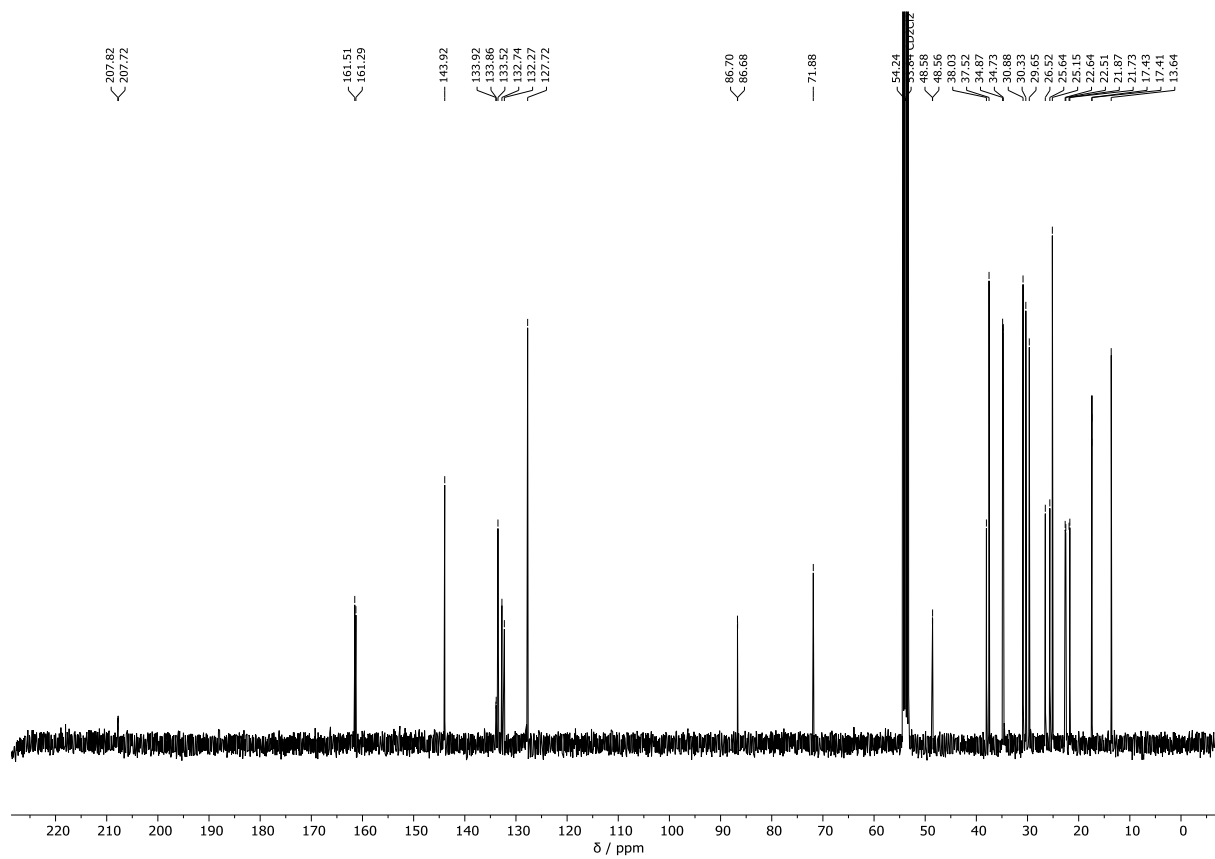
Compound 205d: ^{31}P NMR (162 MHz, CD$_2$Cl$_2$)
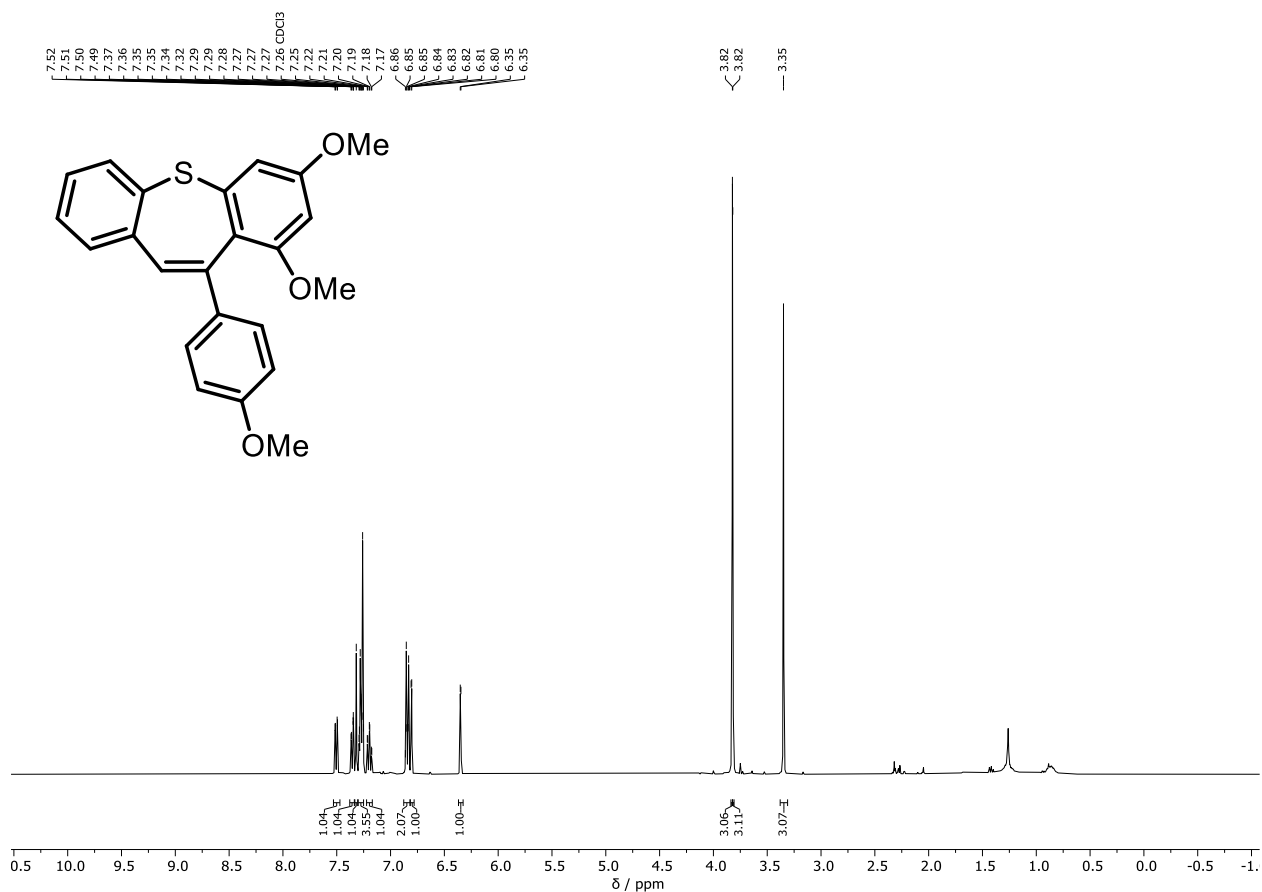

26.30
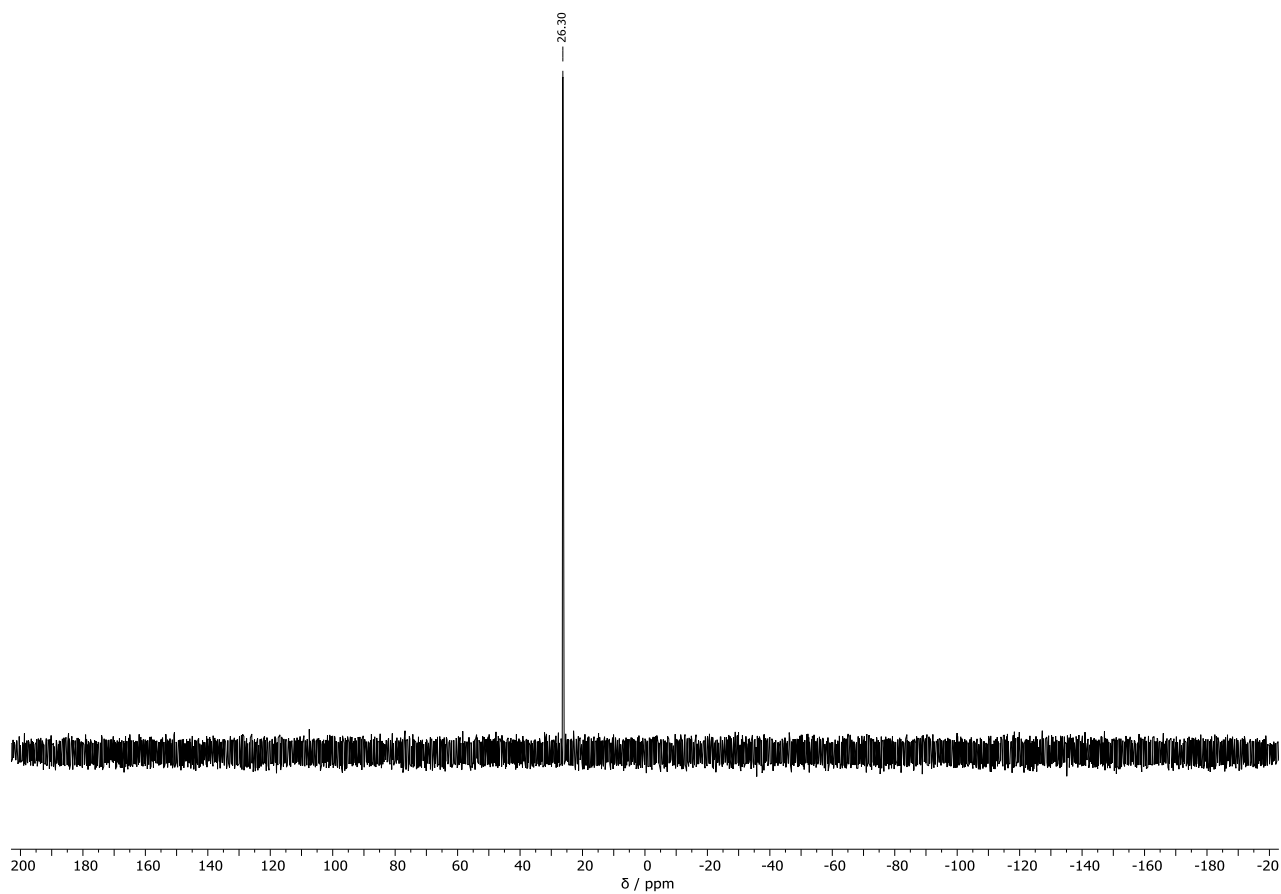
Compound 208: ^{1}H NMR (300 MHz, CDCl$_3$)
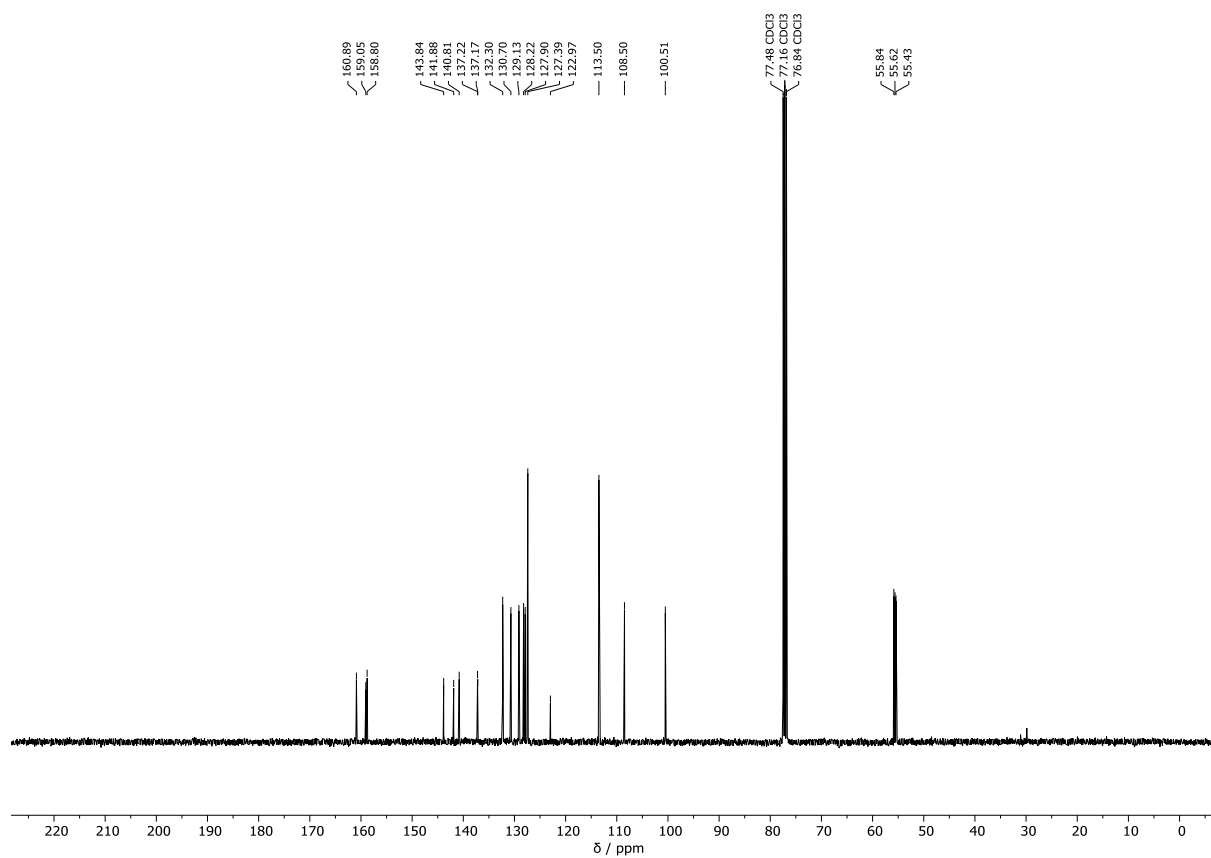

Compound 208: ^{13}C NMR (101 MHz, CDCl$_3$)
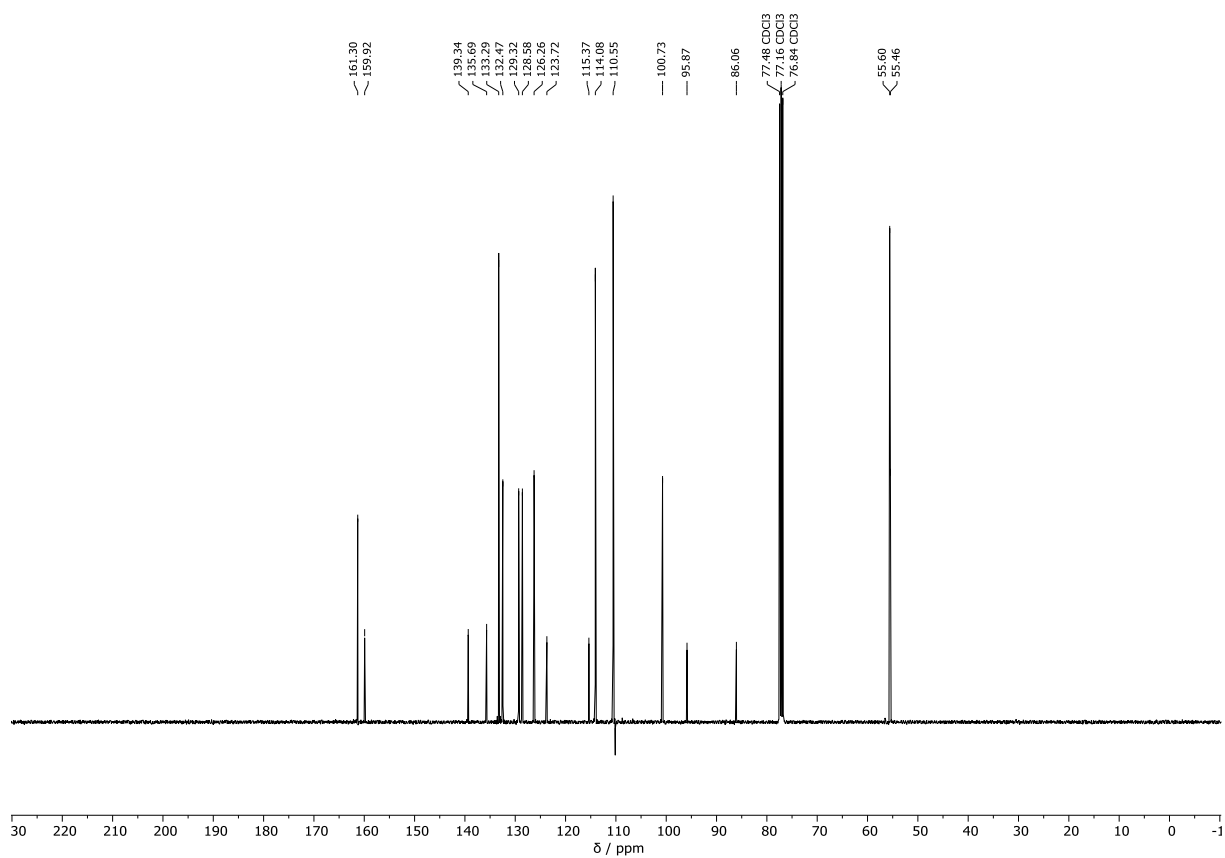
Compound 209: ^{1}H NMR (400 MHz, CDCl$_3$)

Compound 209: ^{13}C NMR (101 MHz, CDCl$_3$)

Compound 210: ^{1}H NMR (300 MHz, CDCl$_3$)
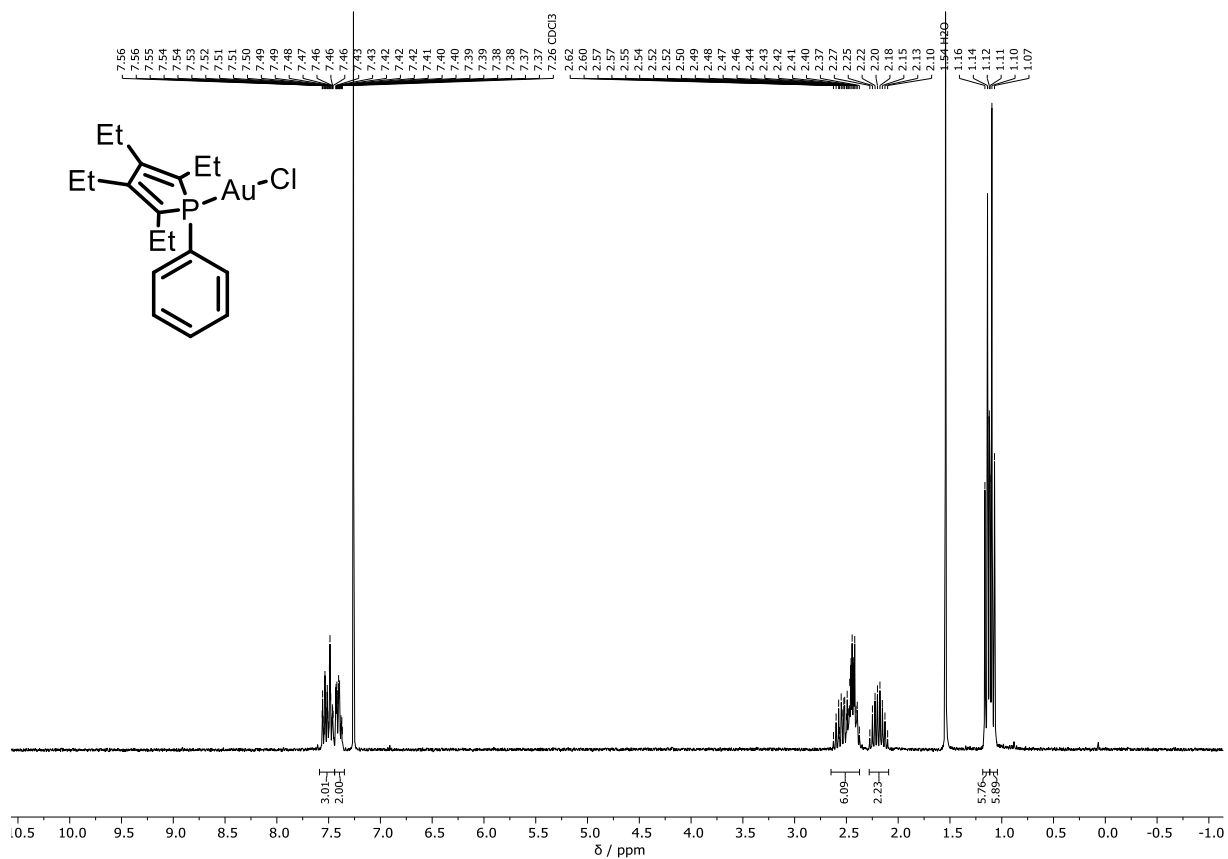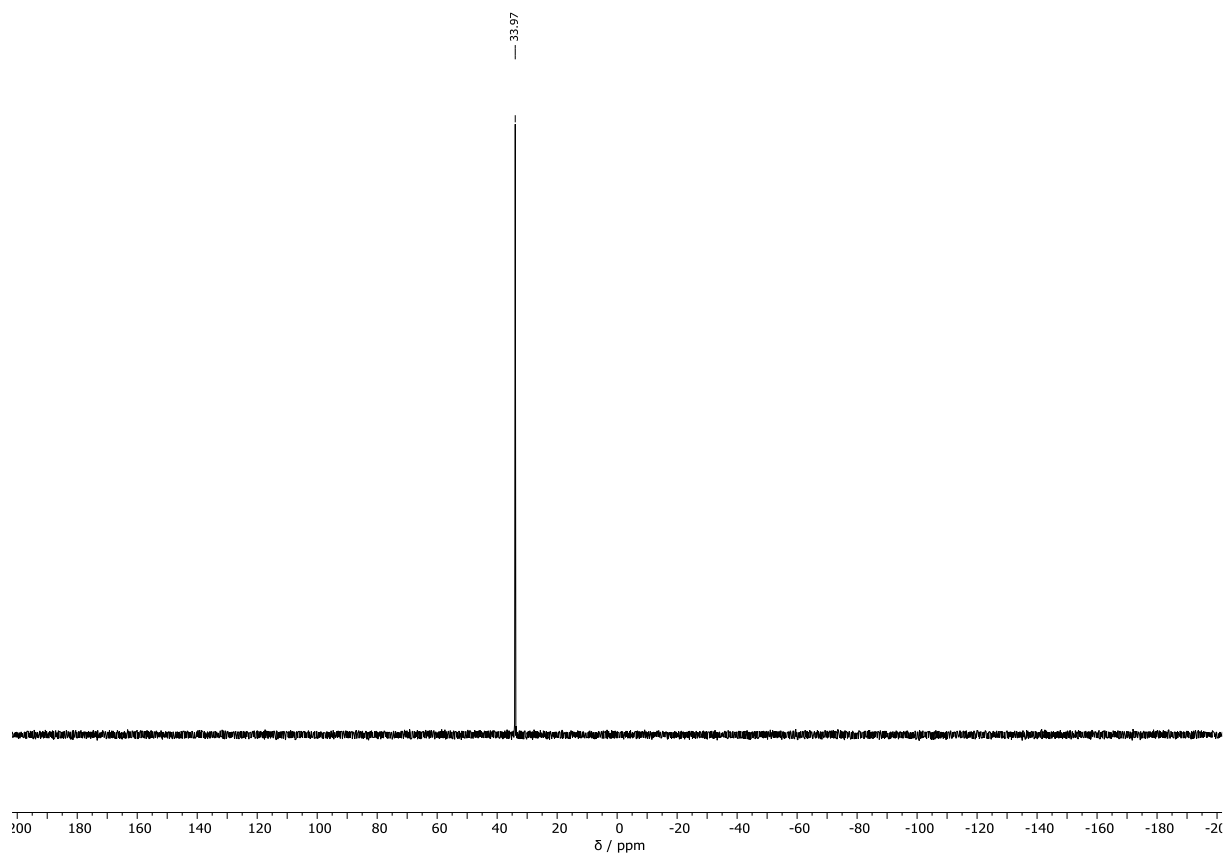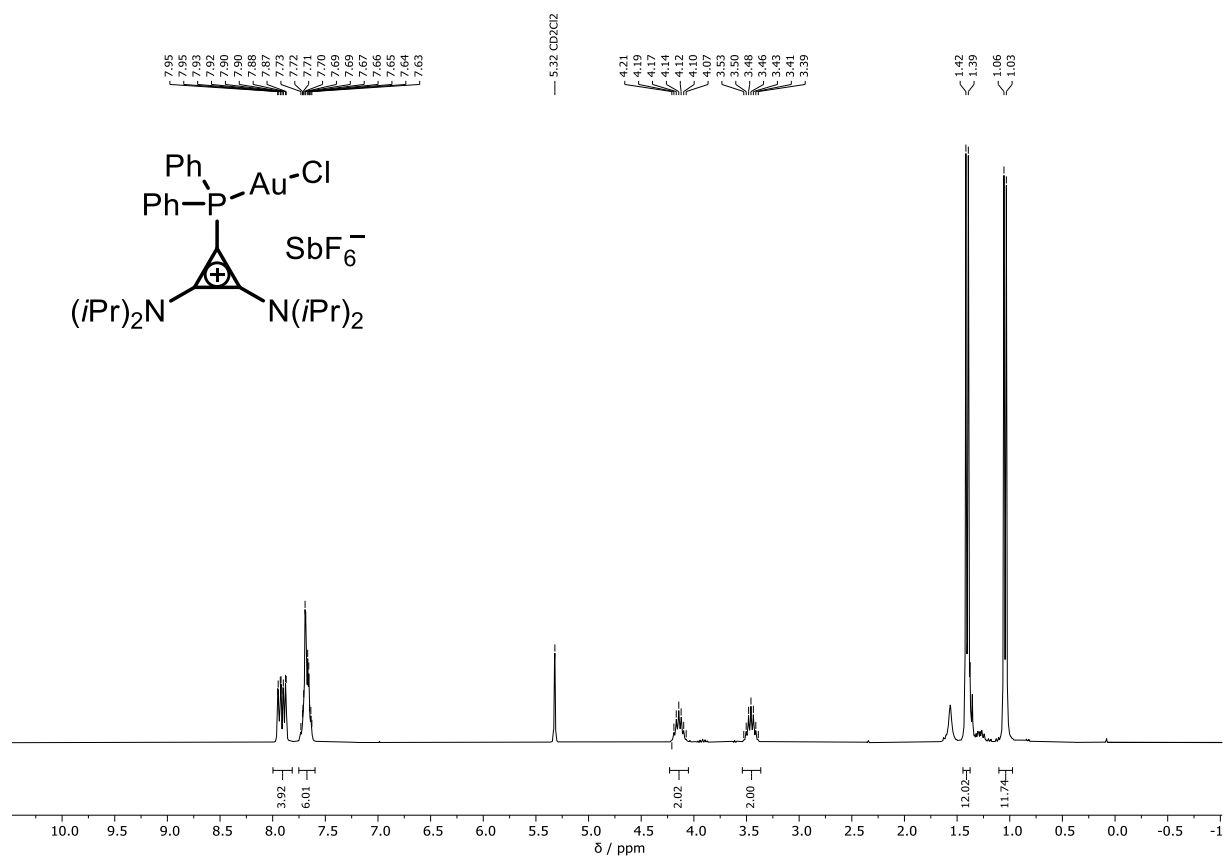

Compound 210: ^{13}C NMR (101 MHz, CDCl$_3$)
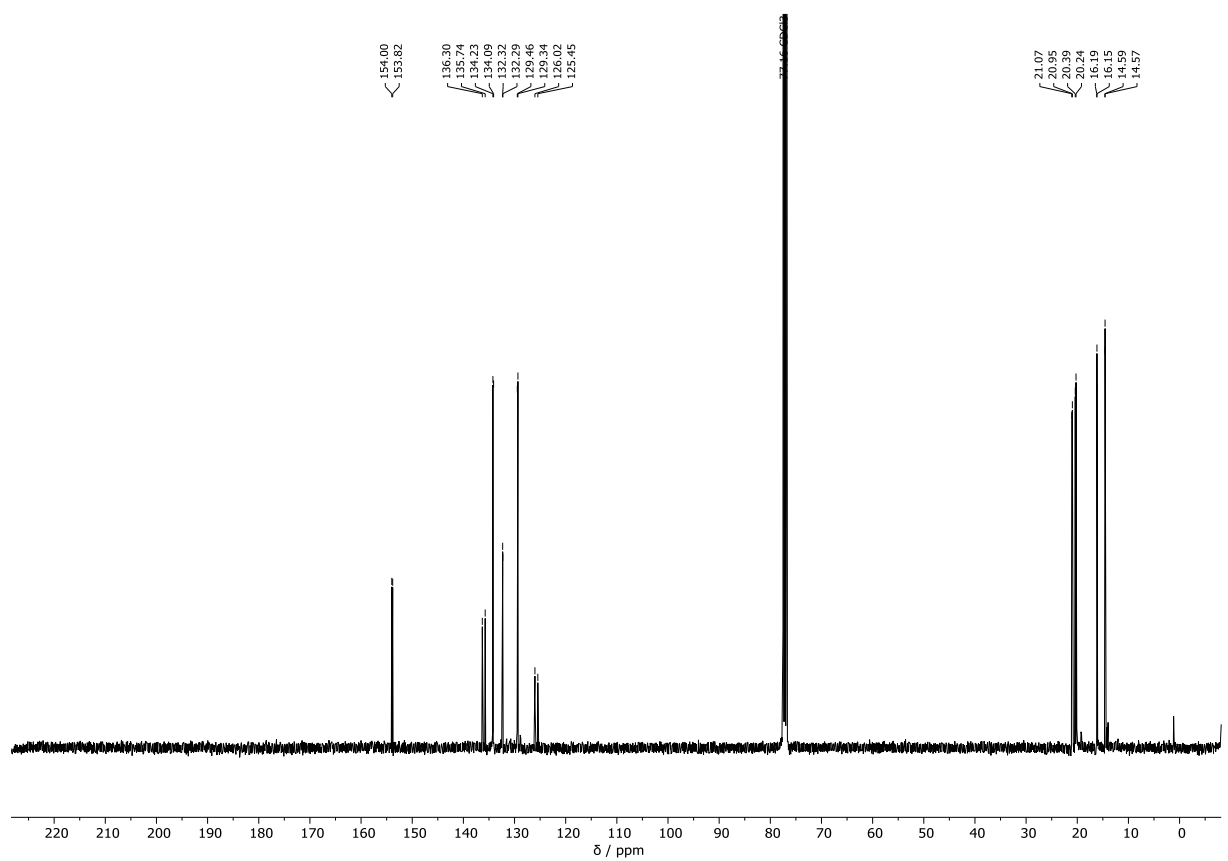
Compound 210: ^{31}P NMR (162 MHz, CDCl$_3$)

Compound 212: ^{1}H NMR (400 MHz, CD$_2$Cl$_2$)

Compound 212: ^{13}C NMR (101 MHz, CD$_2$Cl$_2$)
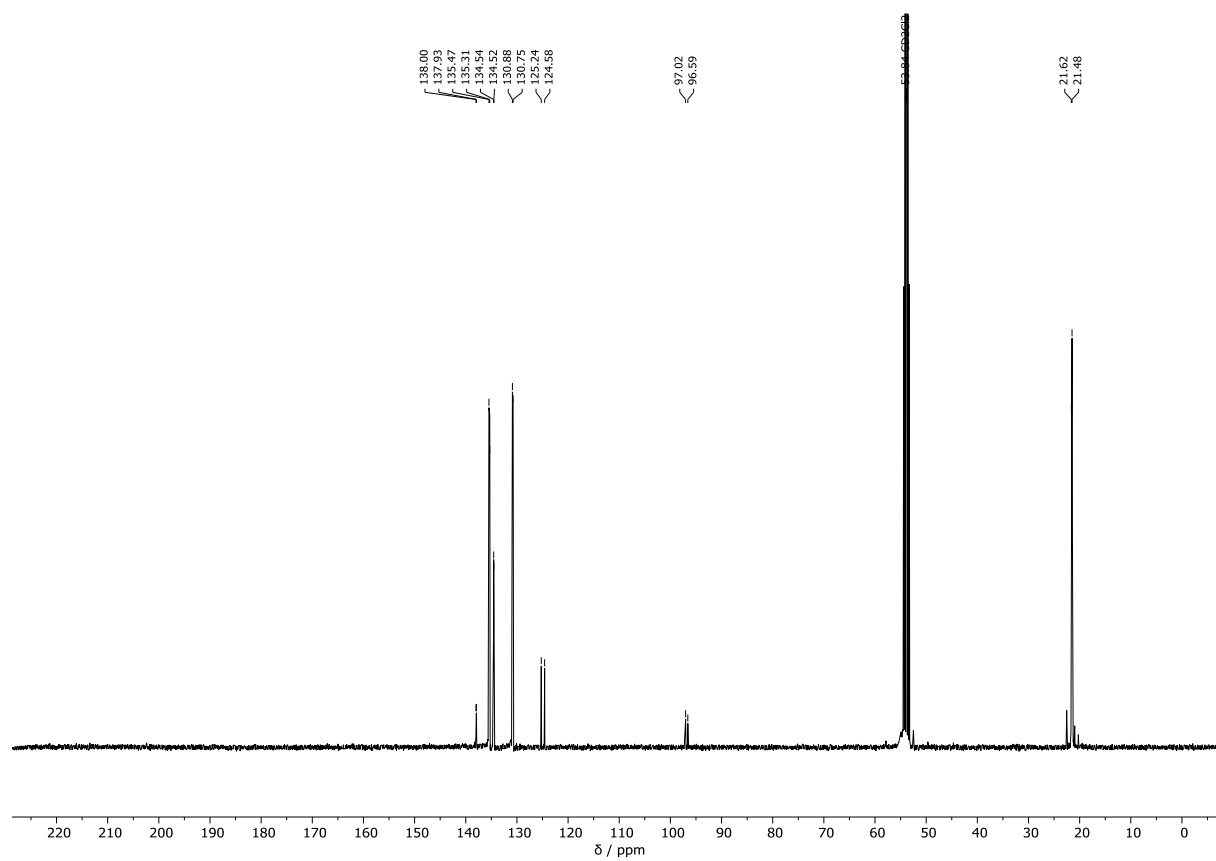
Compound 212: ^{31}P NMR (162 MHz, CD$_2$Cl$_2$)
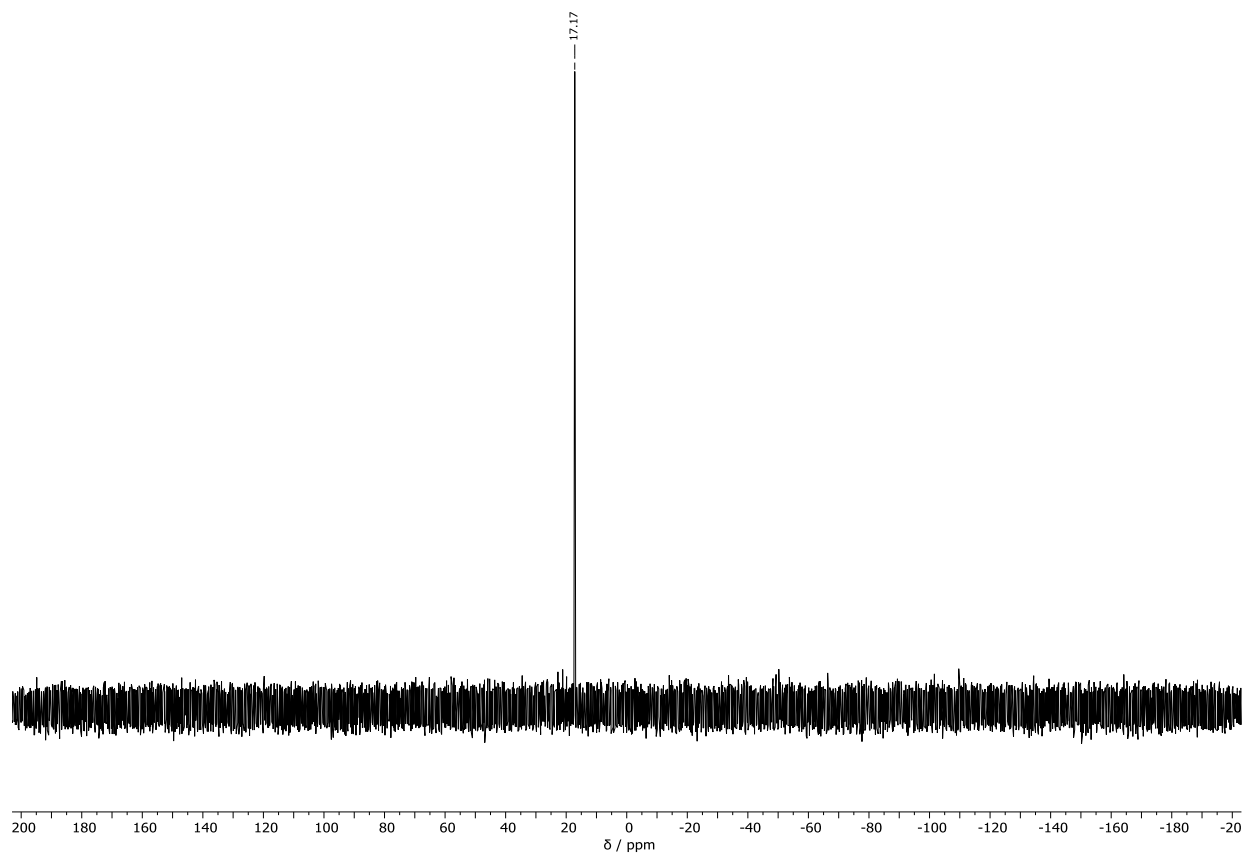
6-chloro-4-iodo-1-tosyl-1,2-dihydroquinoline (216a): ^{1}H NMR (300 MHz, CDCl$_3$)
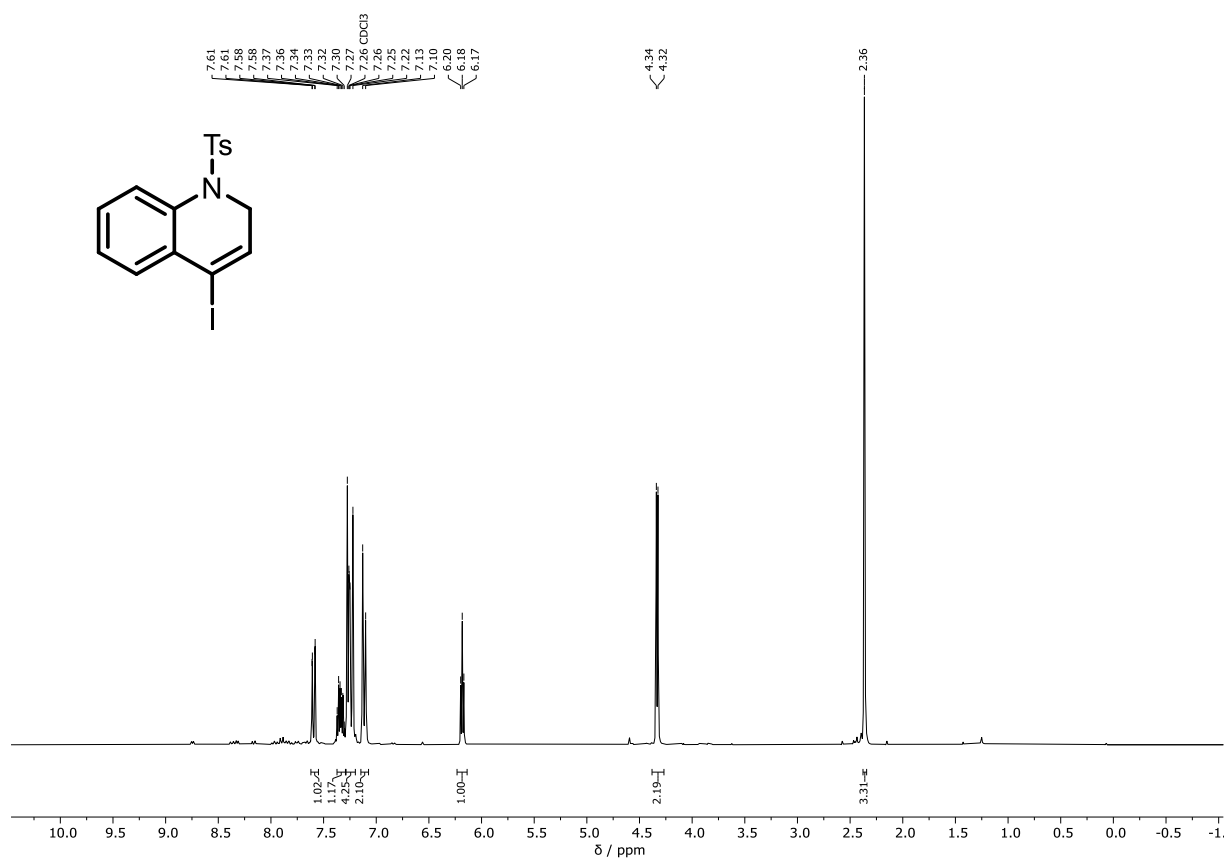
6-chloro-4-iodo-1-tosyl-1,2-dihydroquinoline (216a): ^{13}C NMR (101 MHz, CDCl$_3$)
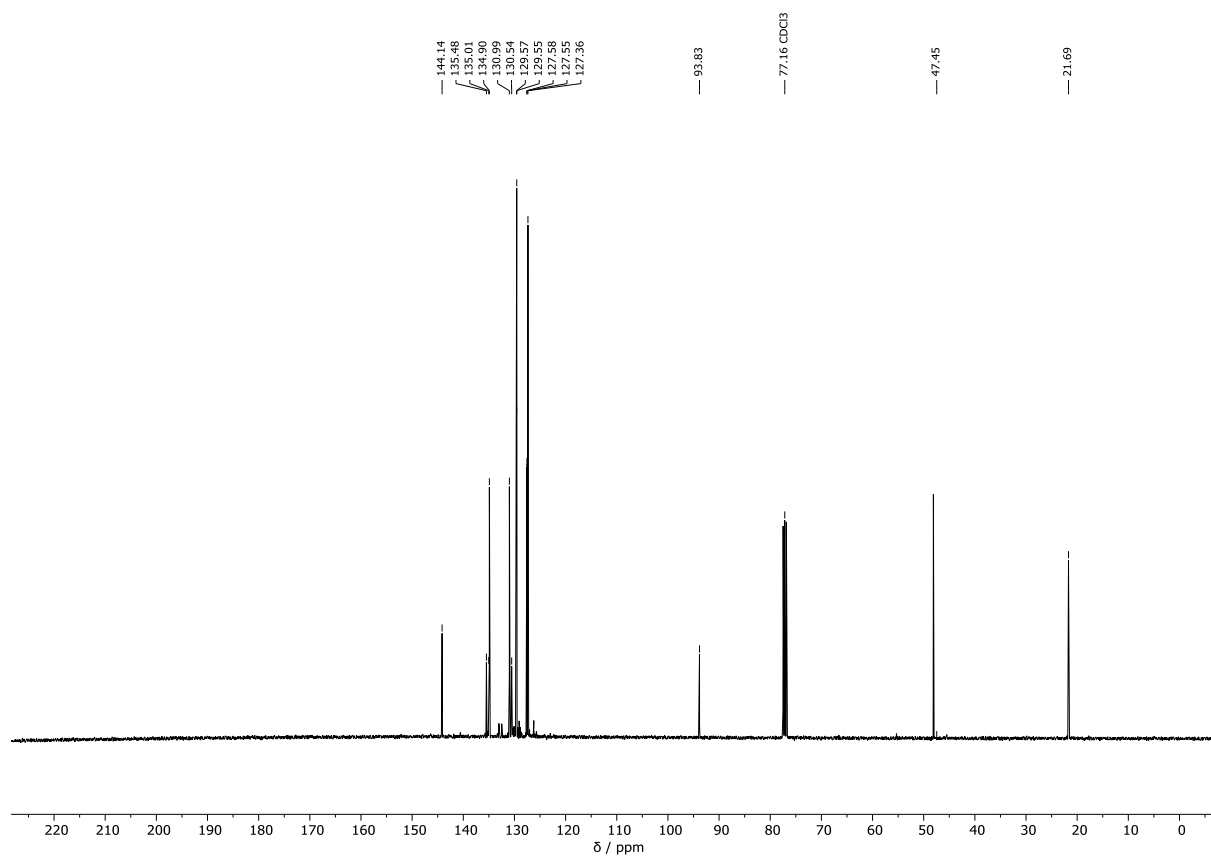
6-chloro-4-iodo-1-tosyl-1,2-dihydroquinoline (216b): ^{1}H NMR (300 MHz, CDCl$_3$)
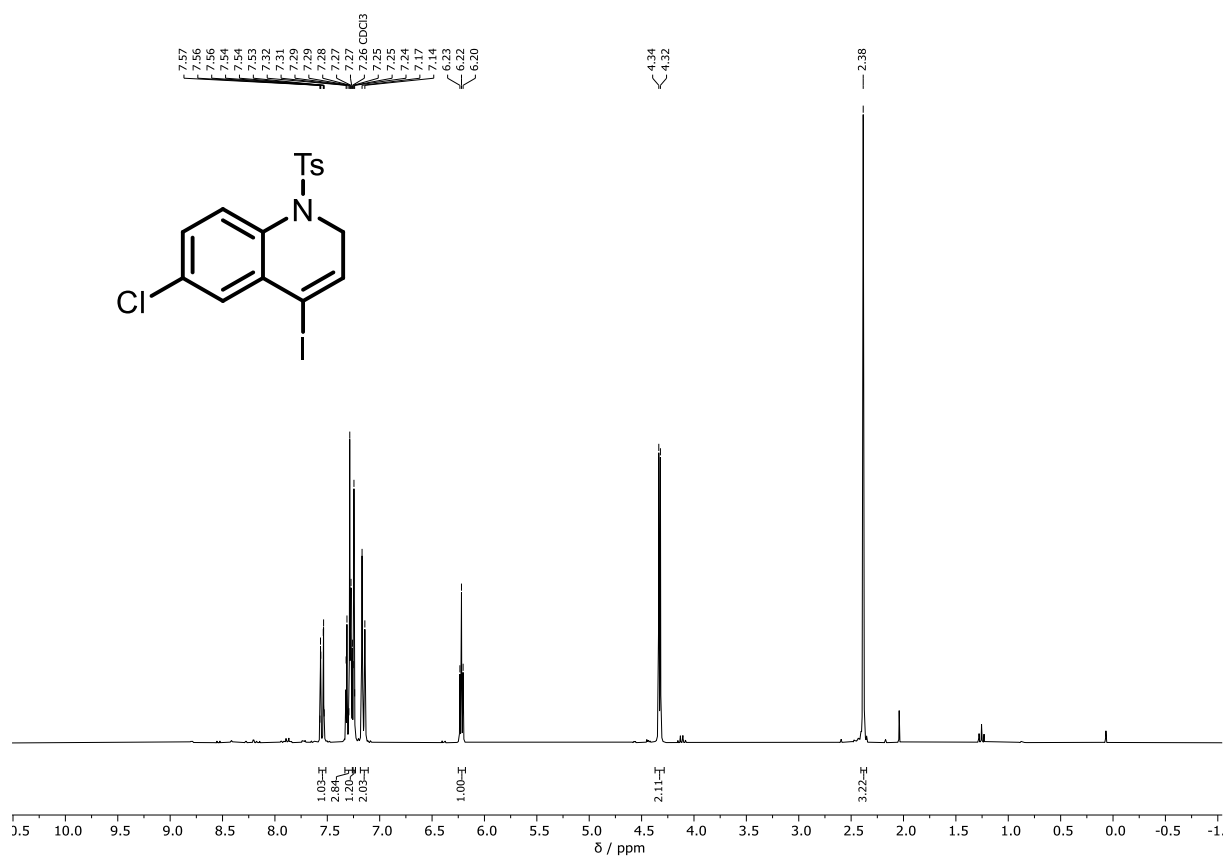
6-chloro-4-iodo-1-tosyl-1,2-dihydroquinoline (216b): ^{13}C NMR (101 MHz, CDCl$_3$)
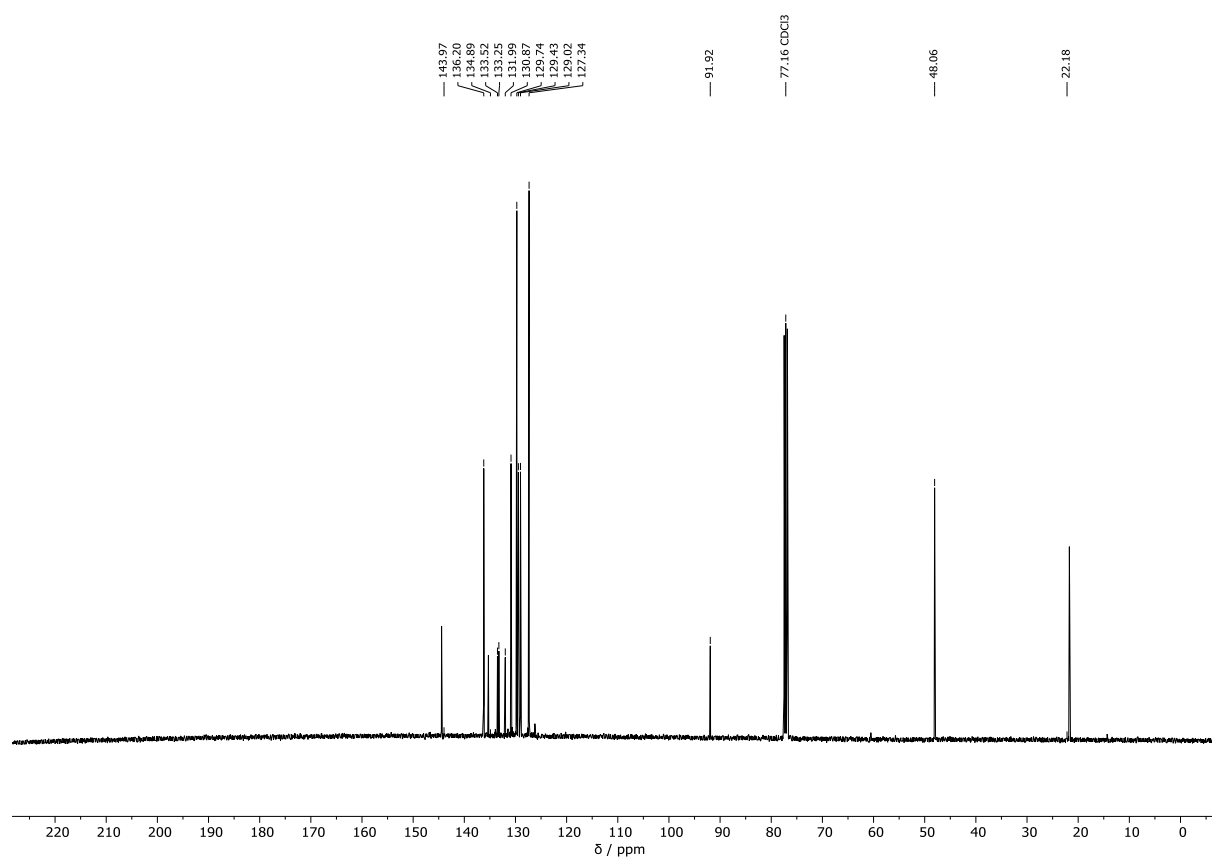
8.2 Crystal Data and Structure Refinement
Compound 172

Figure 23: Full asymmetric unit and labeling scheme of **172**. Hydrogen atoms except hydride omitted for clarity.

Empirical formula	$C_{33}H_{47}ClF_6IrNO_2PSb$
Formula weight	984.08
Temperature/K	100.0
Crystal system	monoclinic
Space group	$P2_1/n$
a/Å	10.0158(7)
b/Å	10.6839(8)
c/Å	36.048(5)
α/°	90
β/°	93.801(4)
γ/°	90
Volume/Å³	3848.9(7)
Z	4

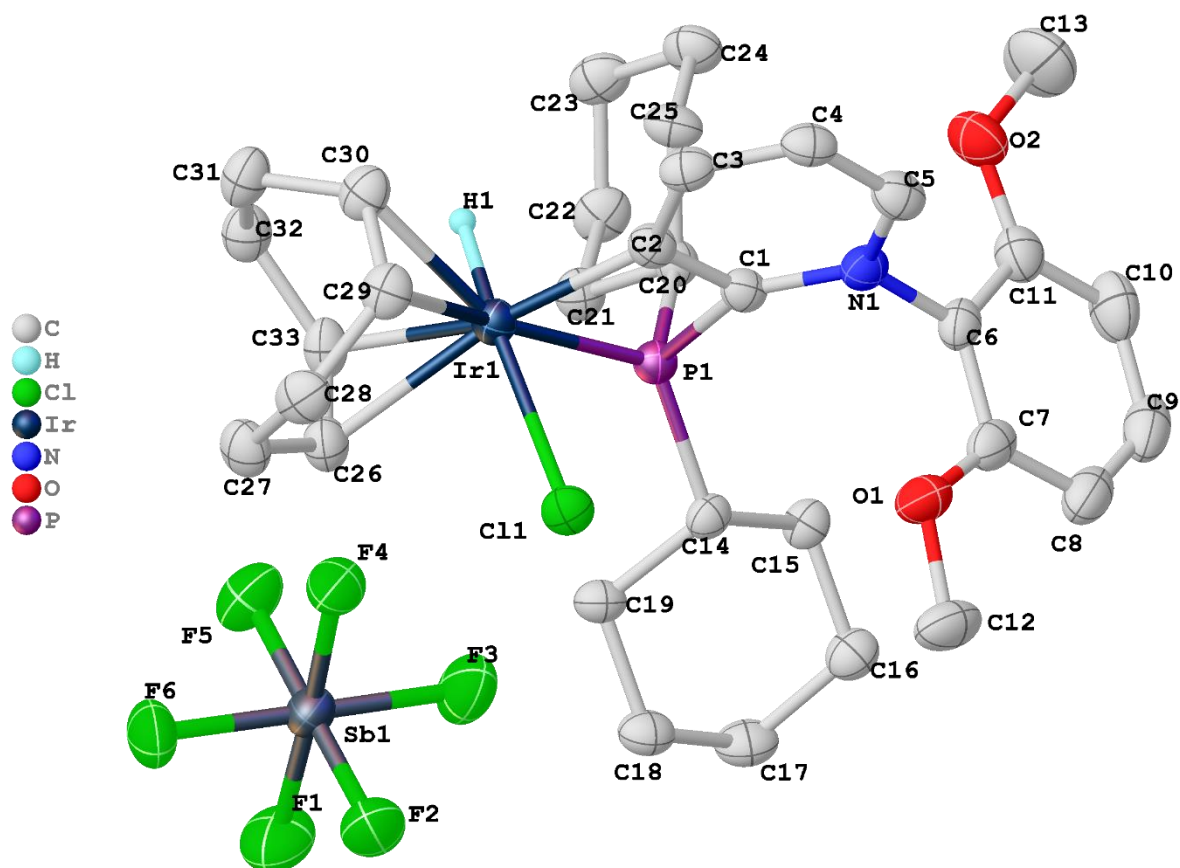|	
ρ_{calc} g/cm^3	1.698
μ/mm^{-1}	4.324
F(000)	1928.0
Crystal size/mm^3	0.16 × 0.107 × 0.017
Radiation	MoKα (λ = 0.71073)
2Θ range for data collection/°	4.434 to 63.052
Index ranges	-14 ≤ h ≤ 14, -15 ≤ k ≤ 12, -48 ≤ l ≤ 53
Reflections collected	38491
Independent reflections	12806 [R_{int} = 0.0377, R_{sigma} = 0.0428]
Data/restraints/parameters	12806/0/421
Goodness-of-fit on F^2	1.053
Final R indexes [I>=2σ(I)]	R1 = 0.0399, wR2 = 0.0923
Final R indexes [all data]	R_1 = 0.0530, wR$_2$ = 0.0980
Largest diff. peak/hole / e Å^{-3}	1.69/-1.24

Compound 174
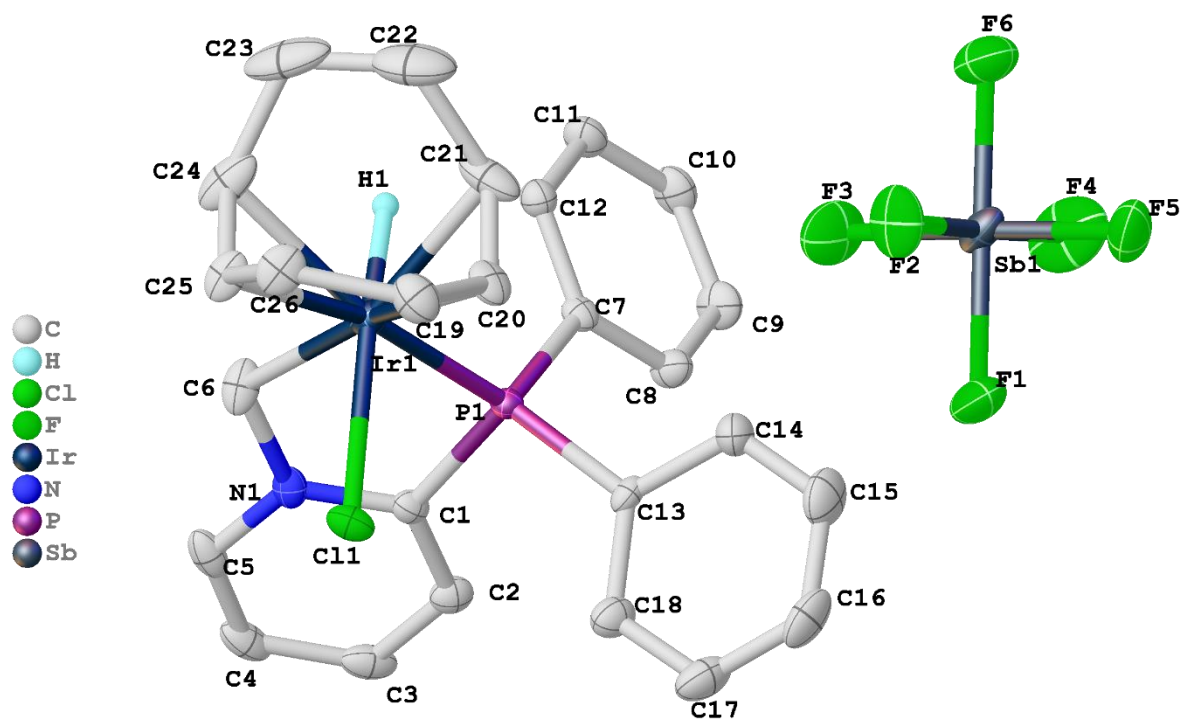
Figure 24: Full asymmetric unit and labeling scheme of **174**. Hydrogen atoms except hydride omitted for clarity.

Empirical formula	$C_{26}H_{29}ClF_6IrNPSb$
Formula weight	849.87
Temperature/K	100.01
Crystal system	monoclinic
Space group	$P2_1/c$
a/Å	11.9033(9)
b/Å	8.2433(7)
c/Å	28.535(2)
α/°	90
β/°	99.672(3)
γ/°	90
Volume/Å^3	2760.1(4)
Z	4
ρ_{calc}g/cm^3	2.045
μ/mm^{-1}	6.008
F(000)	1624.0

Crystal size/mm³	0.073 × 0.05 × 0.025
Radiation	MoKα (λ = 0.71073)
2Θ range for data collection/°	4.88 to 61.2
Index ranges	-16 ≤ h ≤ 17, -11 ≤ k ≤ 11, -40 ≤ l ≤ 31
Reflections collected	40978
Independent reflections	8434 [R_{int} = 0.0390, R_{sigma} = 0.0347]
Data/restraints/parameters	8434/3/338
Goodness-of-fit on F^2	1.173
Final R indexes [I>=2σ(I)]	R_1 = 0.0506, wR_2 = 0.1086
Final R indexes [all data]	R_1 = 0.0573, wR_2 = 0.1109
Largest diff. peak/hole / e Å⁻³	4.35/-2.75

Compound 191a

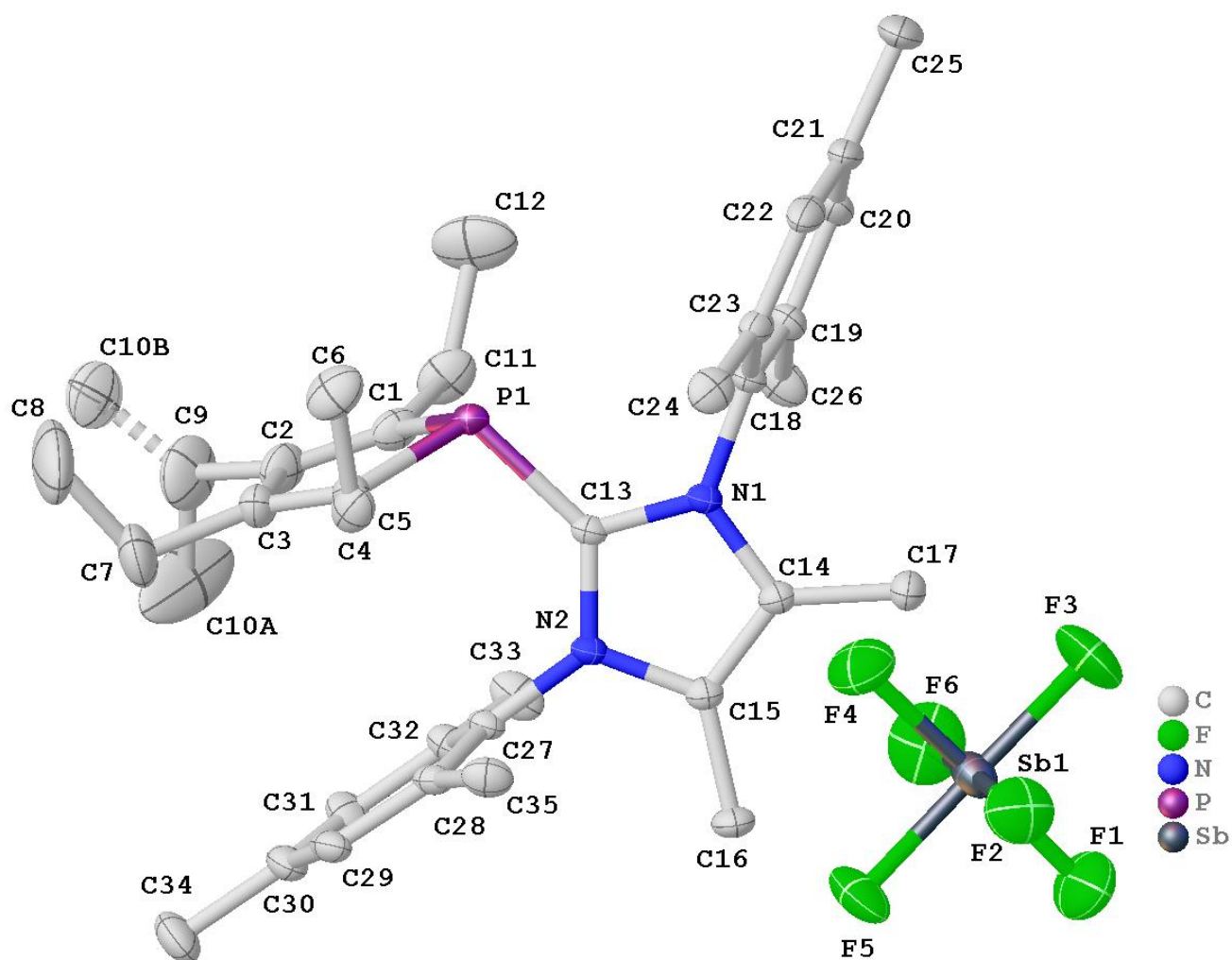**Figure 25**: Full asymmetric unit and labeling scheme of **191a**. Hydrogen atoms omitted for clarity; minor disorder part drawn partly translucent and with stippled cones.

CCDC-Nr.	2006361
Empirical formula	$C_{35}H_{48}F_6N_2PSb$
Formula weight	763.47
Temperature/K	100
Crystal system	trigonal
Space group	R-3
a/Å	33.262(3)
b/Å	33.262(3)
c/Å	18.3912(14)
α/°	90

β/°	90
γ/°	120
Volume/Å^3	17622(4)
Z	18
ρ_{calc}g/cm^3	1.295
μ/mm^{-1}	0.798
F(000)	7056.0
Crystal size/mm^3	0.936 × 0.077 × 0.046
Radiation	MoKα (λ = 0.71073)
2Θ range for data collection/°	4.348 to 59.192
Index ranges	-46 ≤ h ≤ 46, -46 ≤ k ≤ 46, -25 ≤ l ≤ 25
Reflections collected	134818
Independent reflections	11000 [R_{int} = 0.0240, R_{sigma} = 0.0108]
Data/restraints/parameters	11000/0/429
Goodness-of-fit on F^2	1.051
Final R indexes [I>=2σ (I)]	R_1 = 0.0299, wR_2 = 0.0809
Final R indexes [all data]	R_1 = 0.0325, wR_2 = 0.0829
Largest diff. peak/hole / e Å^{-3}	1.85/-0.93

Compound 191b
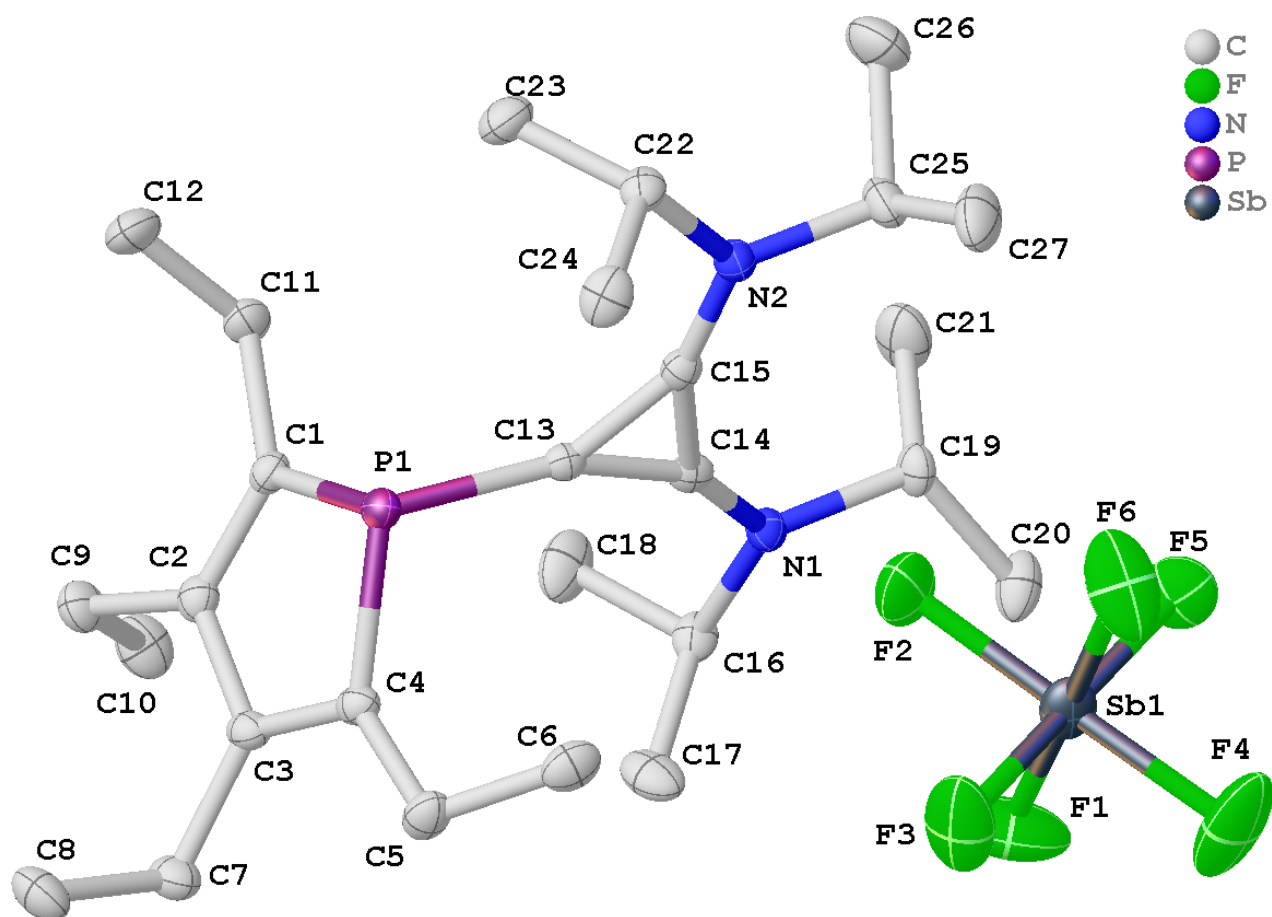
Figure 26: Full asymmetric unit and labeling scheme of **191b**. Hydrogen atoms omitted for clarity.

CCDC-Nr.	2006362
Empirical formula	$C_{27}H_{48}F_6N_2PSb$
Formula weight	667.39
Temperature/K	100
Crystal system	monoclinic
Space group	$P2_1/c$
a/Å	18.438(3)
b/Å	9.0836(15)
c/Å	18.800(3)
α/°	90
β/°	92.155(5)
γ/°	90

|	
Volume/Å^3	3146.4(9)
Z	4
ρ_{calc}g/cm^3	1.409
μ/mm^{-1}	0.981
F(000)	1376.0
Crystal size/mm^3	0.204 × 0.193 × 0.032
Radiation	MoKα (λ = 0.71073)
2Θ range for data collection/°	4.336 to 59.39
Index ranges	-25 ≤ h ≤ 19, -12 ≤ k ≤ 12, -25 ≤ l ≤ 26
Reflections collected	18230
Independent reflections	8480 [R_{int} = 0.0303, R_{sigma} = 0.0478]
Data/restraints/parameters	8480/0/346
Goodness-of-fit on F^2	1.020
Final R indexes [I>=2σ (I)]	R_1 = 0.0380, wR_2 = 0.0753
Final R indexes [all data]	R_1 = 0.0586, wR_2 = 0.0825
Largest diff. peak/hole / e Å^{-3}	0.83/-1.45

Compound 191c
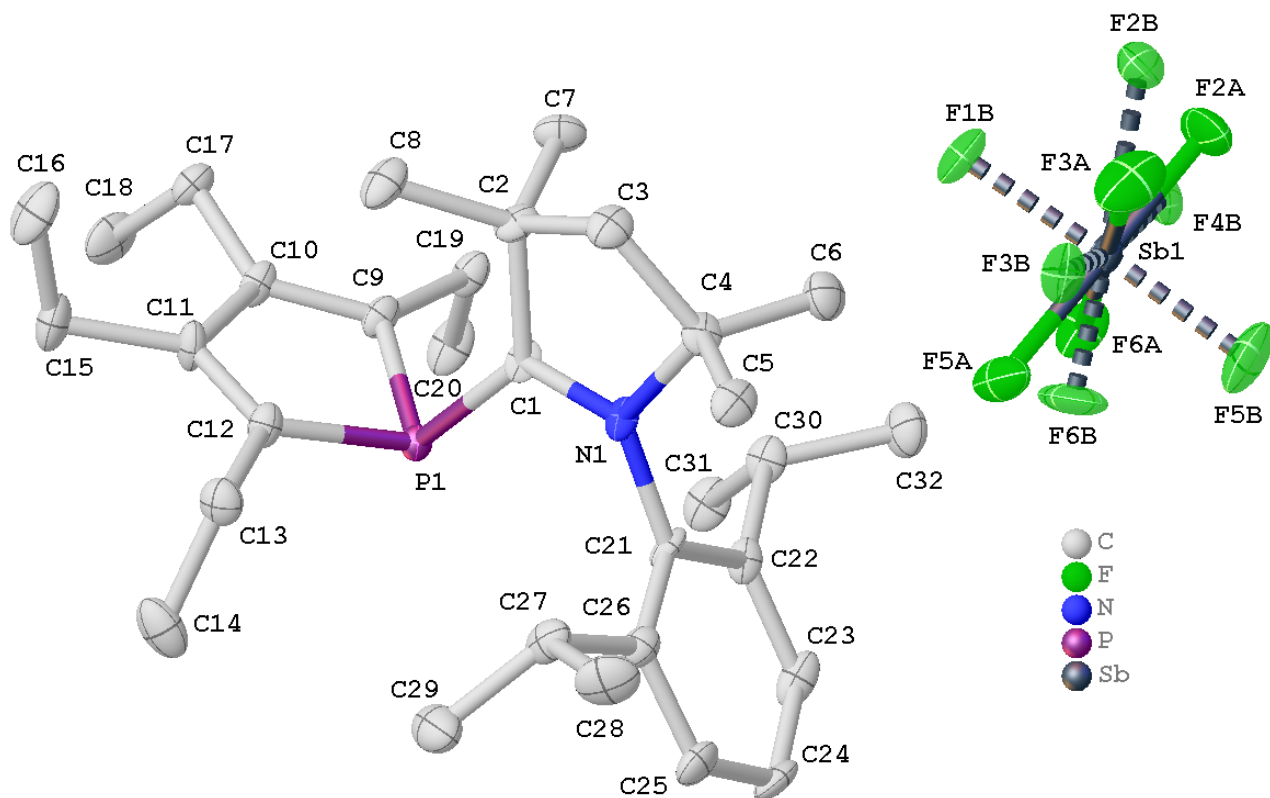
Figure 27: Full asymmetric unit and labeling scheme of **191c**. Hydrogen atoms omitted for clarity; minor disorder part drawn partly translucent and with stippled cones. Final refinement as inversion twin (-1 0 0 / 0 -1 0/ 0 0 -1) as indicated by the Flack parameter of 0.48(4).

CCDC-Nr.	2006363
Empirical formula	$C_{32}H_{51}F_6NPSb$
Formula weight	716.45
Temperature/K	100
Crystal system	orthorhombic
Space group	$P2_12_12_1$
a/Å	10.1524(5)
b/Å	12.2053(8)
c/Å	26.6324(18)
α/°	90
β/°	90
γ/°	90
Volume/Å³	3300.1(4)

|	
Z	4
ρ_{calc}g/cm^3	1.442
μ/mm^{-1}	0.940
F(000)	1480.0
Crystal size/mm^3	0.989 × 0.121 × 0.107
Radiation	MoKα (λ = 0.71073)
2Θ range for data collection/°	5.674 to 60.97
Index ranges	-14 ≤ h ≤ 14, -17 ≤ k ≤ 17, -38 ≤ l ≤ 38
Reflections collected	63408
Independent reflections	10061 [R_{int} = 0.0214, R_{sigma} = 0.0139]
Data/restraints/parameters	10061/30/420
Goodness-of-fit on F^2	1.253
Final R indexes [I>=2σ(I)]	R_1 = 0.0514, wR_2 = 0.1302
Final R indexes [all data]	R_1 = 0.0515, wR_2 = 0.1302
Largest diff. peak/hole / e Å^{-3}	1.69/-2.38
Flack parameter	0.48(4)

Compound 191d
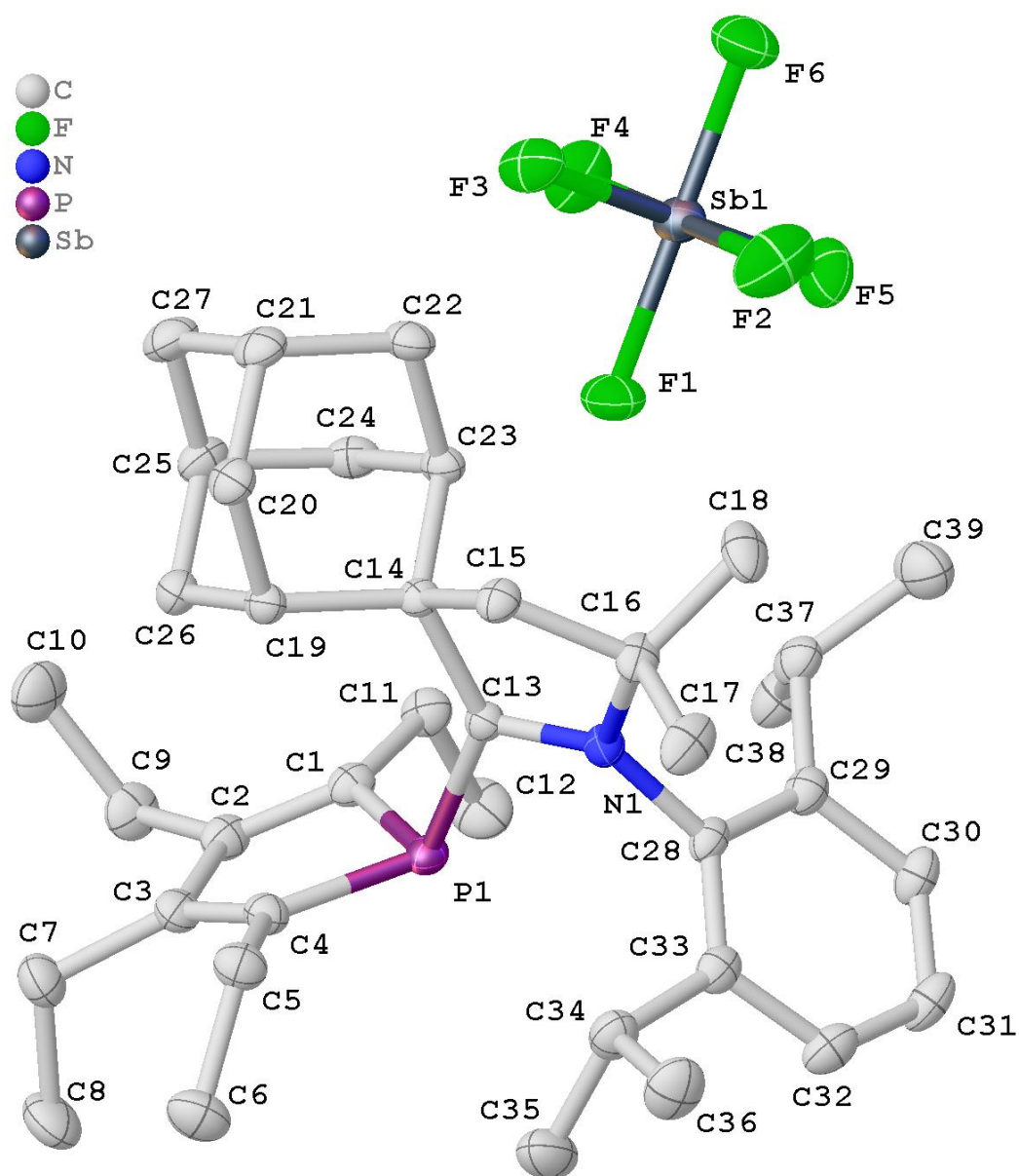
Figure 28: Full asymmetric unit and labeling scheme of **191d**. Hydrogen atoms omitted for clarity.

CCDC-Nr.	2006364
Empirical formula	$C_{39}H_{59}F_6NPSb$
Formula weight	808.59
Temperature/K	150
Crystal system	triclinic
Space group	P-1
a/Å	11.1164(15)
b/Å	11.903(2)

|	
c/Å	15.772(2)
α/°	92.353(4)
β/°	94.304(4)
γ/°	112.664(5)
Volume/Å³	1914.9(5)
Z	2
ρ_{calc}g/cm³	1.402
μ/mm⁻¹	0.819
F(000)	840.0
Crystal size/mm³	0.378 × 0.321 × 0.052
Radiation	MoKα (λ = 0.71073)
2Θ range for data collection/°	4.696 to 55.998
Index ranges	-15 ≤ h ≤ 14, -15 ≤ k ≤ 15, 0 ≤ l ≤ 21
Reflections collected	9069
Independent reflections	9069 [R_{int} = 0.0456, R_{sigma} = 0.0259]
Data/restraints/parameters	9069/0/443
Goodness-of-fit on F²	1.046
Final R indexes [I>=2σ(I)]	R_1 = 0.0341, wR_2 = 0.0769
Final R indexes [all data]	R_1 = 0.0404, wR_2 = 0.0797
Largest diff. peak/hole / e Å⁻³	0.52/-1.10

Compound 193
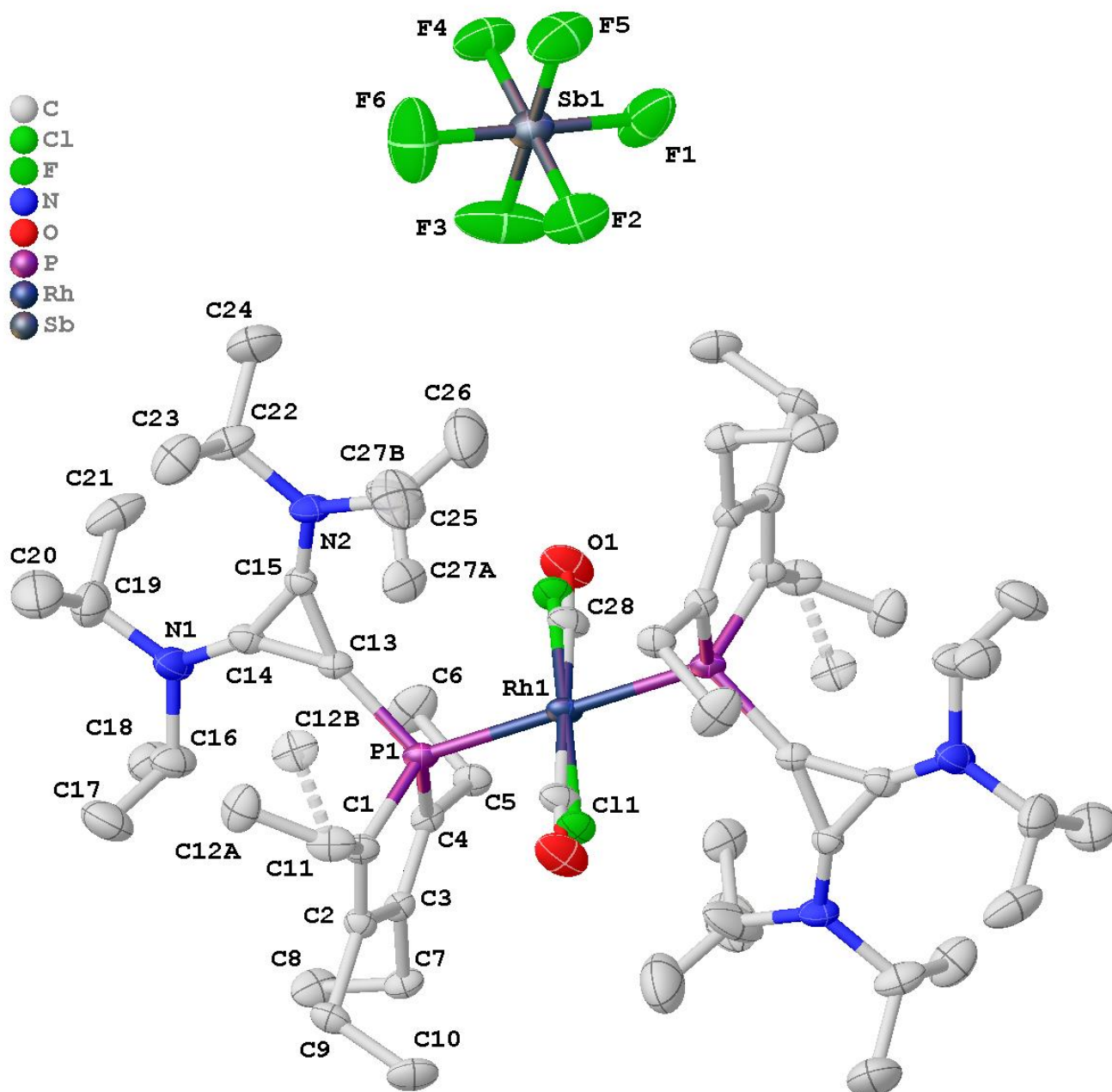
Figure 29: Grown asymmetric unit and labeling scheme of **193**. Hydrogen atoms omitted for clarity; minor disorder part drawn partly translucent and with stippled cones. Rh1 is located on crystallographic symmetry center; full molecule generated by symmetry operation 1-X, -Y, 1-Z. Non-merohedral twinning found for **193**, twin domain transformation matrix is (-1 0 0/ 0 -1 0/ 1.05 0.93 1), the twin batch scale factor on the final data was 0.3584(6).

CCDC-Nr.	2006365
Empirical formula	$C_{55}H_{94}ClF_{12}N_4OP_2RhSb_2$
Formula weight	1499.14
Temperature/K	100

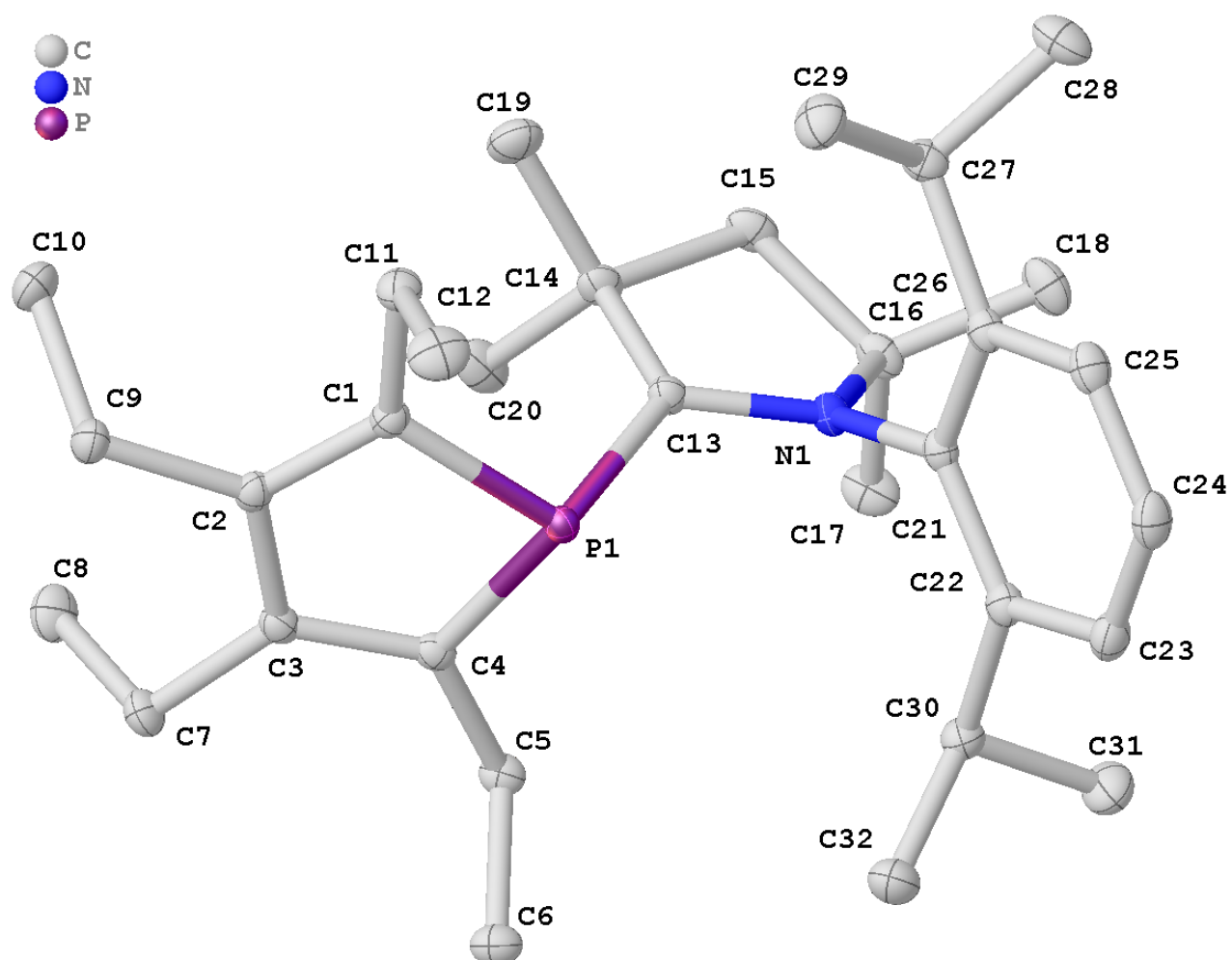| Crystal system	triclinic
Space group	P-1
a/Å	9.8649(11)
b/Å	13.4259(12)
c/Å	14.6785(16)
α/°	113.416(3)
β/°	108.710(3)
γ/°	94.580(3)
Volume/Å^3	1640.9(3)
Z	1
ρ_{calc}g/cm^3	1.517
μ/mm^{-1}	1.228
F(000)	762.0
Crystal size/mm^3	0.2 × 0.2 × 0.15
Radiation	MoKα (λ = 0.71073)
2Θ range for data collection/°	4.488 to 56.6
Index ranges	-13 ≤ h ≤ 12, -17 ≤ k ≤ 16, 0 ≤ l ≤ 19
Reflections collected	7995
Independent reflections	7995 [R_{int} = ?, R_{sigma} = 0.0283]
Data/restraints/parameters	7995/63/402
Goodness-of-fit on F^2	1.053
Final R indexes [I>=2σ(I)]	R_1 = 0.0318, wR_2 = 0.0713
Final R indexes [all data]	R_1 = 0.0367, wR_2 = 0.0746
Largest diff. peak/hole / e Å^{-3}	0.87/-0.92

Compound 196

Figure 30: Full asymmetric unit and labeling scheme of **196**. Hydrogen atoms omitted for clarity.

CCDC-Nr.	2006366
Empirical formula	$C_{32}H_{51}NP$
Formula weight	480.70
Temperature/K	100
Crystal system	triclinic
Space group	P-1
a/Å	8.8773(13)
b/Å	10.0498(14)
c/Å	16.575(3)
α/°	91.202(6)
β/°	92.757(5)

|	
γ/°	100.845(4)
Volume/Å^3	1449.9(4)
Z	2
ρ_{calc}g/cm^3	1.101
μ/mm^{-1}	0.114
F(000)	530.0
Crystal size/mm^3	0.283 × 0.199 × 0.052
Radiation	MoKα (λ = 0.71073)
2Θ range for data collection/°	4.678 to 59.168
Index ranges	-12 ≤ h ≤ 12, -13 ≤ k ≤ 13, -23 ≤ l ≤ 23
Reflections collected	51851
Independent reflections	8092 [R_{int} = 0.0223, R_{sigma} = 0.0167]
Data/restraints/parameters	8092/0/319
Goodness-of-fit on F^2	1.078
Final R indexes [I>=2σ (I)]	R_1 = 0.0332, wR_2 = 0.0862
Final R indexes [all data]	R_1 = 0.0358, wR_2 = 0.0883
Largest diff. peak/hole / e Å^{-3}	0.38/-0.27

Compound 197a
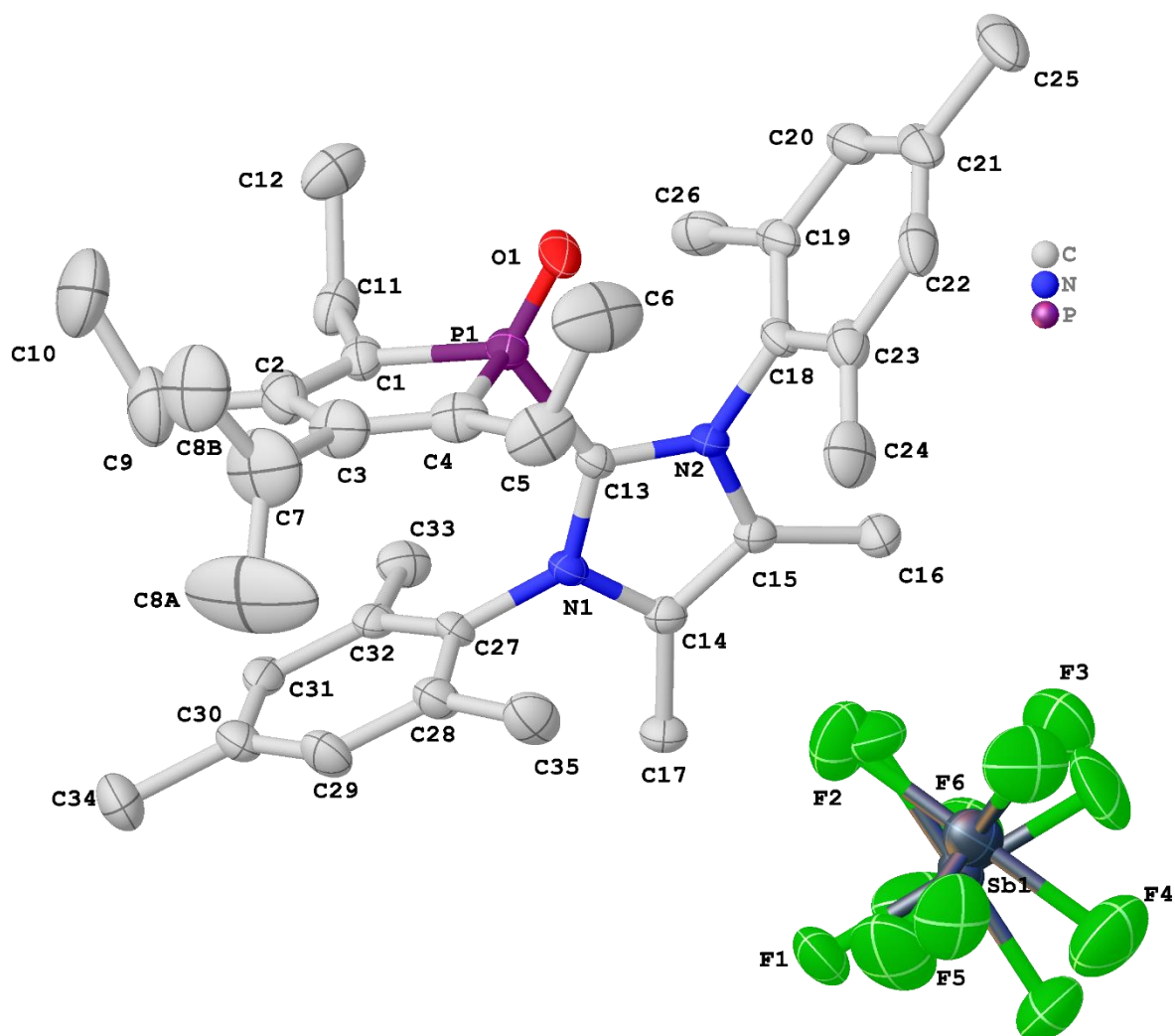
Figure 31: Full asymmetric unit and labeling scheme of **197a**. Hydrogen atoms omitted for clarity.

Empirical formula	$C_{36}Cl_2F_6H_{50}N_2O_{0.11}PSb$
Formula weight	850.16
Temperature/K	100.0
Crystal system	trigonal
Space group	R-3
a/Å	33.2550(14)
b/Å	33.2550(14)
c/Å	18.4232(8)
α/°	90
β/°	90

γ/°	120
Volume/Å^3	17644.5(17)
Z	18
ρ_{calc}g/cm^3	1.440
μ/mm^{-1}	0.937
F(000)	7828.0
Crystal size/mm^3	0.688 × 0.082 × 0.046
Radiation	MoKα (λ = 0.71073)
2Θ range for data collection/°	4.346 to 54.234
Index ranges	-42 ≤ h ≤ 42, -42 ≤ k ≤ 42, -23 ≤ l ≤ 23
Reflections collected	100764
Independent reflections	8665 [R_{int} = 0.0429, R_{sigma} = 0.0200]
Data/restraints/parameters	8665/99/502
Goodness-of-fit on F^2	1.058
Final R indexes [I>=2σ (I)]	R_1 = 0.0357, wR_2 = 0.0793
Final R indexes [all data]	R_1 = 0.0437, wR_2 = 0.0833
Largest diff. peak/hole / e Å^{-3}	0.53/-0.49

Compound 197c
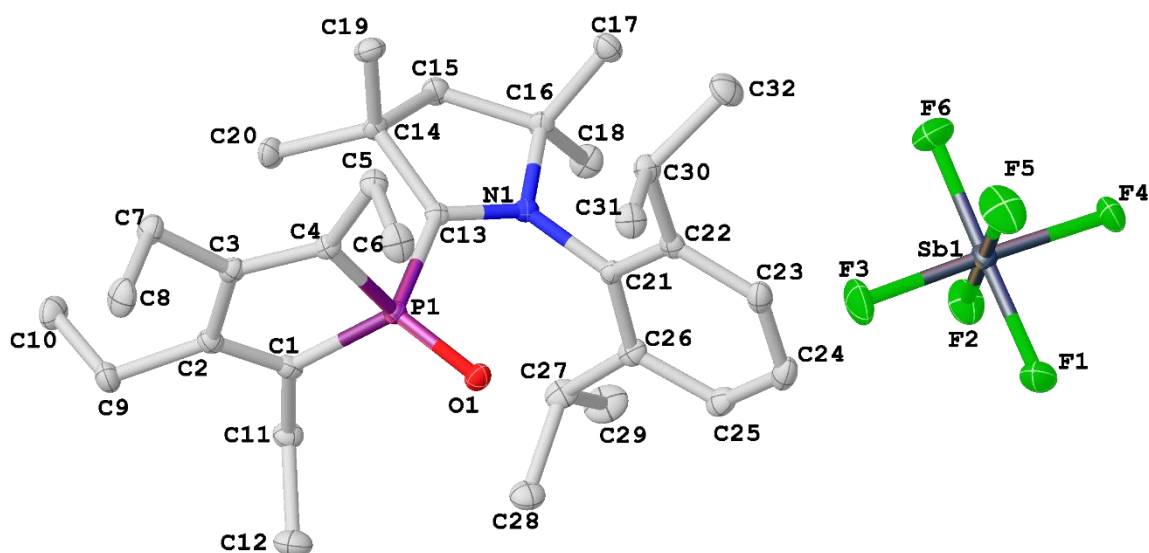
Figure 32: Full asymmetric unit and labeling scheme of **197c**. Hydrogen atoms omitted for clarity.

Empirical formula	$C_{32}H_{51}F_6NOPSb$
Formula weight	732.45
Temperature/K	99.99
Crystal system	orthorhombic
Space group	$Pna2_1$
a/Å	26.7100(10)
b/Å	12.1962(4)
c/Å	10.1295(4)
α/°	90
β/°	90
γ/°	90
Volume/Å^3	3299.8(2)
Z	4
ρ_{calc}g/cm^3	1.474
μ/mm^{-1}	0.944
F(000)	1512.0
Crystal size/mm^3	0.798 × 0.038 × 0.036
Radiation	MoKα (λ = 0.71073)
2Θ range for data collection/°	4.522 to 57.446

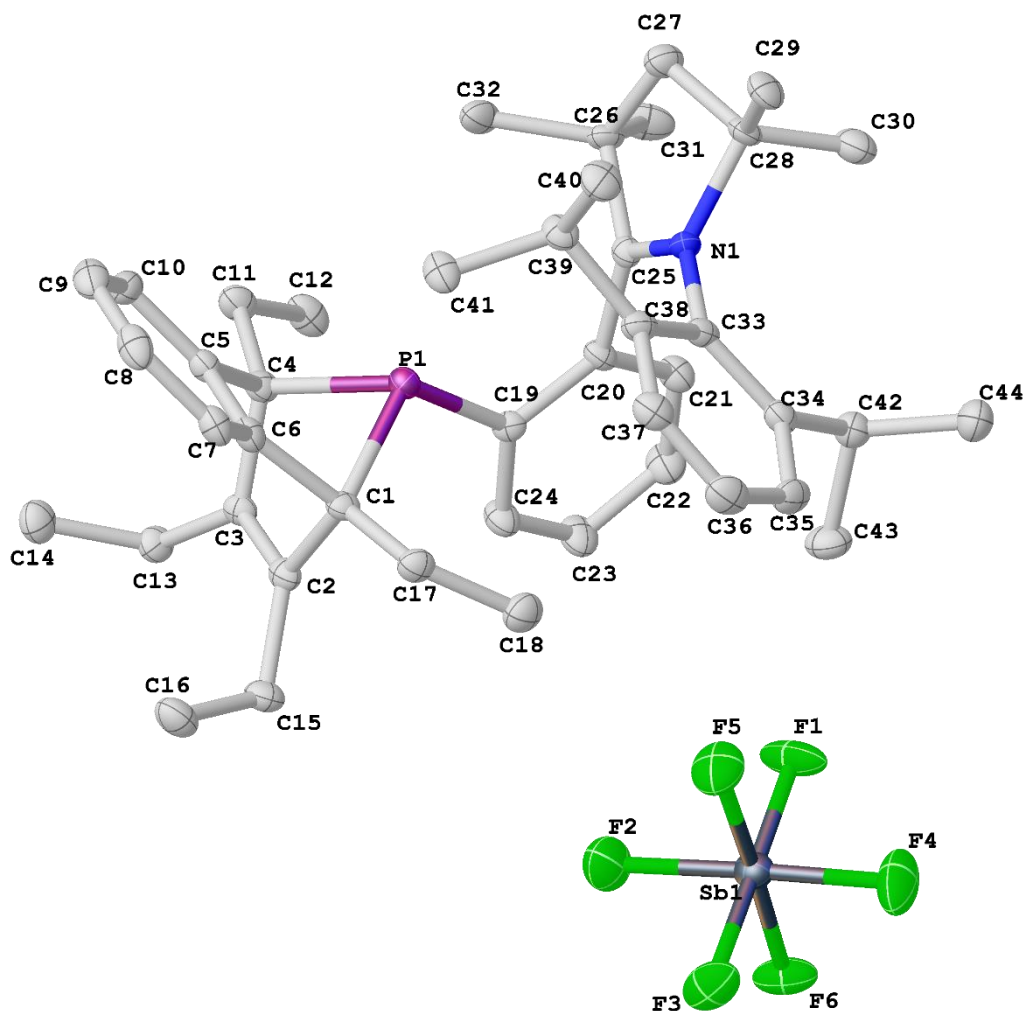|	
Index ranges	-36 ≤ h ≤ 36, -16 ≤ k ≤ 16, -13 ≤ l ≤ 13
Reflections collected	241305
Independent reflections	8532 [R_{int} = 0.0343, R_{sigma} = 0.0107]
Data/restraints/parameters	8532/1/391
Goodness-of-fit on F^2	1.083
Final R indexes [I>=2σ(I)]	R_1 = 0.0149, wR_2 = 0.0370
Final R indexes [all data]	R_1 = 0.0156, wR_2 = 0.0375
Largest diff. peak/hole / e Å^{-3}	0.33/-0.38

Compound 203

Figure 33: Full asymmetric unit and labeling scheme of **203**. Hydrogen atoms omitted for clarity.

Empirical formula	$C_{44}H_{59}F_6NPSb$
Formula weight	868.64
Temperature/K	100.0
Crystal system	orthorhombic
Space group	$P2_12_12_1$
a/Å	9.7316(5)
b/Å	10.6595(7)
c/Å	40.191(3)
α/°	90
β/°	90
γ/°	90

|	
Volume/Å^3	4169.2(4)
Z	4
ρ_{calc}g/cm^3	1.384
μ/mm^{-1}	0.758
F(000)	1800.0
Crystal size/mm^3	0.355 × 0.339 × 0.036
Radiation	MoKα (λ = 0.71073)
2Θ range for data collection/°	4.306 to 54.988
Index ranges	-12 ≤ h ≤ 12, -13 ≤ k ≤ 13, -52 ≤ l ≤ 52
Reflections collected	54644
Independent reflections	9554 [R_{int} = 0.0375, R_{sigma} = 0.0266]
Data/restraints/parameters	9554/0/491
Goodness-of-fit on F^2	1.227
Final R indexes [I>=2σ(I)]	R_1 = 0.0403, wR_2 = 0.0862
Final R indexes [all data]	R_1 = 0.0420, wR_2 = 0.0871
Largest diff. peak/hole / e Å^{-3}	0.80/-1.19

Compound 205a
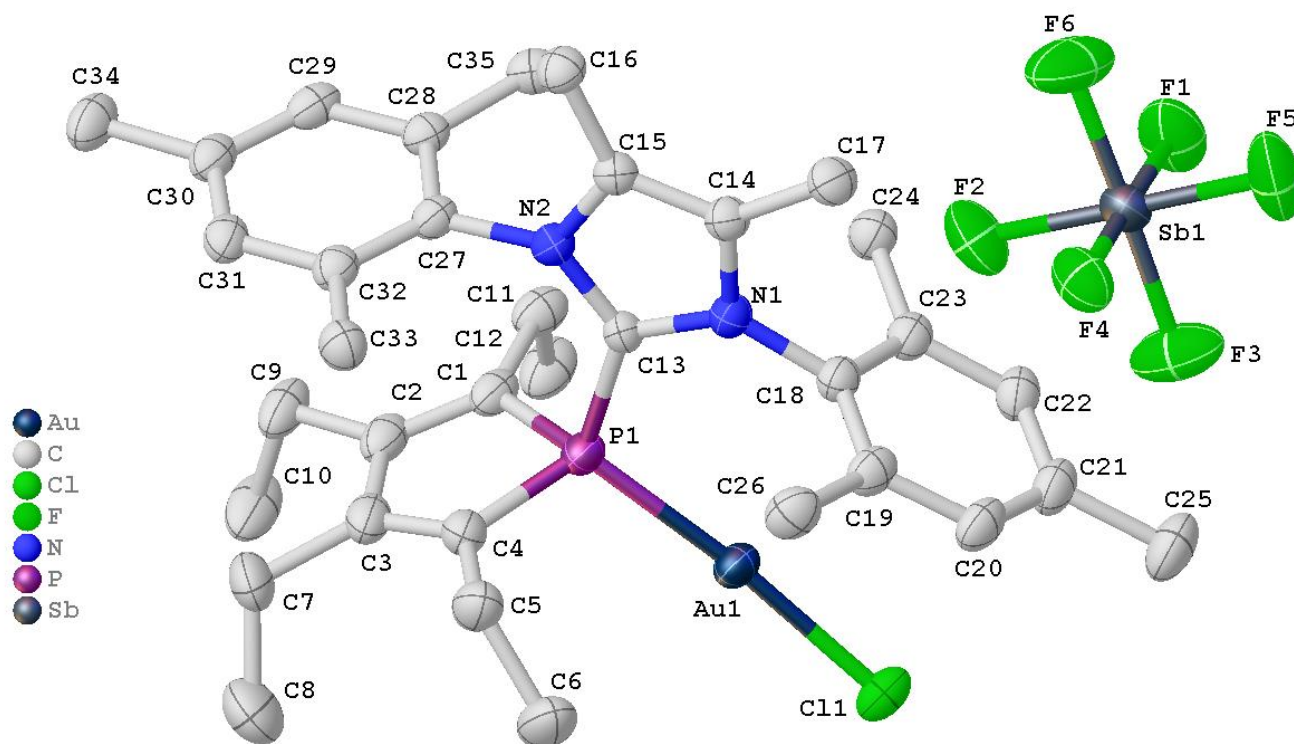
Figure 34: Full asymmetric unit and labeling scheme of **205a**. Hydrogen atoms omitted for clarity. Solvent mask was applied, that is consistent with two disordered molecules of dichloromethane.

CCDC-Nr.	2006367
Empirical formula	$AuC_{37}Cl_5F_6H_{52}N_2PSb$
Formula weight	1165.74
Temperature/K	100
Crystal system	monoclinic
Space group	$P2_1/c$
a/Å	8.7304(6)
b/Å	12.8507(8)
c/Å	38.866(2)
α/°	90
β/°	95.138(2)
γ/°	90
Volume/Å^3	4342.9(5)
Z	4
ρ$_{calc}$g/cm^3	1.783

μ/mm^{-1}	4.396
F(000)	2288.0
Crystal size/mm^3	0.297 × 0.181 × 0.122
Radiation	MoKα (λ = 0.71073)
2Θ range for data collection/°	4.684 to 67.544
Index ranges	-13 ≤ h ≤ 13, -20 ≤ k ≤ 20, -60 ≤ l ≤ 60
Reflections collected	201662
Independent reflections	17302 [R_{int} = 0.0246, R_{sigma} = 0.0117]
Data/restraints/parameters	17302/0/436
Goodness-of-fit on F^2	1.161
Final R indexes [I>=2σ(I)]	R_1 = 0.0433, wR_2 = 0.1225
Final R indexes [all data]	R_1 = 0.0438, wR_2 = 0.1228
Largest diff. peak/hole / e Å^{-3}	2.52/-2.13

Compound 205b
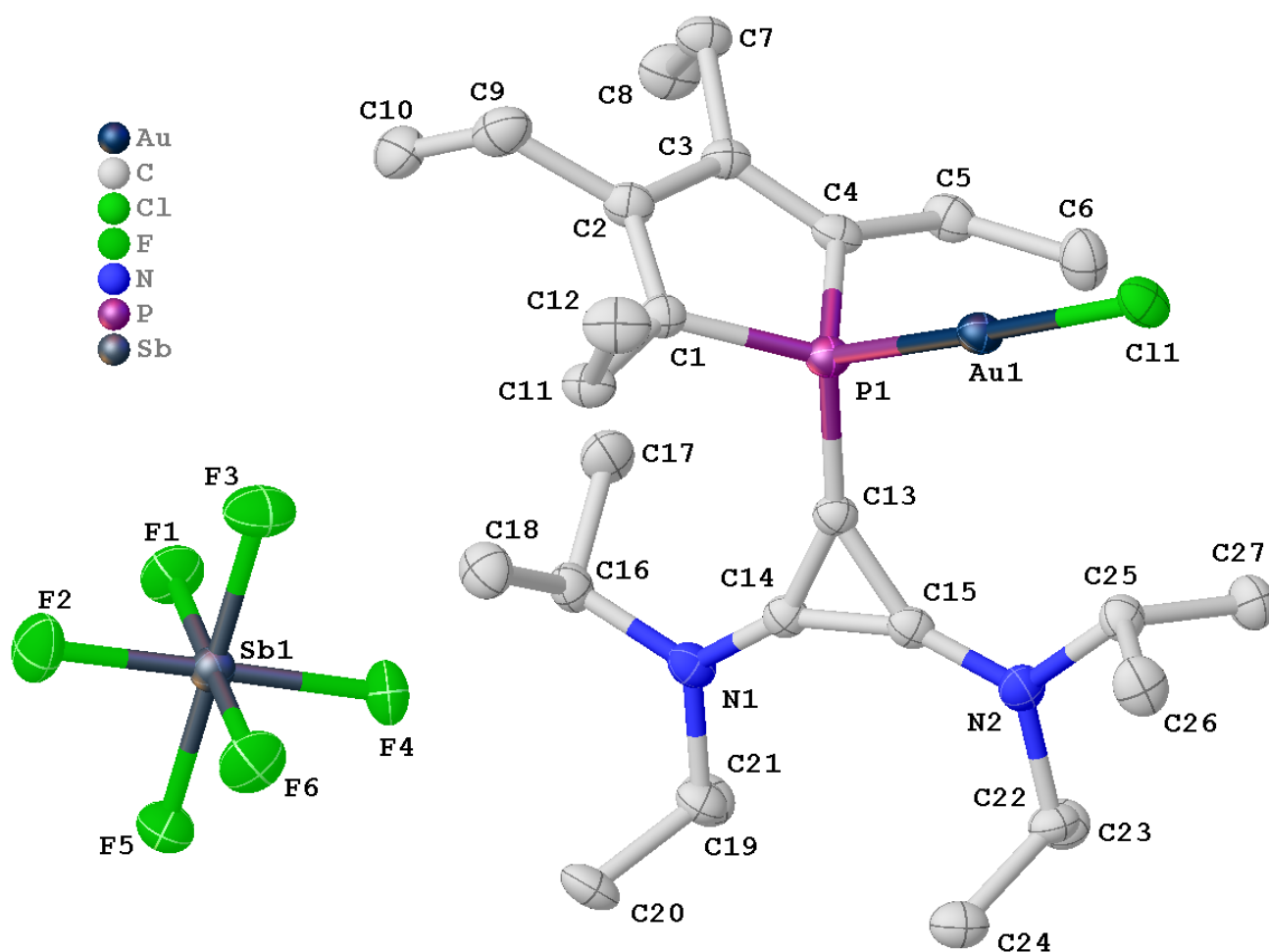
Figure 35: Grown asymmetric unit and labeling scheme of **205b**. Hydrogen atoms omitted for clarity Non-merohedral twinning found for **6b**, twin domain transformation matrix is (-1 0 -0.47/ 0 -1 0/ 0 0 1), the twin batch scale factor on the final data was 0.4827(13).

CCDC-Nr.	2006368
Empirical formula	$C_{27}H_{48}AuClF_6N_2PSb$
Formula weight	899.81
Temperature/K	100
Crystal system	monoclinic
Space group	$P2_1$
a/Å	12.4343(8)
b/Å	10.3293(7)
c/Å	13.6792(8)
α/°	90

β/°	104.910(2)
γ/°	90
Volume/Å^3	1697.77(19)
Z	2
ρ_{calc}g/cm^3	1.760
μ/mm^{-1}	5.289
F(000)	880.0
Crystal size/mm^3	0.273 × 0.15 × 0.136
Radiation	MoKα (λ = 0.71073)
2Θ range for data collection/°	5.004 to 63.122
Index ranges	-18 ≤ h ≤ 18, -15 ≤ k ≤ 15, -20 ≤ l ≤ 20
Reflections collected	11367
Independent reflections	11367 [R_{int} = ?, R_{sigma} = 0.0189]
Data/restraints/parameters	11367/1/365
Goodness-of-fit on F^2	1.044
Final R indexes [I>=2σ(I)]	R_1 = 0.0391, wR_2 = 0.1072
Final R indexes [all data]	R_1 = 0.0393, wR_2 = 0.1074
Largest diff. peak/hole / e Å^{-3}	1.27/-0.55
Flack parameter	0.238(7)

Compound 205c
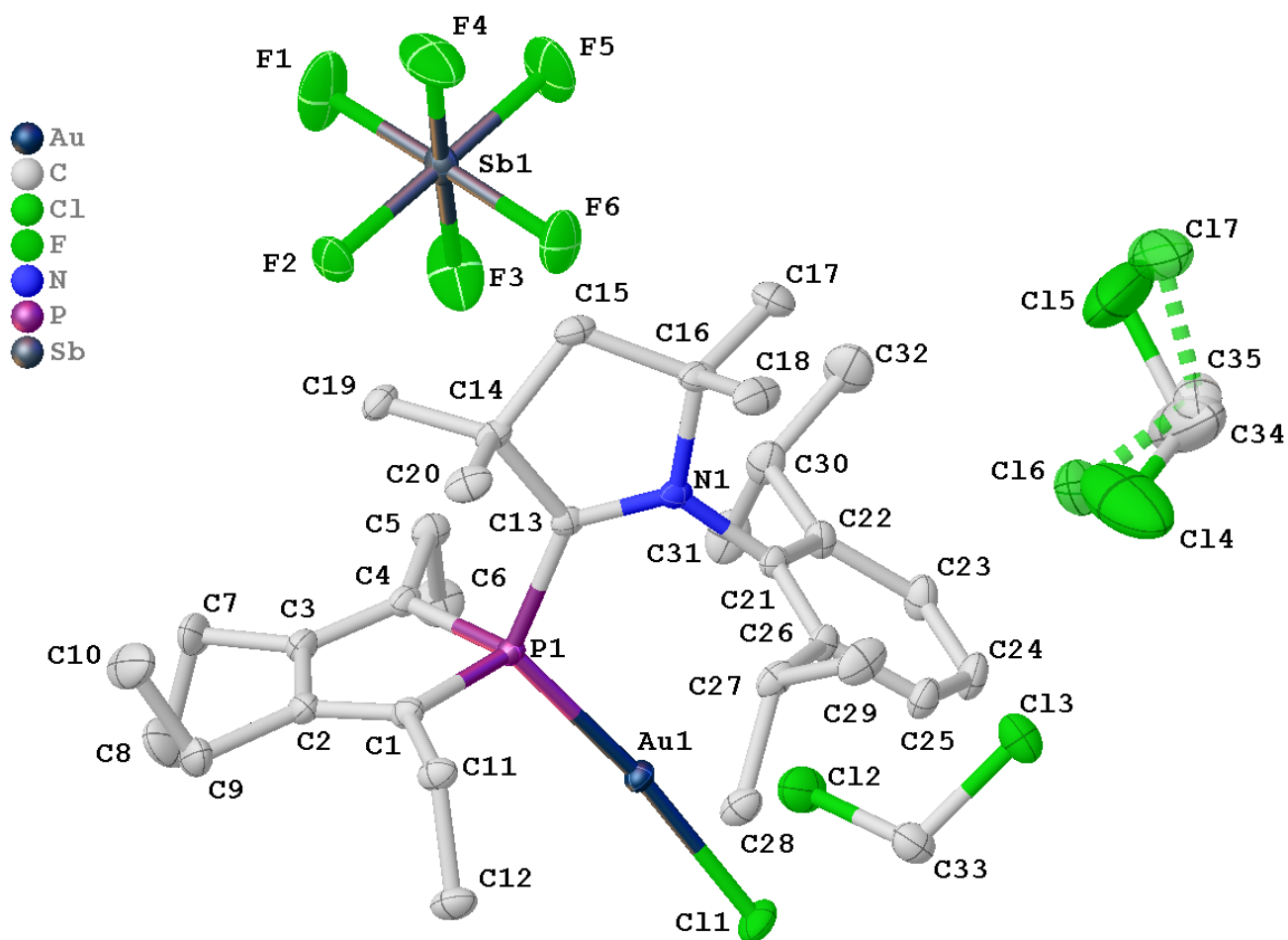
Figure 36: Full asymmetric unit and labeling scheme of **205c**. Hydrogen atoms omitted for clarity; minor disorder part drawn partly translucent and with stippled cones

CCDC-Nr.	2006369
Empirical formula	$C_{34}H_{55}AuCl_5F_6NPSb$
Formula weight	1118.72
Temperature/K	100
Crystal system	monoclinic
Space group	Cc
a/Å	10.8988(3)
b/Å	36.9447(10)
c/Å	11.0805(3)
α/°	90
β/°	106.7770(10)

γ/°	90
Volume/Å^3	4271.7(2)
Z	4
ρ_{calc}g/cm^3	1.740
μ/mm^{-1}	4.464
F(000)	2200.0
Crystal size/mm^3	0.23 × 0.229 × 0.057
Radiation	MoKα (λ = 0.71073)
2Θ range for data collection/°	5.116 to 65.246
Index ranges	-16 ≤ h ≤ 16, -56 ≤ k ≤ 56, -16 ≤ l ≤ 16
Reflections collected	67597
Independent reflections	15511 [R_{int} = 0.0208, R_{sigma} = 0.0173]
Data/restraints/parameters	15511/23/482
Goodness-of-fit on F^2	1.052
Final R indexes [I>=2σ(I)]	R_1 = 0.0146, wR_2 = 0.0355
Final R indexes [all data]	R_1 = 0.0151, wR_2 = 0.0357
Largest diff. peak/hole / e Å^{-3}	0.67/-0.93
Flack parameter	-0.0086(8)

Compound 205d
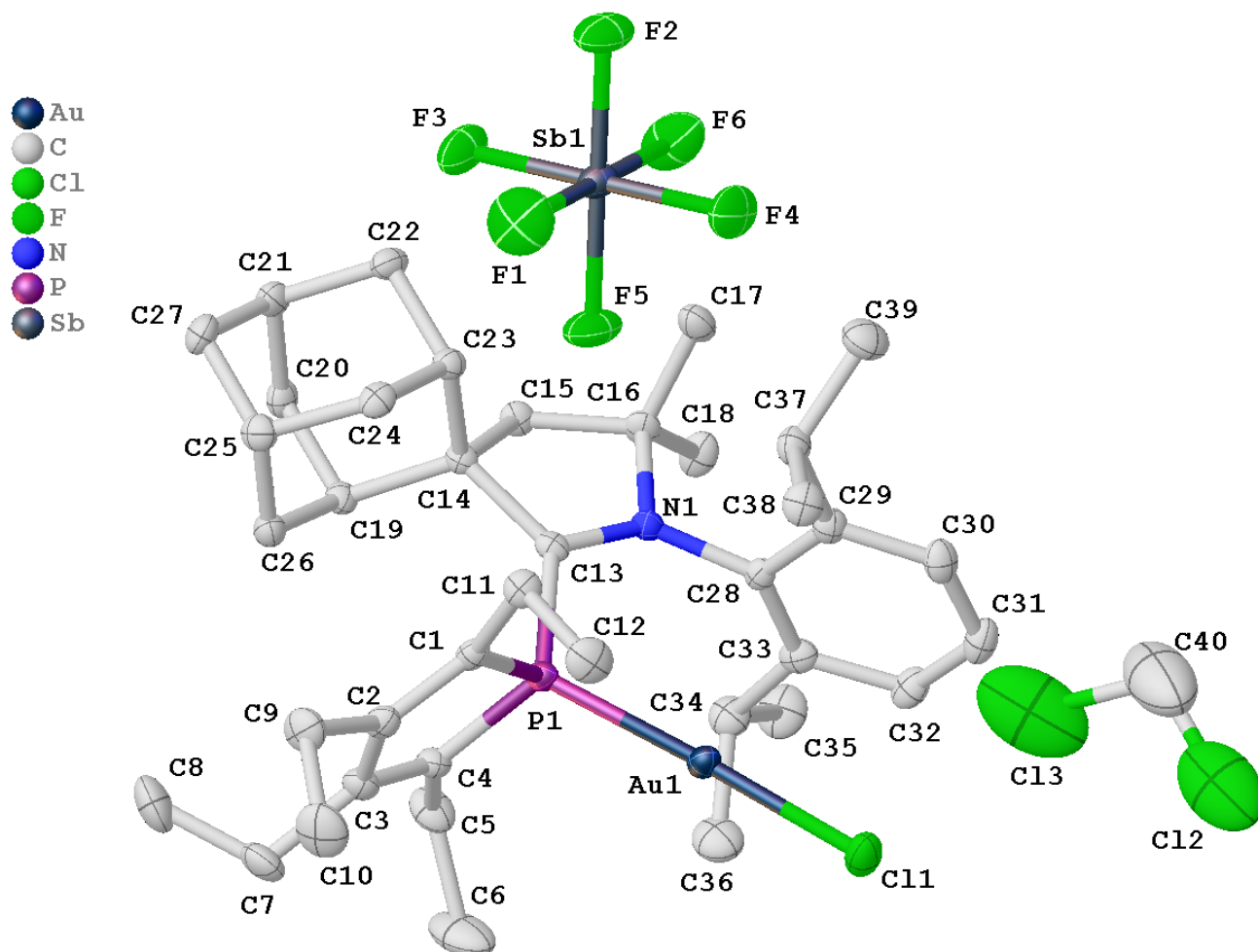
Figure 37: Full asymmetric unit and labeling scheme of **205d**. Hydrogen atoms omitted for clarity.

CCDC-Nr.	2006370
Empirical formula	$C_{40}H_{61}AuCl_3F_6NPSb$
Formula weight	1125.93
Temperature/K	150
Crystal system	monoclinic
Space group	$P2_1/c$
a/Å	11.0872(9)
b/Å	36.375(3)
c/Å	11.6998(10)
α/°	90
β/°	111.442(3)

γ/°	90
Volume/Å^3	4391.9(6)
Z	4
ρ_{calc}g/cm^3	1.703
μ/mm^{-1}	4.225
F(000)	2232.0
Crystal size/mm^3	0.489 × 0.434 × 0.038
Radiation	MoKα (λ = 0.71073)
2Θ range for data collection/°	4.476 to 57.566
Index ranges	-14 ≤ h ≤ 14, -41 ≤ k ≤ 49, -15 ≤ l ≤ 15
Reflections collected	70021
Independent reflections	11334 [R_{int} = 0.0304, R_{sigma} = 0.0228]
Data/restraints/parameters	11334/0/537
Goodness-of-fit on F^2	1.221
Final R indexes [I>=2σ(I)]	R_1 = 0.0337, wR_2 = 0.0648
Final R indexes [all data]	R_1 = 0.0365, wR_2 = 0.0657
Largest diff. peak/hole / e Å^{-3}	1.51/-1.79

8.3 Voltammograms

Squarewave voltammogramm of 169a
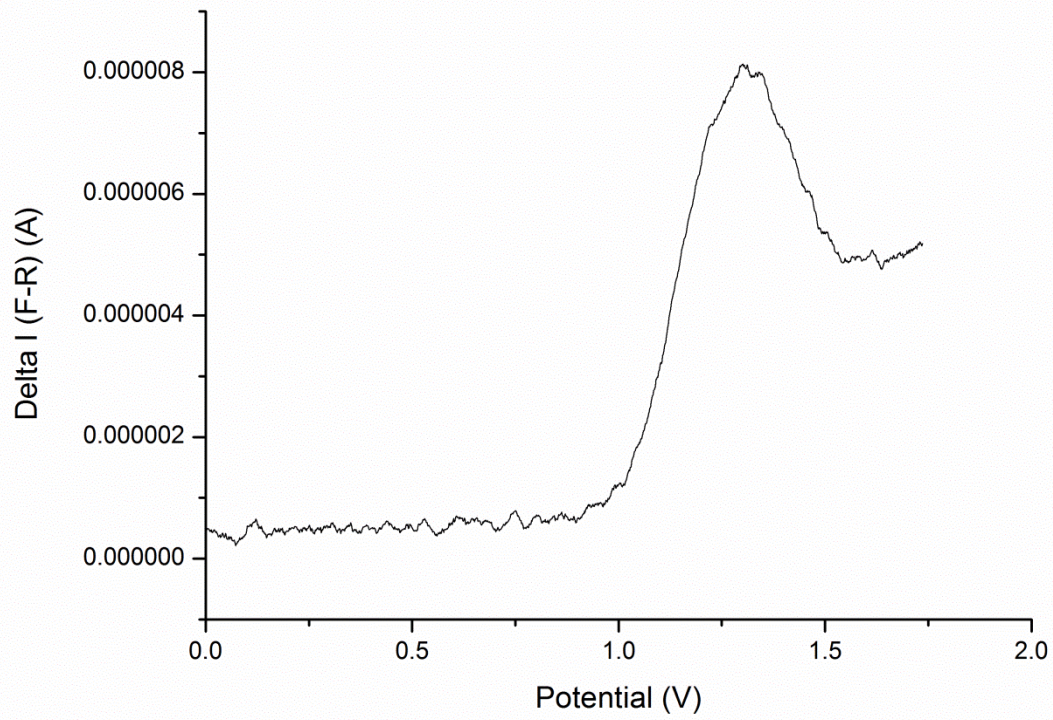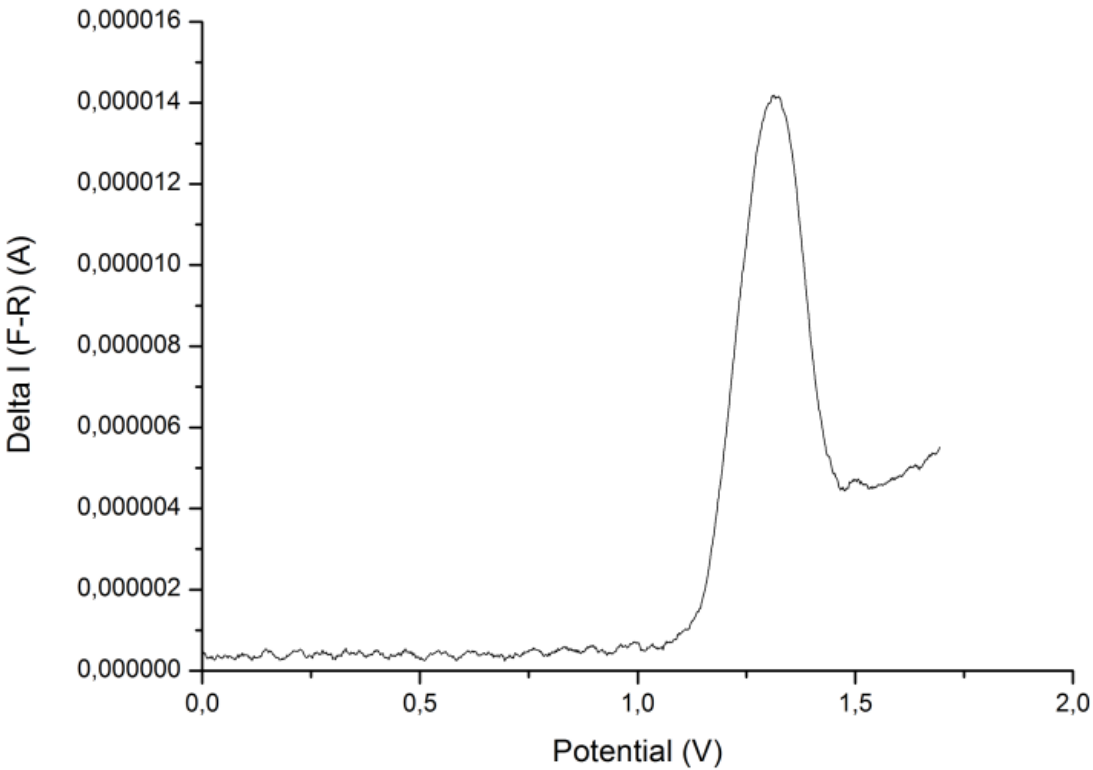

Squarewave voltammogramm of 169b
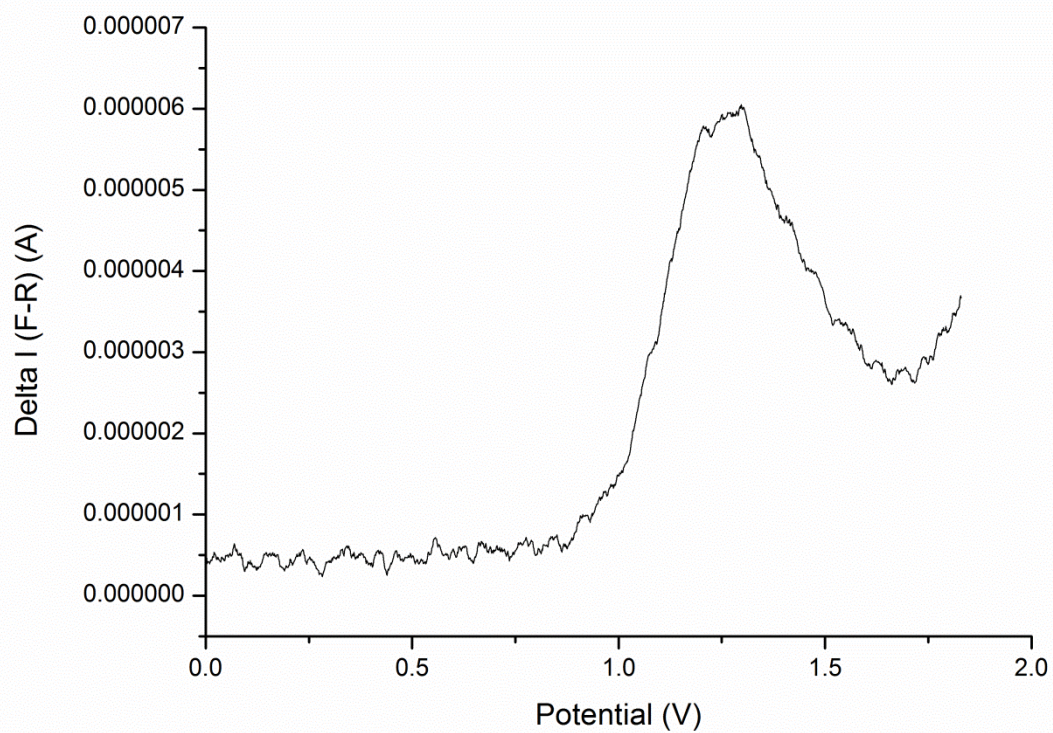
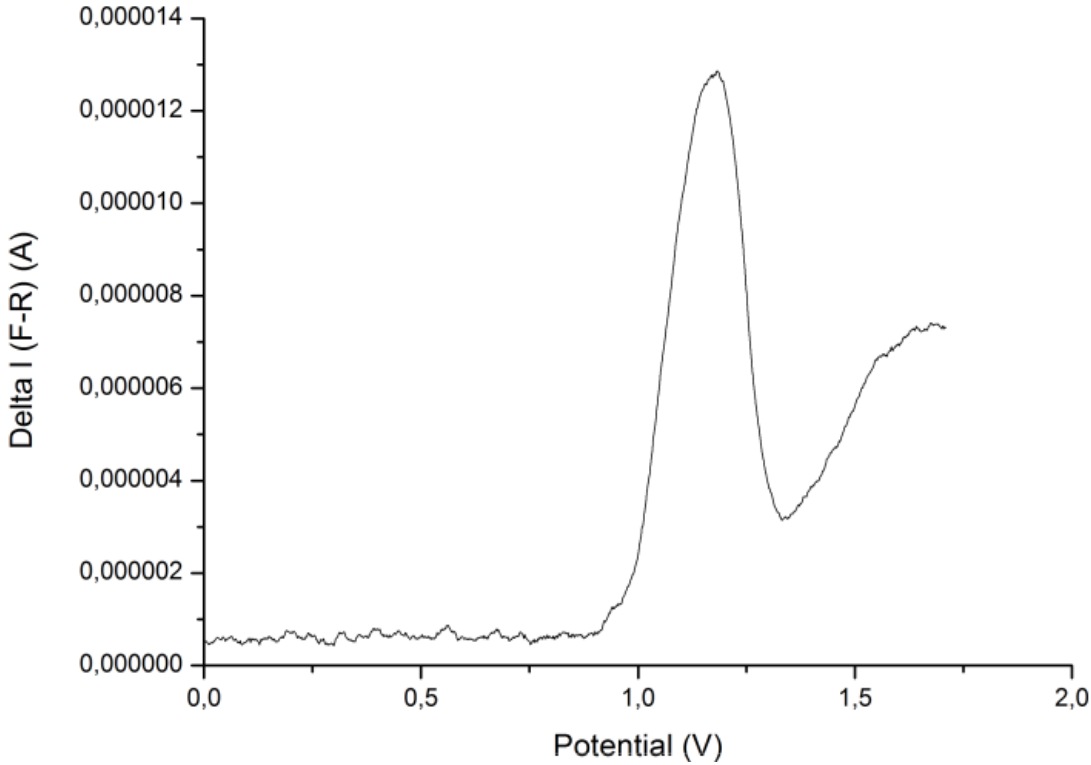**Squarewave voltammogramm of 169g**
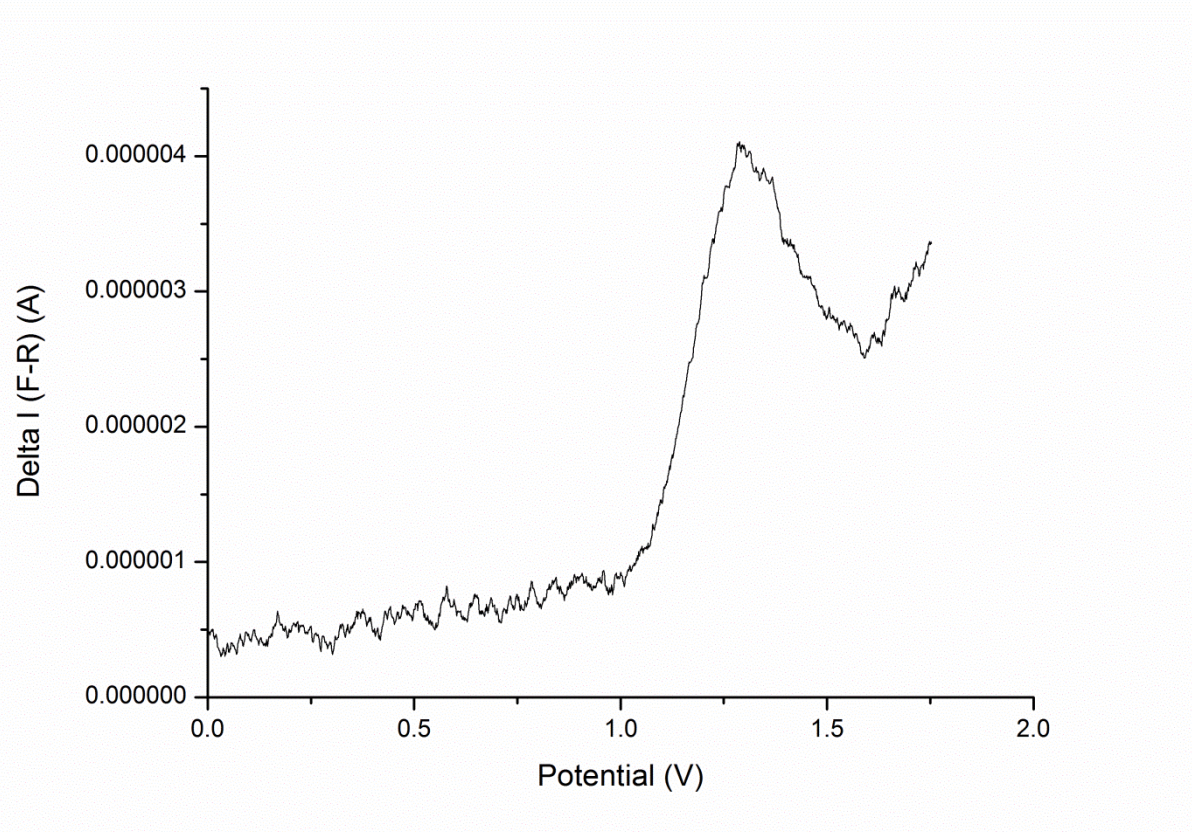
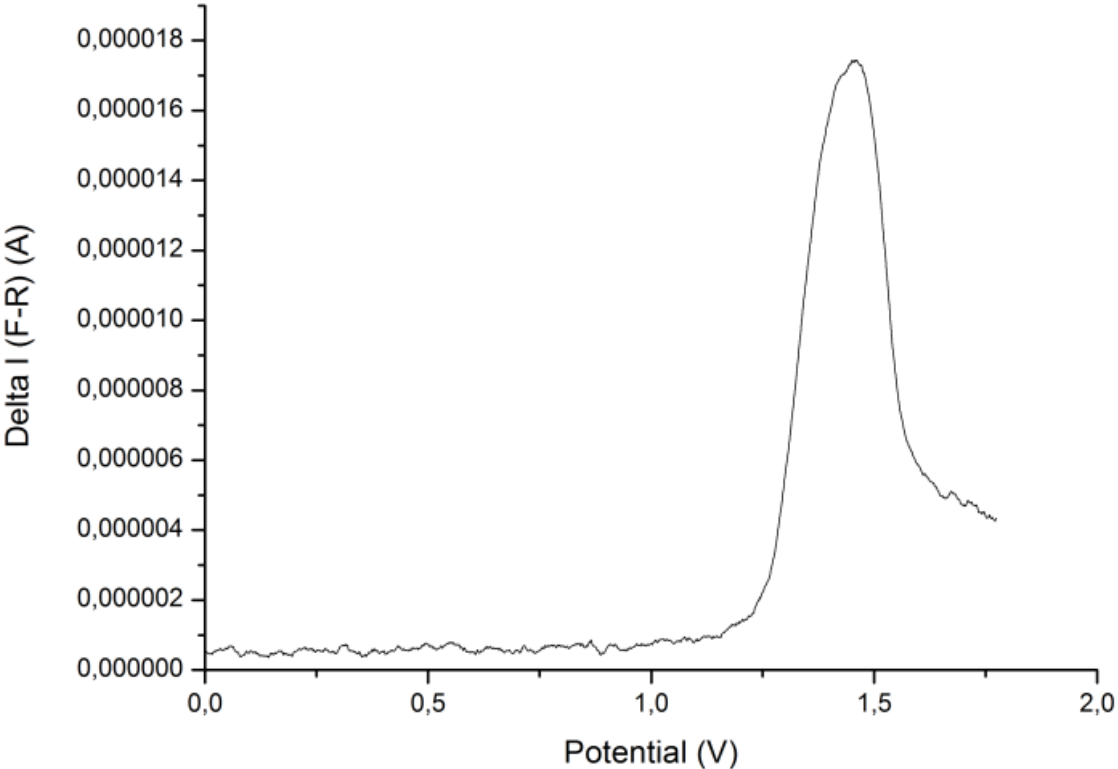
Squarewave voltammogramm of 169h
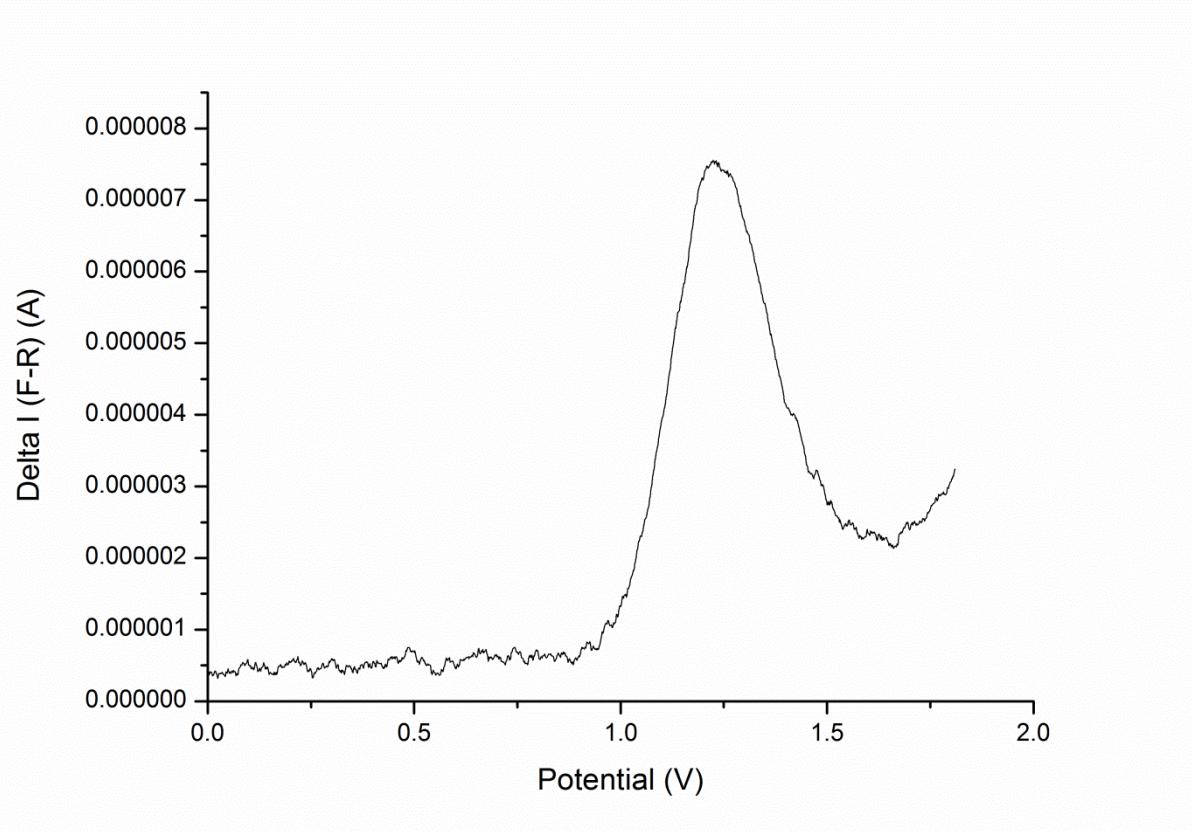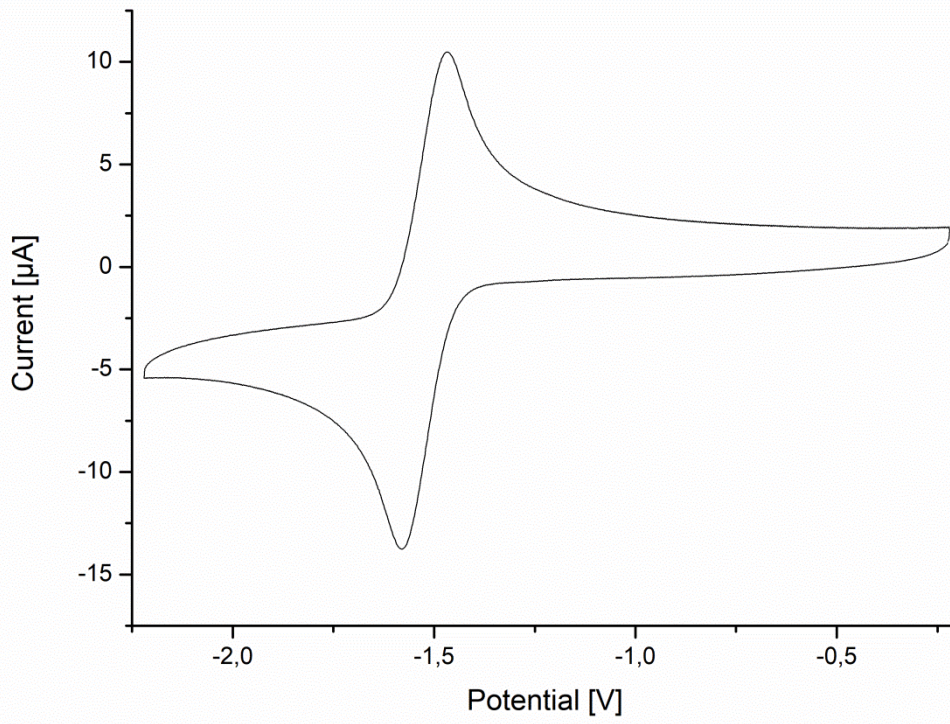
Squarewave voltammogramm of 191a
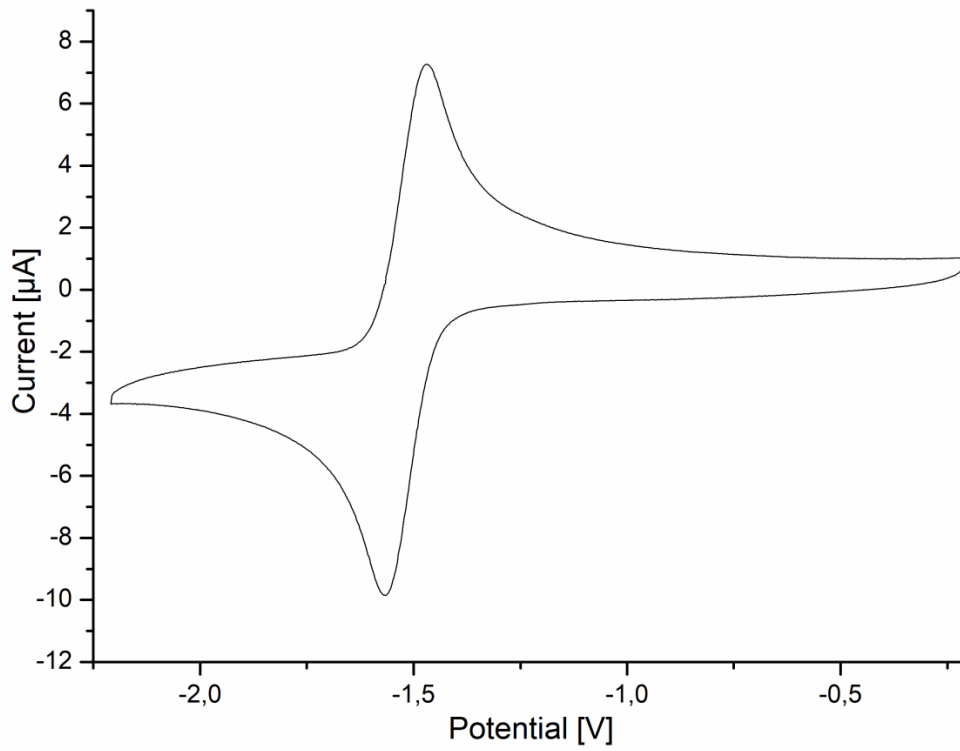

Squarewave voltammogramm of 191b
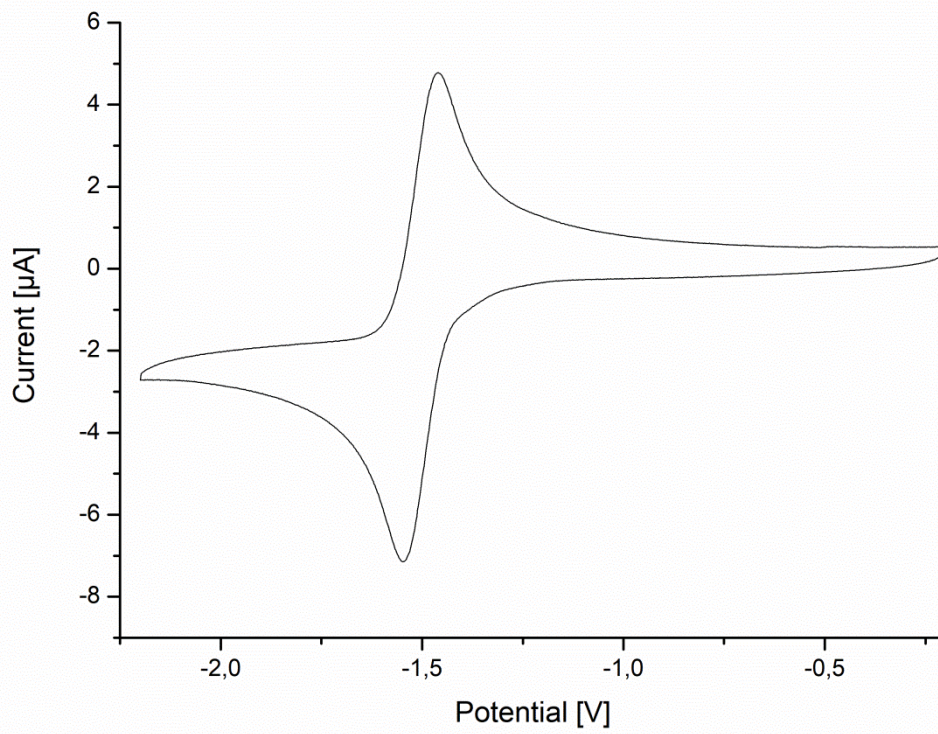
Squarewave voltammogramm of 191c

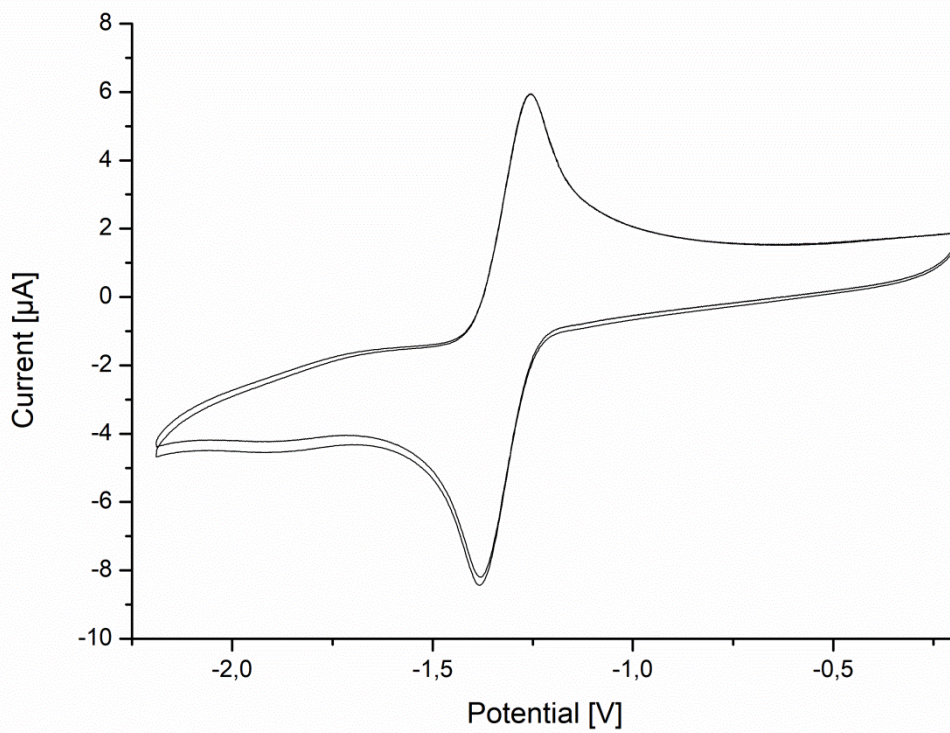**Cyclic voltammogramm of 191c** at 0.2 V/s scan speed

Cyclic voltammogramm of 191c at 0.1 V/s scan speed
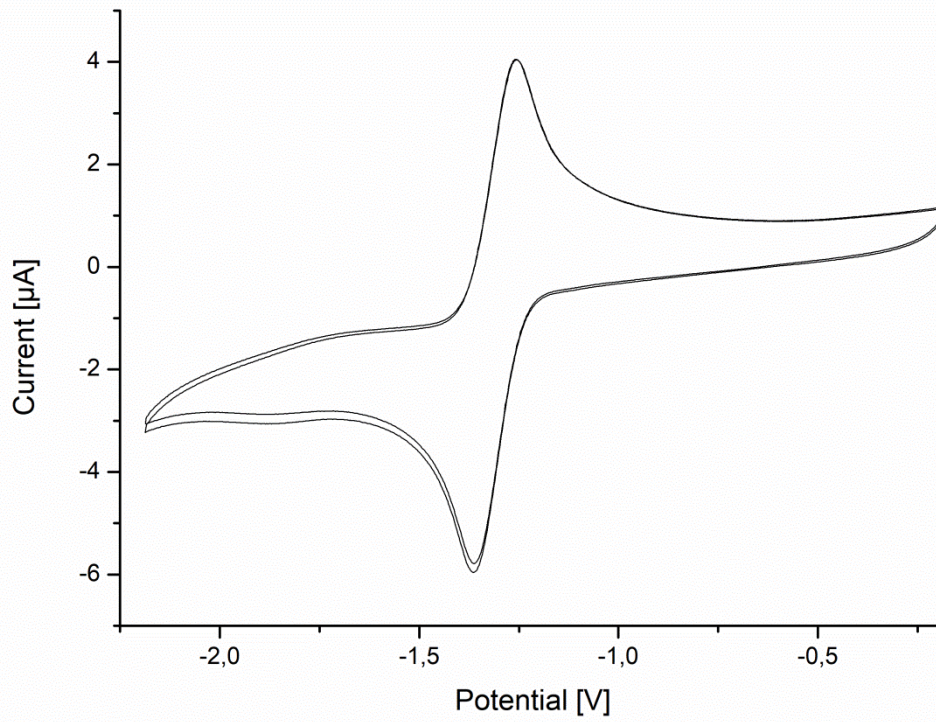
Cyclic voltammogramm of 191c at 0.05 V/s scan speed
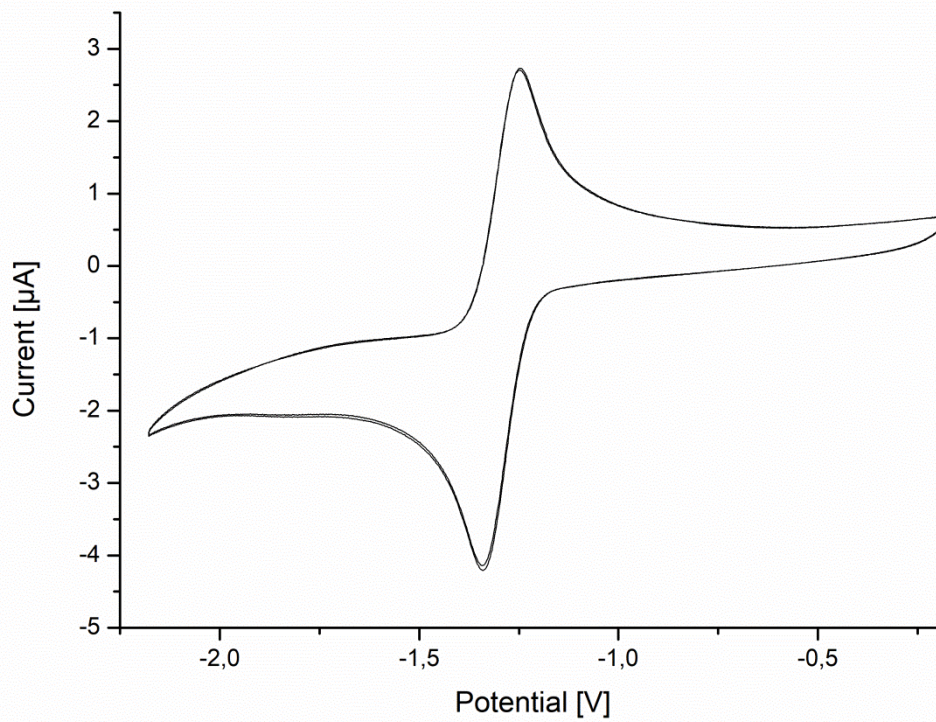

Cyclic voltammogramm of 191d at 0.2 V/s scan speed

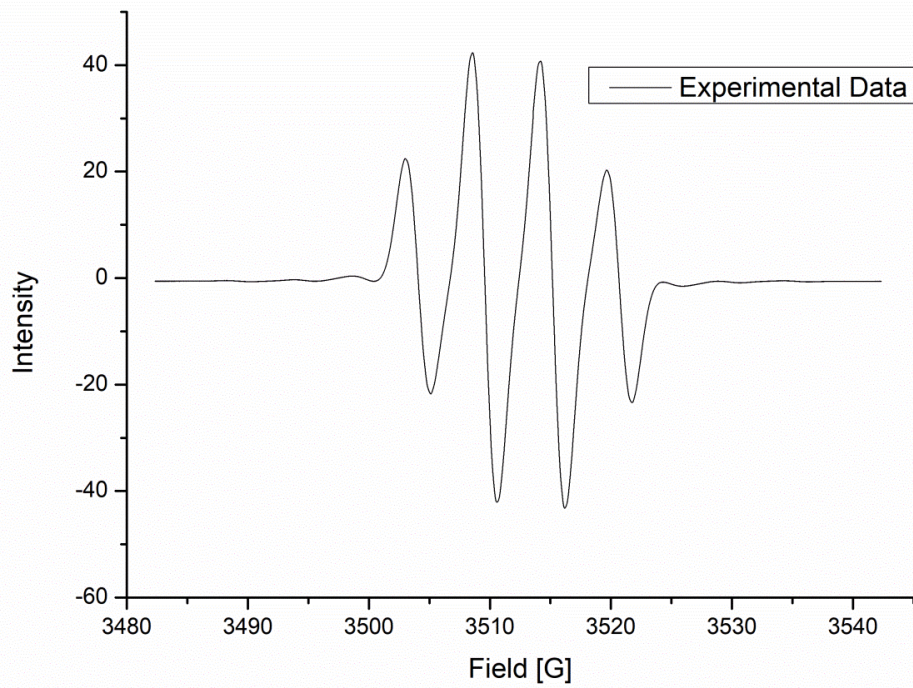**Cyclic voltammogramm of 191d** at 0.1 V/s scan speed

Cyclic voltammogramm of 191d at 0.05 V/s scan speed

8.4 EPR-spectra

Measured spectrum of **196**

Calculated spectrum of **196**
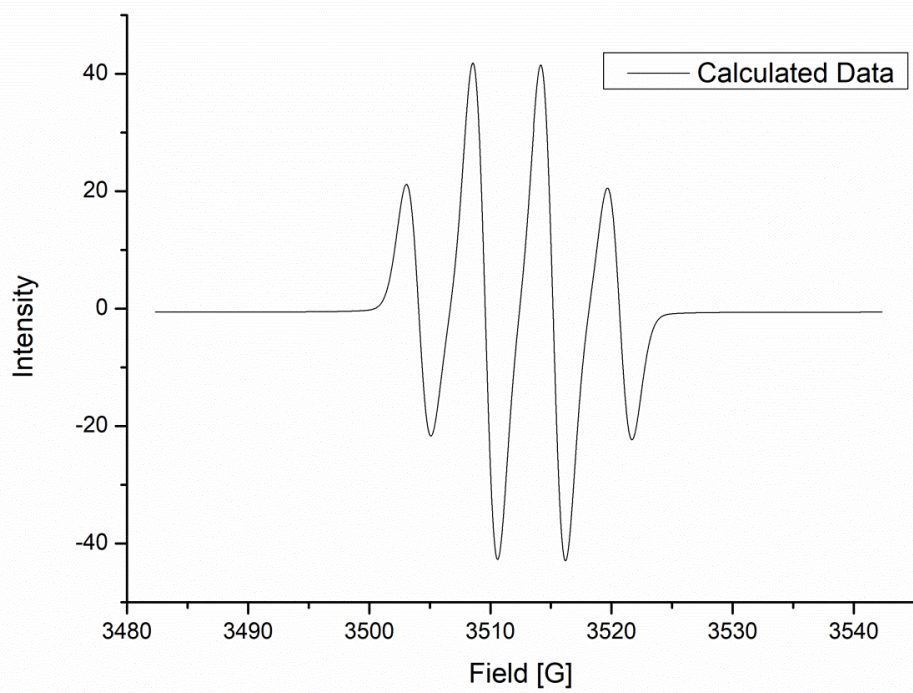
8.5 Buried Volume Determinations

Steric maps for the cationic phospholes **191** were calculated using the online tool sambVca 2.1[128] available online at: https://www.molnac.unisa.it/OMtools/sambvca2.1/index.html. The buried volumes were calculated without hydrogen atoms. The crystal structures of the corresponding Au(I) complexes (**205**, also shown in the figures below) of each ligand were used.

Calculated buried volume of **191a**
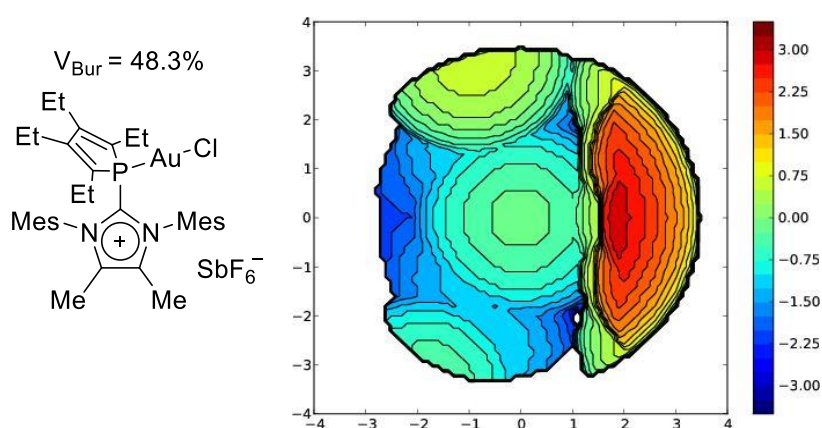
Calculated buried volume of **191b**
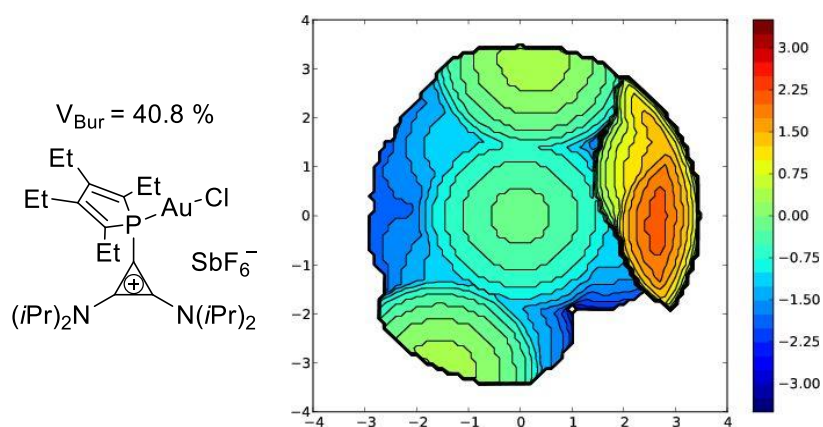
Calculated buried volume of **191c**

V_{Bur} = 52.9%
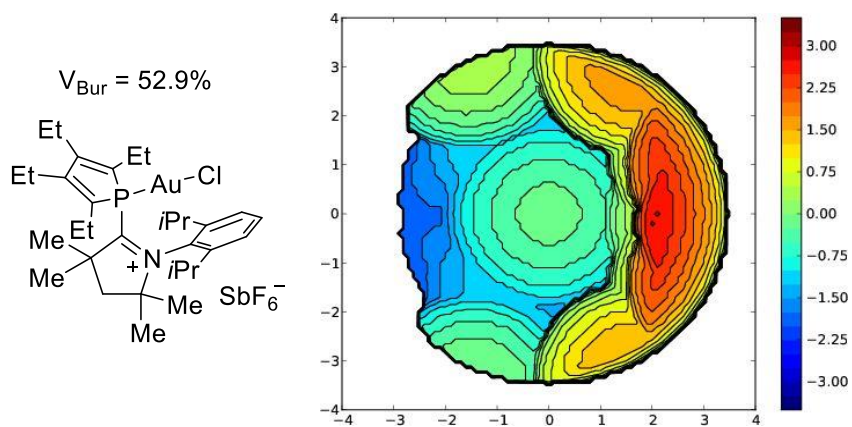
Calculated buried volume of **191d**

V_{Bur} = 56.2%
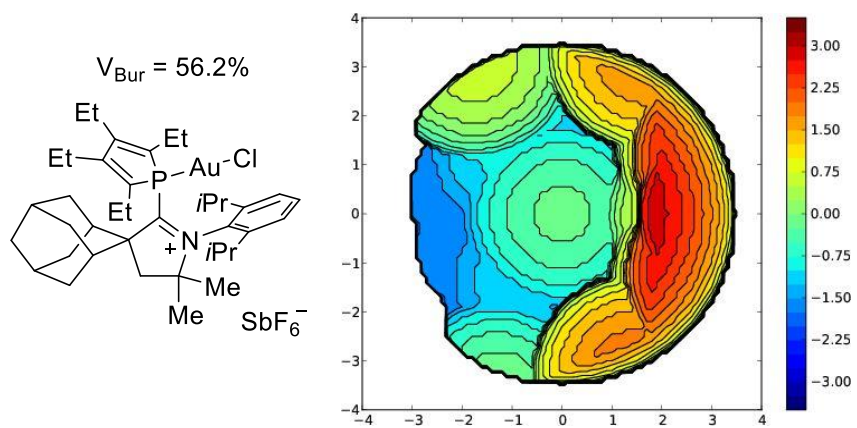
9. Computational methods

Calculations were done by Dr. Christopher Golz with Gaussian 16, Rev A. 03 and the input files were generated with GausView 6.0.16. The level of theory was unrestricted B3LYP/def2-TZVP with CPCM approximation for dichloromethane and empirical dispersion correction (GD3BJ). The minimum was confirmed by frequency calculations at the same level of theory; no imaginary frequency was found for minima. Total Spin density and SOMO plots were prepared within GaussView. [129]
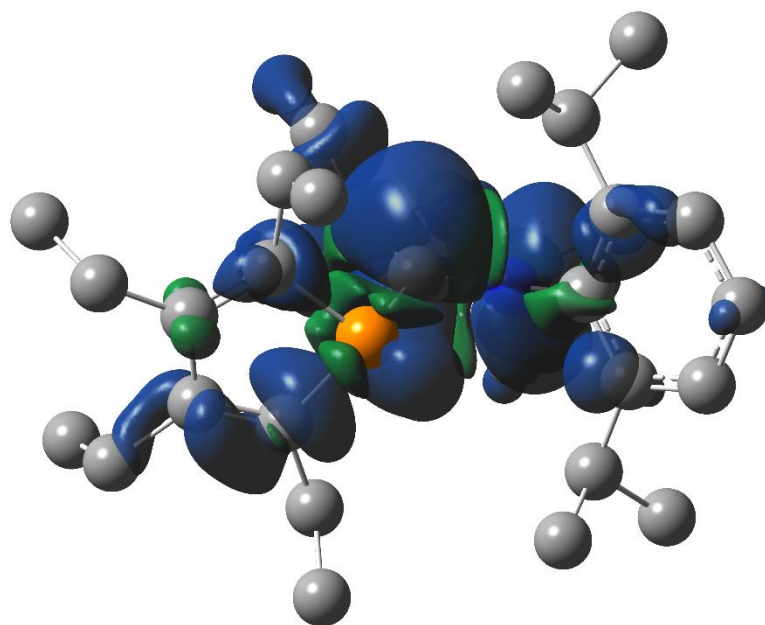
Figure 38: Total Spin density drawn at ISO=0.0005.
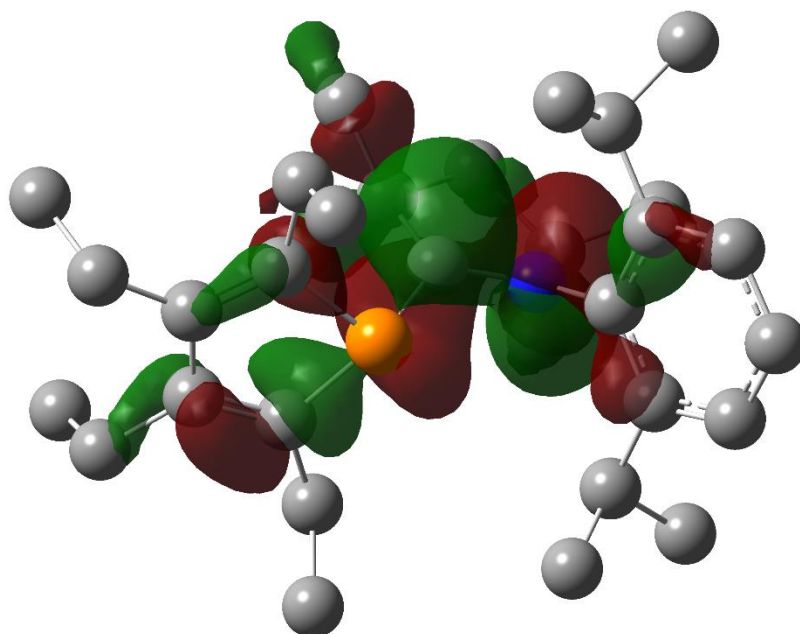
Figure 39: SOMO drawn at ISO=0.025.

Table 9: Coordinates of optimized minimum of **196**.

Tag	Symbol	X	Y	Z
1	P	-0.84202	0.027928	-0.764327
2	N	1.437535	0.152963	0.806975
3	C	0.108257	-0.250822	0.72821
4	C	-0.413157	-0.604129	2.120028
5	C	0.864094	-0.478071	2.983785
6	H	0.648071	-0.098991	3.982327
7	H	1.324997	-1.460968	3.096052
8	C	1.833501	0.436713	2.220318
9	C	1.592836	1.911997	2.575652
10	H	2.332292	2.556938	2.107399
11	H	1.67013	2.044458	3.656152
12	H	0.604459	2.241215	2.2623
13	C	3.289928	0.093845	2.499287
14	H	3.496559	-0.956407	2.311992
15	H	3.508797	0.30151	3.547547
16	H	3.9652	0.693804	1.888699
17	C	-1.53354	0.327528	2.609905
18	H	-1.240939	1.375339	2.583378
19	H	-1.799737	0.074381	3.639071
20	H	-2.419026	0.215646	1.988981
21	C	-0.949222	-2.043623	2.188054

22	H	-1.855537	-2.148153	1.594323
23	H	-1.188613	-2.300266	3.22358
24	H	-0.213015	-2.759618	1.822611
25	C	-2.139059	-1.232879	-0.850647
26	C	-3.366668	-0.64793	-0.819973
27	C	-3.341107	0.800721	-0.549234
28	C	-2.089267	1.313381	-0.431379
29	C	-1.729914	2.747963	-0.178608
30	H	-0.69881	2.804514	0.176678
31	H	-2.347274	3.150487	0.628822
32	C	-1.87724	3.64539	-1.415084
33	H	-2.916766	3.703862	-1.738313
34	H	-1.2935	3.254139	-2.24717
35	H	-1.531639	4.659738	-1.203908
36	C	-4.596964	1.612684	-0.349034
37	H	-5.431483	1.159313	-0.886127
38	H	-4.467989	2.607085	-0.777268
39	C	-4.978406	1.764468	1.130946
40	H	-5.126824	0.794138	1.604875
41	H	-5.902565	2.336477	1.235798
42	H	-4.194561	2.282167	1.684888
43	C	-4.64607	-1.410423	-1.054587
44	H	-4.452632	-2.237306	-1.739264
45	H	-5.375911	-0.771556	-1.555843
46	C	-5.267471	-1.970725	0.231228
47	H	-4.567428	-2.636252	0.739294
48	H	-6.175401	-2.535519	0.009955
49	H	-5.529162	-1.173671	0.926683
50	C	-1.866742	-2.674969	-1.158795
51	H	-2.708336	-3.288119	-0.829798
52	H	-1.006725	-3.013704	-0.581086
53	C	-1.604239	-2.936088	-2.646985
54	H	-1.377476	-3.989252	-2.827142
55	H	-0.760939	-2.340867	-3.001154
56	H	-2.474683	-2.665343	-3.247496
57	C	2.387445	0.020958	-0.254694
58	C	2.828523	1.15702	-0.957265
59	C	3.816247	1.008906	-1.931341
60	H	4.1631	1.880437	-2.470892
61	C	4.352078	-0.231852	-2.22788
62	H	5.119773	-0.328802	-2.985143

63	C	3.890072	-1.351422	-1.554482
64	H	4.301305	-2.322671	-1.796528
65	C	2.91152	-1.252197	-0.567793
66	C	2.44013	-2.528815	0.101306
67	H	1.72383	-2.257351	0.871377
68	C	3.578934	-3.311571	0.766316
69	H	4.293201	-3.677042	0.02641
70	H	3.176343	-4.178574	1.29398
71	H	4.128451	-2.703975	1.484914
72	C	1.717657	-3.421593	-0.91522
73	H	0.948623	-2.864655	-1.445041
74	H	1.247976	-4.272002	-0.416764
75	H	2.418551	-3.811416	-1.656137
76	C	2.248002	2.536302	-0.727831
77	H	1.472969	2.442757	0.02827
78	C	3.303175	3.52521	-0.218006
79	H	3.816879	3.147242	0.666557
80	H	2.838652	4.479664	0.038042
81	H	4.059534	3.716094	-0.981836
82	C	1.587433	3.070381	-2.003768
83	H	2.323231	3.222971	-2.795437
84	H	1.102514	4.027818	-1.807793
85	H	0.8345	2.37249	-2.369326